UNIVERSITÀ DI PISA

Scuola di Dottorato in Ingegneria "Leonardo da Vinci"

Corso di Dottorato di Ricerca in
SICUREZZA NUCLEARE E INDUSTRIALE

Tesi di Dottorato di Ricerca

CONTRIBUTION TO THE ASSESSMENT OF CFD CODES FOR IN-VESSEL FLOW INVESTIGATION

Autore:

Fabio Moretti

Relatori:

Prof. Francesco D'Auria

Prof. Walter Ambrosini

Anno 2009

ABSTRACT

The present research aims at contributing to the CFD code assessment process for nuclear reactor applications, and particularly for the predictive analysis of the fluid-dynamic phenomena occurring inside the reactor pressure vessel of a pressurized water reactor. The importance of such phenomena relies, for instance, on the influence that they can have on the spatial and temporal distribution of coolant properties (such as temperature or boron concentration) at the core inlet during certain accident transients involving perturbations of such properties with respect to nominal conditions; furthermore, in-vessel mixing phenomena can also affect the thermal interaction between coolant and pressure vessel during pressurized thermal shock scenarios.

The contribution provided by this work consists in the proposal of a general and systematic methodology to be applied in the CFD code assessment for in-vessel flow investigations. Within the proposed approach, the relevant modelling issues are identified and discussed, so as to point out the main capabilities and limitations in the present state-of-the-art tools and methods. Then, the main steps of the code application procedure are described and discussed analytically, thus providing guidance for a quality-oriented use of the codes, and complementing the existing best practice guidelines for this specific problem.

Furthermore, the research addresses the problem of the quantification of the accuracy for numerical predictions (both from CFD and integral codes) about coolant properties perturbations at the core inlet. As a result, a methodology is proposed based on a set of accuracy indicators, which can represent a means for judging whether the code results are sufficiently close to experimental data, once acceptance thresholds have been defined and the method has been completely assessed.

The work is supported by extensive CFD code validation and application results obtained in the frame of several international research projects and co-operations, and by a continuous interaction with the involved International scientific community.

LIST OF CONTENTS

LIST OF FIGURES

LIST OF TABLES

ABBREVIATIONS AND ACRONYMS

ABWR	Advanced Boiling Water Reactor
APWR	Advanced Pressurized Water Reactor
ASCII	American Standard Code for Information Interchange
BC	Boundary Condition
BCM	Boiler-Condenser Mode
BDBA	Beyond Design Basis Accident
BIC	Boundary and Initial Conditions
BPG	Best Practice Guidelines
BWR	Boiling Water Reactor
CAD	Computer Aided Design
CCL	CFX Command Language
CEA	Commissariat à l'Energie Atomique
CFD	Computational Fluid Dynamics
CFR	Code of Federal Regulations
CHT	Conjugate Heat Transfer
CL	Cold Leg
CSNI	Committee on the Safety of Nuclear installation
CVCS	Chemical and Volume Control System
DBA	Design Basis Accident
DNB	Departure from Nucleate Boiling
DNS	Direct Numerical Simulation
ECCS	Emergency Core Cooling System
EC	European Commission
ESBWR	Evolutionary Simplified Boiling Water Reactor
EU	European Union
FDA	Final Design Approval
FFTBM	Fast Fourier Transform Based Method
FP	Framework Programme
FSAR	Final Safety Analysis Report
FSER	Final Safety Evaluation Report
FSI	Fluid-Structure Interaction
FZD	Forschungszentrum Rossendorf
GGI	General Grid Interface
GPMF	Gidropress Mixing Facility
GRNSPG	Gruppo di Ricerca Nucleare – San Piero a Grado
GSI	General Safety Issue
GUI	Graphical User Interface
HL	Hot Leg
IVF	In-Vessel Flow
LDA	Laser Doppler Anemometry
LES	Large Eddy Simulation
LOCA	Loss Of Coolant Accident
LOOP	Loss Of Offsite Power
LP	Lower Plenum
LWR	Light Water Reactor
MCPR	Minimum Critical Power Ratio

MS	Mixing Scalar
MSLB	Main Steam Line Break
NEA	Nuclear Energy Agency
NK	Neutron Kinetics
NPP	Nuclear Power Plant
NRS	Nuclear Reactor Safety
OECD	Organization for the Economic Cooperation and Development
PHWR	Pressurized Heavy Water Reactor
PSU	Pennsylvania State University
PTS	Pressurized Thermal Shock
PWR	Pressurized Water Reactor
RANS	Reynolds-Averaged Navier-Stokes
RCP	Reactor Coolant Pump
RCS	Reactor Coolant System
RHR	Residual Heat Removal
RMS	Root Mean Square
RNG	Re-Normalized Group ($\kappa-\varepsilon$ turbulence model)
ROCOM	ROssendorf COolant Mixing (Model)
RPV	Reactor Pressure Vessel
SAR	Safety Analysis Report
SB-LOCA	Small Break LOCA
SCM	Second Closure Model
SG	Steam Generator
SGTR	Steam Generator Tube Rupture
SRP	Standard Review Plan
SST	Shear Stress Transport
SYS	System (code, analysis)
TH	Thermal Hydraulics
UNIPI	University of Pisa
UP	Upper Plenum
USNRC	United States Nuclear Regulatory Commission

1. INTRODUCTION

In many statements about the need to further validate Computational Fluid Dynamics (CFD) codes for nuclear reactor applications, there is an underlying belief that, behind the attractive features of CFD interfaces, there is not a completely reliable predictive tool, at least not reliable enough for being applied to safety related problems.
CFD codes are not yet – generally speaking – fully reliable tools: being inherently "three-dimensional" and "local" does not constitute *per se* a sufficient condition for assuring that 3D and local phenomena are accurately predicted. Colourful pictures and high definition movies that can easily be produced with CFD post-processing tools often give the illusion of a realistic and trustworthy representation of the reality, but may hide code deficiencies in achieving the needed level of accuracy.
On the other hand, intensive CFD code development and assessment work has been and is being carried out in recent years, made more and more effective by the availability of increasing computing resources.
Such advancements are certainly oriented to obtaining reliable and efficient predictive tools; however, some additional efforts are necessary to meet the quality assurance requirements that would make such tools applicable to the nuclear reactor technology, and in particular to the safety analysis within the licensing process.

1.1. Objectives of the research

This research is aimed at contributing to the assessment of CFD codes in their application to problems related to nuclear reactor safety and technology, in particular for the predictive analysis of in-vessel flows in pressurized water reactor (PWR) systems and of the related transport and mixing phenomena affecting the space and time distribution of coolant properties at core inlet.

This aim is pursued by:

- directly contributing to the CFD code validation in selected applications;
- suggesting a general methodology for the code validation against the existing experimental database;
- examining critically and analytically each step of the validation process, evidencing the limitations in the state-of-the-art tools and approaches, proposing solutions and improvements;
- proposing a systematic approach to accuracy evaluation.

The approaches and methodologies proposed are partly extendable to thermal-hydraulic system (TH-SYS) codes with three-dimensional capabilities (e.g. RELAP5-3D®, CATHARE 3D, etc.), since data related to the space and time distribution of coolant properties at core inlet are handled in the same form if it comes either from CFD or system code results, or from experimental measurements.

The result of this work can also represent a sort of extension of the existing Best Practice Guidelines (BPG) for application of CFD to nuclear reactor technology

(see Section 2.3), which represent the state-of-the-art as far as the quality assurance of CFD calculations is concerned. In fact such guidelines are still rather general and incomplete and do not address in detail the specific nuclear reactor issues for which CFD is expected to bring a real benefit to the safety assessment. The present work addresses one of such issues, i.e. the analysis of in-vessel flows, systematically and can hopefully contribute to improving the existing tools for achieving the due quality in CFD.

The work is the result of the following CFD-related activities carried out within the San Piero a Grado Research Group (GRNSPG) – University of Pisa:

- CFD analyses for various purposes such as code assessment, phenomena investigation, supporting system code assessment and application, supporting nuclear reactor safety and design studies, etc.;
- participation in international meetings, workshops and events, being in contact with several internationally recognized experts;
- planning and coordination of all CFD-related activities at GRNSPG.

Next sub-section provides a picture of the framework of the activities performed.

1.2. Framework

The research has been carried out in the framework of the CFD-related activities and international research projects in progress at the University of Pisa –GRNSPG, and has thus profited of the availability of large experimental databases and numerical resources, as well as of the connection to a wide number of internationally recognized experts in the fields of nuclear reactor safety and thermal-hydraulic and CFD code development and assessment.
A representative list of the main international Projects that have constituted the framework of this research is given below.

Project TACIS R2.02/02, “Simulation tools for transients involving spatial variations of coolant properties”
This project funded by the European Commission was a part of the TACIS programme (Technical Assistance to the Commonwealth of the Independent States), and was conducted in the period January 2005 to June 2007. The work was conducted by a Consultant – a consortium formed by AREVA (the Project leader), the University of Pisa (UNIPI) and the Forschungszentrum Dresden-Rossendorf (FZD) – in cooperation with a Director of Experiments (the Russian utility Gidropress), and had as a “beneficiary” the Rosenergoatom, i.e. the Russian Ministry for the atomic energy.
The objective of the project was to provide a validation database for a set of selected Russian thermal-hydraulics system codes, regarding the investigation of mixing inside the RPV during transients involving perturbation of the coolant properties distribution at the core inlet. The validation database achieved is constituted by ten experiments conducted in the Gidropress mixing facility (GPMF) and pre- and post-test calculations with the selected system codes. All experiments were also simulated (both by UNIPI and FZD) with the CFD code ANSYS CFX,

which provided a valuable support to the system code validation process (see Section 4.4.1). The CFD validation was obviously a useful by-product of the activity.

Agreement UNIPI-FZD

A long lasting research cooperation agreement exists between FZD and the Department of Mechanics, Nuclear and Production Engineering (DIMNP). In this framework, FZD provided UNIPI specialists with measured data from some ROCOM experiments for code validation purposes; such experiments have been simulated both with CFD codes (such as ANSYS-CFX, Fluent and Trio_U) and the system code RELAP5-3D (see ANNEX A, A.1).

NURESIM Integrated Project (EU 6th FP), "European Platform for Nuclear Reactor Simulations"

This project, part of the 6th Framework Programme of the EURATOM, was conducted by a consortium of more than twenty European participants (including University of Pisa) in the period 2005-2007, with the objective of developing and establishing a common European software platform for nuclear reactor simulation. One of the five sub-projects dealt with the development and the validation of thermal-hydraulics tools, and in particular of specific models to be implemented into the French CFD code NEPTUNE_CFD (owned by CEA and EDF) for the simulation of two-phase phenomena occurring in light water reactors during accidental scenario (e.g., boiling crisis and pressurized thermal shock).
NURESIM is also a long-term development programme, of which the NURESIM IP was the fist step. The next step is the Project NURISP which is just starting.
Authors' contributions to the CFD validation activities can be found in Refs. [1] and [2].

Research Agreement between UNIPI and N.A.-S.A.

UNIPI and the utility Nucleoeléctrica Argentina – Sociedad Anonima (N.A.-S.A.) have established a cooperation agreement in 2006, within which UNIPI provides support to the safety analysis of the pressurized heavy water reactor (PHWR) Atucha-II (currently under construction in Argentina).
In this context, many CFD investigations have been and are being performed among other studies, addressing specific issues relevant to the safety and operation of Atucha-II reactor (including in-vessel flow). Further information can be found in technical documentation of the activity (e.g. Ref. [3] and [4]).

OECD/NEA/CSNI Writing Groups on CFD Issues

Three international groups of experts were established since 2002 by the Committee on the Safety of Nuclear installation (CSNI), and have periodically met to deal with the following topics (respectively):

1. writing Best Practice Guidelines (BPG) for the application of CFD codes to nuclear reactor safety problems;
2. identifying, characterizing and prioritizing the reactor safety issues which require (or would benefit of) the application of single-phase CFD, and making a state-of-the-art on the assessment of current tools;

3. making a state-of-the-art as regards the currently available multi-phase CFD tools.

The Author of the present work participated in the meetings of the above three groups as representative of UNIPI and contributed to the issue of the following two reports: "*Best Practice Guidelines for the use of CFD in Nuclear Reactor Safety Applications*" (Ref. [5]) and "*Assessment of CFD Codes for Nuclear Reactor Safety Problems*" (Ref. [6]).

OECD "V1000CT-2" Benchmark, "VVER-1000 Coolant Transient: Coolant Mixing Tests and MSLB"
This international benchmark, in which UNIPI participated, had the purpose of testing existing tools for computation of coolant mixing in reactivity transients, such as for instance a Main Steam Line Break (MSLB) scenario in a PWR. The benchmark was based on measured plant data from Kozloduy NPP Unit 6. Both system codes and CFD codes were adopted by the participants (including UNIPI) to simulate the transient and quasi steady-state phases of the scenario (Refs. [7], [8] and [9]).

OECD – NUPEC "BFBT" Benchmark
This international benchmark was based on NUPEC BWR Full-size Fine-mesh Bundle Tests (BFBT) and was aimed at assessing the boiling flow modelling capabilities of existing CFD and sub-channel codes. The test facility had provided in the past very accurate measurements of the void fraction at the outlet of a boiling channel (0.3 mm space resolution) for several experiments at different operating conditions, and such data constitute a valuable database for two phase flow CFD code validation.
UNIPI participated in the benchmark performing CFD simulations with both CFX and NEPTUNE_CFD codes.

1.3. Preliminary remarks

The following considerations constitute the basis and the framework for the present work.

1. The attention focuses on the application and assessment of CFD codes for single-phase flows; multiphase-flow CFD applications are addressed only marginally.
2. The fluid-dynamic phenomena that are the main object of the above mentioned CFD investigations are those occurring inside the reactor pressure vessel (RPV) of pressurized water reactors (PWR), including those of Russian technology (i.e. VVER), and pressurized heavy water reactors (PHWR) such as Atucha-I and Atucha-II. Reference will often be made to "in-vessel flow" (IVF). In many cases, the CFD applications deal with experiments conducted on test facilities that reproduce (usually at reduced scales) such kind of reactors.
3. The mentioned IVF phenomena are relevant to the reactor safety because they affect the space and time distribution of the coolant properties (such

as the temperature and the boron concentration) at the core inlet and its deviation from nominal conditions during incidental scenarios. Therefore, the prediction of the "perturbation" of such properties distribution is often the main objective of the CFD analysis.

4. Unless differently specified, the CFD analyses performed by the Author were run using a commercial, general-purpose CFD code, namely ANSYS CFX (releases 10.0 and 11.0, Ref. [10]). Analogously, most computational grids were developed with ANSYS ICEM-CFD package (releases 10.0 and 11.0, Ref. [11]).

1.4. Basic nomenclature

Assessment
It is considered, in this context, as a synonym of the term "qualification" (see below).

Demonstration calculations
Demonstration calculations are often run with the purpose of checking the capabilities of a given code to perform certain calculations, obtaining information on the computational resources required and thus helping in the decision making as regards the code assessment process. They are performed when experimental information for code validation is not yet available or is still incomplete. Demonstration calculations are, in a sense, a support to the validation and cannot in any way replace it.

Mixing Scalar (MS)
Any "perturbation" (see below) of coolant properties transported by the fluid can be expressed in a non-dimensional normalized form with respect to reference values for the unperturbed (i.e. nominal) and perturbed conditions. The resulting quantity is often called the "mixing scalar" (name that was probably introduced by FZD scientists in the framework of ROCOM investigations, Ref. [12]).
The MS, as a function of time and space, can be thus obtained as in Equation 1, where *C* represents any coolant property (such as temperature, boron or tracer concentration, etc.), while the subscripts *0* and *1* indicate the two reference conditions.

$$MS = \frac{C\left(\vec{x},t\right) - C_0}{C_1 - C_0} \qquad \text{Equation 1}$$

For example, C_0 and C_1 may be respectively the boron concentration in a PWR's coolant in normal operation and in a deborated or low-borated slug which has formed during reflux-condensing mode, or due to a malfunctioning of the Chemical and Volume Control System (CVCS). Otherwise they may represent the normal coolant temperature at core inlet and the temperature of a cold slug which has formed following a Steam Line Break event, or the minimum and the maximum electrical conductivity in a mixing experiment where a salt tracer is utilized to simulate a perturbation in coolant properties (such as in ROCOM, for example).
If the two reference values are extreme values i.e. (a minimum and a maximum), then the MS will range between *0* and *1*. Otherwise it can assume also values

greater than *1* (such as, for instance, in the injection-type experiments performed on Gidropress mixing facility, Ref. [13]).

Perturbation

"Perturbation" here means any deviation from normal conditions value of a coolant property (namely: core inlet temperature or boron concentration in a NPP, or tracer concentration in a test facility). It can be easily quantified by the "mixing scalar" (see above).

Qualification

The "qualification" or "assessment" process, as herein conceived, involves both verification and validation (see below).

Sometimes the terms "qualification" and "assessment" are used as synonyms of "validation".

The following definition of validation can be found in Ref. [14]: "*Determination of adequacy of the conceptual model to provide an acceptable level of agreement for the domain of intended application.*"

Validation

The validation process aims at answering the following questions: is the code able to simulate and reproduce the real behaviour? Does it solve the proper equations and use the proper models?

The validation involves comparison against experimental data.

The following definition of validation can be found in Ref. [14]: "*The process of determining the degree to which a model is an accurate representation of the real world from the perspective of the intended uses of the model.*"

According to another effective definition, validation means to check that a code "*solves the right equations*" (see analogous definition for "verification").

Verification

The verification process aims at answering the following question: are the equations, which describe the real phenomena, correctly implemented in the code?

The verification involves the debugging of the code.

The following definition of validation can be found in Ref. [14]: "*The process of determining that a model implementation accurately represents the developer's conceptual description of the model and the solution to the model.*"

According to another effective definition, validation means to check that a code "*solves the equations right*" (see analogous definition for "validation").

2. STATE-OF-THE-ART IN THE APPLICATION OF CFD CODES TO NRS PROBLEMS

2.1. General remarks

An exhaustive description of the state-of-the-art in the application of CFD codes to nuclear reactor safety (NRS) problems has recently been produced by the three "Writing Groups on CFD" already mentioned in Section 1.2. Those groups of experts were created by the CSNI in 2002, and have periodically met (twice per year) with the aims of providing BPGs (WG1), evaluating the existing CFD assessment database and related limitations (WG2), and exploring the possibilities of extension to two-phase flows (WG3). They have met until the end of 2006, 2007 and 2008 respectively, and the result of their work consists of three reports (Ref. [5], [6] and [15])[1].

Moreover, several experimental campaigns and code development and assessment activities have been carried out in the recent years, both in international and national frameworks, as well as international workshops and conferences devoted to the CFD application in the nuclear field.

This Chapter includes information from the aforementioned CSNI reports (in particular the first two, since two-phase flow is not addressed in this document), as well as from the surveyed literature. Furthermore, the main achievements from the mentioned research activities and international events are briefly summarized.

2.2. Identification of NRS issues requiring CFD

An important outcome of the work done by one of the CSNI Writing Groups on CFD was a sort of classification of a number of NRS problems identified as needing the support of CFD. Such problems are indicated in Table 1 (extracted from Ref. [6]), along with the following information:

- to which part of the nuclear system they are related (reactor core, primary/secondary circuit, containment);
- whether they are relevant to normal operation, DBA or BDBA;
- whether they involve single-phase or two-phase flow (or both).

Information on the current modelling capabilities and limitations and on the availability of experimental data for validation was gathered and reported for each of the above problems in Ref. [6].

[1] The Author of the present work participated in the meetings of all the three groups since 2004, as a representative of the University of Pisa.

Table 1 – NRS issues needing CFD (from Ref. [6])

	NRS problem	System classification	Incident classification	Single- or multi-phase
1	Erosion, corrosion and deposition	Core, primary and secondary circuits	Operational	Single/Multi
2	Core instability in BWRs	Core	Operational	Multi
3	Transition boiling in BWR/determination of MCPR	Core	Operational	Multi
4	Recriticality in BWRs	Core	BDBA	Multi
5	Reflooding	Core	DBA	Multi
6	Lower plenum debris coolability/melt distribution	Core	BDBA	Multi
7	Boron dilution	Primary circuit	DBA	Single
8	Mixing: stratification/hot-leg heterogeneities	Primary circuit	Operational	Single/Multi
9	Heterogeneous flow distribution (e.g. in SG inlet plenum causing vibrations, HDR experiments, etc.)	Primary circuit	Operational	Single
10	BWR/ABWR lower plenum flow	Primary circuit	Operational	Single/Multi
11	Waterhammer condensation	Primary circuit	Operational	Multi
12	PTS (pressurised thermal shock)	Primary circuit	DBA	Single/Multi
13	Pipe break – in-vessel mechanical load	Primary circuit	DBA	Multi
14	Induced break	Primary circuit	DBA	Single
15	Thermal fatigue (e.g. T-junction)	Primary circuit	Operational	Single
16	Hydrogen distribution	Containment	BDBA	Single/Multi
17	Chemical reactions/combustion/detonation	Containment	BDBA	Single/Multi
18	Aerosol deposition/atmospheric transport (source term)	Containment	BDBA	Multi
19	Direct-contact condensation	Containment/ Primary circuit	DBA	Multi
20	Bubble dynamics in suppression pools	Containment	DBA	Multi
21	Behaviour of gas/liquid surfaces	Containment/ Primary circuit	Operational	Multi
22	Special considerations for advanced (including Gas-Cooled) reactors	Containment/ Primary circuit	DBA/BDBA	Single/Multi

DBA–Design Basis Accident; BDBA–Beyond Design Basis Accident; MCPR–Minimum Critical Power Ratio

2.3. State-of-the-art in CFD quality assurance

The application of numerical analysis tools to problems connected to nuclear technology should be performed so as to reduce the related uncertainties and inaccuracies as far as possible, to collect all the necessary information to assess the degree of reliability of the results, and to optimize the exploitation of the available computational resources. This is what, in other terms, can be referred to as the “quality assurance” of the analyses.

An efficient means to implement a quality-oriented approach in the use of codes consists in providing the user with written guidance on the “best practice” to follow when addressing given problems, where the “best practice” is the synthesis of all the experience achieved by the most advanced users on those problems and of the common knowledge about capabilities and limitations of the tools.

2.3.1. Historical remarks

The idea of providing best practice guidelines (BPG) for the application of CFD to nuclear reactor problems is rather recent. This reflects the fact that only recently (say in the past 10-15 years) the use of CFD in industrial applications has become so widespread, owing to the dramatic increase in the computing power. BPGs for CFD use in the non-nuclear industry have appeared first, such as:

- BPGs for marine applications of CFD (MARNET-CFD, Ref. [16]);
- ERCOFTAC best practice guidelines for the application of CFD (Ref. [17]);
- EU 5th Framework Programme "QNET-CFD network" best practice advices (www.qnet-cfd.net).

In 2002, the "BPGs for the CFD Code Validation for Reactor-Safety Applications" were produced as the first deliverable of the ECORA Project (see Section 2.4.2.3, and Ref. [18]): these are the first official guidelines oriented to nuclear applications, and represent thus a milestone, even though they are quite general and do not address specific problems in a detailed way.

The need of establishing BPGs was then recognized by the CSNI, which assigned the task of producing a new document to one of the above mentioned Writing Groups. A panel composed by 15-20 experts of CFD and nuclear reactor technology have thus met twice a year for three years and has finally come out with the "Best Practice Guidelines for the use of CFD in Nuclear Reactor Safety Applications" (Ref. [5]), which represent a further milestone in the process of quality assurance establishment.
Again, also the latter document is incomplete and not exhaustive. It provides useful guidance for a range of single phase applications to a relatively general level of detail; however, a deeper level of specificity is envisaged for each application, but not covered by the document, which is thus intended as the preliminary part of a wider set of (future) guidelines addressing thoroughly many specific problems.
A brief description of the CSNI BPGs is provided in the following.

2.3.2. The CSNI BPGs for CFD application to nuclear reactor problems

The topics covered by the CSNI BPGs are reported in the list below, which also indicates the structure of the BPGs report.

1. Problem definition:
    a. isolation of the problem;
    b. phenomena identification and ranking table (PIRT);
    c. considerations on special phenomena.
2. Selection of appropriate simulation tool:
    a. classic thermal-hydraulic system code;
    b. component code (porous CFD);
    c. CFD code;
    d. potential complementary approaches (e.g. CFD-1D coupling).
3. User selection of physical models:
    a. guidelines for turbulence modelling in NRS applications;
    b. buoyancy model;

    c. heat transfer;
    d. free surface modelling;
    e. fluid-structure Interaction.
4. User control of the numerical model:
    a. transient or steady model;
    b. grid requirements;
    c. discretization schemes;
    d. convergence control;
    e. free surface consideration.
5. Assessment strategy:
    a. demonstration of capabilities;
    b. interpretation of results.
6. Verification of the calculation and numerical model:
    a. error hierarchy;
    b. round-off errors;
    c. spatial discretization errors;
    d. time discretization errors;
    e. software and user errors.
7. Validation of results:
    a. validation methodology;
    b. target variable and metrics;
    c. treatment of uncertainties.
8. Documentation.

A detailed discussion of the above topics is not presented here. However it is worth placing stress on the fact that each single step of the analysis, from the definition of the problem through the meshing, the simulation set-up and the result post-processing and comparison to the final documentation, is identified and considered analytically.
In particular, a special effort is required to assess the errors affecting the results, which implies that a number of sensitivity analyses have to be performed. This is clearly that aspect which makes the systematic application of the BPGs so difficult, since the computational expense to be allocated can easily grow by one order of magnitude or more.
Obviously, this is not to be regarded as a weak point of the BPGs, but rather as a limitation that is embedded in the state-of-the-art methods, tools and resources, and that will hopefully be removed soon by the progress in technology.

A stated above, what is still missing from the BPGs is a set of guidelines devoted to each specific type of problems of those identified as relevant to the reactor safety and as requiring the CFD application. For example, general guidance is given on mesh generation, i.e. on common strategies to achieve high-quality grids and thus reduce the errors associated with spatial discretization as far as possible, but no detailed discussion is provided yet on the specific meshing problems to be faced when dealing with a RPV lower plenum, or a fuel assembly spacer, or a pump, etc.

The main part of this dissertation (Chapters 4 and 5) deals particularly with one of those types of nuclear reactor problems (i.e. the in-vessel flow investigation) and

provides guidance on how to conduct the analysis. For this reason, it can be a candidate to be a first integration to the CSNI BPGs.

2.3.3. Concluding remarks on CFD quality assurance

As explained above, a systematic application of the BPGs usually implies the execution of a large number of calculations for each single problem addressed, which normally results to be prohibitive for most users. Therefore, in most cases only a partial application of the BPGs is possible. For example, grid sensitivity studies are often missing in published works and demonstrations of the achievement of grid-independence of the results are very rare.

Nevertheless, the efforts to follow this quality-oriented approach as far as allowed by the available resources appear to be rapidly growing, as testified by the increasing amount of references to the BPGs in published works on CFD analysis of nuclear reactor problems. In other words, the idea that demonstrating the quality of the performed CFD analysis is an essential step of the analysis itself is becoming more and more widely accepted, which was exactly the intention of the BPGs Authors.

Two international workshops have already been organized by the CSNI Writing Groups on CFD[2], under the sponsorship of the OECD/NEA and of the IAEA, with the purpose of collecting and exchanging information on the most recent advancements in the development, validation and application of CFD methods for nuclear reactor problems. The participants had been invited to follow the BPGs as far as possible, and the submitted papers were evaluated, among various criteria, also on the basis of the efforts made in that sense. Noticeable improvements in the participants' attitude to quality assurance were noticed from the first workshop to the second one.

It is also worth recalling the IAEA/NEA Technical Meeting on the "Use of CFD codes for safety analysis of reactor systems", which was hosted by the University of Pisa in 2002, and which provided a comprehensive view of the current state-of-the-art (see Ref. [19]).
The recommendation to establish BPGs for the application of CFD codes to nuclear reactor safety problems was one of the main outcomes of the meeting.

[2] 1) "CFD4NRS: Benchmarking of CFD Codes for Application to Nuclear Reactor Safety", Garching, Germany, 5-7 September 2006. 2) "XCFD4NRS: Experiments and CFD Code Applications to Nuclear Reactor Safety", Grenoble, France, 10-12 September 2008. The Author was a member of the Scientific Committees of both workshops.

2.4. Review of existing CFD code assessment database related to IVF investigation

2.4.1. Experimental database

Several experimental facilities have been realized by industries and research institutions to investigate the IVF phenomena and provide reference data for CFD code validation. A brief review of the most relevant ones is reported hereafter.

2.4.1.1. ROCOM facility

The Rossendorf Coolant Mixing (ROCOM) test facility was constructed by FZD in 1998. It is a 1:5 scaled model of a German PWR KONVOI; it includes a Plexiglas RPV model and four loos with fully controllable coolant pumps (Figure 1). The geometry of RPV internal is accurately reproduced up to the core support plate, while the core region and the upper plenum are represented in a simplified way.
Salt tracer is used to simulate the presence of slugs of deborated or overcooled water; its space and time distribution inside the RPV is obtained via electrical conductivity measurements (by the so-called "wire-mesh sensors") and proper calibration procedures. Moreover, other additives (such as glycol or alcohol) are used to alter the fluid density for the investigation of buoyancy effects.
In addition to salt concentration measurements, also laser Doppler anemometry (LDA) is also used in some tests for velocity measurement in the downcomer.

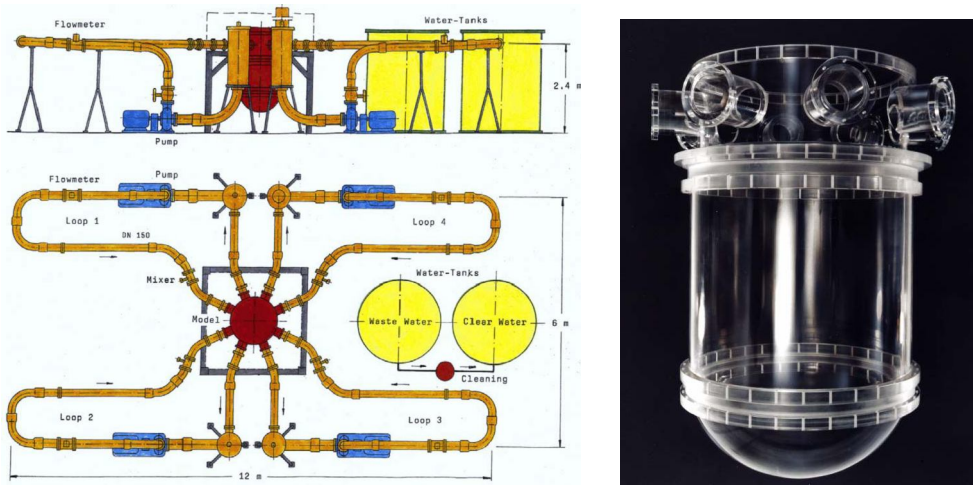

(a) (b)

Figure 1 – ROCOM facility: a) sketch of the facility; b) Plexiglas RPV model

Many experiments have been and are being conducted at ROCOM facility, reproducing a wide range of loop operation configurations and of fluid properties perturbations. Normally, each experiment consists of multiple repetitions of the same tests in the same conditions, which allow quantifying the measurement uncertainties via statistical processing and defining confidence intervals for comparison with code simulation results.

Measured data for some tests are available at the University of Pisa and have been used by the Author for CFD code validation purposes (Section A.1).

ROCOM experiments have been used for code validation also in the frame of FLOMIX-R Project (see Section 2.4.2.4).
Many published works exist which deal with ROCOM experiments and related CFD simulations (e.g. Refs. [12] and from [20] to [32]).

2.4.1.2. Gidropress mixing facility

The Gidropress mixing facility, located in Podolsk (Moscow region, Russia), reproduces a VVER-1000 reactor at a 1:5 scale.
In its current configuration (Figure 2-a) it includes a metal RPV and four independent loops, and the measurement system is based on the use of salt tracer (and other additives for altering the slug density) and electrical conductivity sensors. 60% of the core coolant channels are equipped with conductivity probes, while no concentration measurement is made in the downcomer. Local probes are installed also at each inlet and outlet nozzle. Loop flowrates are measured, while no measurement is made about the in-vessel velocity distribution.
The facility has been operated in the frame of TACIS Project R2.02/02 mentioned in Section 1.2 for the conduction of ten mixing experiments (see Ref. [33]) which have then been used for CFD and system code validation (see, for instance, Section A.3). Several repetitions were made of each experiment in order to provide statistical information on measurement uncertainties.

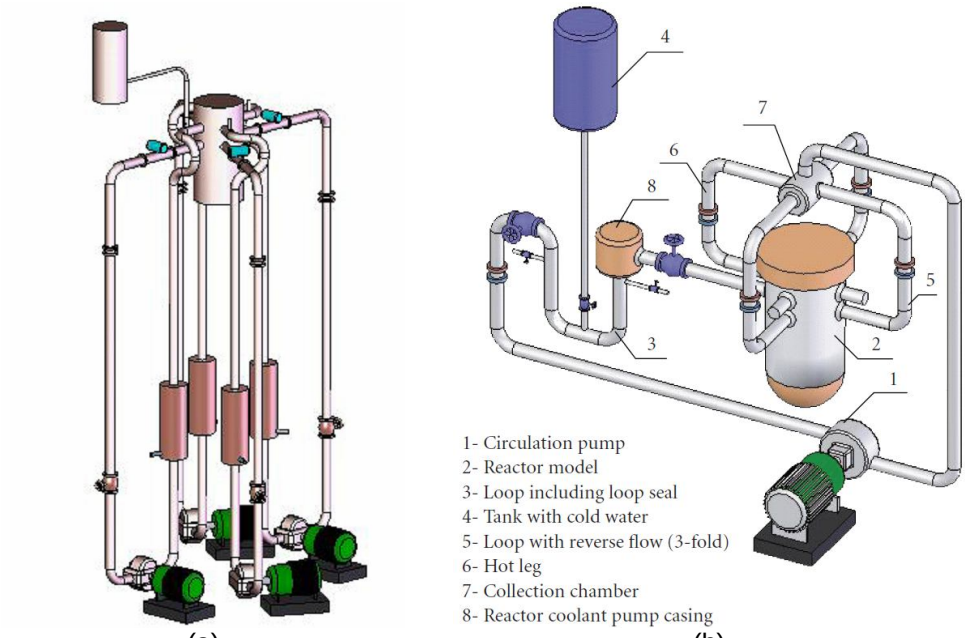

Figure 2 – Sketch of Gidropress mixing facility: a) new layout; b) old layout

As in ROCOM, the RPV internals up to the core bottom are accurately reproduced (apart from some minor simplifications), while the core region is occupied only by the conductivity probes supporting structures.
Although the facility is not as sophisticated as ROCOM, it produced a valuable experimental database for code assessment.

In the past, the same facility used to have a different loop configuration, which is illustrated in Figure 2-b. Measured data from experiments conducted in that facility were used for code validation in the frame of FLOMIX-R Project (Section 2.4.2.4, and Ref. [34]).

2.4.1.3. Vattenfall mixing facility

The Vattenfall mixing facility is a 1:5 scaled model of a 3-loop Westinghouse PWR. The RPV is made of acrylic glass (except the upper part). All geometrical details which affect the in-vessel flow distribution and mixing are accounted for. Two of the four loops are idle and allow for inverse flows. Salt is used as a tracer to simulate deborated water; electrical conductivity measurements are made at the inlet of 181 coolant channels. Alcohol is used for water density adjustment. Further information can be found in Refs. [24] and [35].
As in the ROCOM facility, LDA techniques have been adopted in this facility for flow velocity measurements.
Also Vattenfall mixing experiments were utilized for the CFD code validation activities carried out within the FLOMIX-R Project (Section 2.4.2.4). Obviously, only slug mixing experiments featuring a pump start-up can be conducted on this facility.

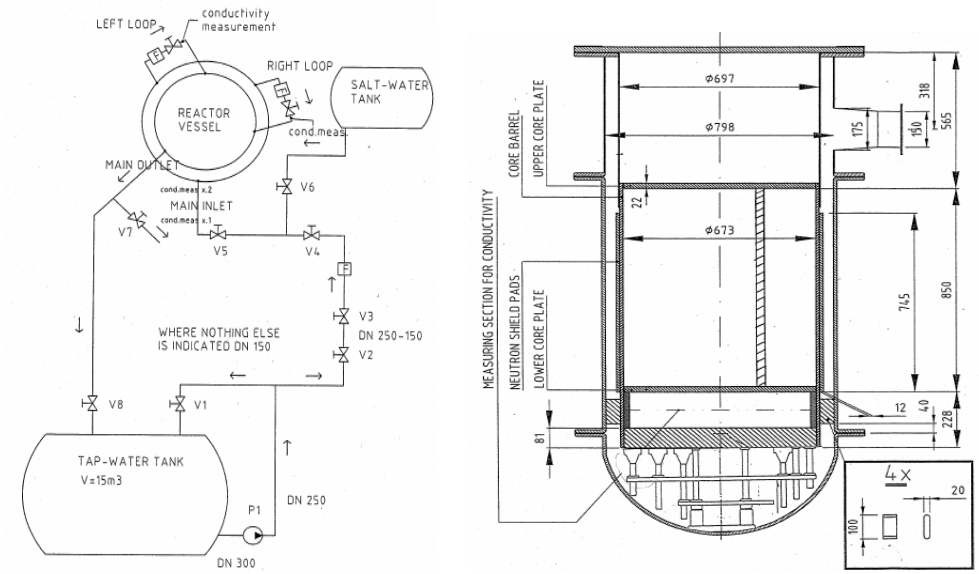

Figure 3 – Vattenfall test facility: a) facility layout; b) RPV cross-section

2.4.1.4. Fortum PTS test facility

The Fortum mixing facility was constructed in 1983 to study thermal mixing phenomena occurring during safety cold injection during scenarios relevant to PTS. The facility is a 1:2.56 scaled model of the Loviisa VVER-440 reactor. The RPV model, made of acrylic glass, reproduces only one half of the real RPV. Three of the six cold legs are partially included. The measured quantity is the fluid temperature (ranging between 10 °C and 75 °C). A salt is added to enhance the density effects. More of 60 thermocouples are installed in the downcomer and in the cold leg where the cold injection is made.

Measured data from some selected tests were used for code validation purposes in the frame of the FLOMIX-R Project (Section 2.4.2.4); further information can be found in Ref. [21]. Moreover, CFD investigations of Fortum PTS experiments are presented in Ref. [36].

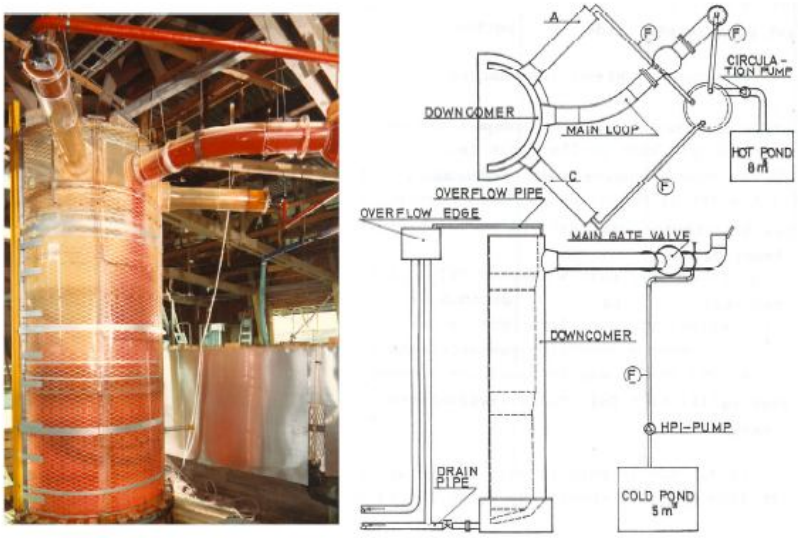

Figure 4 – Fortum mixing test facility (Ref. [21])

2.4.1.5. University of Maryland 2x4 loop facility

The University of Maryland, College Park 2x4 Thermal-Hydraulic Loop Facility (Figure 5) is a scaled down model of the Three Mile Island Unit-2 Babcock & Wilcox PWR (Refs. [36] and [38]).

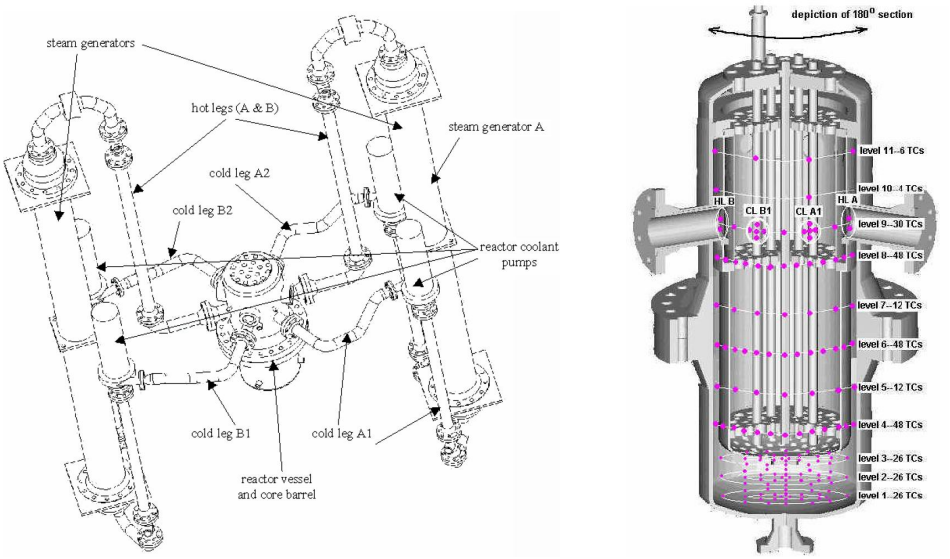

(a) (b)

Figure 5 – University of Maryland 2x4 loop facility: a) overall sketch; b) inside view of the RPV, showing thermocouple locations

Several mixing experiments were performed on this installation within the OECD/CSNI International Standard Problem (ISP) No. 43 (see Section 2.4.2.1). The following experiments were executed, where the presence of a deborated slug is simulated by cold water:

A. 16 “front mixing” redundant tests (infinite slug of cold water entering the RPV);
B. 6 “slug mixing” redundant tests (finite slug of cold water entering the RPV).

Fluid temperature in DC and LP was measured in about 300 locations by thermocouples. Pressure difference between LP and hot led was measured as well. Both buoyancy-driven and momentum-driven flow patterns were observed.

Further information on the experimental investigation carried out at this facility is given in Section 3.5.2.

2.4.1.6. UPTF

The UPTF facility was constructed by Siemens/KWU in Germany in the eighties; it is a full-scale replica of the primary system of a 4-loop Westinghouse PWR (see three-dimensional view in Figure 6). It was designed to perform separate-effect investigations on multi-dimensional thermal hydraulic phenomena in the upper plenum, across the upper core tie plate, in the downcomer and the loops, as well as in the surge line and the pressurizer during various simulated accidents (Ref. [39]).

The “Tram-C3” test series dealt with boron dilution events which may take place during postulated LOCA scenarios. The mixing of hot and cold water in the RPV was investigated, as well as thermal stratification phenomena after the restart of natural circulation. The measured data have recently been utilized in the frame of the validation of the French CFD code Trio_U (Ref. [40]).

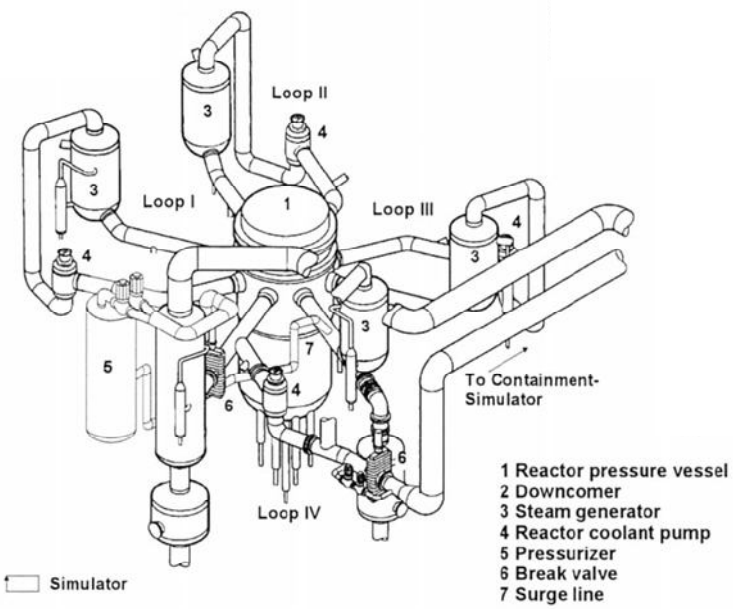

Figure 6 – Sketch of UPTF facility (Ref. [39])

2.4.1.7. Kozloduy NPP VVER-1000

During the plant-commissioning phase at the Kozloduy NPP Unit 6 (a VVER-100/320 reactor), several experiments were conducted by Bulgarian and Russian engineers. Measured data from some of those tests, which simulated MCP start-up and main steam line break transients, have been adopted for system and CFD code validation, within the OECD Benchmarks V1000CT-1 and V1000CT-2[3].

2.4.1.8. Paks NPP VVER-440

Useful data for code validation came also from the commissioning tests of Paks NPP (Hungary) performed in the years 1987-1989. The tests addressed the mixing among coolant loop flows in the downcomer and up to the core inlet in forced flow conditions. The goal of the tests was investigation of potential loop temperature asymmetry that might occur and significantly affect power distribution in the core.
Also those data were utilized in the frame of the FLOMIX-R Project (Section 2.4.2.4).

[3] Information on those Benchmarks can be found on this website: http://www.nea.fr/html/science/egrsltb/v1000ct/index.html.

2.4.2. International activities and events on CFD code assessment

2.4.2.1. OECD-NRC ISP-43

The above mentioned ISP-43 ("Rapid Boron-dilution Transient Tests for Code Verification") was organized by the OECD/NEA/CSNI and sponsored by the United States Nuclear Regulatory Commission (USNRC) with the purpose of demonstrating the capability of CFD codes to predict boron mixing in the downcomer of a reactor vessel. The ISP-43 was based on experiments carried out at the University of Maryland 2x4 loop facility (see Section 2.4.1.5).
Several "blind" CFD simulations were performed by the participants to the ISP-43, using specified boundary conditions. Later on, open recalculations followed. See Ref. [41] for further information on the CFD simulations.

The main achievement of the ISP-43 was that CFD codes have reached a sufficient degree of maturity for being applied to the investigation of single-phase mixing problems in PWRs, in particular those related to boron dilution events, from the point of view of both the model development and the availability of computing power. Nevertheless, further efforts are needed for improving the accuracy of the results, which is mainly affected by the turbulence modelling and by the mesh refinement.

2.4.2.2. OECD Benchmark V1000CT-2

A short description of this Benchmark has already been given in Section 1.2. Measured data from Kozloduy VVER-1000 NPP were used for code validation (Section 2.4.1.7).
Information on the code validation activity performed by the Author in this framework is reported in Section A.2, and interesting information on the results obtained by other researchers can be found in Ref. [42].
The final re-elaboration of the Benchmark results is still in progress; therefore no reference is available yet to published papers or reports which summarize the main achievements.
However, it is worth mentioning here that this activity placed stress on the "downcomer flow rotation" issue in VVER-1000 RPV, and on the difficulties to predict such phenomenon with current CFD methods (see also Section 4.2.4.2).

2.4.2.3. ECORA Project

The ECORA Project ("Evaluation of Computational Fluid Dynamics Methods for Reactor Safety Analysis") was part of the EURATOM 5th FP. It started in October 2001 for a 36-month duration, and was led by GRS-Garching (Germany). See Refs. [43] to [46].
The ECORA project was aimed at evaluating the capabilities of CFD codes for the simulation of the primary system and containment of nuclear reactors, in particular of those thermal-fluid-dynamic problems which are inherently multi-dimensional and cannot be accurately simulated by traditional one-dimensional thermal-hydraulics system codes.
One of the main topics addressed in the project is the establishment of standard quality criteria, on a European basis, for the application of CFD to problems related to nuclear reactor safety; as already mentioned in Section 2.3.1, a major outcome

of this was a document containing BPGs for the use of CFD for nuclear reactor safety applications (Ref. [18]), which has then constituted a basis for the development of upgraded BPGs in the OECD/CSNI framework (Ref. [5]).
Another topic addressed within ECORA was the evaluation of the present state of the CFD code assessment process regarding the primary loop flow. The existing experimental databases were reviewed, as well as the CFD analyses addressing the primary circuit thermal-hydraulics (e.g. reactor core, PTS, boron dilution, asymmetric loop operation etc.) As a result, the main limitations and capabilities of available CFD modelling approaches were pointed out. The evaluation was partly extended also to two-phase flow and heat transfer.
Moreover, several problems typical of nuclear systems were addressed through CFD simulations, model development and validation, in order to demonstrate current capabilities.
In particular, the following CFD investigations were performed (Ref. [45]).

- Verification calculations:
  - oscillating manometer;
  - liquid sloshing;
- Validation calculations:
  - jet impingement with heat transfer;
  - water jet into air (no heat transfer);
  - water jet on a free surface;
  - contact condensation on stratified steam/water flow;
- Demonstration calculations:
  - UPTF Test 1 (single-phase mixing in cold leg and downcomer);
  - UPTF Test 2 (steam/water phenomena in cold leg and downcomer during cold safety injection with RPV filled with steam).

Eventually, the ECORA Project gave a valuable contribution to the improvement of quality in CFD calculations, by:

- establishing BPG;
- identifying capabilities and limitations in current CFD methods for addressing primary system and containment flows;
- identifying needs for extension in the experimental databases for code verification and validation;
- identifying needs for improvements and development in CFD codes;
- developing and validating improved turbulence and two-phase flow models for the simulation of PTS phenomena in PWR.

2.4.2.4. FLOMIX-R Project

Like ECORA, also the FLOMIX-R Project (“Fluid Mixing and Flow Distribution in the Primary Circuit “) was part of the 5th FP. It started in October 2001 for a 36-month duration, and was led by FZR (Germany). See Refs. [20], [21] and [23].
The Project had the following three objectives:

1) obtaining complementary data on slug mixing and improving the understanding of the basic mixing processes affecting the concentration distribution at the core inlet;
2) based on the mixing experimental data available, determining the flow distribution and the thermal mixing phenomena within the primary circuit and assess their influence on RPV structural integrity (e.g. for PTS events);
3) contributing to the CFD codes assessment by comparison against experimental data.

Experimental data from several test facilities (mentioned in Section 2.4.1, and more thoroughly reviewed in reviewed in Ref. [21]), were extensively used for validation purposes, and the CFD codes CFX4, CFX5 and FLUENT were used for simulating those experiments.

Extensive use was made of the ECORA BPGs to assure high-quality of calculations. In particular, sensitivity analyses were performed upon the following parameters and modelling features:

- grid size;
- convergence criteria;
- round-off error;
- time-step size;
- turbulence model;
- inlet boundary location and condition;
- outlet boundary location;
- internal geometry;
- used code.

Such detailed sensitivity analyses allowed gathering a large amount of information on the code capabilities to address the IVF investigation and all the related phenomena, and represents, to the Author's opinion, the most valuable contribution to the CFD code assessment for this category of problems, within the available published literature.

Some considerations on the achievements of the validation work performed within FLOMIX-R are reported hereafter.

- The concept of "production grid" is introduced and discussed: production grids are the finest grid usable, consistently with the available computational resources, although they are not fine enough to provide grid-independent results.
- Best results were obtained when transient calculations were performed also for steady-state conditions, in order to capture macroscopic flow fluctuations which would be filtered out by a steady-state solver.
- The post-test calculations of steady-state mixing tests gave good predictions from the qualitative point of view, but showed some under estimation of the mixing in the DC.

- The influence of inlet conditions (especially the effect of the mixing device in ROCOM tests) was also evidenced.
- No unambiguous conclusion could be drawn as regards the effect of turbulence model, wall function, and position of outlet boundary.
- Simulations of slug mixing experiments were also gave good qualitative results, while showing some discrepancies from the quantitative point of view.
- Recommendation is provided to use a combination of SST model, automatic wall function and higher-order differencing schemes.

Moreover, an attempt was made to perform a systematic quantitative comparison between numerical results and measured data. This represents a clear advancement with respect to the previous works as far as the accuracy quantification is concerned.
The following quantitative parameters (also referred to in Chapter 5) were adopted:

- DEV3_SIGN (as defined in Section 5.3.2.7);
- DEV3_ABS (as defined in Section 5.3.2.7);
- maximum perturbation;
- time of maximum perturbation;
- maximum of average;
- time of maximum of average;
- accumulated perturbation.

The comparison of time trends of maximum and core-averaged perturbation was made accounting for confidence intervals based on the standard deviation of experimental data.
For the steady-state experiments, the quantitative comparison shown that the spreading of the tracer in horizontal direction is always under-predicted.

Conclusions from the FLOMIX-R Project
The first major achievement regards the information obtained from the sensitivity analyses performed to comply with the BPGs recommendations.
As regards the mesh sensitivity, the computing power was a strong limiting factor, due to which mesh independent solutions could not be obtained or demonstrated. This also prevented a systematic estimation of the solution error. It is anticipated that meshes counting several million cells will probably permit to achieve grid independency.
Then, relevant information was collected about the sensitivity to the parameters and modelling choices mentioned above. Concerning the turbulence modelling, in particular, the turbulence models which had given the best results for the various experiments conducted on different facilities were identified; somewhat contradictory outcomes were thus obtained[4], which did not allow drawing general conclusions on which modelling approaches are best suited for a given experiment.

[4] Probably due to the grid-independency having not been achieved.

Some dependence was also observed upon the used CFD codes, for example when the same slug-mixing experiments were simulated both with Fluent and CFX5 using the same grid.

As regards the steady-state mixing tests, the comparison of numerical predictions against measured data (in terms of flow distribution in the downcomer and perturbation distribution at the core inlet) showed good qualitative agreement, also in cases of asymmetric loop operation. However, the mixing in the downcomer is generally under-predicted.

Concerning the transient slug-mixing tests, different behaviours were observed depending of the experimental facility.
ROCOM tests were well qualitatively well predicted, and also good agreement was obtained in terms of global maximum perturbation, while relatively large local discrepancies were observed. In presence of buoyancy effects, the mixing was under-predicted.
Likewise, good results were obtained for the Vattenfall experiment, including the prediction of the maximum perturbation; however the spatial distribution of the perturbation over the core inlet was not well predicted.
Somewhat larger discrepancies were obtained from the simulations of Gidropress slug mixing tests, probably due to poor characterization of boundary conditions.
For the FORTUM Buoyant mixing tests, good qualitative results were obtained but the quantitative analysis of the mixing showed poor agreement.

A general conclusion from such intensive validation activity was that the quantitative agreement between CFD predictions and measured data for in-vessel mixing experiments is not yet satisfactory enough, and further development is still needed. In particular, advancements are needed towards:

- finer computational grids (until mesh-independence is achieved);
- finer temporal discretization;
- improved turbulence modelling;
- improved numerical efficiency (to reduce computational costs, which are limiting the use of finer grids and the application of the BPG).

2.4.2.5. TACIS R2.02/02 Project

A brief description of the TACIS R2.02/02 Project has already been provided in Section 1.2. It can be remarked here that a valuable validation database has been produced within this framework, including:

- 10 mixing experiments reproducing different scenarios;
- ~110 system code pre-test and post-test simulations of the above experiments (performed with four different Russian codes);
- ~30 CFD code simulations of the above experiments, performed by UNIPI, FZD and Gidropress specialists using ANSYS CFX 10.0 code.

The work carried out on UNIPI side[5] within this Project provided useful material for the purposes of the present research, as often recalled in this dissertation. An example of the CFD validation activity is reported in Section A.3.

Beside the achievement of the objectives of the Project (which were mainly related to system code validation), an important by-product of the whole work was a contribution to the assessment of CFD against scenarios involving asymmetric operation. In particular, based on the comparison of CFD results against the measured data in terms of perturbation distribution at the core inlet, it was pointed out that:

- the symmetrical and steady scenarios are always well predicted from the qualitative point of view, while some quantitative discrepancies appear;
- such discrepancies usually indicate a tendency to under-predict the turbulent mixing effectiveness;
- the "downcomer flow rotation" occurred in some experiments, but could never be predicted by the CFD simulations;
- experiments featured by strong asymmetries in pump operation and/or transient behaviour (e.g. pump start-up) are more challenging; the CFD code showed to be capable of capturing the basic phenomena, the flow distribution and the perturbation morphology, but relatively large discrepancies resulted from the quantitative analysis.

Furthermore, CFD was demonstrated to be a valuable support to the system code assessment process. This aspect is discussed further in Section 4.4.

2.4.2.6. Further existing validation databases

Additional CFD code validation for IVF investigation has been carried out by researchers from many organizations outside the framework described above, even though the great majority of the published works still relate to the mentioned experimental databases.

For example, CFD simulations of ROCOM experiments were performed by the Author and his colleagues at the University of Pisa in the frame of an agreement with FZD, as mentioned in Section 1.2. Some details about such validation work are reported in Section A.1.

[5] UNIPI was in charge of coordinating the Tasks dealing with all pre-test and post-test analyses. This work is documented in Refs. [13] and [47].

3. RELEVANCE OF IVF INVESTIGATION TO NUCLEAR REACTOR SAFETY

This Chapter is the outcome of a survey of the open literature (international journals, conference proceedings, and various documents available on the web) performed in the framework of the above mentioned TACIS Project R2.02/02, and reported on Ref. [48].

3.1. General remarks

Perturbations of the spatial distribution of the coolant physical properties at core inlet – namely, both a reduction of core inlet temperature as well as of the boron concentration – are potential causes of reactivity insertions, with consequent local power excursions. If the local power density reaches relatively high levels, then the consequences may be either:

- departure from nucleate boiling (DNB), with potential for cladding damage; or
- excessive energy release in fuel during power pulse with potential for fuel break-up and core damage.

In case of anomalous temperature or boron distribution at core inlet, the perturbation is affected by the mixing phenomena occurring in the RPV, between the coolant from the perturbed loop and the unperturbed loops.
In fact, a peaked and localized perturbation reaching the core may determine a local power excursion; on the other hand, mixing effects tend to dilute the perturbation on a larger area and to smear its gradients, and thus reduce the potential danger.

The analysis tools traditionally adopted for nuclear reactor safety evaluation (i.e. integral thermal-hydraulic codes) are not capable of predicting the three-dimensional turbulent mixing phenomena affecting the IVF and the distribution of coolant properties at the core inlet, therefore the safety analyses have been relying either on strong conservative assumptions about the mixing effects, or on the use of “engineering mixing models”.
Making conservative assumptions basically consists in neglecting the mixing effects at all and assuming bounding conditions in terms of timing, location and intensity of the perturbation.
On the other hand, engineering mixing models are normally bounded to specific reactor types and operating conditions and are based on proprietary measured data; therefore their applicability is normally quite restricted.

The application of CFD represents, potentially, the way to overcome such limitations. In facts, it can predict the 3D mixing phenomena and the actual time and space distribution of the perturbations, and thus allows removing – or, at least, relaxing – the above conservative assumptions and uncertainties (with the related safety margins). Moreover, the dependence on specific geometries and operating conditions is also removed, owing to the CFD inherent ability to simulate the basic phenomena.

As already mentioned in Chapter 1, such direct application of CFD to safety analysis is not yet fully mature since further code assessment is still necessary. However, the recent progress in code development and assessment and the dramatic increase in computing power are quite promising, and CFD already plays an important role as a support to reactor safety analysis.

3.2. Relevant scenarios

Basically, there are two categories of accidental scenarios that can induce the above mentioned perturbations in a PWR[6]:

1. boron dilution transients, i.e. transients featuring the accumulation of slugs with deborated or diluted water in the primary loop;
2. scenarios determining an overcooling of the coolant in one primary loop, and then the accumulation of a cold water slug.

In all cases, if the cold or diluted slugs are transported throughout the core, a reactivity insertion may occur.
A short description of such scenarios is provided in the following.

3.2.1. Boron dilution transients

3.2.1.1. Historical remarks

During the nineties, the possibility of return to core criticality as a consequence of a boron dilution event begun to be regarded as a safety concern, also due to the impulse given by several inadvertent dilution occurrences in the operated reactors.
Intense research activity has been carried out both in Europe (mainly France, Germany, Sweden, Finland) and in the United States to investigate (and prioritize) this issue. The focus was on the identification of the possible initiating events and of the sequences of events leading to unplanned dilution, as well as on the estimation of the events probability, on the transport and mixing of deborated water slugs, and of course on the consequences of the associated reactivity insertion (in terms of fuel damage due to power excursion).
In this framework, relevant research contributions came from the United States Nuclear Regulatory Commission (USNRC) and Industry, especially as regards probabilistic assessment and evaluation of the consequences and of the risk to the public, as well as from research context. A clear example is represented by the studies on transport and mixing carried out at the University of Maryland (see Section 3.5.2).
Relevant information concerning the state-of-the-art on the boron dilution issue was gathered in 1995 by the “CSNI specialists meeting on boron dilution reactivity transients”, held at State College, Pennsylvania, USA, and sponsored by the USNRC, in collaboration with the OECD/NEA/CSNI and the Pennsylvania State

[6] Pressurized water reactors of eastern technology, such as VVER-1000 and VVER-440 are also referred to as PWRs in the following, unless differently specified.

University (PSU, Refs. [49], [50] and [51]). The main goal was to contribute to the identification and quantification of the following factors in relation to the boron dilution issue:

- the risks associated with boron dilution events;
- the probabilities of such events;
- the relevant phenomena involved (including fuel damage and pressure boundary failure mechanisms);
- the behaviour of high burn-up fuels;
- the uncertainties related to experimental and analytical investigations.

The main outcomes of the CSNI meeting are summarized hereafter. They give an idea of the level of understanding of the boron dilution issue as it was about fifteen years ago.

- The return to criticality initiated by boron dilution events constitutes a potential safety risk.
- The quantification of the above risk is still affected by large uncertainties.
- The quantification of the event probabilities is also affected by large uncertainties.
- The relevant mechanisms involved in boron dilution scenarios have been identified.
- The factors that mostly affect the consequences of a boron dilution event are:
    - the quantity of deborated or low-borated water that accumulates;
    - the mixing of normally-borated and diluted water, both in reactor coolant system (RCS) piping, and in RPV as well;
    - the core response as the deborated slug is swept through it.
- The above factors are plant-specific, thus also the probabilities, risks, consequences, and possible design and operating “solutions” are, generally speaking, plant-specific.
- The probabilistic risk assessment is mainly based on the investigation of:
    - dilution origin (either external or inherent);
    - system behaviour (especially flow regimes: natural circulation, RCP restart, boiler-condenser mode, etc.)
- A larger shutdown margin (achieved by increasing the number of rods, or by burnable poisons, or by increasing the negative fuel coefficients) would allow eliminating the need of using boron for the chemical shim and thus to solve the problem radically; however, the costs associated with those design changes could be very high.
- Changes in the plant hardware and in the operating procedures may be adopted in order to reduce the probabilities of certain events or mitigate their consequences (this has already been done by several industries).
- High burn-up fuel is characterized by lower energy release limits above which damage occurs. Thus the role played by high burn-up fuel consists in reducing the acceptability thresholds.
- Much effort is still needed to:
    - reduce uncertainties in thermal-hydraulic analyses;

- reduce uncertainties in quantification of mixing (many issues exist related to numerical diffusion, turbulence modelling, high computational costs involved);
- reduce uncertainties in determining the core response;
- improve the understanding of the basic phenomena and qualify the computational tools by further experimental investigation.

Since then, much progress has been made and the uncertainties above have been reduced (although not eliminated). The high degree of conservatism that has characterized the early studies has been partially removed, thanks to the use of coupled code approaches (like thermal-hydraulics and neutron-kinetics coupling), to the relatively high maturity reached by CFD codes, and to the extension of the experimental database made available to the scientific community for code assessment (see Section 2.4).

Such progress is reflected also in the evolution of the position of the USNRC, in relation to the boron dilution issue and its relevance to licensing, since the eighties up to now, as well as by the contributions given by industry and research institutions to the understanding of the problem. Those aspects are discussed in Section 3.3.

3.2.1.2. Origin of a boron dilution event

As described in Ref. [49], two conditions are required for a "boron dilution event" to occur:

1. the accumulation of a stagnant slug of low-borated water in the RCS piping, in particular in the loop seal;
2. the rapid transport of such slug through the reactor core.

A stagnant zone can exist only if all RCPs are turned off. This can occur both in normal operation conditions (for example, during refuelling outages and all normal cold shutdown conditions), and in abnormal conditions, e.g. following a loss of offsite power (LOOP).

Boron dilution can either be external or inherent.

- External dilution occurs when low-borated water is introduced in the RCS from outside, e.g. from the chemical and volume control system (CVCS), and accumulates in a stagnant region. This introduction can either be the result of a normal procedure (as, for instance, during reactor start-up), or occur inadvertently.
- Inherent dilution occurs when low-borated water forms inside the RCS due to some "distillation" process, without any external intervention. Namely, this happens in the SGs during a small-break loss of coolant accident (SBLOCA), when the system is in boiler-condenser mode (BCM) of operation: in such abnormal conditions, steam – which does not contain boron – is generated in the core and flows through the voided hot leg to

SG tubes, where condensation takes place; deborated water thus accumulates in the SG outlet plenum and in the loop seal.

3.2.1.3. Consequences of a boron dilution event

As described in Ref. [52], if a deborated slug is swept through the reactor core at the beginning of fuel cycle, the inserted reactivity may overpass the shutdown criticality margin and determine a return to criticality. This may lead to fuel damage and, in the worst scenario, to the loss of integrity of the RCS pressure boundary (due to mechanical stresses determined by the pressure waves following molten fuel dispersion).

Two failure mechanisms are possible for the fuel:

1. brittle fracture of the cladding caused by oxidation (no fuel dispersal or severe core damage);
2. fuel pellet and cladding melting, with dispersal of molten fuel into water (severe core damage).

In the case of unirradiated and intact fuel, the first failure mode occurs when the energy release in the fuel reaches 210 to 220 cal/g (in terms of radially averaged peak fuel enthalpy), while for the second failure mode to occur the energy must reach about 300 cal/g. Those failure thresholds decrease as the fuel is irradiated.
The acceptability thresholds currently referred to by the US Nuclear Regulatory Commission (NRC) are the following: 280 cal/g (peak radially averaged), to ensure fuel coolability, and for boiling water reactors 170 cal/g, as the measure of fuel rod cladding failure (by boiling transition).
The possible need to reduce those limits, so as to account for high burn-up fuel behaviour, is being discussed.

It has to be remarked, however, that the core damage frequencies involved are very small ($\sim 10^{-8} \div 10^{-7}$ / reactor-year), which noticeably relieves the safety relevance of the boron dilution issue (Ref. [52]).

3.2.1.4. Boron Dilution Scenarios

As mentioned above, two types of boron dilution scenarios can be anticipated, which involve external and inherent dilution respectively:

1. those originated by dilution events that occur during shutdown and refuelling conditions (normal operation);
2. those originated by dilution events following a SBLOCA event.

As described in Section 3.3, on the USNRC side the first kind of scenarios is addressed by General Safety Issue (GSI) 22 “Inadvertent Boron Dilution Events”, while those of the second kind are addressed by GSI 185 “Control of recriticality following small-break LOCAs in PWRs” (see Ref. [50], and Section 3.3).

In the following, reference is made to the following USNRC classification of the operational modes:

Mode 1 - Power operation
Mode 2 - Start-up
Mode 3 - Hot standby
Mode 4 - Hot shutdown
Mode 5 - Cold shutdown
Mode 6 - Refuelling

The following six boron dilution scenarios have been identified in Ref. [49] as representative of the first category.

Scenario A – Dilution during RCS filling (Modes 4, 5)
The reactor is shutdown and being cooled by the residual heat removal (RHR) system. The RCS is being filled and pressurized. The initiating event is a CVCS malfunction or operator error, due to which for some period diluted water is supplied to the charging pumps, and then to the RCS. Therefore, a slug of colder and deborated water accumulates in a loop seal and is assumed not to be revealed either by boron sampling or source range count rate. When the RCP of that loop is started, the slug is transported through the core.
The frequency for this event has been estimated to be very low (10^{-10} / reactor-year).
In a slightly different version of this scenario, the dilution could be voluntarily made by the operator during RCS filling, but ill-advised and associated to a CVCS malfunction.
It should be considered that operating procedures of all US plants require that boron dilution be not performed before reaching hot zero power conditions.

Scenario B – Steam Generator in-leakage ("Swedish scenario")
The reactor is shutdown and being cooled by the RHR system. The initiating event is a SG tube leak, which causes secondary water to enter the primary circuit and accumulate in the loop seal. When the RCP of that loop is started, the slug is transported through the core. The slug is assumed not to be revealed (although it could). The only difference from the Scenario A is the origin of the diluted slug.
Also the frequencies estimated for this scenario are quite low (10^{-10} / reactor-year).

Scenario C – Loss of AC power during dilution ("French scenario")
The reactor is being started-up (Mode 2) after refuelling, and boron dilution is in progress (as a normal start-up procedure) by charging clean water into the RCS. The initiating event is a LOOP, followed by the trip of all RCPs. Natural circulation, if ever present, is weak due to low decay heat. When the emergency power supply (i.e. the diesel generators) is restored, the charging pumps are automatically restarted, so that dilution continues. The operator is assumed to fail to secure the dilution, and the entire volume control tank (VCT) inventory is discharged into the RCS. Moreover, the charging flow may also be cold (because the letdown has been isolated by the loss of AC power, and the water is not heated any longer by the regenerative heat exchanger). Then deborated water accumulates in the RCS, and when the power supply is restored, it is swept through the reactor core (if the operator inadvertently restarts a RCP).

Note that when the VCT level is low, the charging pump suction is switched to the refuelling water storage tank (RWST), which contains borated and cold water. This stops the dilution process, but in the addressed scenario the RCP restart is assumed before such switching.
Electricité de France (EdF) reduced the probability of such dilution event by installing an automatic system that switches the charging pump suction from the VCT to a borated source when a LOOP occurs[7].

Scenario D – Unborated water in RHR system
The RHR system, which is assumed to be totally boron-free, starts-up and injects deborated water into the RCS and then through the core. No mixing is assumed to take place. Analyses performed in the eighties by the French of the Commissariat à l'Energie Atomique (CEA) showed that the dilution is terminated by the RHR system rupture (due to overpressure caused by power generation) well before fuel damage limits are reached. The frequency estimated for this event is in the order of 10^{-8} /reactor-year.

Scenario E – Boration after shutting off RCPs
During the refuelling shutdown, the RCS is being cooled down. The initiating event consists in prematurely turning off the RCPs, when the RCS temperature is still high and the coolant has not yet been borated to the concentration prescribed for refuelling operations. It is assumed that RHR flow is not capable of forcing circulation through the SG tubes, and a deborated slug accumulates in the loop seal, where it remains during the subsequent RCS draining and refilling.
The operating procedures of all US plants require that RCPs are not switched off until refuelling boron concentration is reached.

Scenario F (Dilution of refuelling cavity)
The reactor is shutdown for refuelling (Mode 6). The initiating event is the formation of a layer of diluted water at the top of the refuelling cavity: this may happen because unborated water is sprayed on the internals to minimize airborne contamination, and since borated water is denser than clear water, stratification occurs. Moreover, in order to keep constant the cavity water level during the refuelling operation, some water may be drained from the bottom (where more borated water is present). During the following draining operations the diluted layer is lowered, and then reaches the RPV, enter the cold legs and eventually goes into the RHR pumps suction, is re-injected into the cold legs piping and is forced to reach the RPV. This scenario involves neither an inadvertent RCP restart nor natural circulation flow transporting deborated slugs towards the core.

Another possible scenario to be considered is the introduction of cold unborated water into the loop seal through the RCP seal. If the RCP are turned off and the natural circulation is sufficiently low, this may lead to a deborated and cold slug formation, which could be transported towards the RPV and through the core following the inadvertent restart of a pump.

[7] The expression "French scenario" is due to the fact that the French were the first to address this scenario in safety evaluations.

As regards the seconds category of boron dilution events (inherent dilution following SBLOCA), basically the following scenario, sometimes referred to as the "Finnish scenario", can be anticipated.
A SBLOCA occurs, the break size being sufficiently large to decrease the RCS inventory, but not to depressurize the system. When the inventory has dropped below a certain threshold, the natural circulation terminates and the BCM occurs, leading to the formation of deborated water slugs which accumulates in the loop seals. If there is a restart of circulation (either natural or forced by RCPs), the deborated slugs are transported to the core, with a consequent risk of recriticality.

According to Ref. [49], up to 1995 several analyses had been performed on the possible consequences of the above mentioned scenarios on different NPPs, and the results did not allow excluding, in general, the possibility of severe core damage under the assumed transient conditions. The conclusion of this was that proper countermeasures should be implemented in order to ensure very low probability of occurrence for the initiating events (i.e. those leading to the accumulation of deborated slug), particularly in terms of operational procedures.

3.2.2. Overcooling transients

As mentioned above, power excursions can be expected if water at a lower temperature than the nominal value reaches the core inlet through one primary loop.
An overcooling of the primary water (and thus the accumulation of a cold water slug) may be induced by a temporary increase in the heat transfer from primary to secondary circuit in a SG. This may happen in the following accidental scenarios:

- main steam line break (MSLB);
- inadvertent opening of a turbine valve;
- feedwater malfunctioning, leading to:
    - flowrate increase;
    - temperature decrease.

Obviously, for reactivity insertion to occur, it is necessary that the cold slug is transported into the RPV by either forced or natural circulation in the affected loop.

In case of a MSLB, the postulated initiating event is a double-ended rupture of one steam line upstream of the cross-connect. As a consequence, a loss of secondary coolant occurs, the affected SG depressurizes and the heat transfer is enhanced due to the increased flow rate. This determines an overcooling on the primary side of the affected loop, which thus feeds the RPV with colder water than the other loops. Such temperature differences between the water coming from different loops, if not sufficiently mitigated by the turbulent mixing, may lead to power excursion.

3.3. The Position of the USNRC

3.3.1. Generic safety issues

Section 3 of NUREG-0933 (Ref. [53]) includes several “new generic issues”, a few of which are related to boron dilution (either during plant startup or following a SB-LOCA):

- ISSUE 22: Inadvertent boron dilution events
  This issue was established to check whether the degree of protection of the operated reactors was adequate, in relation to the possibility of core recriticality following inadvertent boron dilution during refuelling and maintenance operations. The question was raised by USNRC in the early eighties following several boron dilution occurrences (although none of these had resulted in core recriticality). A possible solution to this problem could be the installation of instrumentation able to detect the inadvertent dilution and either to stop it automatically or to alert the operators. However, on the basis of USNRC probabilistic analyses, the Issue 22 was considered resolved, without the establishment of new requirements.
- ISSUE 104: Reduction of boron dilution requirements
  In the framework of USNRC internal discussion regarding the resolution of Issue 22, the question was addressed whether Section 15.4.6 of the Standard Review Plan (SRP) could be deregulated. This Issue was resolved by stating that SRP Section 15.4.6 was not to be deregulated, so as to avoid an increase in the probability of an inadvertent core recriticality following a boron dilution event, which is in any case considered an unacceptable event. Therefore SRP Section 15.4.6 should continue to be applied.
- ISSUE 185: Control of recriticality following SBLOCA in PWRs
  Investigations carried out in the late nineties had shown that high burn-up fuels may be susceptible of more serious consequences in case of reactivity insertion events (like boron dilution events), and also that severe consequences may come from a boron dilution event following during a SBLOCA in Babcock & Wilcox (B&W) reactors. Thus, in 1999 the possibility to re-open the Issue 22 was considered, in order to account for that new information. However, since the new concerns were related to a different scenario (SBLOCA) from those addressed by Issue 22 (which involved shutdown or refuelling conditions), this new Issue was established.

Issue 22 was raised in the early eighties, while Issue 185 at the end of the nineties. In the meantime, several studies have been conducted by USNRC, industry and research institutions, which led the USNRC to “reconsider” the problem after it had been assigned a low priority.
The historical evolution of USNRC position as regards the inadvertent boron dilution problem is documented in NUREG-0933 reports, in the letters and information notices issued by the USNRC, and in some papers by USNRC experts (Refs. [49] to [64]).

The Issue 185 started to be addressed for resolution by USNRC in October 2004, for all operating B&W, Westinghouse and Combustion Engineering PWRs (Ref. [63]).
Within the prioritization procedure required by NUREG-0933, new analyses had recently been performed by USNRC and documented in a draft NUREG report (Ref. [64]). Those analyses, which addressed boron dilution accidents associated with SBLOCA[8] tried to remove part of the conservatism of the previous studies[9] by using more advanced computational approaches. In particular:

- The FLUENT CFD code was used to calculate the mixing of borated and deborated water in the RCS; the code was validated against experimental data from University of Maryland integral test facility and DC mixing facility; the CFD model gave conservative predictions of the mixing.
- The PARCS-RELAP5 coupled codes were used to simulate the thermo-hydraulic and neutron-kinetic behaviour; the code was validated by comparison with French and Russian codes.

The following conclusions were achieved:

- As regards Westinghouse and ABB–Combustion Engineering systems, the SBLOCA boron dilution event is not expected to cause any core recriticality, both in case of natural circulation restoring and RCP restart, because the volumes of the SG outlet plena, loop seals and RCPs are relatively small and the corresponding slug volume that can be formed is not sufficient to represent a recriticality concern.
- In B&W systems with lowered loop seals, the resumption of natural circulation may lead to limited core recriticality, but without causing any core damage (i.e. the energy release would keep below the acceptability thresholds).
- In B&W systems with lowered loop seals, the inadvertent restart of a RCP may lead to core recriticality with limited fuel damage, with without any severe damage (i.e. the coolability of the geometry would be preserved).
- The postulated event is very unlikely to occur, because of several factors:
  1. small range of break sizes allowing BCM;
  2. failure of high-pressure injection system assumed;
  3. only a fraction (1/5) of the fuel cycle is concerned;
  4. much time required for accumulating sufficient deborated water (BCM will most probably be stopped before, unless operator errors occur);
  5. inadvertent RCP restart assumed.
- On these bases, GSI-185 must be considered resolved.

[8] Break sizes ranging from 0.5 to 2 in were considered, i.e. large enough to decrease the RCS inventory, but not large enough to depressurize the system.
[9] Performed both by USNRC and Framatome Technology.

3.3.2. Standard Review Plan

3.3.2.1. Boron Dilution

The Section 15.4.6 of the USNRC Standard Review Plan (SRP), “Chemical and volume control system malfunction that results in a decrease in boron concentration in the reactor coolant (PWR)” (contained in NUREG-0800, Ref. [65]), provides guidance for the review of Safety Analysis Reports (SAR), in their parts related to the analysis of boron dilution accidents (due to CVCS malfunctioning).
Here is a brief description of the content of such Section.

The postulated inadvertent boron dilution event is due either to an operator error or a malfunction of the CVCS, and leads to a decrease in the shutdown margin. The operator must stop the dilution before such margin is lost. This situation may occur in different plant operating conditions (refuelling, startup, power operation either manually or automatically controlled, hot standby, cold shutdown), each determining a different sequence of events that must be taken into account in the review.
The reviewers must check that the safety analyses performed by the applicant assure that acceptance criteria are met. Those criteria are based on General Design Criteria 10, 15 and 26 (10 CFR 50 – Appendix A, Ref. [66]), and have the purpose of achieving the following two objectives:

1. “The consequences of these events are less severe than the consequences of another transient that results in an uncontrolled increase in reactivity and has the same anticipated frequency classification, or
2. The plant responds to the events in such a way that the criteria regarding fuel damage and system pressure are met and the dilution transient is terminated before the shutdown margin is eliminated.”

The acceptance criteria are:

1. “Pressure in the reactor coolant and main steam systems should be maintained below 110% of the design values. (see ASME III NB-7000)
2. Fuel cladding integrity shall be maintained by ensuring that the minimum departure from nucleate boiling ratio (DNBR) remains above the 95/95 DNBR limit for PWRs based on acceptable correlations (see SRP Section 4.4)
3. An incident of moderate frequency should not generate a more serious plant condition without other faults occurring independently.
4. An incident of moderate frequency in combination with any single active component failure, or single operator error, shall be considered and is an event for which an estimate of the number of potential fuel failures shall be provided for radiological dose calculations. For such accidents, the number of fuel failures must be assumed for all rods for which the DNBR falls below those values cited above for cladding integrity unless it can be shown, based on an acceptable fuel damage model (see SRP Section 4.2), that fewer failures occur. There shall be no loss of function of any fission product barrier other than the fuel cladding.

5. If an operator action is required to terminate the transient, the following minimum time intervals must be available between the time when an alarm announces an unplanned moderator dilution and the time of loss of shutdown margin:
    a. During refuelling: 30 minutes.
    b. During startup, cold shutdown, hot standby, and power operation: 15 minutes."

The reviewer has also to check the analytical model used by the applicant: such model must have been accepted by the staff as qualified; otherwise it has to be evaluated by the staff.
The application of the analytical model should be based on conservative assumptions, such as the following ones (which are considered acceptable by the USNRC):

I. "For analyses during power operation, the initial power level is rated output (licensed core thermal power) plus an allowance of 2% to account for power-measurement uncertainty.
II. The boron dilution is assumed to occur at the maximum possible rate.
III. The core burnup and corresponding boron concentration are selected to yield the most limiting combination of moderator temperature coefficient, void coefficient, Doppler coefficient, axial power profile, and radial power distribution. This will usually be the beginning-of-life (BOL) condition.
IV. All fuel assemblies are installed in the core.
V. A conservatively low value is assumed for the reactor coolant volume.
VI. For analyses during refuelling, all control rods are withdrawn from the core.
VII. For analyses during power operation, the minimum shutdown margin allowed by the technical specifications (usually 1%) is assumed to exist prior to the initiation of boron dilution.
VIII. For each event analyzed, a conservatively high reactivity addition rate is assumed taking into account the effect of increasing boron worth with dilution.
IX. Conservative scram characteristics are assumed, i.e., maximum time delay with the most reactive rod held out of the core."

3.3.2.2. Asymmetrical Temperature Distribution

According to the USNRC, the events listed below, which involve an unplanned increase in heat removal by the secondary system and then an overcooling of the moderator, must be discussed in the safety analysis reports (SAR), and are addressed in Sections 15.1.1 – 15.1.4 of the SRP (Ref. [65]).

a) feedwater system malfunctions that result in a decrease in feedwater temperature (PWR and BWR);
b) feedwater system malfunctions that result in an increase in feedwater flow (PWR and BWR);
c) steam pressure regulator malfunctions or failures that result in increased steam flow (PWR and BWR);
d) inadvertent opening of a steam generator relief or safety valve (PWR only).

Some other events involve an increase in core reactivity due to decreased moderator temperature, moderator boron concentration, or core void fraction, and are addressed in Sections 15.4.4 – 15.4.5 of the SRP (Ref. [65]):

e) startup of an idle recirculation pump (BWR);
f) flow controller malfunction causing increased recirculation flow (BWR);
g) startup of a pump in an initially isolated inactive reactor coolant loop where the rate of flow increase is limited by the rate at which the isolation valves open (PWR with loop isolation valves);
h) startup of a pump in an inactive loop (PWR without loop isolation valves).

The safety review of the above mentioned events must ascertain that for the most limiting events the criteria regarding fuel damage and system pressure are met:

1. “pressure in the reactor coolant and main steam systems should be maintained below 110% of the design values;
2. fuel cladding integrity shall be maintained by ensuring that the minimum DNBR remains above the 95/95 DNBR limit for PWRs and the CPR remains above the MCPR safety limit for BWRs based on acceptable correlations;
3. an incident of moderate frequency should not generate a more serious plant condition without other faults occurring independently;
4. an incident of moderate frequency in combination with any single active component failure, or single operator error shall be considered and is an event for which an estimate of the number of potential fuel failures shall be provided for radiological dose calculations; for such accidents, fuel failure must be assumed for all rods for which the DNBR or CPR falls below those values cited above for cladding integrity unless it can be shown, based on an acceptable fuel damage model that fewer failures occur; there shall be no loss of function of any fission product barrier other than the fuel cladding;
5. to meet the requirements of General Design Criteria 10, 15, 20,30 and 26 the positions of Regulatory Guide 1.105, "Instrument Spans and Setpoints," are used with regard to their impact on the plant response to the type of transient addressed in this SRP section;
6. the most limiting plant systems single failure, as defined in the "Definitions and Explanations" of Appendix A to 10 CFR Part 50, shall be identified and assumed in the analysis and shall satisfy the positions of Regulatory Guide 1.53”.

The analytical methods used must be conservative. For instance, the following assumptions should be made:

- high initial power level (consistently with the number of loops initially assumed operating), plus 2% to allow for measurements uncertainties;
- conservative scram characteristic (i.e. for a PWR: maximum time delay with the most reactive rod stuck in the fully extracted position; for a BWR: a factor 0.8 times the calculated negative reactivity insertion rate);

- core burnup selected so as to yield the most limiting combination of moderator temperature coefficient, void coefficient, Doppler coefficient, axial power profile, and radial power distribution;
- mitigating systems actuated in the analyses at setpoint with allowance for instrument inaccuracy.

3.4. The Position of US Industry

3.4.1. Existing Reactors

3.4.1.1. Westinghouse

The position of Westinghouse concerning the boron dilution issue, up to the early nineties, was presented by Burnett in Ref. [49] and is summarized hereafter.
Studies conducted in 1971, in which a rapid boron dilution event was analyzed (including both point kinetics and three-dimensional analyses), had shown that the insertion of reactivity could lead to fuel damage, although without loss of integrity of RCS. Thus Westinghouse decided to adopt protection-grade interlocks circuits to prevent inadvertent startup of an isolated loop, thus allowing removing the analyses of dilution events from design basis evaluation. Then the analyses of dilution events in FSARs have been limited to gradual and limited dilution events, which do not involve local reactivity effects.
Other studies have been conducted more recently (published in 1992), after which the position of Westinghouse was not changed: some scenarios can be hypothesized (namely, the startup of a RCP after the accumulation of a large slug of deborated water) which can lead to unacceptable consequences (i.e. to core damage), and those scenarios must be prevented.

The above studies were focused in particular on the external boron dilution scenarios which are described in the Introduction.

The dilution during a RCS filling, due to CVCS malfunction was estimated to have a very low frequency. However the frequency estimation is plant-dependent. For instance it would be higher in those reactors where the RCS filling is routinely done via the RCP seals. This scenario is identical to the Swedish scenario (see below), except for the mechanisms leading to the formation of the deborated slug.

As regards the French scenario, it was found that high conservatism had been used in previous non-U.S. analyses, for instance in relation to the assumption that no natural circulation exists in the loop which is assumed to receive the deborated charging flow. Westinghouse performed calculations assuming a decay heat of 0.05 % the nominal power, and found a natural circulation flow rate of about 800 gpm per loop (i.e. 7-8 times the postulated charging flow). On the basis of their analyses, perfect mixing of the unborated water with borated water would be expected.

In the Swedish scenario the accumulation of a diluted slug in the loop seal is caused by a SG leakage from the secondary to the primary circuit. This is a “credible” event, which has some historical precursors out of U.S. (e.g. Blayais reactor, France, 1990) and may result for instance from SG maintenance operations. A RCP inadvertent restart is expected to lead to re-criticality.
Burnett (Ref. [49]) refers of Swedish analyses that assumed a 280 ft^3 slug volume (accumulated in the loop seal during several days due to secondary-to-primary leak), and the restart of a RCP. The boron concentration at core inlet was calculated by a particle tracking analysis with the PHOENIX code, and the core response was calculated with the SIMULATE-3 three-dimensional steady-state

code, yielding a reactivity excursion lower than the 15% shutdown reactivity margin. However, considering a lower shutdown margin (e.g. 10 %, like in some reactors in operation), the reactivity excursion would leave quite a small shutdown margin, which is unacceptable because of the uncertainties affecting this kind of analyses.
The results above are applicable to Swedish reactors, but cannot conservatively be extrapolated to US reactors. In fact the latter have higher enrichments and lower shutdown margins (5%), and the distribution of fresh fuel assemblies over the core follows a different criterion (i.e. “low leakage”) than the Swedish reactors. Therefore those transients would be more severe in a US reactor.

The startup of the RHR when it contains totally deborated water was estimated to have such a low frequency (10^{-8}/reactor-year) that it is not to be further considered.

As regards the formation of a diluted slug during RCS cooldown at the beginning of a refuelling shutdown, assuming that all the RCPs are turned off is also considered very unlikely, since it is common practice to keep the RCP operating until refuelling boron concentration is reached. This scenario is similar to the Swedish scenario.

The local dilution of the refuelling cavity water during refuelling operations, which is in principle a credible event (and also happened two cases), may lead to recriticality, but without severe core damage.

Then, according to Burnett, the position of Westinghouse in particular with respect to the Swedish scenario is that analyses performed with reasonable conservatism lead to unacceptable results (i.e. severe core damage) in some cases, which means that, in general, scenarios with a large volume of unborated water in the RCP suction may potentially cause severe core damage. Therefore the presence of a deborated slug prior to the RCP restart must be prevented.

In order to ensure a very low probability of occurrence for the scenarios “Dilution during RCS filling”, “Swedish scenario” and “Boration after shutting off RCPs”, Westinghouse recommended the following precautions:

- verifying the leak-tightness of the RCS following SG maintenance operations, and before filling and venting the RCS (e.g. by visual inspection);
- keeping a RCP running when diluting;
- performing dilution only in conditions such that natural circulation would be expected if the RCPs were tripped (avoid dilution when one SG is hotter than RCS);
- keeping a RCP running when performing a shutdown boration;
- if the RCS is filled through the RCP seals, reviewing the administrative procedures and the design to ensure the an inadvertent filling with deborated water has a negligible likelihood;
- whenever possible, boron sampling in the loop seal before restarting the RCPs and before filling the RCS.

3.4.1.2. Babcock & Wilcox

As described in the USNRC report on Issue 185 (NUREG-0933, Ref. [53]), in between 1995 and 1998 B&W Owners Group and Framatome Technology provided USNRC with results of analyses showing that BCM following a SBLOCA in a B&W plant, in case of resumption of natural circulation or inadvertent restart of an idle RCP, would lead to a possible core recriticality and to core damage. Those analyses were based on conservative assumptions (in particular taking no credit of the mixing effects on boron concentration distribution), and according to B&W Owners Group the results supported their position that it was an operational issue and not a safety issue (i.e. a concern requiring regulating actions).

The last analyses performed in the framework of the research activities aimed at resolving Issue 185, led to the conclusions that among the existing PWRs, the lowered-loop B&W plants are those where a boron dilution event can determine the highest reactivity excursions. This is basically due to the fact that in B&W systems the volumes of SG, loop seal and RCP are much larger, and the volume of deborated water that may accumulate is thus much greater than in W and CE plants. Therefore, whereas for the latter no boron dilution event is expected to yield any fuel damage, for B&W plants even severe fuel damage can result from the inadvertent RCP restart, especially if high burn-up fuel is used[10].

3.4.1.3. ASEA Brown Boveri – Combustion Engineering (ABB-CE)

The ABB-CE response to the boron dilution issue that arose in the early nineties, in relation to the System 80+ reactor, can be found in Ref. [67] (mentioned by Attard, Ref. [51]).

ABB-CE performed analyses on a SBLOCA scenario resulting in the accumulation of deborated water in the RCS loop seals (during the BCM). They found that such dilution process may occur for small break diameters between 2.54 and 7.62 cm. Furthermore they made conservative analyses (both thermal-hydraulic and neutron-kinetic) assuming that an infinite deborated slug enters the RPV, transported by the natural circulation flow occurring in the RCS refill phase with ECC injection, and also assuming that no mixing takes place. The results showed that recriticality occurs in the core when the deborated slug begins to be swept through the core, but then neutron power spike is rapidly terminated by Doppler effect first, then power oscillations occur which are dumped and reduced at a low amplitude by moderator temperature feedback (as the water is being heated). It was found that the minimum average boron concentration required to avoid the return to criticality at BOC and with all rods inserted depends on the temperature of the coolant (e.g. 550 ppm at 149 °C and 200 ppm at 260 °C).

More realistically, the deborated slug would not be “infinite”, since new highly borated water (4400 ppm) would come from the ECC injection. Moreover, mixing is expected to occur in the loop seal (between the ECC water and the deborated condensate), in the downcomer and in the lower plenum.

---

[10] However the assessment of the entity of the core damage depends on energy release thresholds, the values of which are still matter of discussion, also within USNRC.

The above considerations permitted to conclude that a SBLOCA boron dilution event followed by a natural circulation flow sweeping the deborated slug through the core would not be a concern. However, the question arises of what would happen if a RCP is restarted. If enough time has elapsed since the onset of natural circulation for the slug to completely pass through the core, no reactivity insertion occurs. On the other hand, if a pump is restarted when some deborated water is present upstream the core the consequences may be serious.
According to ABB-CE analyses, 20 min of natural circulation are sufficient for the deborated slug to pass though the core and then efficiently mix with normally borated water. However, the USNRC raised concerns that the onset of natural circulation might be not properly recognized by the operators, or they could err in determining for how long it is established. So ABB-CE was asked by the USNRC to produce further analyses that demonstrate that the event is not credible, the consequences are not serious, or to provide additional protective measures.

ABB-CE responded to USNRC request by performing a PRA of a SBLOCA deboration scenario in the System 80+ reactor, accounting for the factors listed below:

- probability of a SBLOCA;
- amount of boron mixing in the cold leg piping during the refill phase of the event;
- reestablishment of natural circulation in the RCS;
- probability of a premature RCP restart before the establishment of natural circulation.

Moreover, ABB-CE changed the System 80+ Emergency Operations Guidelines so as to ensure that the operator will not inadvertently restart the RCPs during a SBLOCA, by emphasizing the importance of maintaining the natural circulation before turning on the RCPs. Such modifications were considered satisfactory by the USNRC.
In addition, ABB-CE performed also CFD analyses (with the FLUENT code) aimed at assessing the boron mixing efficacy in the RCS in the event that a RCP is erroneously restarted by the operator. Several conservative assumptions were made that underestimated the mixing effects (e.g. by simplification of the flow paths). The results were that the boron concentration at core inlet strongly depends on the initial slug volume, and that the calculated average concentrations corresponding to all the postulated slug volumes were far above the critical concentration (i.e. the concentration above which criticality does not occur).

Following the review of the ABB-CE analyses results, the USNRC concluded that:

- the inadvertent restart of a RCP before the fully establishment of natural circulation is very unlikely to occur;
- even if a RCP is restarted, there is enough mixing to prevent core recriticality.

Thus the SBLOCA Boron Dilution issue is to be considered resolved.

Some details of the analyses carried out by ABB-CE for the System 80+ reactor, before that USNRC issued the Final Design Approval (FDA), were described by Longo et al. (Ref. [68]).

3.4.2. Innovative Reactors: Westinghouse AP-600 and AP-1000

3.4.2.1. Boron Dilution

In September 2004 the USNRC issued the final safety evaluation report (FSER) for the AP1000 design (Ref. [69]). Such document is the results of the safety review of the AP1000 Design Control Document that the USNRC staff made in order to check whether the new reactor design met the requirements of the Subpart B of Title 10 of the Code of Federal Regulations (10 CFR) Part 52 (Ref. [66]).
The FSER was issued as a support to the contextual issuance of the Final Design Approval for the AP1000 design: "This FDA allows the AP1000 design to be referenced in an application for a construction permit or operating license under 10 CFR Part 50, or an application for a combined license under 10 CFR Part 52."

Hereafter a brief description is given of how the issues related to boron dilution are dealt with in the FSER of the AP1000.

Deboration due to DWS or CVCS malfunction

The inadvertent boron dilution caused by malfunctioning of the DWS or the CVCS is addressed in Section 15.2.4.6[11] of the SRP.
The two systems above "are designed to limit the dilution rate to values that allow sufficient time for automatic or operator actions to terminate the dilution before the shutdown margin is lost", i.e. several alarms exist to alert the operator of an undergoing dilution process.
In the Design Control Document the boron dilution event was analysed by Westinghouse for all modes of operation, by using a generic fluid mixing model, assuming a dilution rate of 12.6 l/s of unborated water (i.e. the maximum flowrate provided by the two charging pumps).
The following modes of operation are considered (in the same order):

1. Mode 6 – Refueling
2. Modes 3, 4, and 5 – Shutdown
3. Mode 2 – Startup
4. Mode 1 – Power operation

Uncontrolled boron dilution event during refuelling (Mode 6) mode is not considered a credible event, because the RCS is isolated from the CVCS by specific valves locked closed, and is connected to the boric acid tank, which supplies makeup water.

[11] Section 15.2.4.6: "Chemical and Volume Control System Malfunction that Results in the Boron Dilution in the Reactor Coolant". This section, which is part of Chapter 15, "Transient and Accident Analysis", corresponds to Section 15.4.6 of the Standard Review Plan (Ref. [65]).

As regards the shutdown conditions (Modes 3, 4 and 5), the analyses made by Westinghouse were based on the following assumptions:

- minimum shutdown margin (1.6 %);
- minimum initial reactor coolant volume;
- one RCP operating;
- minimum amount of water in the RCS assumed to mix with incoming unborated water (such amount is depends on the assumed mode of operation);
- the source-range flux multiplication signal is assumed to actuate an alarm in the control room and close the DWS isolation valves when the neutron flux increases by 60 percent over any 50-minute period.

The results of the analyses were that the DWS would terminate the boron dilution before the subcriticality margin is consumed, so the requirements of SRP Section 15.4.6 are met.

The reactor startup mode (Mode 2) is operated at the beginning of each cycle. The rod control is manual. The Westinghouse analyses were based on the following assumptions:

- dilution rate of 12.6 l/s;
- shutdown margin of 1.6 %;
- four RCPs operating.

As shown by the results of the analyses, “a reactor trip from a signal on the intermediate-range neutron flux will initiate closure of the DWS isolation valves, terminate the boron dilution, and maintain the plant in a subcritical condition”, so also in this case the requirements of SRP Section 15.4.6 are met with respect to core subcriticality.

Concerning the boron dilution during power operation (Mode 1), both the manual mode and the automatic mode were analyzed by Westinghouse.
In case of manual operation, the results of the analyses showed that the boron dilution event is terminated by the reactor trip following an overtemperature signal, and followed by closure of the DWS isolation valves, and that no posttrip return to criticality would occur.
In the automatic mode case, the reactor trip is avoided by the slow insertion of the control rods following the power increase determined by a boron dilution event. At the same time, several alarms (based on neutron flux and rod position) alert the operator that a boron dilution event is occurring. It is demonstrated that sufficient time exists for the operator to detect the event and terminate the dilution before loss of shutdown margin.

So, Westinghouse analyses have shown that:

- for refuelling mode, inadvertent boron dilution events are prevented by design and procedures;

- for refuelling modes and manual control operating mode, the reactor is always maintained in a subcritical condition thanks to the automatic closure of the DWS isolation valves;
- for operating mode with automatic control, several alarm systems allow the operator to detect the dilution event and terminate it before loss of subcriticality.

Therefore the requirements of the SPR Section 15.4.6 are met, as regards the operator action time and core subcriticality.

In addition, Westinghouse specified a required minimum core flow rate of 630 l/s, which on the basis of analyses supported also by experimental tests would be sufficient to assure well-mixed flow conditions in boron dilution events.
On this basis, also the Generic Issue 22, discussed in NUREG-0933 (Ref. [53]), is considered as resolved for the AP1000 design by the USNRC.

Deboration during SBLOCAs
The boron dilution occurring during a SBLOCA is addressed in Section 15.2.8.
On the basis of the analyses performed by Westinghouse (and approved by the USNRC staff), the boron dilution associated with the SBLOCA - BCM (often referred to as the "Finnish scenario") is not a concern for the safety of AP1000 reactors. In fact, during a SBLOCA, the SGs behave like heat sources rather that heat sinks, and no production of boron diluted slugs due to BCM occurs in the SGs. Another potential source of unborated coolant could be represented by the passive residual heat removal exchangers (PRHR HX), which works as a heat sink for the RCS, and may function in BCM. On the other hand, no loop seal is present in the AP1000 primary circuit piping, and thus there is no point where a dilute slug could accumulate. The water condensed in the PRHR HX tubes is continuously drained to the Loop 1 SG outlet plenum, and then to Loop 1 cold legs and to the RPV. Moreover, the analyses show that the water entering the RPV efficiently mixes with the highly borated water already present there and that injected by the accumulators and/or by the core make-up tanks (CMTs). In such analyses the relatively large flow rates from accumulators and CMTs, and the relatively large volumes of the downcomer and of the lower plenum were taken into account. In addition, it has to be recalled that the boron concentration in AP1000 reactors is much lower than in previous PWRs (i.e. 1000 ppm instead of 4400 ppm). All this leads to the conclusion that good mixing exists in the RPV an critical boron concentrations are not reached.
The Westinghouse evaluations about the degree of mixing occurring in the RPV of an AP1000 were supported by experimental investigations.
The conclusion is that "recriticality of the core is not of concern for SBLOCA scenarios."
On this basis, also the Generic Issues 22 and 185, discussed in NUREG-0933 (Ref. [53]), are considered resolved for the AP1000 design by the USNRC staff.

PRA of severe accidents: boron dilution events
Chapter 19 of the FSER deals with the safety analysis of severe accidents, i.e. of those scenarios which are potentially expected to lead to substantial core damage. In particular, Section 19.1.4 deals with probabilistic safety assessment of initiating

events related to the shutdown operation, among which the boron dilution events are addressed in Section 19.1.4.3.7.
The AP1000 design has several features that reduce the shutdown core damage frequency (CDF) with respect to the shutdown CDF of operating PWRs, some of which are related to boron dilution events.
The addressed scenario is the following. A LOOP occurs during an RCS deboration during startup. Then the charging pumps are restarted by the emergency diesel generators, while the RCPs keep at rest, so the dilution continues and the deborated water is transported through the cold legs and reaches the RPV, where it accumulates in the lower plenum. If the offsite power is recovered and one of the RCPs is restarted, the diluted slug will go into the core causing a power excursion.
Such scenario is prevents by design from occurring in an AP1000, because the protection and safety monitoring system (PMS) is designed in such a way to produce boron-dilution signals that terminate the dilution by connecting the CVCS pump suction to the boric acid tank (BAT).
The conclusion is that these events are a negligible contributor to the AP1000 shutdown CDF estimate.

3.4.2.2. Asymmetric Temperature Distribution

The MSLB scenario is included among the transients considered in the safety analyses for the AP1000 licensing (Ref. [69], Section 15.2.1.5: Steam system piping failure). Such scenario consists in the following sequence of events: a pipe break occurs in the main steam system; RCS temperature and SG pressure decrease due to the steam release; the lower temperature of the coolant in the affected loop results in a positive reactivity insertion (due to the negative moderator temperature coefficient) and thus in a power excursion; a low pressure signal causes the reactor trip, a trip of the RCPs, and the actuation of the CMT.
Westinghouse safety analyses were conducted using the LOFTRAN code for the system transient, and the VIPRE-01 code to check whether the DNB had occurred during the transient (using LOFTRAN results as boundary conditions).
The reactor was conservatively assumed to be at zero-power conditions, because the average coolant temperature is lower and less energy is stored in the fuel, and thus the cooldown induced by the steam line break is more severe).
Other assumptions were made to maximize the overcooling effect:

- most reactive rod cluster control assembly fully withdrawn after reactor trip;
- end-of-cycle / zero power conditions;
- Steam flow calculated by the Moody model, neglecting the pipe friction losses (to maximise blowdown);
- Maximum cold startup feedwater flow, and nominal 100% main feedwater
- Four RCPs operating initially;
- No moisture in the blowdown steam;
- Manual actuation of the PRHR at the initiation of the event;
- Availability of offsite power (in case of LOOP the RCS cooldown effect would be reduced).

The analysis conducted by Westinghouse was considered acceptable by the USNRC staff, since it was shown to be based on conservative assumptions (in terms of cooldown, and potential damage to the fuel), and resulted in RCS temperature always lower than the saturation temperature throughout the transient, in a minimum DNBR above the acceptable limit and in a peak RCS pressure below 110% of the design value.

The “Startup of an Inactive Reactor Coolant Pump at an Incorrect Temperature” was not analyzed by Westinghouse because the Technical Specifications do not allow operation with an idle RCP for Modes 1 and 2 (Section 15.2.4.4 of Ref. [69]).

3.5. US Research Context

3.5.1. BNL

In a recent work by Brookhaven National Laboratory (BNL, Ref. [52]) a study was carried out on boron dilution events in PWRs following SBLOCA. The aim was to estimate the consequences (in terms of core damage) of either the establishment of natural circulation or the restart of an idle RCP after the accumulation of a diluted slug in a loop seal (caused by the SGs being in BCM for a certain time period).
Hereafter a brief description is provided of those analyses.

The analyses consist in coupled neutron kinetics and thermal-hydraulics calculations; they address several plant designs (B&W, W, CE) and consider a number of varying parameters like the volume of the deborated slug, and its boron concentration. The used coupled codes are PARCS v. 1.05 (for simulating both steady-state and transient reactor behaviour), and the RELAP5 (for thermal-hydraulics).
A reactor core model was developed based on TMI-1 B&W reactor at BOC, for the above codes. The PARCS model account for each of the 177 fuel assemblies and of the 64 reflector assemblies (4 radial nodes; 28 axial nodes), and for the control rod banks. The cross sections were calculated with the CASMO-3 code. The RELAP5 model represents the core with 30 parallel thermo-hydraulic channels (each one accounting for a number of assemblies lumped together to reduce computational cost), with 24 axial nodes, connected at the inlet and the outlet by shared volumes.
The ex-vessel mixing model proposed by Di Marzo (Ref. [70]) was used to provide boundary conditions to the RELAP5/PARCS model. Such mixing models represent the RCS piping and components from the SGs to the vessel, and simulates the transport and mixing of a deborated slug towards the RPV, and was validated against experimental data from the UMCP 2x4 Integral Test Facility. Diamond et al. adapted that model to several plant designs (2-loop B&W, 3-loop W, 2-loop 4-pump CE), and used it to provide boron concentration at RELAP/PARCS core inlet, making the conservative assumption that no mixing occurs inside the vessel.
In the case that a natural circulation flow is assumed in a B&W, the calculated maximum value over time of the fuel pellet radial average enthalpy is about 90 cal/g, which yields a maximum fuel centreline temperature lower than 2000 °C.

In the case that a forced circulation (RCP restart) is assumed in a B&W, the maximum fuel enthalpy reaches 190 cal/g and in many fuel assemblies the peak fuel centreline temperature exceeds the melting point.
Similar calculations were performed also using boundary conditions obtained for W and CE plants (but using again the PARCS/RELAP TMI core model). In these cases the slug volumes are much smaller (3.5 m^3 instead of 42.5 m^3), thus sensitively reducing the time period during which positive reactivity is inserted into the core. In such cases, the energy release resulted to be far from causing core damage.
As regards the acceptance thresholds for the fuel enthalpy, a reference value currently used by USNRC for BWRs is 170 cal/g for fuel damage inception, whereas 280 cal/g is considered by USNRC as the enthalpy threshold above which unacceptable core damage occurs (i.e. with loss of fuel coolability). On the other hand, the possibility of drastically reducing those threshold is currently being discussed, on the basis of new experimental information, and also to take into account that high burn-up fuel is more sensitive. According to the proposal under discussion, the acceptance criterion for fuel enthalpy should be reduced as low as 100 cal/g.
Based on the above considerations and results, no unacceptable fuel damage is expected in the cases of natural circulation resumption, while the restart of a RCP may lead to unacceptable core damage only when large deborated volumes are involved, like in the lowered-loop B&W plants.
It has to be remarked that the addressed scenarios have a very low probability of occurrence. According to Diamond et al., a rough estimation of the CDF yields about 10^{-8} / reactor-year.

3.5.2. University of Maryland

The University of Maryland has been deeply involved in the research activities on the boron dilution scenarios in PWRs, also in collaboration with the USNRC as a support to the discussion on the prioritization of Issue 185.
A relevant contribution to this research has come from the UMCP[12] integral test facility (see Section 2.4.2.1), which is a down-scaled model (1/470 volume) of a lowered-loop B&W plant (like Three Mile Island Unit 2). The facility can be operated at high temperature, has a design pressure of 2.1 MPa, and is equipped with a RPV, four cold legs, two once-trough SGs, two RCPs with variable speed and high pressure safety injection system. Salt solutions are used as a tracer and to simulate density differences. Instrumentation is present to measure temperatures, pressures and concentrations. Spatially placed thermocouples allow measuring the slug velocity. Single-phase Natural Circulation can be established, and used as initial condition for simulating SB-LOCAs and boron dilution scenarios (when BCM is also operated).
As an example, the experiments performed in 1996 by Tafreshi and Di Marzo (Ref. [71]) were aimed at studying the transport of salt-free slugs in two cases: RCP startup either with the system in SNC or in BCM, with water at mid loop levels. In

[12] University of Maryland – College Park. Descriptions of the facility can be found in Refs. [71], [36] and [38], as well as in many other publications by UM researchers.

the experiments on the second case, the RCP impeller is partially submerged, and flashing phenomena occur that hinder the establishment of a continuous flow, so that the slug transport may show some intermittency (which delays the time needed to reach the RPV).
More recently (2000), the experimental data from the UMCP facility were used for the validation of the simple fluid-dynamic model proposed by Di Marzo (Ref. [70]) for simulating the transport and mixing of a deborated slug from the SG to the core RPV of a B&W reactor.

As mentioned in Section 2.4.2.1, the OECD-NRC International Standard Problem No. 43, was in close connection with the University of Maryland research activities described above.

3.5.3. The OECD/NEA - USNRC PWR Main Steam-Line Break Benchmark

This benchmark, organized by OECD/NEA (NSC and CSNI) and the USNRC, and co-ordinated by the Pennsylvania University, had the purpose of assessing the capabilities of 3D-neutronics/thermal-hydraulics coupled codes to perform best-estimate simulations of transients relevant to the nuclear reactor safety, involving core-plant interaction.
The addressed problem was a MSLB occurring in a PWR, upstream the main isolation valves, followed by reactor trip (also assuming a stuck control rod) and leading to asymmetric core cooling. The reference plant was the Three Miles Island NPP Unit 1 (TMI-1), from which “experimental” data were available to comparison purposes.
The benchmark included the following exercises:

1. point kinetics simulation to test the primary and secondary system model responses;
2. coupled 3D neutronics / core thermal-hydraulics response evaluation using inlet and outlet core transient boundary conditions;
3. best-estimate coupled core – plant transient modelling.

Many organizations from all over the world took part into the benchmark. Among the main achievements of this research activity were the demonstration of the capabilities of the best-estimate 3D coupled codes and their applicability to reactor transients, both for safety analysis and reactor operation. Moreover, the need of further development and a common approach for sensitivity/uncertainty analysis in neutronics and thermal-hydraulics was highlighted.

3.6. Brief review of EU Projects related to computational tools

The research projects mentioned below have been (or are being) carried out within the 4^{th}, 5^{th} and 6^{th} EURATOM Framework Programmes (FP), i.e. in the periods 1994-1998, 1998-2002 and 2002-2006 respectively. Their scope and achievements are relevant or related to the safety analysis of asymmetrical boron concentration / temperature events in pressurized water reactors.

3.6.1. EUBORA

EUBORA Project ("EU Concerted Action on Boron Dilution Experiments") belonged to the 4th FP; it started in September 1998 for 14-month duration, and was led by FORTUM (Finland).
The Project (see Ref. [72]) had the following objectives: 1) "…to discuss and evaluate the needs for a common European experimental and analytical research programme to validate the computational methods for assessing transport and mixing of diluted and boron-free slugs in the primary circuit during relevant reactor transients"; 2) "…to discuss how the boron dilution issues should be addressed within the EU."

3.6.2. EUROFASTNET

EUROFASTNET Project ("EU Project for future advances in sciences and technology for nuclear engineering thermal-hydraulics") was part of the 5th FP; it started in September 2000 for 18-month duration and was led by CEA (France). See Ref. [73].
The Project was aimed at discussing and identifying the needs for R&D activities to be carried out in the field of the thermal-hydraulics applied to nuclear reactor safety, design and economic operation issues.

3.6.3. ECORA

This Project has already been described in Section 2.4.2.3.

3.6.4. ASTAR

The ASTAR Project ("Advanced Three-Dimensional Two-Phase Flow Simulation Tools for Application to Reactor Safety") belonged to the 5th FP. It started on September 2000 for 39-month duration, and was led by CEA (France). See Ref. [74].
The project was aimed at improving the accuracy and robustness of the two-phase flow numerical three-dimensional methods, by validation and development activities. The CFX and NEPTUNE codes were used (and further developed).

3.6.5. FLOMIX-R

This Project has already been described in Section 2.4.2.4.

3.6.6. VALCO

The VALCO Project ("Validation of Coupled Neutronics / Thermal Hydraulics Codes for VVER Reactors") was part of the 5th FP. It started in January 2002 for a duration of 24 months and was led by FZR (Germany). See Ref. [75].
The Project was aimed at improving the validation of coupled neutron kinetics / thermal-hydraulics codes for VVER reactors.

3.6.7. CRISSUE-S

The CRISSUE-S Project ("Revisiting Critical Issues in Nuclear Reactor Design / Safety by Using 3-D Neutronics / Thermal-hydraulics Models: State-of-the-Art") was part of the 5th FP. It started in January 2002 for a duration of 24 months, and was led by University of Pisa. See Ref. [76].
The Project, conducted in co-operation with the VALCO Project (see above) was aimed at re-evaluating fundamental issues in the technology of LWRs with emphasis on the interactions between NK & TH, and had the following objectives:

1) establishing the state-of-the-art;
2) providing results of best estimate analyses in existing reactors;
3) identifying areas of the NPP design where the design/safety requirements can be relaxed;
4) providing recommendations to target Institutions.

3.6.8. NURESIM

The NURESIM Integrated Project ("European Platform for Nuclear Reactor Simulations") belonged to the 6th FP. It started on February 2005 for a 36-month duration, and was led by CEA (France). See Ref. [77].
The Project aims at establishing the basis for the realization of a common European standard software platform for nuclear reactor simulations. The key objectives of the Project are the following:

1) "the integration of advanced physical models in a shared and open software platform;
2) promoting and incorporating the latest advances in reactor and core physics, thermal-hydraulics, and coupled (multi-) physics modelling
3) progress assessment by using deterministic and statistical sensitivity and uncertainty analyses, verification and benchmarking;
4) training, dissemination, best practice and quality assurance."

3.6.9. BOROND

The BOROND Project ("Addressing Boron Relevant Accidents in PWR and VVER-1000 Nuclear Reactors") was part of the 6th FP. It started in February 2007 for a duration of 24 months and is next to completion. It has been carried out in the frame of a EURATOM Training Fellowship by a researcher hosted by the University of Pisa. See Ref. [78].
The Project has addressed boron dilution events in PWR and VVER-1000 reactors (originated both by inherent and external dilution), and focused on the transport of the deborated slug, on the slug mixing and on the core response. Three-dimensional Neutron Kinetics and Thermal-Hydraulics codes have been used, and a glance was has also at CFD codes, whose capabilities and degree of qualification have been analysed.

3.7. The position of IAEA

The sequences described hereafter, which are taken from an IAEA report (Ref. [79]), are all characterized by a potential for a core power excursion due to asymmetric temperature or boron concentration at core inlet.

Incorrect connection of an inactive reactor coolant system loop

This event is typical, although not exclusively, of VVER-440 reactors with a main isolation valve (MIV) installed in both the hot and cold legs of all circulation loops. The reactor may be operated with one of the loops isolated, and containing colder and less borated water. The possible initiating events (all due to erroneous operator action) are:

- startup of the MCP of the isolated loop, followed by opening of MIVs;
- startup of the MCPs in an inoperable non-isolated loop;
- inadvertent opening of a MIV

The event results in a reactivity initiated accident, due either to the lower core inlet temperature or to higher mass flow rate, thus power excursion and reduction of the DNBR are expected.

The core response is mainly governed by the moderator temperature coefficient, which in conservative analyses must be considered as high as possible (i.e. at end-of-cycle). As regard the core inlet conditions, turbulent mixing plays a major role in mitigating the reactivity insertion. Low mixing in DC and LP is a conservative assumption, since it favours a more intense and localized perturbation. 3D neutron kinetics and thermal-hydraulics models are suggested for the analysis.

Concerning the acceptance criteria, the prescribed limits for DBAs must be not exceeded, namely those related to:

- the radially averaged fuel pellet enthalpy;
- the fuel rod cladding temperature;
- fuel melting at any axial location;
- the RCS pressure.

Boron dilution

Boron dilution (i.e. inadvertent decrease of the boron concentration in the primary coolant), may be homogeneous or inhomogeneous.

In the former case, which may occur due to CVCS malfunction or operator errors, the circulation in the RCS is sufficient to assure uniform mixing. The dilution process is slow and can be easily mitigated by operator intervention. This event is classified as an anticipated operational occurrence.

The inhomogeneous dilution is characterized by the accumulation of a slug of deborated or low-borated water in stagnant loops. This may happen due to inherent dilution (when the reactor enters in boiling-condensing mode during accidents with decreased reactor coolant inventory) or to external dilution (i.e. injection of deborated water from the CVCS, or primary-to-secondary leak transient with reversal of the flow through the break).

Due to pump restart or re-establishment of natural circulation the deborated slug may be transported to the core inlet, leading to rapid power excursions.

Any boron dilution accident is governed by the following aspects:

- formation of a deborated slug;
- mixing of the deborated slug with the normally borated coolant during its transport to the core;
- core power response.

The following acceptance criteria are suggested:

- in case of inhomogeneous external boron dilution events with MCP startup and transport of the deborated slug into the core, no recriticality of the core (after reactor scram) is allowed;
- in case of inherent boron dilution events, where it is assumed that the slug is transported to the core by re-establishment of natural circulation, the acceptance criteria have to be combined with the acceptance criteria of the initial accident concerning the fuel heat-up.

For conservative analyses of boron dilution accidents, assumptions should be made that maximize the initial boron concentration and the deborated water volume, and minimize the mixing of deborated water with primary coolant. The analyses should take into account the overall system behaviour, the dilution processes, the turbulent mixing occurring in the RPV DC and LP (by the use of 3D thermo-hydraulic computer codes including mixing models), the core response to the reactivity insertion (by the use of 3D neutron kinetics models) and the mechanical response of the fuel.

Steam line break

In the accident scenario initiated by a rupture of a steam line, a depressurization of the secondary coolant and an overcooling of the RCS occur. The second effect represents a potential for positive reactivity insertion and core power excursion, induced by the lower coolant temperature in the core section adjacent to the affected loop.

The same acceptance criteria mentioned above for the “incorrect connection of an inactive reactor coolant system loop” must be respected.

The following suggestions are made for the analysis of such accident:

- both hot full power and hot zero power operation conditions should be considered, with and without MCPs running;
- the possibility of return to criticality should be maximized by considering end-of-cycle conditions;
- for conservatism, the most effective control rod should be assumed stuck-out, and located in the “cold” core region;
- sensitivity analyses should be made with respect to cooldown rate, change in primary coolant boron concentration (following HPIS intervention), ECCS configuration, etc.;
- maximum power peaking factors should be used when using point kinetics for core response calculations;
- DNBR calculations should be performed using a sub-channel approach;

- the use of 3D dynamic neutronics models is recommended, or at least 3D steady-state neutronics models coupled with 1D thermal-hydraulics system codes.

Inadvertent opening of steam relief valves

This event is similar to the steam line break, in that it is characterized by the steam outflow from the secondary system. On the other hand the loss flow rate is lower and the system experiences slower changes. Thus this event is much less relevant.

Feedwater system malfunction

Malfunctions of the feedwater system, leading either to an increase of the feedwater flow rate (e.g. failure of a feedwater control valve) of to a decrease of the feedwater temperature (e.g. failure of a feedwater preheater) may determine a reduction of the primary coolant temperature and reactivity feedback, like in the case of steam line break described above.

Some other accidental scenarios addressed in the above mentioned IAEA report (Ref. 79) are featured by asymmetric perturbations of the core inlet flow conditions, which mainly affect the core cooling and lead to exceed the core thermal limits (i.e. the DNBR), rather than inducing core power excursion. Also for those cases (which are listed below) the flow mixing in the downcomer and in the lower plenum may have a mitigation effect.
Those events are:

- single or multiple MCP trip;
- feedwater line break;
- feedwater pump trip;
- reduction of steam flow from steam generator for various reasons.

4. ASSESSMENT METHODOLOGY FOR IVF INVESTIGATIONS

4.1. General remarks

The purpose of this Chapter is to describe analytically all the important steps involved in a CFD investigation of single-phase IVF aimed at code validation.
In other words, a general assessment methodology is outlined for this class of NRS related problems, which synthesizes the lessons learned from the code validation and application activities performed in the frame of the PhD research, as well as from the close contact with the international scientific community and with state-of-the-art studies.

The reactor transients considered in this framework are those leading to perturbation of coolant properties at core inlet. Their relevance to the nuclear reactor safety has already been addressed in Chapter 3. Basically, reference is made to transients such as those mentioned hereafter-

- Boron dilution / deboration:
    - malfunctioning of CVCS → inadvertent injection of deborated water into the primary circuit;
    - reflux/condensing mode in SG (following SB-LOCA) → accumulation of deborated water in loop seal.

  Combined with:
    - symmetric or asymmetric steady pumps operation;
    - inadvertent pump start-up;
    - onset of natural circulation.
- Temperature distribution anomalies:
    - MSLB in PWR → enhanced heat transfer causing cold plug formation;
    - SG isolation in reactors with positive moderator temperature coefficient → hot plug formation.

To a certain extent, the methodology for CFD investigation of IVF can be extended also to single-phase PTS analysis, since the target phenomenon (i.e. the heat transfer between coolant and RPV wall) is governed by the in-vessel mixing and flow distribution, as well as by mixing phenomena taking place outside the RPV.

The thermal fluid dynamic phenomena which are involved in the IVF investigation are reviewed in the next sub-section, along with the main issues connected with their experimental investigation and numerical modelling.

Reference is made to the phenomena occurring in the real plant during the relevant transients as well as in experimental facilities reproducing such scenarios.

4.2. Involved phenomena and flow configurations

The following identification of the phenomena and flow configurations relevant to the IVF investigation is a synthesis of (part of) the experience gained addressing the CFD simulations of several RPV-type systems such as:

- ROCOM test facility (section A.1, Refs. [22], [31], [32], [80]);
- Gidropress Mixing Facility (section A.3, Refs. [13] , [47], [81], [82]);
- VVER-1000, Kozloduy-6 NPP, V1000-CT Benchmark (section A.2, Ref. [7]);
- Atucha-II PHWR (Refs. [3], [4]).

4.2.1. Pipe flow in cold and hot legs

The IVF is clearly influenced, at least in part, by the coolant flow in the rest of the primary circuit, and in particular in the piping directly connected with the RPV (which may also be part of the computational domain of a CFD simulation). Examples are provided below.

4.2.1.1. Cross-sectional profiles

In normal operation conditions a highly turbulent flow develops in a PWR loops (Re ~ $10^7 \div 10^8$). The length of cold legs (e.g. ~10 m in typical 4-loop PWR Westinghouse) is not large enough for a fully developed turbulent flow to establish. Therefore, the cross-sectional profiles of the thermal fluid dynamic quantities characterizing the flow (such as velocity, temperature, turbulence parameters, boron concentration, etc.) will be somewhat in between the uniform distribution and the fully developed flow distribution.
This obviously has a potential influence on the IVF and has to be accounted for in the simulation BC definition.
In most situations the RPV inlet conditions are related to the CL flow. However, off-normal cases in which the coolant pumps are switched-off may feature inverse flows, with coolant entering the RPV from HL and leaving the RPV from the corresponding CL. This also has to be considered in modelling.

4.2.1.2. Thermal stratification

Thermal stratification in CL can occur following the intervention of the ECCS during a LOCA scenario, which leads to cold water mixing with the coolant.
This condition is particularly relevant to PTS. This topic is further discussed in Section 4.2.2.

4.2.1.3. Effect of elbows

Bends in a pipe always cause distortions in the cross-sectional profiles, secondary flows, increase in pressure losses, mixing enhancement, etc. Such effect may have a big influence on the RPV inlet conditions and must always be checked.
The hypothesis has been formulated that CL elbows may play a role in inducing or affecting the “flow rotation” effect, which is typical of VVER-1000 reactors[13]. CFD simulations of Atucha-II IVF performed at UNIPI (Ref. [3]) have predicted such type influence, as shown in Figure 7. The elbow effect determines an angular momentum of flow, with respect to the RPV axis, entering the RPV itself; the

[13] This issue has been addressed in the frame of OECD Benchmark V1000-CT2, Ref. [8]. See also Refs. [9] and [41].

contributions from both CLs sum up, due to the central symmetry of the system, and the resulting angular momentum drives the flow rotation in the downcomer.

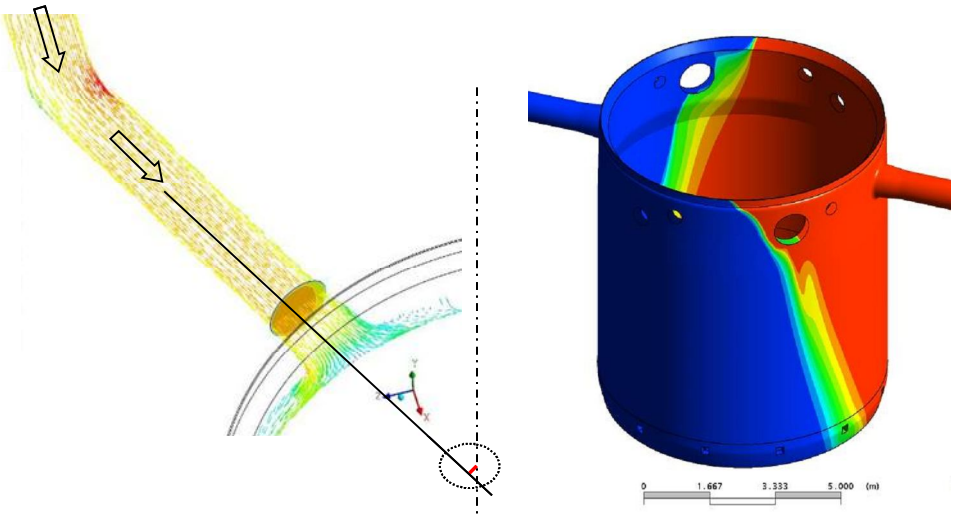

Figure 7 – Effect of CL elbow on RPV inlet flow

4.2.1.4. Effects due to circulation pump outlet

The CL flow is in turn influenced by the circulation pumps. In fact, the pump impellers induce swirling flows that are transported along the pipe and may eventually reach the RPV and affect the IVF.

The CL cross section at the connection with the pump outlet can be partially obstructed by a sort of "dam", the function of which is to prevent back flow in some accidental conditions featuring steam/water stratified flow in CL[14]. That "dam" can also be affecting the CL pipe flow and produce asymmetries and secondary flow structures.

Also the effects mentioned above can be suspected of playing a role in inducing the "DC flow rotation"; however this still requires to be deeply investigated.

4.2.1.5. Experimental issues

The pipe flow upstream of the RPV inlet is usually not very well characterized in experiments aimed at the IVF investigation. A reason for this is that some of the instrumentation needed for that (thermocouples, electrical conductivity sensors, etc.) would probably result too much invasive in the flow and actually alter the RPV inlet conditions.

Information on the turbulence parameters and on the secondary flows is usually not available to the experimentalists, and this obviously introduces some uncertainties

[14] This happens, for example, in Atucha-II reactor.

in the code assessment process, especially when boundary conditions for code simulations are defined, which may not accurately describe the actual conditions.

An example of “good” characterization of the RPV inlet conditions is represented by the ROCOM facility and by the instrumentation adopted in it to measure the salt tracer time and space distribution, that is the so-called wire-mesh sensors (see e.g. Ref. [12]). In particular, such a sensor is placed at the inlet nozzle of the loop which is used for the tracer injection (see Figure 8). The advantage is that the non uniformity of the tracer distribution across the pipe section[15] can be measured and taken into account in CFD code simulations (an example of this is provided in Section A.1; see also Ref. [32]).

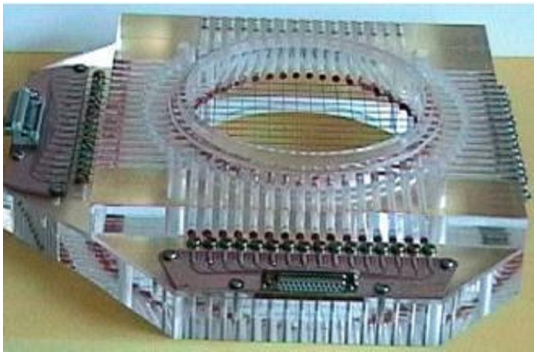

Figure 8 – Wire-mesh sensor at ROCOM inlet nozzle (≈200 measuring points over the cross-section)

Another issue is the “isolation” of external mixing effects in the loop. Let us consider for instance a slug of tracer accumulated in some part of a test facility. During its transport along the circuit that slug (or at least its front and back sides) undergoes some mixing with the pure water, then the RPV inlet is reached by a relatively smooth concentration front instead of a sharp front (as it would be in absence of any external mixing). This effect was particularly evident in the experiments conducted on the GPMF (see section 5.4.3, and Ref. [33]): in the slug-type tests a tracer slug previously accumulated in one cold leg was transported to the RPV following a pump start-up; the concentration probe close to the RPV inlet showed a “smoothed” trend like the one indicated by the black continuous curve in Figure 9 (the blue dashed curve representing the passage of an ideal slug, in absence of external mixing). A proper definition of boundary conditions for a code simulation should account for such a profile, instead of defining ideally sharp concentration fronts (which could result in excessive under-prediction of overall mixing).

[15] ROCOM injection system is equipped with a “mixing device” to obtain a good mixing between the injected solution and the water flowing in the main circuit, nevertheless a perfect uniformity of tracer concentration cannot be achieved, and variations around the mean concentration can be in the order of 10%.

The difficulty in doing this is often related to the lack of experimental information: in fact a single concentration probe at the RPV inlet (such as in Gidropress facility) is not sufficient to provide a complete picture of the inlet tracer concentration because the non uniformities in spatial distributions cannot be revealed. The wire-mesh sensors mentioned above represent an optimal solution, but they have not yet been installed in any other mixing facilities than ROCOM.

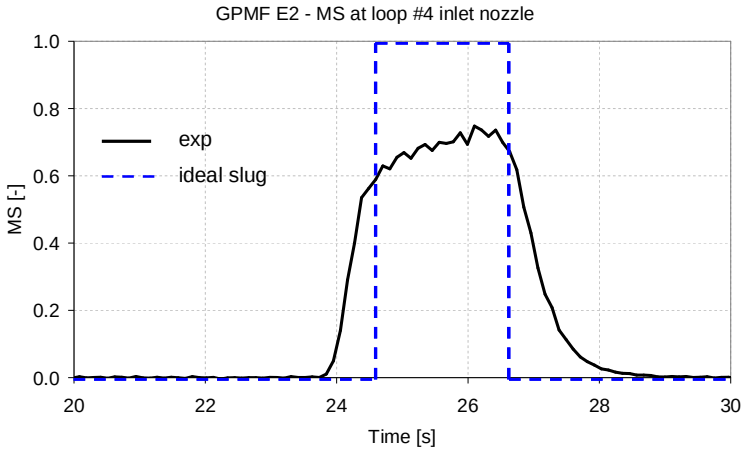

Figure 9 – External mixing: MS at RPV inlet during GPMF slug-mixing test #2

4.2.1.6. Numerical and modelling issues

In this framework, two major numerical and modelling issues associated with the pipe flow simulation are: the prediction of the secondary flows in the duct cross-section and the control of the numerical diffusion.

Secondary flows (the origins of which have been mentioned above) can yield additional difficulties as regards turbulence modelling. They may require advanced RANS 6-equation models, capable of dealing with the turbulence anisotropy, or they may even require LES, if the turbulence is featuring relatively large space and time scales.
The turbulence modelling becomes even more challenging if thermal mixing at the ECC injection is to be dealt with for PTS or thermal fatigue analysis purposes (see next section).

Numerical diffusion is a common issue whenever dealing with numerical simulations. It appears due to the effect of truncation error on the numerical prediction, which can be often mainly dissipative (i.e. smearing sharp fronts) and sometimes also dispersive (different velocities in perturbation harmonic components).
When mixing phenomena are the object of the numerical simulation, then the numerical diffusion deserves particular attention since it provides an extra undue contribution to the predicted mixing and thus can lead to non-conservative over-predictions. Such contribution should always be checked and reduced as far as

possible, by means of a proper choice of numerical schemes and the use of sufficiently fine and high-quality grids.

4.2.2. ECC injection into CL

Several issues are connected with the ECC injection into the CL, especially in relation to PTS scenarios. Some aspects have already been mentioned above in connection with the CL pipe flow. Some further issues are discusses below, owing to their relevance to and influence on IVF.

4.2.2.1. Jet impingement

A real jet impingement situation takes place where the ECC injection occurs. The geometry configuration is quite complex compared to an axisymmetric jet impinging against a plane, infinite wall. The resulting flow is highly turbulent and characterized by large velocity gradients, strong curvature in the streamlines, and anisotropy. Turbulence modelling in this situation is difficult, although extensive model development and validation against experiments have been carried out for many years and is still ongoing in many research centres all over the world.

Validation activities on the jet impingement problem have been performed also at UNIPI (Ref. [83]).

4.2.2.2. Inducing thermal stratification

The injection of colder water will probably not be followed by a perfect mixing. The non uniformity combined with the density effects can lead to thermal stratification in the CL, which must be appropriately taken into account when defining inlet conditions for an IVF simulation for PTS analysis purposes.
The CFD modelling of thermal stratification is not trivial because of the common difficulties in turbulence modelling combined with those associated with the buoyancy modelling in a turbulent flow. This is another aspect which still needs development and validation efforts.
This kind of phenomenology has been investigated in the past in the UPTF facility (Refs. [39] and [84]). As mentioned above regarding the tracer concentration measurements, obtaining detailed experimental information on the RPV inlet conditions is difficult, and this introduces noticeable uncertainties in the simulation and in the code assessment process.

4.2.2.3. Inducing thermal oscillations

The unsteady nature of the turbulent flow can reveal itself in the form of temperature oscillations in the mixing flow downstream of the ECC injection and then on the CL walls. This represents a potential for thermal fatigue structural damage, and is a typical problem of fluid-structure interaction (FSI).
Experimental investigation and code development are currently in progress to tackle this problem.
From the point of view of CFD modelling, accurate prediction of such oscillations still represent a tough task. Obviously, LES is necessary to address this problem.

4.2.2.4. Connection to two-phase flow conditions

The modelling issues mentioned above become much more difficult when two-phase flow conditions occur in the primary circuit (e.g. during a large break LOCA scenario), such as a steam/water stratified flow in CL, with cold water being injected. The phenomenology associated with the ECC injection becomes much more complex, since it will include the condensation effects (both around the cold water jet and on the free surface), the bubble entrainment, the jet instability, the wave propagation over the free surface, the turbulence enhancement in the liquid phase due to the entrained steam bubbles, etc. The development and the validation of CFD models for all such phenomena have constituted some important tasks of the NURESIM Project (see Section 3.6.8, and Ref. [77]).

However, two-phase modelling issues are not part of the scope of the present work, and have been mentioned only for the sake of completeness.

4.2.3. RPV inlet

The region where the CLs connect to the RPV – also referred to as the inlet nozzles region – is always included in the computational domain of an IVF CFD simulations. The way the flow distributes in this region strongly affects the flow distribution and the mixing in the rest of the domain, especially in the DC.

4.2.3.1. Jet impingement

The flow entering the RPV from a CL impinges against the barrel, and its streamlines are forced to an abrupt change of direction. In ideal conditions of symmetry the inlet flow would spread uniformly around the nozzle, while in a real RPV (as well as in a test model) the flow distribution will result from the combination of the bounding geometry (the RPV, the barrel, and in particular the barrel flange, which separates the DC from the UP and prevents upwards flow) and the interaction with the flow being injected from the other inlet nozzles (see Figure 10).

CFD modelling of this region presents all the known problems common to jet impingement situations, especially those related to turbulence modelling.

Some further issues are discussed below.

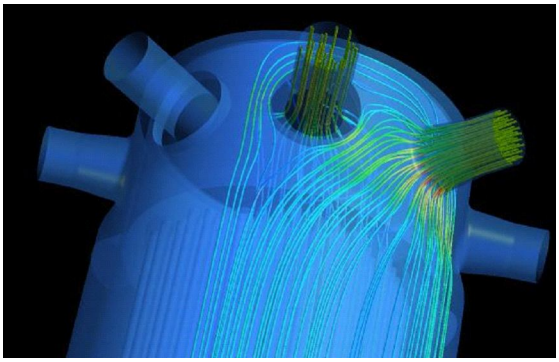

Figure 10 – RPV inlet (CFD model)

4.2.3.2. Effect of fillets and diffusion regions

RPV inlet and outlet nozzles normally present a fillet on the inner side instead of a sharp circular edge. This geometrical feature has an influence on the impinging jet behaviour and on the flow distribution, and should always be reproduced in the CFD model. An example of such an effect is shown in Figure 11, which refers to CFD simulations of one ROCOM steady-state experiment, performed by the Author with two different grids (with and without the fillet); the azimuthal profile of the velocity in the DC is plotted for both cases.

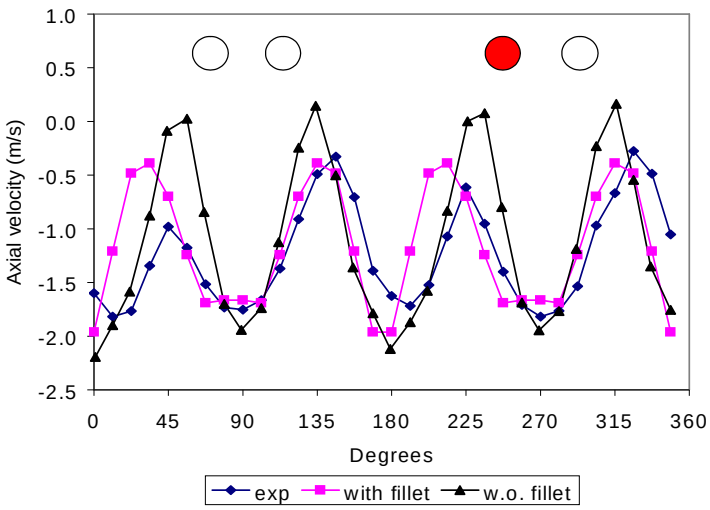

Figure 11 – Effect of inlet nozzle fillet on flow distribution in the DC

4.2.3.3. Meshing issues

The geometry of the inlet nozzle region does not usually include complex features, small details, etc. and is therefore relatively easy to mesh.

Obtaining tetrahedral meshes is straightforward; at least if commercial tools such as Gambit or ANSYS ICEM-CFD are used, and to "inflate" prism layers at wall boundaries is also an easy and fast operation.

On the other hand, if hexahedral grids are to be produced, some difficulties may arise, in particular if a block-structured meshing approach is adopted[16] (as is done with ICEM). In fact, it is rather difficult to obtain a block-structure that accounts for the fillet at inlet nozzle connection without loosing quality in the mesh, where "quality" is intended as that class of mathematical parameters which "measures"

[16] This method is used when generating hexahedral grids with ICEM. The domain is subdivided into several parts which can be topologically associated with parallelepipeds ("blocks"). Then a space discretization is defined for the three directions of each block, but meshes on adjacent blocks are constrained to be conformal on the interface. In this way, a "structured grid" can be obtained even from a complex geometry, provided that all its complexity has completely been handled during the block-structuring phase.

how close is the shape of a mesh element to the ideal element (a cube in this case).
Examples are shown in Figure 12. The mesh on the left was developed by the Authors and his colleagues at UNIPI for CFD simulations of GPMF experiments (Ref. [81]); it was made with ICEM, with the block-structuring technique; the overall quality of the mesh is good, however the grid spacing in the inlet nozzle zone is not optimized and some elements show rather high skewness and poor quality. The grid on the right side, recently developed by the Author for ROCOM simulations, was obtained with the same tools, but with a different (and more complex) sub-division into blocks. Several lower-quality ROCOM meshes have been developed by the Author during the past years, and this last one represents, to his opinion, practically the highest quality level achievable for this kind of geometry.

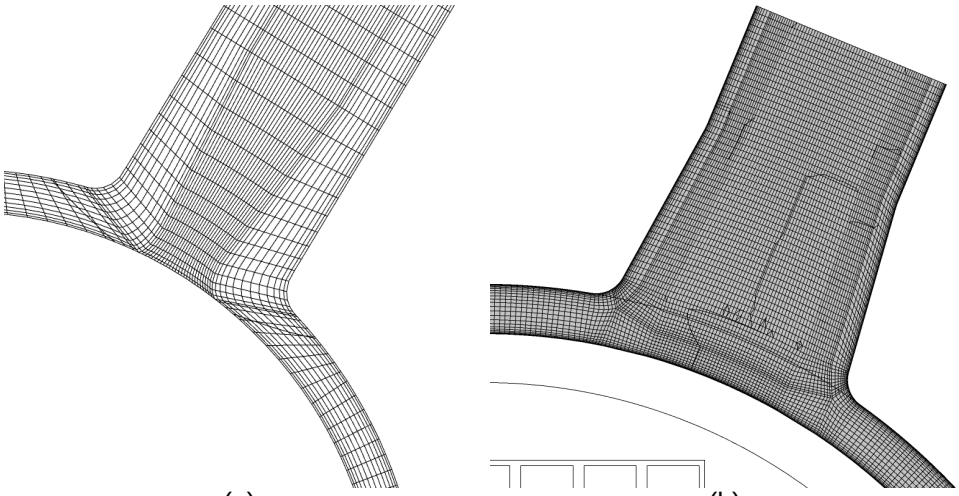

(a) (b)

Figure 12 – Meshing the inlet nozzles: a) improvable quality; b) excellent quality

4.2.3.4. BC issues

Closely related to the RPV inlet is the definition of boundary conditions for IVF simulations, at least when the computational domain starts from the inlet nozzles and does not include the cold legs.
As discussed above in relation to the CL pipe flow, the RPV inlet flow conditions may noticeably deviate from ideal profiles. The appropriate definition of cross-sectional profiles for velocity, turbulent parameters, transported scalars (e.g. temperature or concentration) must be addressed with care, as well as the related sensitivity and uncertainty issues (see Section 4.3.5.6).

Inlet nozzles may also behave as “outlet” nozzles in cases of inverse flows, for example when all pumps are switched-off and their isolation valves are left open, then a pump start-up inadvertently and back flows establish on the other loops. In such situations the boundaries have to allow for an outflow or even for the possibility of flow in both directions.

4.2.3.5. Coupling with TH-SYS

The RPV inlet would most probably be the location for coupling interfaces between a CFD and a system code. The CFD/TH-SYS coupling is not yet an established technology, and only few preliminary results have appeared in the literature in the last decade (see for instance Refs. [85] and [86]).
Basically, such coupling can be intended in two ways: either the CFD model replaces the RPV description in a system code nodalization (i.e. the IVF belongs to the CFD model only, while the external flow is dealt with by the system code) or the CFD model of the RPV overlaps with the corresponding part of a system code nodalization and provides a sort of "correction" to it. In any case, both codes will have to exchange information about the CL flow, and then problems arise related to the loss of information when data is transferred from CFD to system code and to the lack on information (and thus the need of some "arbitrary" input from the user) when transfer is from system code to CFD.
This is really interesting matter for future research and development.

4.2.4. Downcomer flow

The downcomer flow, despite the relatively simple geometry, is the most critical part of the IVF. Most of the mixing effects take place in the DC (although the "lower plenum mixing" is more often mentioned), and there is a close connection between the DC flow distribution and the morphology of the coolant property perturbations at the core inlet.

4.2.4.1. Flow distribution

The flow distribution in the DC has been widely investigated in the ROCOM test facility and, less recently, in the framework of OECD International Standard Problem ISP-43 (see Section 2.4.2.1, and Ref. [41]), based on experimental data from University of Maryland mixing facility.
The ROCOM facility is equipped with laser Doppler anemometry (LDA) instrumentation, which can measure the azimuthal distribution of the flow velocity in the DC (Figure 11). Moreover, the DC is instrumented also with wire mesh sensors which provide accurate information on the tracer space and time distribution; such data in turn provide indirect information on the flow distribution.
The University of Maryland facility was equipped with several thermocouples in the DC, which also gave indirect information on the flow.

The measurements have pointed out the non-uniformities and the asymmetries affecting the DC flow during several types of experiments, and further qualitative information has been provided by CFD investigations.
The considerations reported hereafter can be made on the observed phenomenology.

- Experiments featuring steady and symmetric pump operation show a prevailing vertical component in the DC flow velocity below the RPV inlet region and a well-defined "flow sector" corresponds to each injecting loop (e.g. 90-degree sectors for 4-loop configurations). Such sector is evidenced in the presence of a tracer injected from one loop. An example of that is shown in Figure 13, which refers to a CFD post-test simulation

(run by the UNIPI specialists) of one experiment conducted at the Gidropress mixing facility.

- There is always a kind of "nozzle effect" on the DC velocity field, so that a uniform azimuthal profile is never achieved (except when loop flowrates are very small). Rather, a pseudo-sinusoidal profile develops as in Figure 11; the low-velocity regions may even show stagnation. The velocity azimuthal gradients obviously play a role in terms of mixing; this is evident for instance in Figure 14, showing the azimuthal profile of the normalized tracer concentration measured by two mesh sensors placed in the upper and in the lower part of the DC during one ROCOM slug-mixing experiment (section A.1)
- Asymmetries in pump operation (e.g. one or more pumps kept switched-off) determine more complex flow distributions in the DC. An example of that is shown in Figure 15, which refers to CFD results for a Gidropress mixing test with only two loops in operation (one of them being affected by tracer injection): strong horizontal velocity components appear in the upper part of the downcomer, along with the presence of inverse flows through the idle loops.
- Most complex flow configurations occur in pump start-up scenarios, due to their transient nature and to the strong asymmetry in the flow entering the RPV. The inlet flow, in fact, tends to "wrap" the barrel and reach the opposite side, where most of the flow and of the transported tracer will then concentrate. This is shown, for instance, in Figure 16, which refers to the results from Author's CFD simulations of a pump start-up experiment conducted in the ROCOM facility. Another similar example is presented and widely discussed in Section A.3.

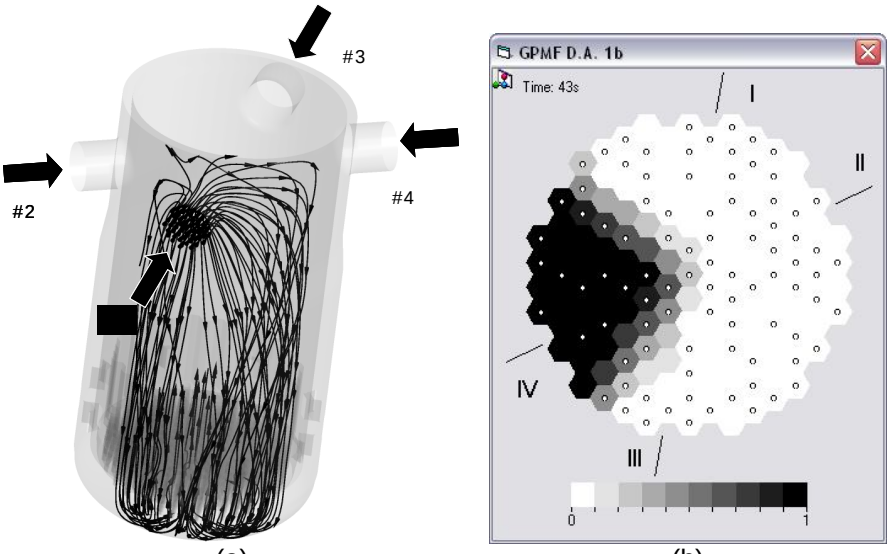

Figure 13 – CFD simulation of symmetric and steady pump operation experiment at Gidropress facility (with tracer injection into loop #4): a) streamlines from loop #1; b) perturbation sector at core inlet (Refs. [13] and [47])

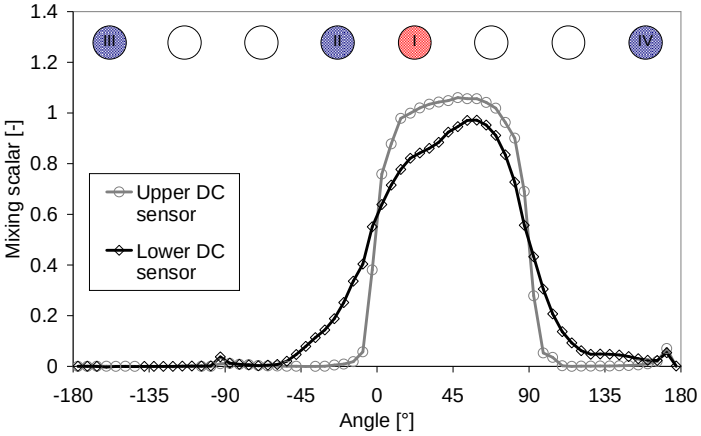

Figure 14 – Effect of mixing in DC (see Section A.1)

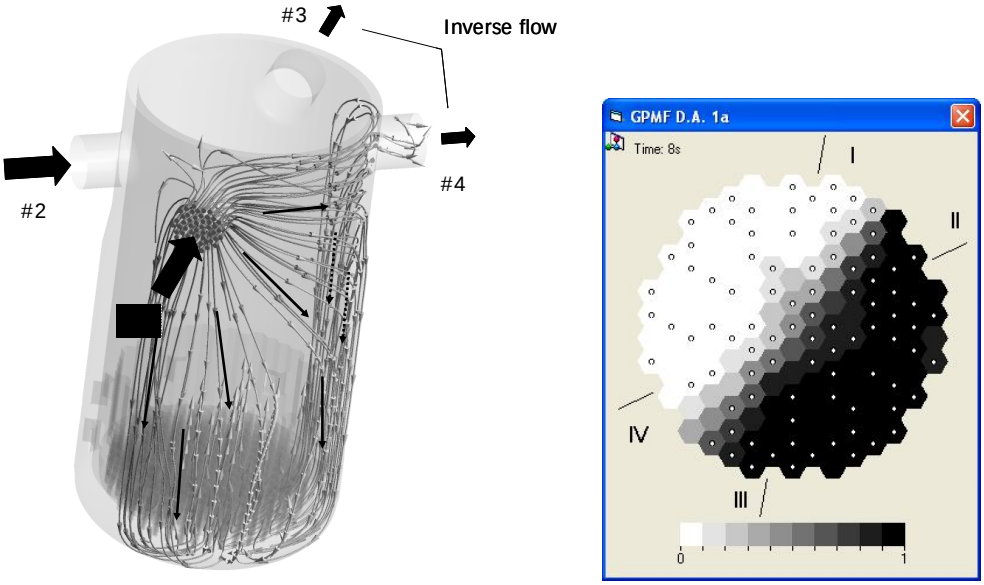

(a) (b)

Figure 15 – CFD simulation mixing experiment at Gidropress facility, featuring pumps no. 1 and 2 in steady operation, and tracer injection into loop no. 4): a) streamlines from loop #1; b) perturbation sector at core inlet (Ref. [47])

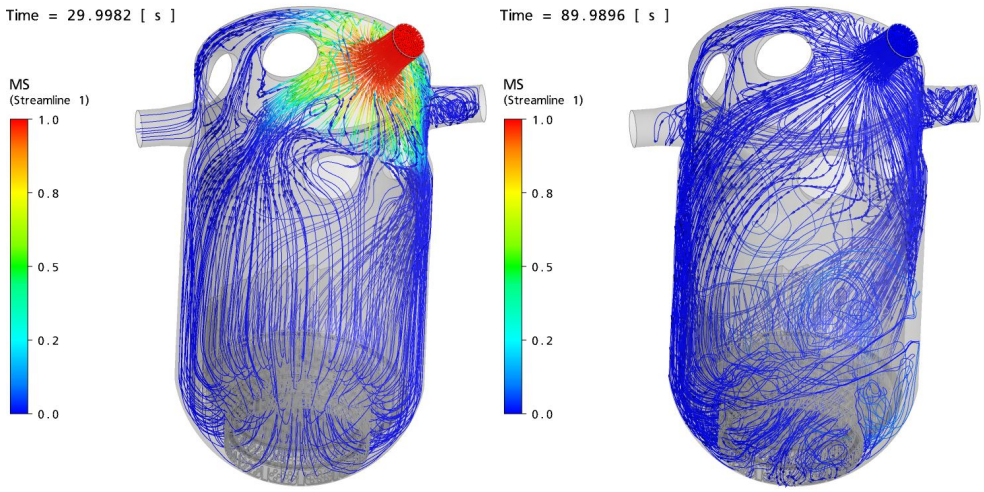

Figure 16 – CFD simulation of ROCOM pump start-up test with tracer injection in starting loop: streamlines and mixing scalar field at two different instants (Ref. [80]).

Accurate characterization of the DC flow demands costly and sophisticated instrumentation.
On the other hand, also the numerical simulation may be a challenging task especially for certain scenarios such as the pump start-up.

4.2.4.2. DC flow rotation

As already mentioned in Section 4.2.1.3, the DC flow in VVER-type systems shows a "flow rotation" effect, which actually determines an angular shift in the position of the perturbation at the core inlet (see also Sections 5.3.1 and A.2) and finally affects the loop-to-loop mixing.

Clear explanations of the origin of this phenomenon cannot be found in the literature, and only limited experimental information is available to the scientific community, namely that from Kozloduy NPP tests on which the OECD Benchmark V1000-CT2 is based (Ref. [8]), and from GPMF (Ref. [47]). Several factors have been hypothesized as possible causes: some of them have already been mentioned above (elbows effect, swirls in CL flow); others can be the pumps start-up procedure and the deviation of the actual geometry from the nominal values (see for instance Ref. [42]). However widely accepted conclusions on this issue are still missing.

Beside, it is an open issue also from the numerical modelling point of view, since only very few CFD applications succeeded in predicting the angular shift (Ref. [42])[17], while in almost all cases CFD has missed the target. This can be observed

[17] The CFD simulations presented by Bieder (Ref. [42]) were performed with the French code Trio_U, using different turbulence modelling approaches, and different

for example in Figure 17, where the perturbation measured at core inlet (left) and the related code prediction (right) are compared, for a GPMF test featuring four pumps in steady operation and tracer injection in loop #4 (Ref. [47]).
It has to be remarked that almost all CFD investigations of IVF have been performed with RANS approaches, which have well-know intrinsic limitations in handling unsteady phenomena, hydraulic instabilities and bifurcation situations. Furthermore, such calculations usually did not account for any geometrical or operational asymmetry.
Probably improvements will be brought by a wider use of LES-type approaches made affordable by increasing computational resources. Moreover, extensive study is necessary to further assess the sensitivity of the CFD results on geometrical and operational asymmetries.

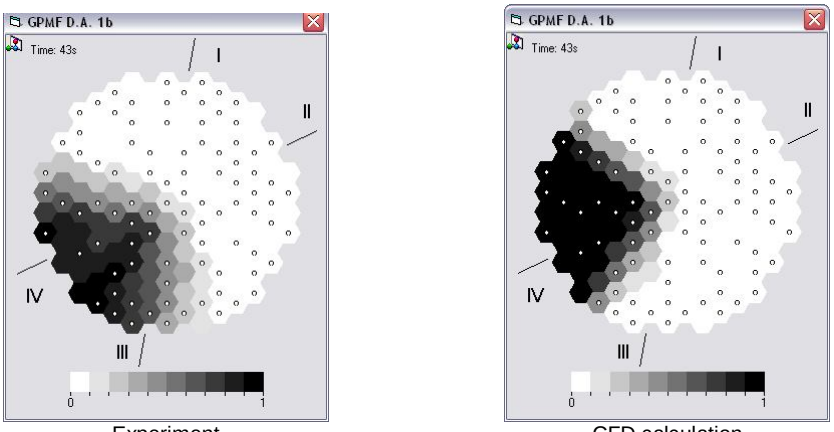

Experiment CFD calculation

Figure 17 – Effect of the downcomer flow rotation on the perturbation at core inlet (Ref. [47])

4.2.4.3. Geometrical features

Spacer devices (sometimes called “consoles”) normally exist between the RPV wall and the barrel, in the lower part of the DC, to assure the correct positioning of the barrel itself and limit its accidental displacements. They have a local influence on the flow and are expected to enhance the mixing, although such effect can be negligible compared to the larger mixing effects occurring in the DC and LP. They should however be accounted for in the CFD modelling, at least with a simplified geometrical description. This was done, for instance, in the Author’s simulations of Kozloduy-6 VVER reactor, as shown in Figure 18 and further discussed in Section A.2.

---

geometrical models, some of which accounted for the deviations of real plant geometry from the nominal values (namely, the actual orientations of CL axes). Some simulations could predict the “swirl”, some others could not. The conclusion was that using LES and including the information on the real geometry are necessary conditions to predict the flow rotation in Kozloduy-6 VVER reactor.

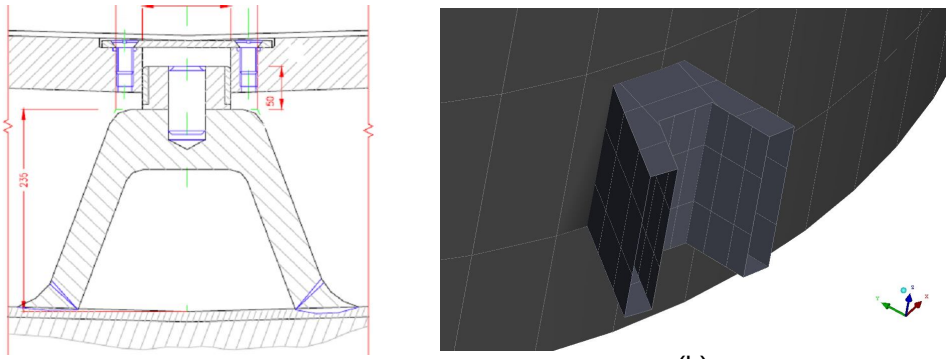

(a) (b)

Figure 18 – Spacer between RPV and barrel in VVER-1000 reactor: a) geometry (Ref. [8]); b) 3D solid model prior to meshing (Section A.2)

Another typical feature of a RPV downcomer in all PWRs (including VVERs) is the RPV wall diameter variation just below the inlet nozzle region (Figure 19-a). This is a “diffusion” zone, where the flow area enlarges and the flow expands, with consequent static pressure increase and possible formation of flow detachment and recirculation phenomena.
Something analogous happens also in Atucha-II PHWR, with the only difference that the diameter increase is in the moderator tank instead of the RPV wall, therefore the flow area decreases and the flow accelerates (Figure 19-b).

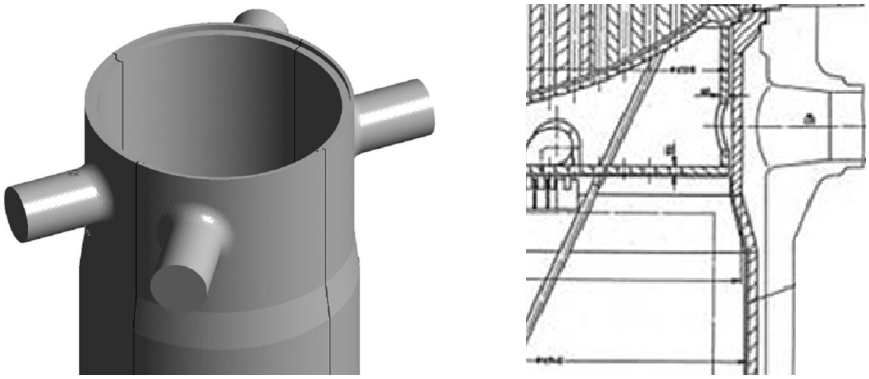

(a) (b)

Figure 19 – Diameter variation below inlet nozzle region: a) VVER-1000 (Section A.2); b) Atucha-II PHWR (Ref. [3])

4.2.4.4. Meshing issues

Obtaining a high-quality hexahedral mesh of a RPV downcomer is a straightforward task, with some possible complications is some obstacles (such as the spacers mentioned above) have to be included.

On the other hand, obtaining a sufficiently fine mesh, compatible with computing resources limitations, may be more problematic.
A means commonly adopted to limit the number of mesh elements consists in using hexahedra with high aspect ratios, lengthened along the vertical direction. This approach relies on the assumption that the flow is mainly directed downwards. However, as discussed before, many IVF situations exist in which the DC flow behaves in a more complex way and horizontal (azimuthal) velocity components may be important in some regions. In such cases, having aspect ratios close to one is desirable because less numerical diffusion is introduced.
In addition, if LES approaches are adopted, then the mesh will necessarily have small aspect ratios.
All this should be taken into account when developing meshes for IVF CFD analysis.

4.2.4.5. Further modelling issues

Many (RANS) CFD investigations of the IVF have shown a tendency to under-predict the turbulent mixing. This is evident from steeper spatial gradients predicted for tracer concentration distribution than measured. An example is shown in Figure 20 and Figure 21, in which the measured and calculated azimuthal profiles of the mixing scalar are plotted both in the upper and in the lower part of the DC, for the same ROCOM test referred to in Figure 14. The code predictions perfectly agree with the measured data just below the nozzles, while at the bottom sensor (which is about 1 m below) a noticeable discrepancy is shown which clearly indicates an under-estimation of mixing effectiveness.
This topic is covered more in detail in section A.1 and in Ref. [32]. Further investigation is still necessary to clarify the source of such under-prediction. However, the explanation is most probably to be searched for in the limited capabilities of current turbulence modelling approaches (especially the eddy viscosity models) in handling the complex and strongly anisotropic flow developing in the downcomer.

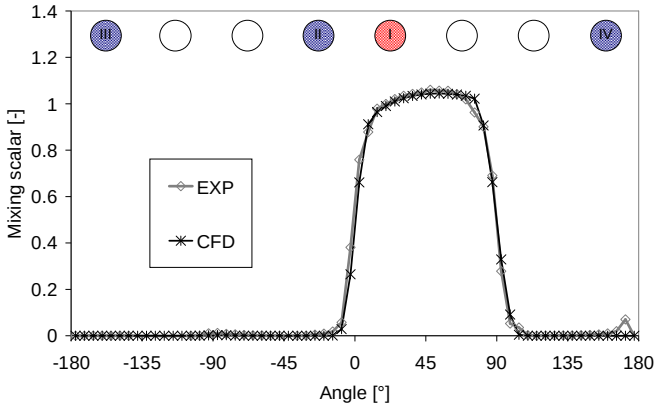

Figure 20 – Perturbation azimuthal profile in DC (top), ROCOM slug mixing test (Section A.1)

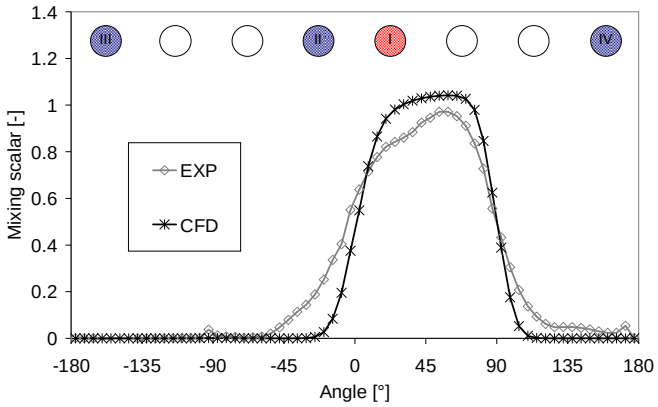

Figure 21– Perturbation azimuthal profile in DC (bottom), ROCOM slug mixing test (Section A.1)

4.2.5. Lower plenum flow

The LP is the region where most of the geometrical complexity is concentrated (along with the related modelling problems), due to the presence of the "internals". Important mixing phenomena take place there, which directly affect the actual distribution of coolant properties at the core inlet.

4.2.5.1. Geometrical features

Basically, the internals encountered in the LP have two different functions: supporting the reactor core, and homogenizing the flow entering the core by filtering the largest turbulent eddies (so as to reduce the vibrations induced on the structures).
In any case, a large number of small geometrical details act as obstacles for the flow (as well as for who is in charge of modelling them).

For example, a cylindrical sieve ("perforated drum") with several hundreds of small holes drilled on it is placed in the LP of KONVOI reactors (and then also in ROCOM facility), with the purpose of enhancing the mixing and breaking the largest eddies (Figure 22-a). A perforated plate, located just above the sieve, constitutes the core inlet (Figure 22-b).

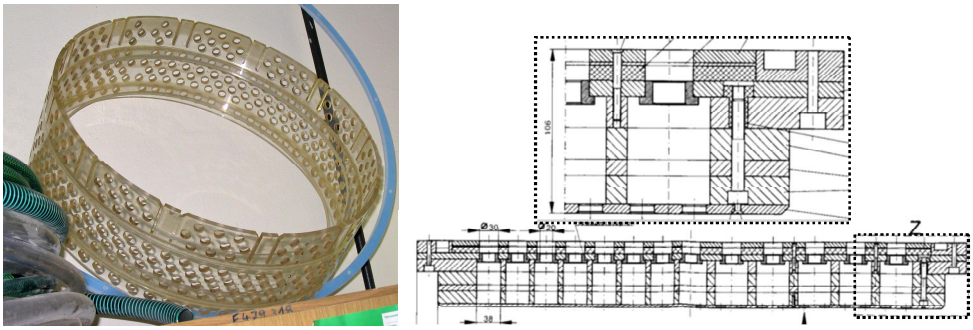

(a) (b)

Figure 22 – ROCOM LP internals: perforated drum (a); core support plate (b)

The LP of a VVER-1000 is quite different from above (Figure 23). The barrel ends with an ellipsoidal perforated bottom where some thousands holes are drilled. Internally, supporting columns (one per coolant channel) bear the weight of the whole core and transmit it to the barrel bottom. Again, a perforated plate is placed below the core, with the only function of positioning the fuel assemblies. The lower part of the supporting columns is thin and solid, while the upper part is larger, hollow and provided with openings: the coolant in fact enters the columns and then moves upwards to reach the fuel assembly.

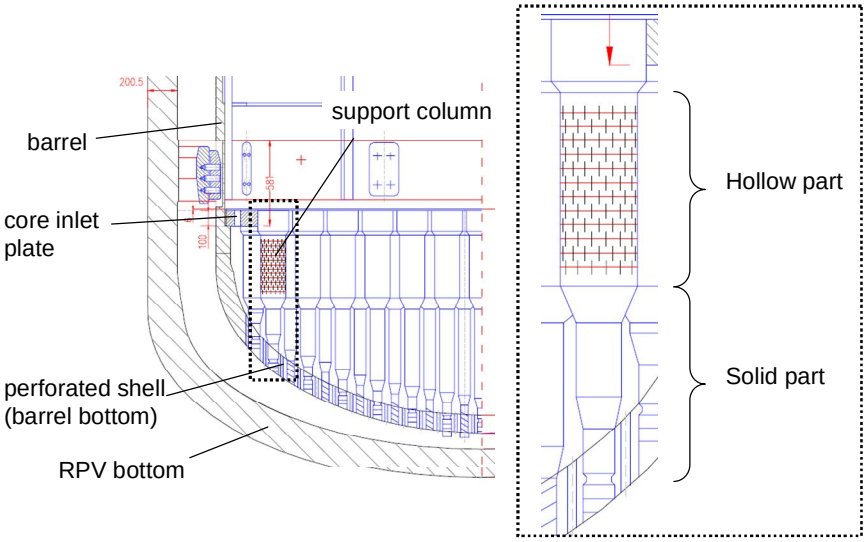

Figure 23 – VVER-1000 LP internals (from Ref. [8])

A rather unusual geometry is encountered in Atucha-II reactor (see Figure 24). The weight of the whole core and of the moderator is supported by a large grid structure below the core inlet plate, which occupies almost the entire LP. Just below it is the so-called “filler”, i.e. a metal structure that has the purpose of minimizing the LP volume (and then the expensive heavy water inventory). Such grid structure

subdivides the LP into around fifty rhomboidal-prismatic sub-plena, and each plenum feeds nine coolant channels.

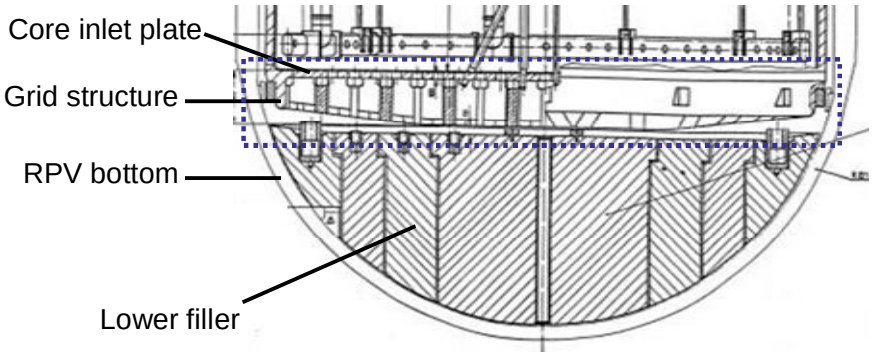

Figure 24 – Atucha-II LP internals (LP region indicated by dashed zone; Ref. [3])

As shown above, a wide variety of geometries can be encountered in the lower plena of nuclear reactors. In all cases, such details have to be taken into account, either with a fine geometrical description or with some modelling simplifications which can properly include the mixing effects as well the greater flow resistance.

4.2.5.2. CFD meshing issues

If the CFD model aims at a fine description of the LP geometry, then a large number of small geometrical details must be explicitly meshed (e.g. hundreds of supporting columns, thousands holes, etc.). This has two main implications:

1. the mesh results in a relatively large number of cells, since the maximum cell size is locally imposed by the geometry scales, which may be very small (in the order of centimetres or millimetres);
2. it is almost impossible to generate high-quality hexahedral grids; tetrahedral grids usually represent the only practicable option.

In typical CFD IVF investigations it is rather common that something like 80% or more of the total mesh budget is invested in the LP (e.g. four millions cells for the LP, and one million cells for the rest of the computational domain, such as DC, inlet nozzles, core region).

The use of tetrahedral meshes in the LP is often combined with hexahedral grids for the DC, thus resulting in hybrid grids assembled via non-conformal mesh interfaces.
More complex meshing approaches involve the use of tetrahedral elements in some sub-regions of the LP, while the rest is meshed with hexahedra. An example is show in Figure 25: in this mesh of the ROCOM LP, recently developed by the Author (the same already shown in Figure 12-b), only the volume surrounding the perforated drum is meshed with tetrahedra, while in the remaining domain a hexa-based grid was created using the block-structuring approach.

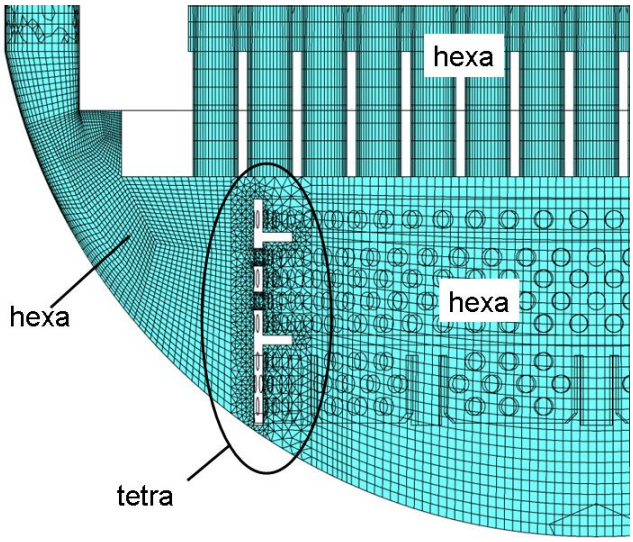

Figure 25 – Hybrid mesh for ROCOM LP

4.2.5.3. Porous media

A different and less complex option than the fine geometrical description is the adoption of geometry simplifications, compensated by adequate modelling. For example, a perforated plate or shell can be replaced by a “porous” region, with noticeable savings in the number of cells. The definition of additional pressure losses (in the form of a sink term in the momentum balance equation) is then necessary to model the flow resistance associated with the plate or the shell, since it is not explicitly “simulated” any more.

Quadratic correlations between momentum sink and local flow velocity are appropriate for such a model (for instance, they are usually implemented in commercial CFD codes, along with other types of correlations), but the problem arises of setting the closure parameters. The Idel’cik manual (Ref. [87]) can provide useful indication in many cases, but in many others experimental information is necessary; otherwise, special CFD investigations can be performed to obtain local information on pressure losses.

Moreover, another issue associated with the use of porous media is how to force the fluid to flow in the right direction. In fact, a flow through a perforated plate is always perpendicular to the plate itself, but if the plate is replaced by a porous medium then transversal velocity components may be present, which yield a non physical description of the flow field. This problem is only partially solved by defining larger transversal flow resistance coefficients.

An example of “porous region” is shown in Figure 26: the perforated drum present in ROCOM LP was modelled (in a simplified variant of the mesh shown in Figure 25) with an annular sub-domain, without explicitly describing the 400 small holes. Additional pressure losses were defined, however, to take the actual flow resistance into account.

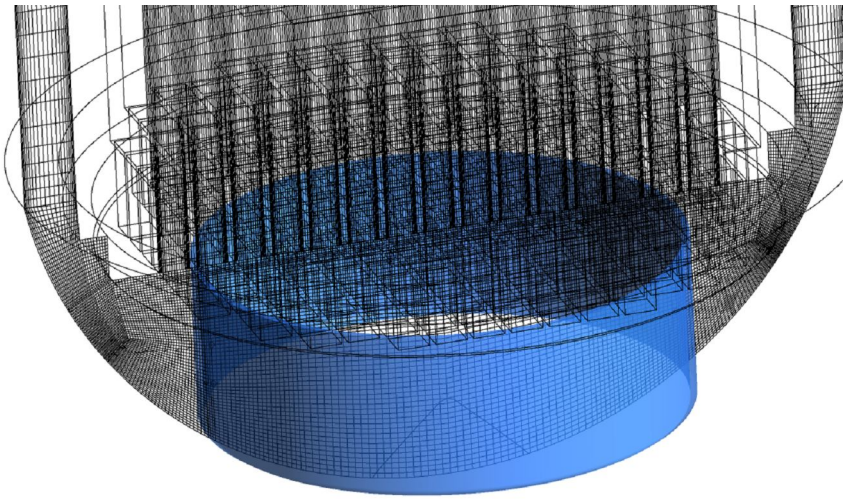

Figure 26 – Porous medium for ROCOM perforated drum (blue)

4.2.6. Core region flow

4.2.6.1. Level of complexity

The core region is the place where the highest level of geometrical complexity is reached, because of the large number of items which compose the nuclear fuel (~10^2 fuel assemblies; ~10^4 fuel pins; ~10^2 spacers). This is obviously true only for real plants, since in experimental facilities the core region is usually represented in a simplified form.

High complexity is involved also from the phenomenological point of view. In fact, the flow along the coolant channels features secondary flows between the fuel pins, and a strong interaction with the spacers, which increase the turbulence diffusion (and consequently the pressure losses and the heat transfer rates).
Conjugate heat transfer (CHT) between fuel pins and coolant is also an important phenomenon. In principle, it can be simulated with common CFD codes in a relatively easy way, since the coupled solution of the heat conduction equation in the solid domain and of the thermal-fluid dynamics balance equations in the fluid domain is usually an available capability[18]. On the other hand, extensive validation on CFD CHT analysis is not yet available in the literature. Moreover, the large amount of fuel pins would inevitably lead to very expansive computational meshes.

In a real plant the convective heat transfer between coolant and fuel is not the only heat source for the coolant, since an important contribution is given also by the

[18] This is true provided that single-phase conditions are kept. In the presence of mass transfer (convective boiling flows), much more complex modelling is necessary, which is currently the object of intense development and assessment work within the international scientific community.

energy deposition from radiation and neutron moderation. This can be taken into account in CFD modelling by means of volumetric power sources.
An example is constituted by the CFD simulations of the moderator flow inside Atucha-II reactor, carried out by the Author and his colleagues (Ref. [4]). In that case, the computational domain represented the moderator tank and was bound by the tank walls, the coolant channel guide tubes crossing the tank, and by four boron injection lances (see Figure 27-a). The power transferred to the moderator by neutrons, gamma radiation, and fuel channels (by convection) was modelled via a volumetric source term in the enthalpy balance equation defined over the whole domain. This allowed predicting, along with the moderator velocity field, also the temperature distribution: as shown in Figure 27-b, thermal stratification occurs since cold moderator enters from the bottom, heats up while flowing upwards and finally leaves the tank from the top.

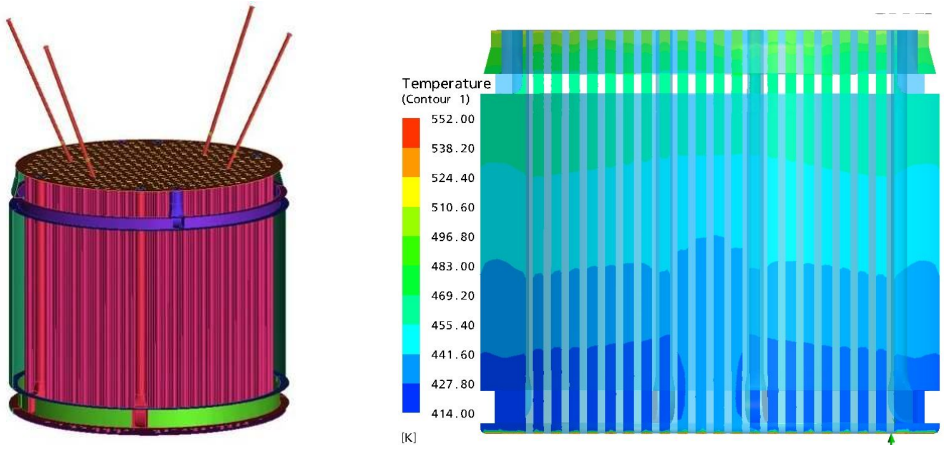

(a) (b)

Figure 27 – CFD simulation of Atucha-II moderator flow: a) computational domain; b) predicted thermal stratification (Ref. [4])

4.2.6.2. Channel-type vs. open space

In ROCOM facility the core is simulated with a bundle of 193 simple tubes, each one representing a “coolant channel”. Therefore there is no cross-flow between adjacent channels. This configuration does not involve any particular modelling difficulty.

A similar situation occurs in the Atucha-II reactor, where coolant channels are independent (Figure 27), like the pressure tubes in a CANDU reactor or the canned fuel assemblies of BWR and VVER.

On the other hand, in common PWRs the fuel assemblies are not canned, then cross-flows are allowed and consequently the pressure distribution tends to equalize.

In Gidropress facility the real plant geometry is reproduced (although in a reduced scale) up to the core inlet plate; above the plate, in lieu of the core, there is a

structure made of around one hundred long and thin tubes that support the electrical conductivity probes. Therefore this region behaves like an open volume, with obstacles inside.

4.2.6.3. Inclusion in the computational domain

The core region is usually not included in the computational domain for CFD analysis of IVF, as long as the perturbation of the coolant properties at the core inlet is investigated. The reason for this is that the flow in the core region is not directly affecting the mixing phenomena upstream of the core inlet.
On the other hand, the pressure field in the core region can influence the flow distribution over the coolant channels, and this has to be taken into account in modelling.

If the core region is not simulated, than the problem arises how to impose outlet boundary conditions above the core inlet plate. One possibility could be to define pressure-controlled BCs at the entrance of each coolant channel; however this approach is rather tricky (one BC has to be handled for each channel) and usually not supported by sufficient information on pressure distribution to implement as BC. A more practicable approach consists in defining a dummy open volume above the plate, and imposing a pressure-controlled BC on the top of such volume. An example of such modelling approach is shown in Figure 28; the “outlet volume” is the dummy volume mentioned above, and the “reduced core” is the core inlet plate. The reduced core consists of simple cylinders (one per channel); additional pressure losses (via momentum sinks in Navier-Stokes equations) can be defined so as to concentrate on the reduced core the pressure losses encountered by the flow across the entire core.

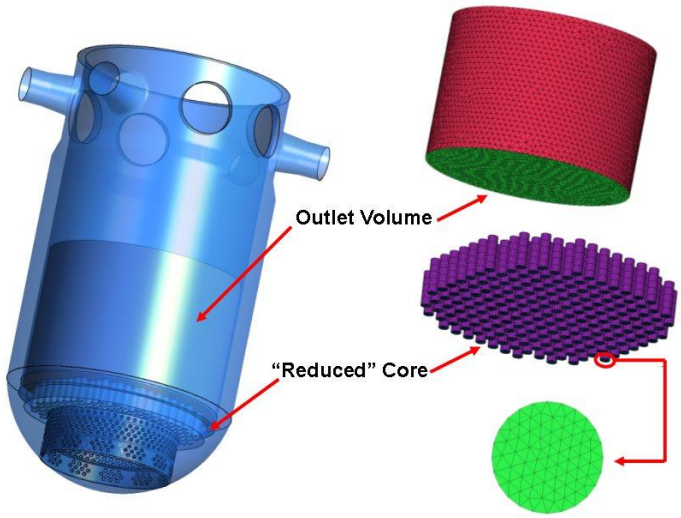

Figure 28 – Simplified modelling for the core region in ROCOM facility (Ref. [22])

The modelling approach described above must always be supported by sensitivity analyses to demonstrate that the outlet boundary location has negligible influence on the flow distribution. This is also recommended by the BPGs.

An example of such sensitivity study is shown in Figure 29, which is taken from Ref. [13], and refers to pre-test simulations (performed by the Author and his colleagues at the University of Pisa) of one Gidropress experiment featuring symmetric and steady pump operation. The azimuthal profile of the vertical velocity in the downcomer is plotted in the figure for three cases: the reference calculation (which did not include CLs); the calculation labelled with “piping” (which included the CLs with their elbows); the calculation labelled with “Extended out volume” (in which the outlet boundary was located at a 50% larger distance from the core inlet compared to the reference case). As can be seen from the figure, the sensitivity of the results on the outlet boundary location is negligible, which indicates that in the reference case such location was defined “far enough” from the core inlet. On the other hand, some influence of the CL modelling is evident; this indicates the results sensitivity on the cross-sectional velocity profiles at the RPV inlet, which are defined as uniform in the reference case, while they are closer to a developed flow in the “piping” case.

In a relatively simple case such as the ROCOM facility, the core region can be explicitly modelled without excessive efforts. This implies that also the upper plenum is included in the computational domain (see Section 4.2.7.1).

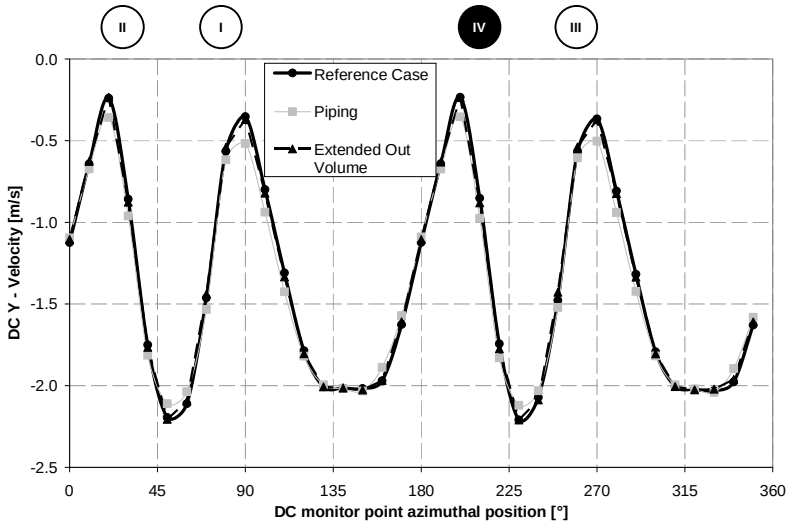

Figure 29 – Sensitivity analysis on location of outlet boundary (Ref. [13])

When dealing with “real plant” geometries the explicit modelling of the core is practically impossible. For instance, a rough description of the core which accounts for all fuel pins (without modelling the spacers) would easily lead to a number of cells in the order of 10^7 to 10^8; as a reference, 10^7 cells is the size of the largest CFD grids used at the University of Pisa on a computer cluster with 40 CPUs.

As an example, Figure 30 shows the computational domain and the mesh used by the Author and his colleagues to simulate a portion of one single fuel assembly of the Atucha-II reactor, for pressure loss estimation purposes. Only one fuel pin spacer was included in the domain, and only one sixth of the cross section was modelled (owing to the symmetries). The coarsest grid developed counted about 3 million cells and more than 1 million nodes, which gives an idea of the unaffordable cost of simulating the whole core.

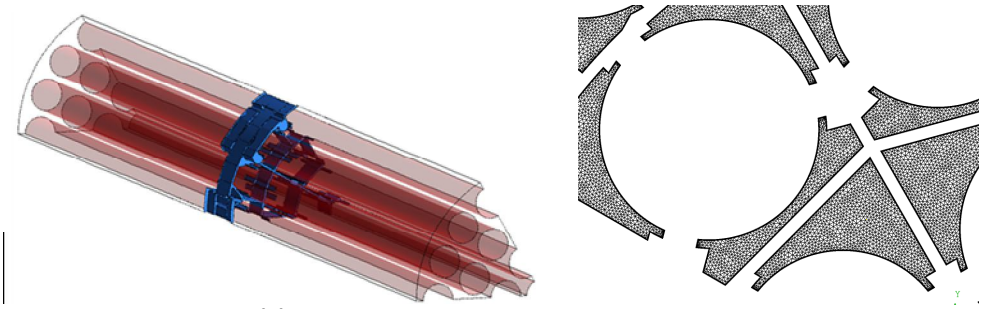

(a) (b)

Figure 30 – Simulation of Atucha-II fuel assemblies: a) computational domain; b) mesh detail

4.2.6.4. Pressure loss assessment

As mentioned above, modelling simplifications may require the definition of additional pressure losses accounting for channel inlet and outlet, FA spacers, etc. Experimental information of this type is usually missing, and the only references for models tuning are the Idel'cik manual (when applicable) and the results of special CFD analyses devoted to the prediction of local pressure losses, such as those mentioned above (see also Section 4.4.3).

This problem was addressed by the Author, for example, when dealing with the pressure losses through ROCOM lower plate (Figure 31, Ref. [22]), in order to define suitable momentum sources in the simplified CFD representation.
With this purpose, a detailed CFD study was performed on a single channel, exploiting the symmetries in the computational domain definition as far as possible, and developing very fine meshes (Figure 32-a). Moreover, a simplified model (Figure 32-b) was developed for the same region, based on a simple cylindrical domain (such as in the global model for the simulation of the entire ROCOM RPV). Then, additional pressure losses were defined on the simplified model and tuned so as to coincide with those predicted by the detailed model. In this way, the source terms to be applied to the global model could be obtained. This procedure is summarized in Figure 33.

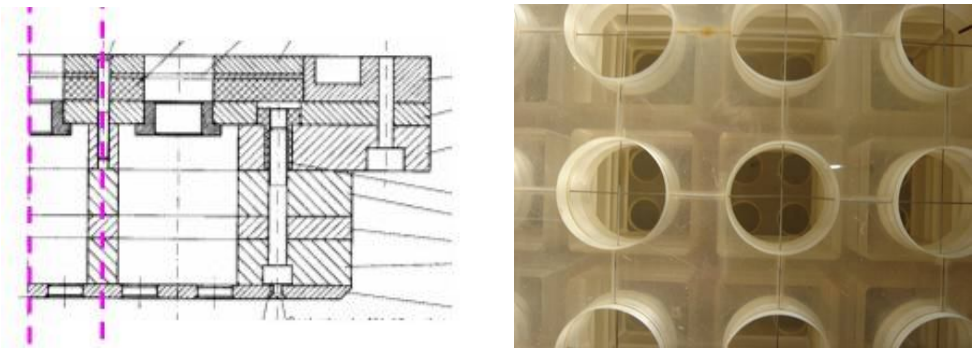

(a) (b)

Figure 31 – ROCOM lower support plate: a) drawing (with indication of sub-region for CFD analysis); b) picture from the top (wire-mesh sensor well recognizable, as well as the thin plate in the bottom, on which small holes are drilled)

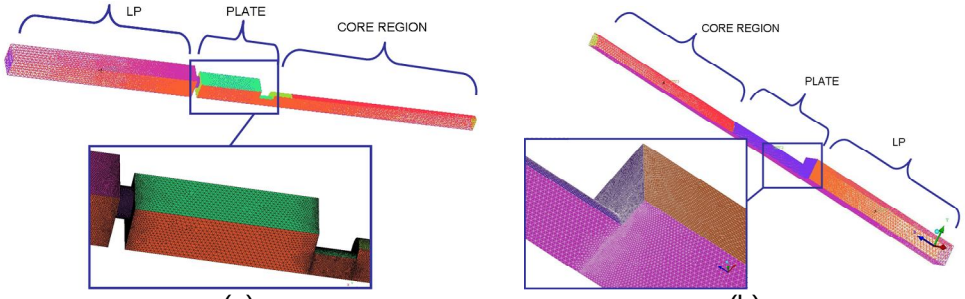

(a) (b)

Figure 32 – CFD mesh for detailed simulation of pressure losses through ROCOM lower plate: a) detailed domain; b) simplified domain

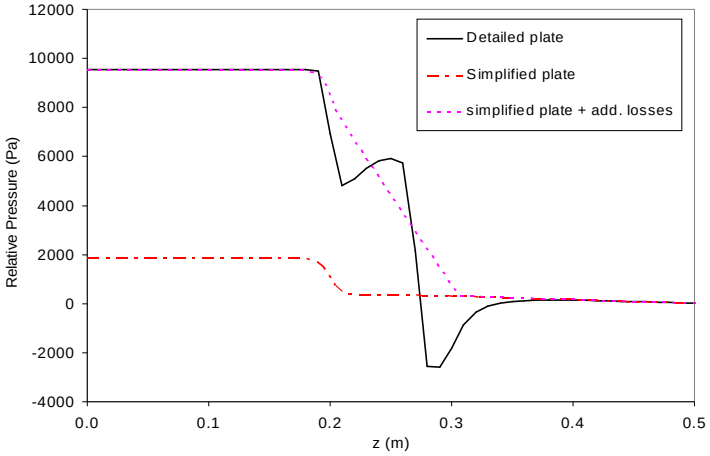

Figure 33 – CFD study of pressure losses through ROCOM lower plate

4.2.7. Upper plenum & outlet nozzle flow

4.2.7.1. Relevance of UP flow

Also the upper plenum and the outlet nozzles, as well as the core region, are usually not included in the computational domain for CFD analysis of IVF. The UP flow has practically no influence on the flow distribution and flow phenomena upstream of the core inlet, which are the main target of the simulations.

On the other hand the UP flow is relevant to the loop-to-loop mixing. In fact, the perturbation coming from one loop will affect to some extent all loops after leaving the core. The proportions to which the perturbation is shared by the loops are a result of the mixing taking place in the whole RPV, including the flow rotation effect. They can be expressed in terms of loop-to-loop mixing coefficients c_{ij}, defined as the relative amount of perturbation coming from loop *i* that will reach loop *j* after core outlet.
Examples of analysis aimed at the estimation of loop-to-loop mixing can be found in the OECD Benchmark V1000-CT (Ref. [8]): in fact, measured temperature data from Kozloduy reactor included information on temperature distribution at the core outlet and in hot legs.

As shown in Figure 34-a, the UP of ROCOM was included by the Author in the computational domain of some meshes for sensitivity analysis purposes (see Section A.1). Furthermore, also the CFD simulations performed by Gidropress specialists in the frame of TACIS R2.02/02 Project (Ref. [13]) included the upper plenum in the domain (Figure 34-b).

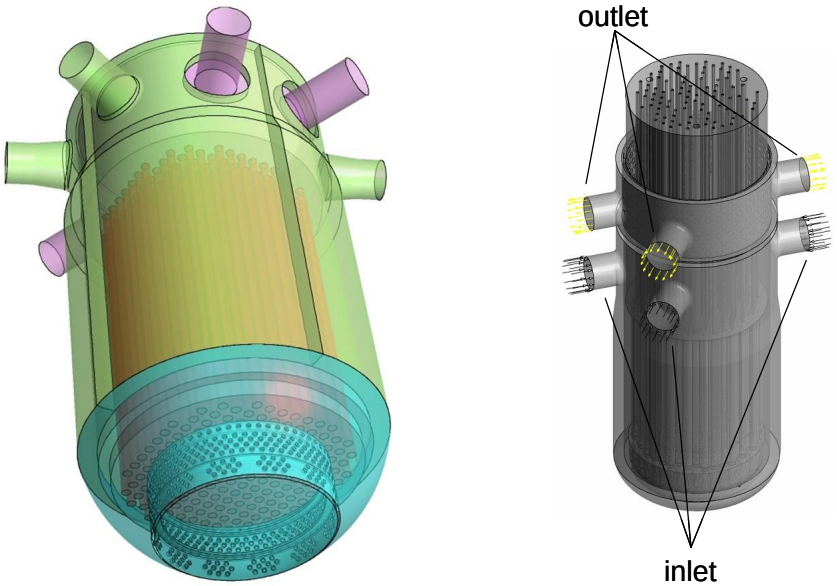

(a) (b)

Figure 34 – Including the UP and the core region in the computational domain for IVF investigation: a) UNIPI simulations of ROCOM (Section A.1); b) Russian simulations of Gidropress facility (Ref. [13])

Moreover, the UP flow can be the object of specific investigations on flow distribution, pressure losses etc., regardless of the issues related to perturbations at core inlet.
Such investigation was performed, for example, for the UP of Atucha-II reactor (Ref. [4]). Figure 35-a shows the computational domain adopted for the CFD analyses, while some results related to the calculated velocity field are plotted in Figure 35-b.

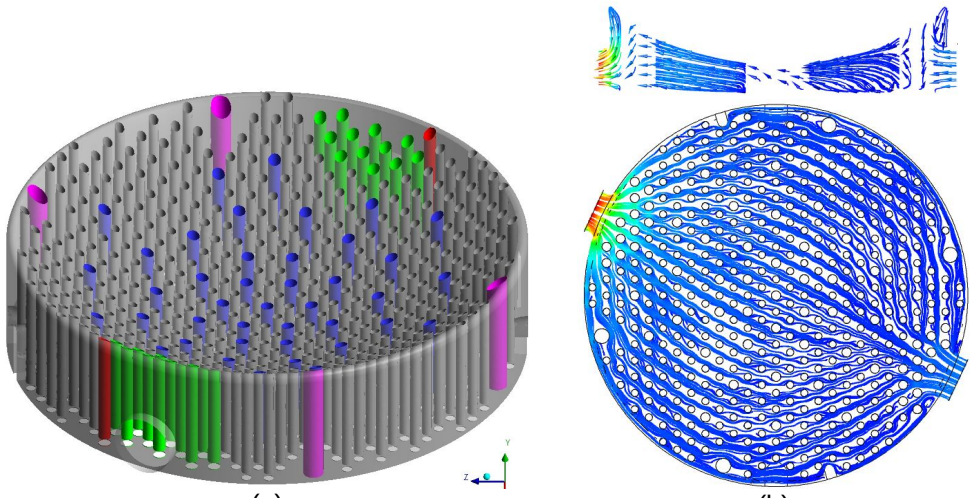

(a) (b)

Figure 35 – CFD analysis of Atucha-II upper plenum: a) computational domain; b) velocity field predicted for a pump shaft break scenario

4.2.7.2. Modelling issues

Modelling issues related to the UP flow are similar to those of LP, due to the presence of internals, such as control rod guide tubes and support columns in common PWR, coolant channel guide tubes in Atucha-II reactor etc.

Actually, far less complex geometry can be found in experimental facilities; for example, ROCOM UP is just an open volume without any internals.

4.3. Main steps of IVF CFD analysis

Many tasks of a CFD analysis aiming at the IVF investigation are common to any CFD study. It is rather obvious that such an analysis will generally require meshing, simulation set-up, solving, post-processing, etc.
On the other hand, each task requires several issues to be addressed, which may be related to the features of the specific problem under study, to the limitations in the capabilities of existing codes or in the state-of-the-art modelling approaches or in the computing resources, to the absence or non-completeness of adequate quality assurance procedures, etc.
Therefore, it is important to identify such issues and to discuss them analytically, so as to provide a sort of guidance on possible choices, necessary steps, expected problems, in connection with the current best practice.
This section aims at providing such guidance, taking advantage of the hands-on experience gathered and synthesizing the lessons learned from the code validation work performed as well as from the connection with the international scientific framework and in particular from that current which is pushing for the spreading and the acceptance of a BPG-based approach.
The result is a kind of “methodology” proposed for addressing the CFD investigation of IVF, especially for code assessment purposes. It has not the ambition to be fully comprehensive and exhaustive; nevertheless it is a starting point for establishing a quality assurance oriented approach.

The main steps of the IVF CFD analysis can be listed as follows:

1. definition of the objectives of the analysis;
2. definition of the computational domain;
3. creation of the 3D solid model;
4. meshing;
5. definition of BIC;
6. CFD simulations set-up;
7. CFD simulations execution;
8. CFD results analysis;
9. accuracy evaluation.

Such steps will be described and discussed in the next sub-sections. They are supported by the discussions on phenomenological aspects already addressed in Section 4.2.

4.3.1. Definition of the objectives of the analysis

The firs step is the definition of the objectives of the CFD analysis. This is necessary for efficiently planning the utilization of the available computing resources.

The CFD analysis may be carried out with the following purposes:

- demonstration;

- phenomena investigation;
- validation;
- application to safety/design issue.

A demonstration calculation (see section 1.4) aims at proving and testing the modelling capabilities, estimating computational costs, checking the feasibility of a certain analysis approach, without involving any accuracy evaluation. Such a calculation could indicate, for example, that a given mesh is not usable for performing a certain transient analysis since it is too fine and would require unaffordable computing resources; or, on the contrary, it may show that there is a margin for mesh refinement. This kind of application is (optionally) part of the code assessment process.

Simulations may aim at investigating the phenomena involved in an IVF, e.g. by providing a qualitative description of the flow distribution inside the RPV regions, or helping to identify locations where certain effects or phenomena occur (such as concentration of flow resistance, recirculation, stagnation, etc.). Such information would then provide guidance for further model or mesh improvement, or for numerical investigations at different scales (e.g. with system codes), as explained in Section 4.4. This kind of application does not require demonstration that the phenomena are “accurately” predicted (in quantitative terms), while confidence that the code predictions are qualitatively correct is necessary. Therefore, this use must be avoided unless the user has already achieved a “reasonable” level of confidence in the code predictions throughout a code assessment process (at least partial). In other words, the user must ask her/himself: “am I sure that the code predictions are physically plausible and realistic?”

If calculations are run for validation purposes, then the objective is rather clear, i.e. to understand if and to which extent the modelling approach adopted is capable of predicting the phenomena. This obviously requires the availability of reference data for comparison (either from experiments or real plant measurements), and implies a quantification of the mentioned capability (or – in other terms – quantification of the accuracy).
Within a validation study, normally several calculations are performed, possibly with different grids and adopting different models, numerical schemes etc., since this is necessary for assessing sensitivity of results on the possible options and choices and the calculation uncertainties. Therefore, computational resources to be allocated are likely to be far larger than for non-validation applications.

Finally, a CFD application may be directly addressing design or safety issues. For example, the results in terms of coolant properties perturbation at core inlet could be transferred as boundary conditions to a neutron kinetics analysis (either via an on-line or off-line coupling) to predict the core response. Another example of safety-related application is the use of the RPV wall temperature distribution predicted by CFD for structural mechanics verifications within a PTS analysis.
The obvious prerequisite of such a kind of use of a tool is that it has already been “sufficiently” validated, in the sense that the applicability to the specific problem has been proved and the numerical uncertainties are known.

Both validation and applicative calculations require accuracy and uncertainty evaluation. Then it is important to define, from the beginning of a numerical analysis, what the "target variables"[19] are, also because some modelling choices depend on them, and so do the settings related to results output.
As far as multi-dimensional target variables are concerned, such as perturbation at core inlet, no systematic methodology has been established yet for numerical accuracy and uncertainty evaluation, and this is an important limitation in the state-of-the-art. This issue is addressed in Chapter 5.

4.3.2. Definition of the computational domain

The CFD modelling starts with the definition of the computational domain. As explained above, the computational domain for IVF investigations aiming at predicting the coolant properties distribution at core inlet will necessarily include the RPV inlet region, the downcomer and the lower plenum.
The option of further extending the fluid domain will then have to be evaluated.

For instance the cold legs may be included, with the advantage that the effects of the CL flow on the IVF are accounted for. The domain inlet boundaries are moved farther and this certainly reduces the sensitivity of the results on the BCs, however the problem of accurately defining the BC still exists. The inlet boundaries may be located, in this case, at the MCP outlets: large uncertainty on the flow profiles must probably be expected there.

In case the thermal mixing associated with ECC injection is to be investigated, it is necessary to include also the ECC nozzles in addition to the CL, and to envisage the need of a local refinement during the meshing phase.

As regards the outlet boundaries, it is not common practice to set them just at the core inlet plate. In such a case, the number of boundaries to handle would be equal to the number of coolant channels, if each channel is accounted for separately; if a "porous medium" replaces the plate than there would be one outlet boundary only, but in this case the representation would be very unrealistic and difficult to justify.
The most common approach consists in defining a dummy outlet volume above the plate, in lieu of the core region. A description of this approach has already been provided in Section 4.2.6). It is worth remarking that the location of the outlet boundary should not influence the flow upstream of the core inlet, and sensitivity analyses must be envisaged to prove this.

As described above, the computational domain can be extended to include the core region and the upper plenum. In this case the core region can be modelled

[19] The expression "target variables" is introduced in the ECORA BPGs (Ref. [49]), in relation to the monitoring of numerical error. Here a more extended meaning is adopted: the target variables are the main results expected from the CFD simulation, for example the space and time distribution of coolant properties at the core inlet.

either with separate channels or with an open porous medium, ending up in both cases with the UP. The outlet boundaries will then be located at the connections between the UP and the HL (outlet nozzles). Such a domain extension can lead to a noticeable increase in the mesh size and then in the computational costs; therefore, it is justified only if the thermal fluid dynamic phenomena taking place in the core region and in the UP are relevant to the investigation, or if there is an influence on the upstream flow conditions.

Another possibility is to include the complete loops in the computational domain and thus to simulate the entire primary circuit. This means that the modelling will have to account for the pumps, the steam generators (or the components which replace the SG in a test facility) and the whole CL and HL.
Such utilization of CFD at a "system scale" is rather unusual; however, an interesting example is a CFD model that the Gidropress developed to simulate some GPMF experiments in the frame of TACIS Project R2.02/02 (Refs. [13] and [47]). In such application the MCP were not included in the domain, and an inlet and an outlet boundary was located respectively upstream and downstream of each pump; related inlet and outlet BC were appropriately linked to close the loops.

The computational domain also can be extended to include a solid domain to allow for a conjugate heat transfer (CHT) analysis. Namely, the RPV wall can be included with the purpose of solving the heat conduction equation in the metal, coupled to the energy balance equation solved for the fluid, in order to implicitly account for the convective heat transfer between the fluid and the solid.

4.3.3. Creation of the 3D solid model

A 3D solid model has to be developed before meshing. Commercial meshing tools such as ANSYS ICEM-CFD and GAMBIT include CAD modelling features for creating and modifying a geometrical model. However, they may be not suitable for handling complex geometries; therefore, the most common procedure consists in importing into meshing packages geometrical models generated with commercial 3D CAD packages (such as Autodesk® Inventor®, Pro/ENGINEER®, SolidWorks®, etc.)

CAD modelling is then a crucial phase of the CFD modelling. The level of detail of the geometrical representation has to be defined at this step. Obviously, the smaller are the details explicitly accounted for in the model, the smaller is the minimum size of the mesh cells and the larger is thus the total number of cells.

The typical geometrical details encountered when modelling IVF have been already mentioned in Section 4.2.6, and the most important ones are listed hereafter:

- inlet and outlet nozzles, with their diameter changes, fillets etc.;
- diameter variations in the downcomer;
- RPV-barrel spacers in the downcomer;
- LP internals:
    - sieves and mixing devices (with their small holes);
    - FA support columns (with their hollow and solid regions);

    - perforated shells and plates;
    - etc.;
- core region:
    - FA, with their fuel pins, spacers, boxes, throttles, etc.;
- UP internals

It is necessary to adopt a quality-oriented procedure since this very preliminary modelling step: the coherence between the reference data (usually drawings and reports) and the CAD model developed must be checked, and a track of the used reference material must be kept in order to allow for a complete referencing during the documentation phase.
Discrepancies between the CAD model and the reference geometry that result from specific modelling choices (e.g. geometry simplifications, or modifications aiming at sensitivity or optimization studies) must be described and justified in the documentation.

After a CAD model has been developed it is imported into the meshing tool using one of the existing standard formats. For example, two common formats for such data transfer are *iges* and *step*.
The geometry import process is a possible source of errors; therefore the imported geometry must be carefully checked before proceeding to mesh generation.

Some auxiliary work may be needed on the imported solid model before meshing: modification of some parts, subdivision of one item into more items, etc.

If a “modular approach” is adopted for meshing (see below), this may require that several solid models are developed and exported from CAD, each one representing a sub-domain. The use must assure the matching of the boundaries of different sub-domains which will have to fit together.

4.3.4. Meshing

The objective of this step is to develop one or more computational grids for the intended CFD analysis, that is – in other words – to define the spatial discretization over the computational domain.

This task must be addressed keeping in mind what requirements the mesh must have, i.e.:

a. being sufficiently fine to resolve the addressed phenomena;
b. having the highest achievable quality, and in any case not lower than acceptable quality parameters (see below);
c. being compatible with the computing resources available (memory, number of processors, time).

Regarding the item a, the definition of “sufficiently fine” mesh is rather arbitrary. The ideal target that should be always achieved is obviously the grid independence of the results; therefore a sufficiently fine grid would be such that further refinement would not bring any accuracy improvement. On the other hand it is well known that

such target is usually almost impossible to reach, at least for complex problems (like the investigation of IVF, for instance), since demonstrating the grid independence would normally require unaffordable computing costs. Then, "sufficiently fine" has, in the common practice, a more relaxed meaning, such as: "fine enough to capture the basic phenomena and provide realistic predictions – at least qualitatively – according to the user's experience, and, in any case, as fine as possible consistently with the resources available".

The BPGs provide useful guidance on mesh generation; in particular, they define the mesh quality based on a number of quantitative parameters that characterize the grid[20], and provide recommendations on how to generate high-quality grids. It has to be remarked that "quality" is both a generic term indicating the class of the above mentioned parameters, and one of those parameter, which has a mathematical definition and quantifies the distortion of an element with respect to its ideal shape. For example, the quality of a tetrahedral element is calculated as "the minimum ratio of height to base length of each side (normalized to 1)", while the quality of a hexahedron has some other mathematical definition involving Jacobian matrices and their determinants (Ref. [10]).

Concerning the item c, the computing resources always represent the most important limiting factor, together with modelling deficiencies, for accuracy.

Finally, the mesh will be the result of a compromise between the need to refine as far as required by an ideal discretization and the practical limitations in computing power and time.

Just to give an idea, the grids developed at UNIPI for IVF investigations have numbers of cells ranging approximately from four to twelve millions, and can take up to two or three weeks to run a slug mixing simulation with CFX code on the adopted 16-CPU cluster[21]. Obviously such values vary from case to case and cannot be taken as a reference for exact estimation of computational costs; however, they help figuring out how tough the task can be.

One important note regards the concepts of "nodes" and "cells" when talking about CFD mesh size. What actually determines the size of a grid, and the amount of information that has to be handled by the code during processing, is the number of control volumes defined by the spatial discretization[22]. The control volumes may or may not be the same as the mesh cells: this depends upon the specific code and the related numerical method implementation. For example, in CFX code – which is based on a hybrid finite volume / finite element approach (Ref. [10]) – the mesh elements and the control volumes do not coincide; on the contrary, a control

---

[20] In ICEM (Ref. [10]) such parameters are referred to as: *Quality, Aspect ratio, Determinant, Min. angle, Max orthogls, Max warp, Max warpgls, Skew*. User-defined quality parameters can also be introduced.

[21] Based on AMD Opteron® processors at 2.2 GHz.

[22] The assumption is made that the CFD code is based on a "finite volumes" approach, as happens in most cases. See Ref. [88].

volume is defined around each node, and is made of portions from each of the surrounding cells (Figure 36). In this case, the most significant quantity to define the mesh size is the number of nodes. The following empirical rule can be used to approximately estimate the number of cells from the number of nodes, and vice versa: in tetrahedral grids, the cells-to-nodes ration is 5; in hexahedral grids it is 1; in hybrid grids it will be something in between.
Another example is the French CFD code Trio_U, developed by CEA.

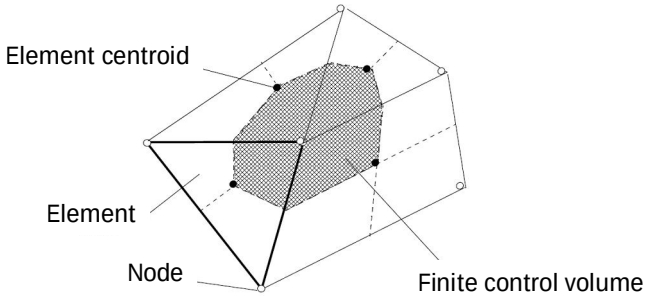

Figure 36 – Definition of finite control volumes from nodes and elements in CFX (2D example), Ref. [10]

In Fluent code, on the other hand, the control volumes coincide with the cells, so the related number is the one which better defines the mesh size.

4.3.4.1. Modular approach

A modular approach was adopted in the development of most of the grids used by the Author for IVF investigations. It consists in meshing separately the sub-domains in which the computational domain has been subdivided, and assembling the sub-meshes so obtained in a final mesh.
The advantages of this approach are the following ones:

- smaller electronic files are handled, thus visualization and pre-processing tasks result faster;
- different meshing strategies can be adopted for different sub-domains (i.e. hybrid grids are produced), so as to better adapt the mesh to different geometrical configurations;
- optimization or local mesh refinement studies become easier and faster, since one may need to replace just one sub-mesh instead of the entire mesh.

There are also some disadvantages:

- special efforts are needed to obtain conformal grids (i.e. such as no discontinuity results at the connection between adjacent sub-meshes); otherwise non-conformal interfaces will have to be accepted, with potential losses if accuracy and computational efficiency (see below);

- a larger number of electronic files have to be handled, which yields some additional complications in data management and quality assurance procedures.

4.3.4.2. Meshing strategies

The meshing normally starts with answering the question which kinds of mesh (tetrahedral, hexahedral or polyhedral elements) will be used.
Which type is better is usually an open issue, and strongly depends on the specific problem. In general, hexahedral grids are less prone to numerical diffusion than tetrahedral grids having the same number of control volumes, and for this reason hexahedral meshes are preferable. One important drawback related to the use of hexahedra is their anisotropic behaviour as regards the numerical diffusion: this effect is smaller when the flow is aligned with the principal directions of the cells, while it is larger for oblique directions. However, in a complex flow it is usually impossible to generate a mesh such that the alignment condition is respected, and then one will have to accept that the numerical diffusion effect will have an erratic behaviour over the domain. On the other hand, a tetrahedral mesh may be featured by a larger but more uniform numerical diffusion.

What actually drives the choice of the mesh type to adopt is the topology of a sub-domain, and the ease with which a hexahedral grid can be obtained.

A circular pipe (e.g. a CL) can be very easily meshed with hexahedra. For instance, it can be subdivided into “blocks” through an O-grid scheme (Refs. [11] and [88]); if a normal flow is expected, mainly oriented in the direction on the pipe axis, the cells can be imposed a large aspect ratio, so as to limit the overall mesh size; also the near-wall grid spacing can be easily controlled. Otherwise, a 2D grid made of quadrangles can be generated on a cross-sectional boundary of the pipe (either on a free or O-grid scheme), then a 3D grid can be obtained from an extrusion of the plane mesh along the pipe axis.

Meshing the RPV inlet zone with hexahedra is more complicate, as already discussed in Section 4.2.3.3. If a block-structuring technique is adopted (e.g. with ICEM) good skills are needed to deal with the fillet at CL-RPV connection and keep a high mesh quality at the same time.
Obtaining a tetrahedral grid in this region is straightforward, regardless of the meshing tools adopted, but the resulting number of cells will probably be much higher than the “budget” envisaged for such a simple geometry.

As regards the DC, it was already pointed out in Section 4.2.4.4 that obtaining a hexahedral grid is rather simple. It is practically as simple as generating a tetrahedral grid, but with a noticeably smaller number of cells, if large aspect ratios are used. However, the user must consider the effect that the aspect ratio may have in the presence of strong transversal velocity components (as in the case of pump start-up scenarios), and the role played by numerical diffusion (as discussed above).

With some effort, a good quality hexahedral mesh for the computational domain from the CL up to the DC can be produced. However, the job usually becomes much more complicate in the LP, where the topology features a greater complexity, and many more details have to be taken into account. Generating a hexahedral mesh of a LP with its internals is normally not a feasible task, unless simplified descriptions (porous media) are adopted for perforated shells and plates. See the related discussion in Section 4.2.5.2.
Several sub-domains can be identified in the LP itself, and different meshing approaches can be adopted for them. This was done for instance when developing grids for simulations of GPMF experiments (Ref. [81])

Most of the meshing difficulties are concentrated in the LP and in the RPV inlet region. In the core region and in the UP simplified geometry description is usually adopted, which makes the meshing much easier. Mesh extrusion can be used for instance to fill simple circular channels (e.g. ROCOM), or a dummy outlet volume. Rather coarse meshes can be used in these regions unless the detailed phenomena taking place there are considered relevant to the object of the investigation.

The result of the whole mesh generation process will usually be a hybrid grid, with hexahedra in some regions (e.g. CL, RPV inlet, DC), tetrahedra in other regions (e.g. in LP or parts of it), extruded prisms[23] somewhere else (e.g. core region).

It is worth mentioning the possibility of generating "polyhedral" grids. This type of mesh is a new feature of Star-CD code, and is claimed to be advantageous both from accuracy and computing efficiency point of view. However the Author has no experience on this type of mesh.

4.3.4.3. Managing interfaces

Once the sub-meshes have been generated, they must be assembled into a single mesh. This can be done with the meshing software, or directly importing the grids into the CFD pre-processor.
The CFX code, for instance, allows an easy management of the meshes within its pre-processing interface. Two adjacent grids will have to be connected together by means of an "interface". If the grids are conformal, then a "1:1" interface can be defined: in this case the two grids will be perfectly merged, and no discontinuity will result. On the other hand, if the grids are non-conformal, the interface will necessarily have to be of the "General Grid Interface" (GGI) type: in this case no matching is possible, then some interpolation is necessary to force the continuity of the solved variables; this process determines a slight increase in computing time and a possible loss of accuracy (that should be assessed by the user).

In order to avoid the use of GGI, one sub-mesh can be "forced", during its generation", to match an adjacent sub-grid at the connecting interface. Let us

[23] Two types of prisms can be present, in relation to their origin and function: 1) prisms inflated at the wall, for turbulence wall treatment; 2) prisms generated in the bulk by extruding 2D elements.

consider, for example, two portions of a circular pipe, one meshed with hexahedra and the other one with tetrahedra. The two faces to be connected will show quadrangles and triangles, respectively. Then the interface region can be modified by inserting a buffer zone made with pyramidal elements, to allow transition from hexahedra to tetra. Such operation can be performed automatically with a special tool available in ICEM. The result is a hybrid grid without any non-conformal interface.
However, this approach can bring benefits only if the local quality of the two connecting grids is relatively high: in fact, the buffer mesh will normally tend to degrade the quality, and thus to give a worse accuracy than if a GGI was used.

4.3.4.4. Mesh sensitivity analysis

Assessing the sensitivity of the target results on the mesh is a crucial task, as far as CFD is applied for validation or for safety/design analysis purposes. But, as discussed above, this may be really hard to achieve.
What the BPGs recommend, for estimating the error associated with the spatial discretization, is to perform systematic refinement studies, based on successive reductions of the cell size by a factor 2, on all three directions, which results in an increase of the total number of cells by a factor 8. This approach however is difficult to apply, and is in most cases inapplicable because of computing power limitations (since each step brings an increase by almost an order of magnitude).

The systematic refinement approach is suited for simple cases. When dealing with IVF investigation different flow phenomena and domain topologies are combined together, and this suggests that grid refinement studies should be performed locally, taking advantage of the modular meshing approach.
For example, one can develop several sub-grids for the RPV inlet region, without modifying the mesh in the remaining parts of the domain, in order to asses the sensitivity of the results on the mesh in that region. This approach is much more practicable and less expensive.

In any case, spending large efforts in mesh sensitivity studies is always necessary and beneficial. Even if the grid-independence of the results is still a target sometimes impossible to reach, it is important to have at least an idea about how far we are from that.

4.3.5. CFD simulations set-up

Most of the choices that the user has to take and that will affect the results are concentrated in the CFD simulation set-up phase.
Commercial CFD codes are always provided with powerful graphical user interfaces (GUI). The main advantage with them is that the simulation set-up can be really fast, since the GUI automatically guides the user through all the necessary steps, and includes many default settings, as well as debugging features to automatically check the consistency of the user's settings. The main disadvantage, on the other hand, is that the user has a more superficial approach to the code structure and the issues related to models closure, numerical schemes etc., and may not be induced to check whether the default settings are actually suitable for the intended analysis.

Normally there is also the possibility of a lower-level access to the code features. For instance, CFX allows translating all simulation settings (except the mesh information) into a sort of script, written on an ASCII file in the so-called "CFX command language" (CCL), Ref. [10]. The resulting *file.ccl* can be edited to change models, boundary conditions, numerical schemes. This obviously requires the user to know the related syntax, and in general to have a deeper knowledge of the code architecture.
Moreover, the use of GUIs may be not comfortable when handling large models (due for instance to graphical memory limitations, larger delays in display refresh etc.), while using CCL (or analogous options) usually allows speeding-up the work (at least for advanced users). Finally, handling "user-readable" scripts files instead of (or along with) non user-readable binary files has advantages also from the point of view of document management for QA purposes.
For the above reasons, the possibility of a more direct access to the core (e.g. via scripting languages) than usually offered by graphical interfaces constitutes an advantage and should be considered – to the Author's opinion – as best practice.

4.3.5.1. Choosing transient vs. steady state

In principle, any simulation of turbulent flow should be transient, due to the inherently non-stationary nature of turbulence. However, if statistical treatment of turbulence is used (i.e. RANS), steady-state simulation of stationary flows is allowed; obviously, it would not in the case of LES.
Normally, the IVF is stationary when the MCP are running at constant speed, such as in normal operation conditions. However, the possibility exists that, despite the steadiness of inlet flow conditions, a steady IVF cannot establish and some kind of large scale vortices, oscillations and instabilities occur (see below).
With steady pump operation and in the presence of a temporary perturbation of coolant properties (a deborated or over-cooled slug, or a tracer slug) the flow will either be unsteady (if the perturbation is associated with density effects, which alter the velocity field) or keep stationary (if no such feedback exists); in any case the "problem" is transient since there are non stationary phenomena.
With unsteady pumps operation the flow is obviously always non stationary.

Decision has to be made whether to use a transient or a steady-state solver. As mentioned in the BPGs, a distinction has to be made between real steady-state solvers, whose formulation does not include any time derivative, and pseudo-transient solvers, in which time has no physical meaning, but is used as an under-relaxation factor to improve the convergence (a solver of this type is available for instance in CFX).
An actual transient behaviour inherent in the flow may be completely cancelled by a steady-state calculation, or revealed by some convergence difficulties when a pseudo-transient scheme is used. This kind of behaviour must be kept in mind, and in particular the steady-state solvers should be used with due care (although their robustness and efficiency make them attractive). Sensitivity analyses in this regard are obviously always recommended.

Even in case of a transient problem, steady-state simulations can be useful for providing flow initialization for transient analyses.

4.3.5.2. Defining material properties

No particular issues emerge related to the definition of thermo-physical properties of the working fluid (density, dynamic viscosity, thermal conductivity, etc.) for the addressed IVF problems. A CFD code normally allows for a wide spectrum of possibilities: constant user-defined values (with the option of adopting default values), user-defined temperature-dependent correlations, imported tables (often available within the code libraries) etc.

Nevertheless, also this step must be subjected to the due quality checks, and appropriately documented. Moreover, it may be useful to envisage sensitivity analyses on the mentioned properties, e.g. to assess the influence of temperature on the phenomena investigated.

4.3.5.3. Turbulence modelling

Turbulence modelling is, as a matter of fact, the biggest issue. A thorough discussion on turbulence model selection is already included in the BPGs, and an extensive assessment work was done within the FLOMIX-R Project (see Section 3.6.5) which pointed out capabilities and limitations in the current turbulence models available in CFD codes. A thorough description of turbulence models can be found in Ref. [89].

To synthesize, the use of RANS approaches[24] can be considered "acceptable" for IVF investigations, unless the time-scales of largest turbulence structures are comparable to the time-scale of the main flow (in which case the LES-type approaches become indispensable). In particular, momentum-driven flows are successfully handled with two-equation models ($\kappa-\varepsilon$ and/or $\kappa-\omega$ based), while 6-equation second closure moment (SCM) models are more suitable for simulating buoyancy-driven flows (Ref. [20]). It is not clearly explained what the best practice is in case of mixed regimes.

Actually, the above conclusions have some weakness, which reveals lacks still existing in the state-of-the-art as regards the model and code assessment process. Basically, the above judgement relies more on qualitative and semi-quantitative analysis of the CFD results and of their discrepancies with respect to experimental data, than on a systematic quantitative assessment of the accuracy (although a noticeable progress came from the FLOMIX-R Project in this sense). Statements such as "the numerical results are in good agreement with the experimental data" are seldom supported by a quantification of such agreement. This topic is further discussed in the Chapter 5.

Coming back to the CFD simulation set-up, the best that a user can do – given the state-of-the-art limitations and capabilities – is to select RANS models among the

[24] Especially their transient formulations (referred to as T-RANS or U-RANS).

most advanced ones available, always plan sensitivity analyses and, if possible, switch to scale-resolving approaches such as LES or LES/RANS hybrid models[25]. For example, the shear stress transport (SST) model available in CFX (Ref. [10]), a two-equation model which is a sort of blending between $\kappa-\varepsilon$ and $\kappa-\omega$, has often shown the best performance for momentum-drive IVF. As regards LES-type approaches, the Author is not in the position to refer to applications of his own; what can be said here is that those models have an intrinsic capability to resolve the unsteady nature of turbulence (at least above certain scales). However, the penalty is that much finer grids and longer computing times are needed and that this approach opens issues still existing in regard to the sub-grid turbulence modelling and the turbulence wall treatment.

A last note regards a model limitation of which a direct experience was gained during the validation work performed in the frame of this research. Namely, the CFD simulations run using two-equation eddy-viscosity models ($\kappa-\varepsilon$, SST, etc.) have often shown a tendency to under-predict the turbulent diffusion (i.e. the turbulence mixing effects), as already shown in Section 4.2.4.5, and it can be hoped that switching to LES will bring improvements in accuracy of code predictions.

4.3.5.4. Defining additional balance equations

In a basic CFD simulation of a 3D turbulent flow the equations solved are: the mass conservation (1 scalar equation), the momentum balance[26] (3 scalar equations), and the transport equations for the turbulent variables that are the unknowns of the selected model (e.g. κ and ε, or κ and ω, or the 6 independent component of the Reynolds stress tensor if a SCM model is used, etc.)

However, an IVF investigation will most probably involve the presence of some transported scalar quantity, such temperature or tracer concentration; therefore an enthalpy balance equation or a generic scalar transport equation will be included too.

4.3.5.5. Defining initial conditions

A transient analysis requires initialization of the solved variables all over the computational domain.

In case of a pump start-up scenario, the velocity field is easily initialized by imposing a zero value everywhere, since all pumps are initially switched off. If also a scalar (temperature/concentration) is solved for, then it will require initialization too. If, for example, there is a slug accumulated somewhere in the domain (normally in a CL), a sub-region will have to be defined so as to impose a different value than in the rest of the domain. There are generally two possible ways to do that: either a sub-domain is defined, with its specific initialization independent on

---

[25] Such as, for instance, Detached Eddy Simulation (DES) and Scale Adaptive Simulation (SAS). See Ref. [10] for further information.

[26] Also known as the Navier-Stokes equations.

the rest of the domain, or the given variable is expressed as a function of spatial coordinates.

In case of a steady pump operation scenario, the initialization cannot be made algebraically; rather the stationary flow field must be calculated with a preliminary steady-state calculation, the results of which will be read during the pre-processing phase. The initialization calculation is run either with a steady-state solver (see above) or with a transient solver combined with constant boundary conditions; in the second case, the simulation is obviously run until the flow field reaches complete stabilization.

A steady-state calculation, in turn, needs initialization too, as any numerical solution scheme. However, in this case the initial flow field, in principle, does not need to be realistic: the solution scheme will actually converge to the solution regardless of the initial guess solution. Nevertheless, the closer is the initialization to the actual flow field, the faster will be the convergence.

4.3.5.6. Inlet boundary conditions

The definition of inlet BCs is a critical point because it directly deals with the balance of the extensive variables that must be conserved (mass, momentum, energy, etc.)
The consistency between the BCs and the analogous conditions on the reference experiment or real plant transient is a necessary condition for getting realistic and accurate predictions. This is quite obvious to any CFD user; nevertheless the systematic check of BCs before a CFD calculation is launched is not always addressed as an essential step for quality assurance.

Some general guidance is provided by the BPGs on BC definition, as well as some indications based on the experience from the FLOMIX-R Project. Some useful guidance may be provided also by the user guides of the CFD codes themselves. For example, the CFX manual (Ref. [10]) gives a sort of rating (in terms of robustness) of the possible configurations for inlet/outlet conditions; the most robust configuration is “velocity/mass flow rate at inlet” and “static pressure at outlet”.

As already mentioned in Sections 4.2.1.1 and 4.2.3.4, the definition of the inlet boundary conditions for an IVF CFD analysis must address flow velocity (or flow rate), turbulence, and transported scalars (temperature or species concentration), wherever the inlet boundaries are located (RPV inlet/outlet nozzles, MCP outlet).

<u>Velocity</u>
As regards the velocity, the easiest choice is to define a uniform inlet profile. In all practical cases this is an approximation of the reality that may introduce noticeable errors in the solution, since the velocity profile through the cross-section of a RPV nozzle can be expected to be much closer to a developed turbulent pipe flow. On the other hand, experimental information on the velocity profile is usually missing. Then, the best practice consists again in accounting for such uncertainty by sensitivity analyses with respect to the inlet boundary location and to the velocity profile.

Non-uniform profiles can easily be implemented either via mathematical correlations (e.g. as a function of the distance from the pipe axis, using the well-know "1/7th power law") or importing a fully or partially developed flow profile from the results of a separate pipe flow CFD simulation.
So, a good practice can be running (at least) two calculations, one with uniform velocity profiles and one with developed profiles (obtained as described above): this will provide indications on the results sensitivity on this parameter.
If the computational domain includes the cold legs, such sensitivity is expected to be lower than in case the inlet boundaries are closer to RPV.
The issue related to inlet velocity profile arises also when the inlet boundary constitute an interface with the computational domain of a one-dimensional system code (e.g. RELAP, CATHARE, etc.), in the frame of a coupled-code analysis: in such a case, no information is provided by the "external" code to the CFD model on the spatial profiles, and it must be introduced somewhat arbitrarily by the user.

One last remark about velocity profiles regards the time-dependence. In transient flow scenarios the flow rates (and thus the velocities) are functions of time; related information is normally available from experimental or plant measurements. The implementation of time-dependent inlet velocities in a CFD simulation set-up is usually a straightforward task, performed – for instance – with the help of user-defined functions which interpolate imported external data. This obviously involves some additional pre-processing steps that must be subjected to due quality checks, to avoid (or to control) the possible introduction of errors and uncertainties.

Turbulence parameters
The definition of inlet turbulence parameters is less "intuitive" and brings additional uncertainty. Turbulence is even more sensitive to the upstream flow conditions than the velocity profiles; moreover, experimental information is almost always missing.
Rough estimates of the turbulence kinetic energy (κ) and its dissipation rate (ε) can be obtained through the correlations provided by the dimensional analysis (on such recipes are based the defaults settings available – for example – in CFX code, Ref. [10]).
However, such estimation procedures are based on arbitrary assumptions of the flow type (i.e. fully developed pipe flow) and on the turbulence intensity (e.g. 1%, 5% and 10% are the pre-defined levels available in CFX as "Low", "Medium" and "High" intensity, respectively).
Again, the best that the user can do to deal with this sort of uncertainty is to perform sensitivity analyses (as insistently recommended by the BPG).

As for the velocity, also the turbulence parameters can be assigned in input either as uniform or non-uniform profiles. In the second case, the profiles are normally the results of previous pipe flow CFD simulations.

Temperature and concentration
Inlet conditions in terms of temperature or concentration may be used to define the presence of a perturbation in coolant properties. For example, in both ROCOM and GPMF experiments a salt tracer is injected into one loop (or a slug is accumulated in the loop before the transient starts), and the tracer passage is revealed by

sensors located close to the RPV inlet: on such information is based the definition of post-test simulations. Similarly, boundary conditions can be defined for UPTF or University of Maryland mixing experiments in terms of temperature.

The cross-sectional profiles of concentration or temperature distribution, however, may be affected by strong non-uniformities, due to the presence of thermal stratification phenomena as well as imperfect mixing of an injected solution. Such non uniformity can be expected to influence the IVF analysis results, and therefore an accurate characterization of inlet boundary conditions is of major importance. On the other hand, presently only the ROCOM facility, with its wire mesh sensors, can provide accurate information on the tracer space and time distribution at RPV inlet (as already mentioned in Section 4.2.1.5).
With some pre-processing, based on user-defined interpolating functions and expressions, such detailed information can be implemented in a CFD simulation set-up. This was done – for example – in CFD simulations of ROCOM experiments (see Section A.1, and Ref. [32]), with substantial improvements in the results with respect to simulations in which uniform tracer profiles had been imposed (see example in Figure 37).

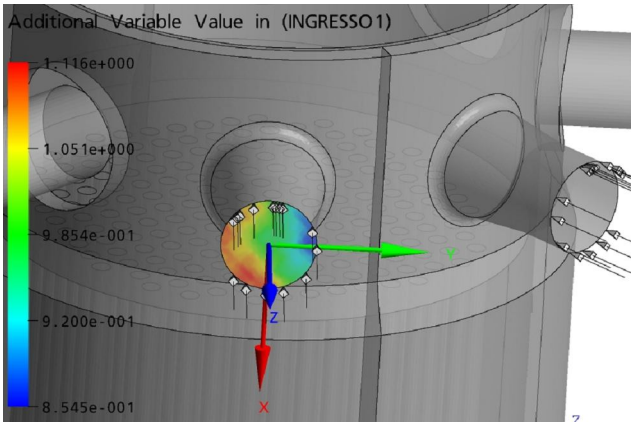

Figure 37 – Non-uniform concentration profile at inlet boundary in a ROCOM test

4.3.5.7. Outlet boundary conditions

For reasons of robustness (see above) the outlet boundary conditions are normally pressure-controlled. This means that a relative or absolute static pressure is imposed at outlet boundaries; in particular, either a uniform pressure profile is imposed, or a surface-averaged value is imposed (so as to allow for some non uniformity implicitly resolved by the code).
To limit the related numerical uncertainties, the best practice is to locate the outlet boundaries where the pressure profile is actually expected to be uniform; otherwise, enforcing a non-physical profile would have an impact on the upstream flow distribution.
If the UP is included in the domain, then the outlet boundaries are located at the outlet nozzles or even farther on the HL; in this case the uniform pressure profile assumption is normally acceptable. On the contrary, if the UP is not included and a dummy outlet volume is defined in the core region (as described in Section

4.2.6.3), then the outlet boundary position may be critical, and sensitivity analyses are necessary to check that it is not affecting the upstream flow.

Outlet conditions may have to be defined at inlet nozzles in cases in which inverse flows develop in some idle loops. This happened for instance in some pump start-up experiments performed in ROCOM and GPMF. In such cases two situations may occur, depending on whether the flow rate through the boundary is known or not. In the first case, the boundary condition is defined in a similar was as an inlet condition (except for the direction of the flow). In the second case, it is simply a pressure-controlled outlet condition, but some provision is needed to account for the flow resistance of the loop (which is not included in the computational domain); this can be done by defining some additional pressure loss concentrated on the boundary, the value of which has to be estimated in some way. The latter situation was encountered during the pre-test analysis of some GPMF tests, and obviously prone to the introduction of large uncertainties.

4.3.5.8. Wall boundary conditions

The wall BCs basically address the momentum transfer and the heat transfer (if present), with some possible corrections to account for the turbulent boundary layer.

A no-slip condition is always used to impose a zero velocity at the wall. Then problems related to the turbulent boundary layer arise. If the mesh in the near-wall region is sufficiently fine to resolve the boundary layer[27], then no additional condition is needed, but the used turbulence model must be appropriate for low-Reynolds conditions. On the other hand, if the mesh is too coarse to resolve the boundary layer, then a "wall function" has to be used, i.e. a special boundary condition that forces the shear stress in the first cell to a value given by an empirical correlation known as the "logarithmic wall law" (Refs. [10] and [88]).
The standard formulation of the "wall function", which is available in some commercial CFD codes, requires the $y+$ parameter to be in the range $10 \div 200$, otherwise this boundary condition is no longer valid. The existence of a lower limit is a strong limitation, since it precludes systematic mesh refinements.
For this reason more advanced wall functions have been developed that allow a smooth transition from the standard wall function to a low-Re formulation.
The use of the advanced formulations (e.g. "Automatic" and "Scalable" wall treatment available in CFX, associated with SST and $\kappa-\varepsilon$ models respectively) is recommended by the BPGs.

The mentioned wall functions include also the possibility to account for the wall roughness: this parameter appears as an additional term in the logarithmic law, which determines an increase in the wall shear stress. However the use of such correction is not well established and still needs validation efforts. Then it has to be used with due care, maybe as a sensitivity parameter. Moreover, the user must

---

[27] This condition is achieved when the non-dimensional distance of the first node from the wall is $y^+ \approx 1$.

check that the mesh size does not drop below the wall roughness otherwise the wall function looses its validity.

In the presence of temperature (i.e. if the enthalpy balance equation is solved), also a thermal BC must be specified at wall. It will be a fixed temperature, an imposed heat flux, or a convective heat transfer coefficient.

4.3.5.9. Spatial discretization

The discretization of the spatial variables is defined by the mesh itself. Then the user has also to select a differencing scheme for advection terms in the solved equations (in particular the Navier-Stokes equation).
As a general rule, low-order schemes are associated with greater robustness, easier convergence but greater numerical diffusion; on the other hand, higher-order schemes are more accurate but less robust and more prone to instabilities, unboundedness, etc. (Ref. [88]).

The schemes available in CFX for a RANS application are named “Upwind” (UW) and “High Resolution” (HR). The former is a first-order scheme; the latter makes a local blending between the UW scheme and a second-order Upwind-type scheme, based on local boundedness criteria.
The usual recommendation is not to use first-order schemes because they introduce too numerical diffusion. Nevertheless, many IVF investigations performed by the Author have encountered a tendency to instability, poor convergence and unphysical predictions when HR scheme was used instead of UW.

The conclusion from the above is that the identification of the most appropriate scheme may be not univocal, and the Author’s recommendation is to include always a sensitivity analysis on the discretization scheme and to treat the related discrepancies as a source of uncertainty, unless a demonstration exists that a given scheme in a given code is giving the best results for a specific problem

4.3.5.10. Time discretization

General guidance provided by the BPGs regarding the selection of time advancement schemes is exhaustive.
A second-order backward Euler scheme is set in CFX as a default; a first-order scheme is available too, but it should be normally avoided. An exception can be the solution of a scalar transport equation: it was observed than using a second-order scheme (for that particular equation) can lead to violations of the solution boundedness, due to local overshoots that, on the other hand, are smeared out when first-order is used (with some additional numerical diffusion introduced, though).

Either a fixed time-step or an automatic time-stepping algorithm can be used. In the first case, the choice of a time-step that is sufficiently small to resolve the relevant time scales of the transient is up to the user, and is thus based on physical considerations. In the second case, the user defines an initial time-step, the

minimum and maximum allowed time-step, and the criteria[28] to decide whether and by which ratio the time-step must be decreased, increased or kept constant; the code automatically decides every *N* time-steps, where *N* is user-defined too.

According to the Author's experience with CFX code, the adaptive time-stepping is usually advantageous because it allows optimizing the time-step so as to minimize the total number of iterations and thus the computing time.
In any case, the time-step should always be addressed in sensitivity analyses, as recommended by the BPGs.

4.3.5.11. Source terms

Source (or sink) terms may be necessary to account for additional production/dissipation of heat or momentum that could not be included explicitly owing to modelling simplifications.
A typical example is represented by the so-called "porous media" often adopted in LP or core region modelling (as already described in Sections 4.2.5.3 and 4.2.6.4); in such cases the geometry simplification always removes flow resistance effects, which have then to be compensated by some artificial pressure losses. This is done by defining momentum sink terms.
As discussed above, arbitrary information is introduced in this way, which should be supported by experimental information and sensitivity analyses.

Source terms can be defined also to account for heat generation from physical phenomena that are not described by CFD models; for instance, volumetric heat source terms can account for the power deposited in the moderator by gamma and neutron radiation.

4.3.5.12. Convergence control

Convergence control is normally done by defining a minimum acceptable threshold for the root mean square of residuals from solved equations. Fixing a convergence target of 10^{-4} (i.e. reduction of residuals by at least four order of magnitude) has almost become a "standard" approach, since it has been observed that such convergence level is satisfactory for most engineering applications. However, convergence behaviour can noticeably vary from case to case, and the user should always assure that the achieved convergence is satisfactory for the specific problem addressed.
A more rigorous approach to the convergence control for a steady-state analysis should, whenever possible, satisfy the following conditions:

A. consistently with the available computing time, the convergence is pushed as far as the "asymptotic region" is reached: this guarantees that the iteration error, for a given simulation, has been reduced to the lowest level

[28] A criterion can be, for example, based on the number of inner iterations needed for the last time-step to converge: the time-step will be reduced, or increased, if such number is larger or smaller than user-defined limits (e.g. 5 and 2, respectively).

achievable; an example is shown in Figure 38, reporting the RMS residuals for some solved variables in a two-phase flow simulation[29];

B. the solution has stabilized with respect to the iterative process, i.e. the solved variables do not show any further appreciable variation with new iterations (or pseudo time steps); this can be easily controlled with the help of some "monitor points" located over the domain (Figure 39);
C. the imbalances of the quantities that must be conserved (mass, enthalpy, etc.) have become negligibly small (Figure 40).

Looking at the three following figures, it can be noted that the 10^{-4} RMS target is reached in around 50 iterations, while 300 iterations are needed to stabilize the monitored variable and 500 to reach the asymptotic region. This gives an idea of the increase in the computational costs if such demanding convergence criteria are applied.

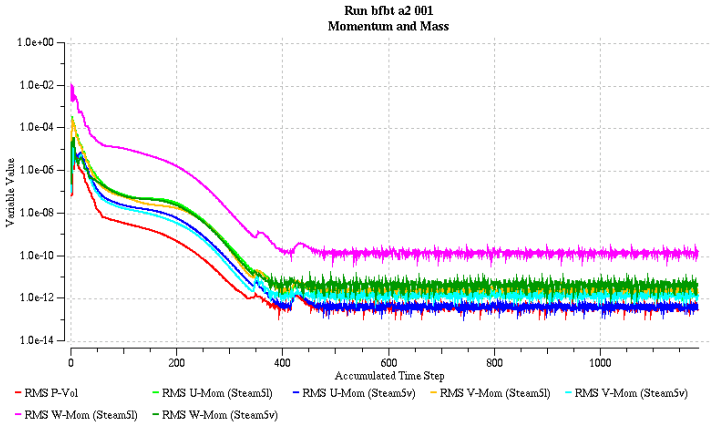

Figure 38 – Convergence control: reaching the "asymptotic region"

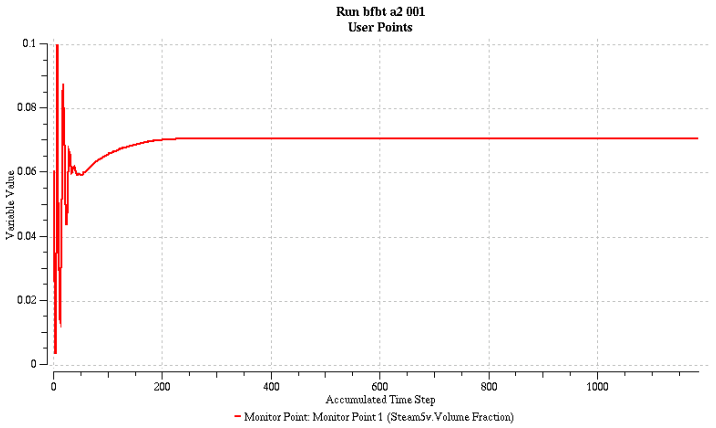

Figure 39 - Convergence control: stabilization of the solution

[29] Simulation of the boiling flow in a BWR FA simulator, performed in the frame of the OECD BFBT Benchmark, see Section 1.2.

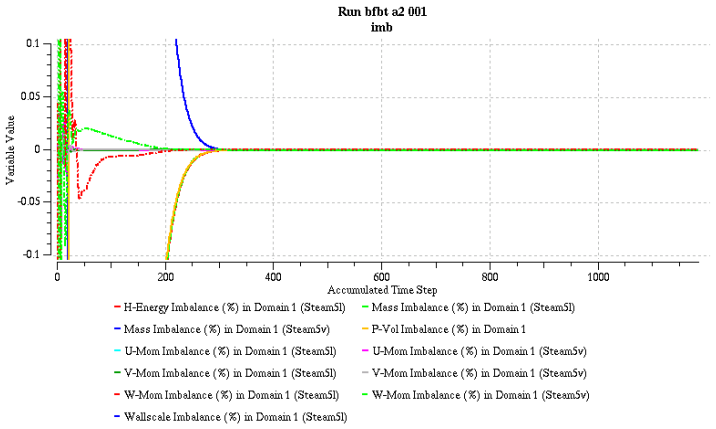

Figure 40 – Convergence control: checking imbalances

In a transient analysis the problem of controlling the convergence exists for each time-step, then adopting the above approach may be prohibitive. Therefore, a target criterion will simply be defined in terms of residuals. The target level, in turn, must be as low as possible, and at the same time it must be above the asymptotic region, otherwise the iterative scheme will proceed until the maximum number of iterations is achieved.
Convergence targets in the range $10^{-5} \div 10^{-4}$ have been used for most IVF investigations performed by the Author.

4.3.5.13. Results storage

A common problem that a CFD user usually must face is the need to limit the size of the results files produced, both because of hardware and software limitations. When dealing with transient simulations of relatively big problems (millions of computational nodes) it is rather usual that tens or hundreds of gigabytes are produced.
To limit the space needed for storage, the user must select – before running the simulation – which solved variables have to be stored and with which frequency (e.g. after each group of *N* time-steps).
The variable selection must be done carefully, having clear in mind what information is needed for post-processing, since disregarded information is totally lost and cannot be retrieved unless a new simulation is run.

A powerful means for monitoring and storing results is represented by the so-called "monitor points": the calculated values of selected variables at given locations can be stored on ASCII files, as "virtual" sensors placed in the flow. This can be done, for example, to register the time history of coolant properties at the inlet of each coolant channel during the transient.
Defining monitor points at the same locations where the temperature or electrical conductivity transducers are placed in an experimental facility, allows a direct comparison between calculated and measured data.

The resulting electronic files have negligible size compared to those that contain calculation results over the whole domain.
Normally, the monitor points are defined through their Cartesian coordinates, which can be input manually by the user, imported via ASCII files, or automatically generated by user-defined algorithms implemented in the code via the scripting languages supported by the code (e.g. the above mentioned CCL).
This technique is widely adopted to track velocity, concentration, temperature etc. at all the relevant locations during an IVF analysis.

4.3.5.14. Sensitivity analyses

Planning sensitivity analyses is an important task, which should be performed before starting the simulations, with the purpose of assessing the uncertainties and estimating numerical errors. Many parameters and modelling choices requiring sensitivity analyses have been identified in the previous sections. They can be summarized in the following (probably not exhaustive) list[30]:

- computational domain:
  - level of detail of geometrical description:
    - effect of CL elbows;
    - effect of fillets at CL-RPV connection;
    - porous media vs. perforated plates or shells;
    - etc.
  - location of inlet boundaries;
  - location of outlet boundaries;
- mesh:
  - mesh type;
  - mesh size (bulk);
  - mesh size (near-wall);
  - interfaces;
- numerical model:
  - transient vs. steady-state solver;
  - material properties;
  - turbulence model;
  - initial conditions;
  - boundary conditions:
    - inlet velocity profiles;
    - inlet turbulence parameters profiles;
    - inlet temperature/concentration profiles;
    - type of outlet BC;
    - wall roughness;
    - turbulent wall function;
  - momentum/heat source terms;
  - spatial differencing scheme;
  - time advancement scheme;
- parallel solving:

[30] Obviously, most of them are explicitly recommended by the BPGs.

- number of processors;
- partitioning algorithm.

It is evident that the computational cost of such an extensive approach to the sensitivity analysis could be prohibitive. Moreover, the number of sensitivity cases is even larger if different combinations of the possible options are tested, e.g. if each of the selected turbulence models is applied with each of the selected meshes. Therefore, the user will normally select only a few of the possible sensitivity analyses, addressing those features which are expected to have a greater influence on the results (e.g. the mesh, the boundary conditions, the turbulence model, and the numerical schemes).
An attempt to perform systematic sensitivity analyses to IVF CFD investigations was made in the frame of the FLOMIX-R Project; however no such an extensive application as described above have ever been carried out, and this – to the Author's opinion – constitutes a weak point in the overall CFD code assessment process.

A further limitation is related to the lacks in the available approaches to the quantitative analysis of the results (see Chapter 5), which is a crucial point since the sensitivity analyses actually aim at quantifying uncertainties. In other terms, the outcome of a sensitivity analysis should be some statement such as «*variations of the parameter A within a range* Δ_A *determines variations of the output variable B within a range* Δ_B», while most common statements are more similar to «*sensitivity analyses on the parameter B showed small influence on the parameter A*».
The obstacles rely in the fact that the target variables consist of distributions over time and space, and it is difficult to define integral and global quantities characterizing the target variables.

4.3.6. CFD simulations execution

The pre-processing phase usually ends up with the generation of a "definition file" (as it is called in CFX language), i.e. a binary file which includes all information related to the computational grid as well as the modelling. If the above mentioned CCL files are used in defining a CFX simulation, then they are finally merged into the definition file. The definition file is directly fed as input to the solver programme, either in batch mode or via a GUI.

No particular consideration or recommendation is necessary for this phase of the analysis, apart from the obvious need of a quality-oriented attitude, based on which all files are handled within a well organized frame, all actions are registered and everything is appropriately documented.

4.3.6.1. Parallel calculation issues

In most cases an IVF simulation will be a parallel calculation run on a computer cluster, simply because a personal computer, or even a workstation, does not provide sufficient computing power and memory to handle such a big problem in reasonable time.
Therefore, before the run is launched, a domain partitioning step is necessary. For that purpose, automatic algorithms are normally available in CFD codes, which are

able to optimize the partitioning in order to reduce the interfaces between the partitions, and thus the latency time needed for data transfer between partitions. There is not much that the user can do in this phase, except testing different partitioning algorithms to assess their possible influence on the results and on the numerical performance (efficiency, convergence, etc.)

4.3.6.2. On-line results monitoring

Monitoring the results during the calculation execution is necessary to check whether the solver is actually converging to a plausible solution. This can be done, for instance, by saving temporary results files and visualizing the results with post-processing tools. A qualitative judgement will thus be made on the evolution of the calculation.

Quite useful to this purpose are also the above mentioned monitor points, which can help checking whether the velocity has stabilized (in a steady flow scenario), or if a perturbation is reaching a certain location as it would expected to do, etc.

The obvious recommendation is that the user be “active” during the calculation in monitoring and checking the solution evolution, especially in order to timely stop an ill-defined simulation, or to change the under-relaxation parameters.

4.3.6.3. On-line convergence monitoring

The important considerations regarding the convergence control and monitoring have already been reported in Section 4.3.5.12.
It is worth remarking that the user must attentively follow the simulation and checking the convergence behaviour, particularly the trend of the residuals, the stabilization of the monitor points, and the imbalances. Anomalies in the solution stability and convergence may thus be timely revealed, so as to allow stopping a badly defined simulation and saving computing time.

4.3.7. Results post-processing and analysis

The post-processing includes all those operations that are necessary to translate the calculation output (results files) into information understandable and usable for results analysis.
Such information consists of:

- pictures showing 3D and 2D distributions of solved variables (either vector or scalar);
- animations (movies) of 3D and 2D distributions of solved variables;
- time-history plots of scalar quantities;
- values of local, integral or global quantities.

4.3.7.1. 2D and 3D plots

Via graphical post-processing pictures, plots and animations are produced. This is mostly done by the GUI of visualization tools available with a CFD code (e.g. the CFX-Post module of CFX).

When processing results of an IVF simulation, the following items are usually produced:

- contour plots of 3D fields (velocity magnitude, velocity components, pressure, concentration, temperature, κ, ε, etc.) over the whole domain or single sub-domains, at selected instants;
- contour plots (of the above variables) on 2D boundaries, interfaces, or user-defined surfaces (e.g. cross-sections), at selected instants;
- velocity streamlines starting from inlet boundaries and crossing the whole domain, at selected instants, coloured by velocity magnitude, or concentration, etc.;
- velocity vectors over the whole domain, at selected instants;
- movies animating the above plots evolution during the transient.

The main purpose of the above plots is to visualize the flow distribution and the relevant flow structures, as well as the space distribution of a perturbation, both over the whole domain and at some specific regions (RPV inlet, DC, LP, core inlet).

Actually, the visualization tools available in the commercial CFD codes nowadays are very powerful and make the production of beautiful and impressive pictures and movies an easy task. They represent a useful support to the qualitative results analysis, but must always be considered only a preliminary step, and not an objective of the CFD analysis.

4.3.7.2. 1D plots

The information gathered by monitor-points (Section 4.3.5.13) can be easily displayed with 1D plots showing the time-history of a given variable at a specified point.
For example, the tracer concentration or the flow velocity can be plotted at the inlet of selected channels, at inlet nozzles or in the downcomer.

With some additional post-processing, the azimuthal distribution of the velocity in the downcomer can be plotted at selected instants.

4.3.7.3. Results analysis

The analysis of the results consists of two main steps: the qualitative analysis, and the quantitative analysis.

The qualitative analysis is based on the above plots and aims at:

- checking that the solution obtained is physically plausible and realistic, based on a sort of “engineering judgement” that is – as such – subjected to some arbitrariness and influenced by the experience of the analyst;
- recognizing and identifying the structures and patterns characterizing the flow distribution and the morphology of the perturbations;
- comparing the above information with experimental data (if available) to assess whether the CFD simulation has captured the relevant phenomena, at least or partly.

The quantitative analysis aims at:

- characterizing the numerical solution (particularly, the target variables) with a number of relevant quantities;
- comparing the above quantities with corresponding experimental values (and related uncertainties) in order to quantify the accuracy of the solution.

As already mentioned in Section 4.3.5.14, the quantitative analysis of three-dimensional results of a CFD analysis is rather problematic and not yet supported by well-established methodologies. The next Chapter is entirely devoted to this issue and proposes some new ideas for the accuracy quantification, as far as the space and time distribution of coolant properties at core inlet is concerned.

4.3.8. Coupling

The activity performed in the frame of this research did not directly address coupling issues; therefore the limited experience achieved does not permit a thorough discussion. Nevertheless some general considerations can be made here to provide a more complete picture of the issues encountered in IVF investigation.

In particular, some situations are indentified that may need some data exchange between a CFD code and a different type of numerical analysis tool.

4.3.8.1. Data transfer between CFD and TH-SYS codes

A situation where a CFD and a system code are coupled for an IVF investigation has already been envisaged in Section 4.2.3.5. Namely, the CFD provides a zoomed-in view on the RPV flow, while the system code analyzes the behaviour of the whole system (the RPV being either modelled also in the system code nodalization, or only by the CFD). An advantage of such a coupling approach is that the loop-to-loop mixing can be taken into account in case some perturbation is affecting a loop, and the information related to the coolant distribution over the core channels and the coolant properties distribution at core inlet can be directly fed to the TH-SYS code.

Interfaces connecting the CFD and the system domain will most probably be located at the inlet and outlet nozzles of the RPV. Apart from the issues related to message passing and to the numerical coupling between the solvers, the problem how to translate 3D CFD data to 1D data, and vice versa, must be addressed. This implies some loss of information in the former case, and the need to introduce some arbitrary information (e.g. on cross-sectional velocity and turbulence profiles) in the latter case.

Moreover, interfaces at the core inlet can be used to transfer information of the coolant flow rate and properties distribution from CFD to system code, while interfaces along the coolant channels can be used to model the convection heat transfer and transfer information on heat flux from system to CFD.

Another option to account for the heat transfer is the definition of volumetric heat source terms in the coolant channels of the CFD model.

4.3.8.2. Data transfer between CFD and neutron kinetics codes

The main purpose of the predictive analysis of in-vessel mixing is to provide boundary conditions for neutron kinetics analysis and obtain a best estimate of the core response following a perturbation of coolant properties. Therefore, a coupled code analysis can be envisaged with an interface at the core inlet, and information being transferred from CFD to a neutron kinetics code.

Another possibility is the transfer of information on time and space distribution of a poison concentration in the moderator. An example is represented by an analysis carried out at the University of Pisa[31] involving the CFD simulation of borated water injection and mixing into the moderator tank of Atucha-II PHWR, and the transfer of information on boron distribution to the NK analysis (Ref. [4]). Such data transfer, however, was performed off-line, without a real software coupling.

4.3.8.3. Data transfer between CFD and structural mechanics codes

PTS analysis requires that the temperature distribution through the RPV wall is estimated and fed to the structural mechanics analysis of stresses and strains (for the subsequent fracture mechanics analysis). The critical aspects for modelling are the mixing phenomena and the heat transfer between coolant and RPV wall; both can be accounted for in a conjugate heat transfer (CHT) analysis performed with a CFD code (since practically all CFD codes can solve the conduction equation in a solid domain). The CHT analysis may be coupled to a structural mechanics code which uses the temperature distribution as a boundary condition.

The CFD analysis may not involve the direct coupling to the solid conduction problem: in such a case the temperature distribution through the RPV wall is calculated by the structural mechanics code, and the heat transfer coefficient between the coolant and the RPV wall must be input by the user because it is not predicted by the CFD code any longer.

[31] The related CFD analyses being performed by the Author.

4.4. Role of CFD in support to TH-SYS code application and validation

One of the achievements of this research is the demonstration of the role that CFD can play as a support to the thermal-hydraulic system code assessment process, as well as to the application of system codes to nuclear reactor problems.
The tasks which can benefit from such support are:

1. interpretation of TH-SYS code results;
2. extension of experimental database;
3. development of TH-SYS nodalizations.

A brief discussion on each of those topics follows.

4.4.1. Interpretation of system code results

Relevant experience in this connection was gathered from the utilization of both CFD and system codes in the framework of the Project TACIS R2.02/02, in which the Author participated together with other University of Pisa's specialists. The main objective of such project was the validation of mixing models implemented in some Russian system codes (KORSAR, DKM, TRAP-KS) against the experiments conducted by the Gidropress mixing facility (already mentioned in Section 1.2).
The same experiments were simulated with CFD codes too and the related results were very effective in providing a clear and plausible description (although only "qualitative") of the velocity field inside the RPV and in helping to understand the phenomena taking place there.
An example is shown in Figure 41, which refers to the CFD predictions of the flow developing inside the Gidropress facility vessel during a pump start-up experiment. The main fact that can be observed in the plot is the complex flow pattern, featured by strong horizontal components: being not counterbalanced by equal flows entering from the other loops, the flow from loop #4 tends to keep its momentum by flowing around the barrel and reaching the opposite side, instead of moving downwards. Therefore, most of the descending flow takes place on the other side than the one of impingement: this means that, if a "perturbed" slug is transported by the flow, its appearance at the core inlet is to be expected on that opposite side.
On the other hand, the flow below the injection nozzle tends to stagnate; some part of the perturbation can reach also this zone, but it will probably persist there longer and then reach the core inlet with some delay compared to the first perturbation appearance. An idea of the tracer distribution during such experiment is given by the two plots in Figure 42, referring to CFD simulations of Gidropress mixing experiments (see Section A.3, and Refs. [13] and [47]): it is evident that the tracer is transported towards the opposite side (Figure 42-a) and on that side makes its first appearance at the core inlet; then a weaker perturbation appears – with some delay – also below the injection side.

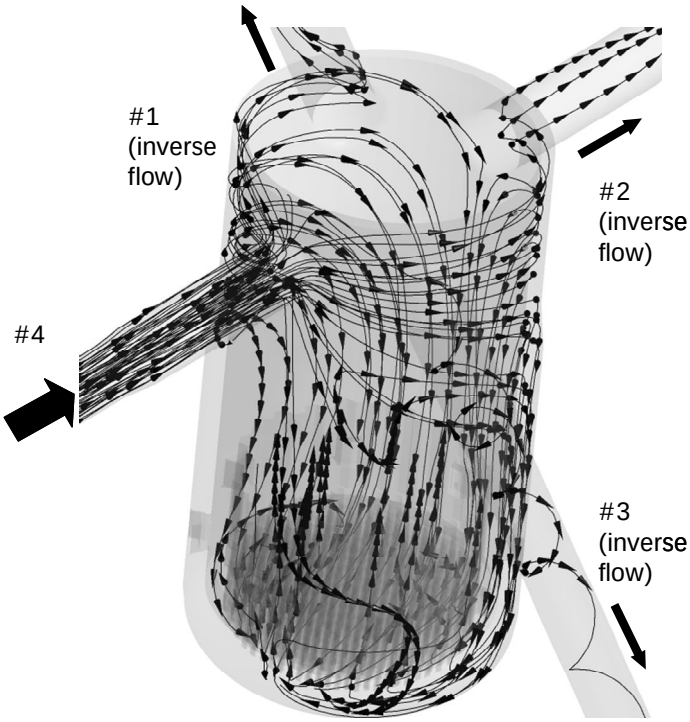

Figure 41 – In-vessel flow distribution during pump start-up scenario (CFD result)

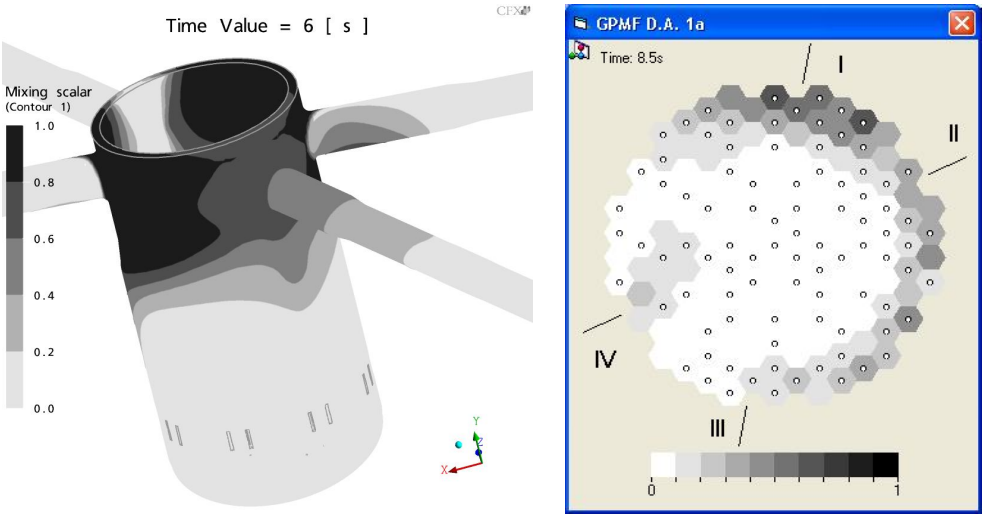

(a) (b)

Figure 42 – Tracer distribution in the downcomer (a) and at the core inlet (b) during pump start-up scenario (CFD result)

All such considerations are not straightforward when system code analyses are performed without the support of any three-dimensional tool such a CFD code. In such a case, realizing that the system code prediction shown for example in Figure 43 for the same pump start-up experiment is definitely far from being realistic, could take quite long (at least as long as needed to compare the results against the measured data).

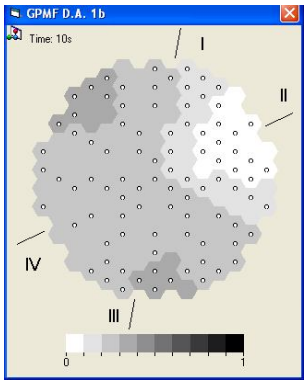

Figure 43 – Tracer distribution at the core inlet during pump start-up scenario (system code result)

In addition, the CFD analysis can reveal *a priori* possible deficiencies of the system codes in dealing with highly three-dimensional and complex IVF (such as in the example above).

4.4.2. Extension of the experimental database

Using CFD as a cheap mean to replace costly experiments is a very attractive idea, which in some cases has already revealed its practical applicability. This happens for instance when Direct Numerical Simulation (DNS) is applied to “simple” fundamental problems, where it is known to yield a very accurate and reliable quantitative description of the observed phenomena, and thus provides the necessary information for the closure of analytical models for multiphase flows simulation, turbulence modelling with LES or RANS approaches, etc.

A similar contribution was initially expected from CFD also for the objectives of the TACIS Project mentioned above, i.e. there was the ambitious intention to perform CFD simulations of scenarios with different operating parameters than in the real experiments (although within the same ranges of values) and thus to obtain a sort of extended “experimental” database, with the underlying idea that CFD results could be trustworthy enough to replace experiments for the system code validation purposes.

Actually, as the results of the CFD simulations of the real experiments have shown (Ref. [47]), CFD codes are still far from being capable of realistic predictions of the most complex in-vessel flows, therefore they cannot replace experiments, but rather they still have to be subjected to intense validation efforts.

Nevertheless, within an optimistic perspective, we can imagine that such challenging target will sooner or later be achieved, not only at DNS scales, but also at macroscopic scales.

4.4.3. Development of TH-SYS nodalizations: pressure loss estimation

One of the most useful ways in which CFD codes can be used to support the application of system codes is the calculation of local pressure losses.
Pressure loss coefficients are normally required as user input in any system code nodalization. Unless very accurate estimates are provided by *ad hoc* experiments, it is common practice to adopt "standard" values known from previous works, or suggested by the user experience, as well as to estimate such coefficients from engineering correlations or handbooks (the most universally known and used of which is certainly the Idel'cik's one, Ref. [87]).
The coefficients so obtained may be affected by relatively large uncertainties. The idea is therefore to obtain more accurate estimates of pressure losses with the help of CFD. Some examples of local geometrical features that may require fine estimation of pressure losses are:

- fuel assembly spacers;
- coolant channel inlet/outlet;
- pipe elbows;
- T-junctions;
- valves;
- rupture devices.

This kind of application is relatively less complex than other problems such as the investigation of the in-vessel flow, since usually it involves steady-state analyses in the absence of heat transfer, and in a limited size domain. On the other hand the geometrical details to be accounted for can make the meshing a really challenging task (as in the case, for example, of fuel assembly spacers), and quite complex turbulent flow phenomena can take place which are difficult to model.
Therefore, achieving a sufficiently high accuracy may be much harder than expected.

Following the BPGs is an efficient way of approaching the CFD calculation of pressure losses, since they require special attention in generating high-quality meshes, in assessing the results sensitivity on geometrical details, mesh size, modelling choices and parameters, boundary conditions etc. and in systematically quantifying the errors that affect the results. On the other hand, the existing BPGs (Refs. [5] and [18]) do not include (yet) any specific section related to pressure loss estimation. This is matter for future development.

4.4.4. Development of TH-SYS nodalizations: investigation of 3D flows

The best practice in developing nodalizations for TH-SYS code analyses requires that the domain discretization of large volumes (such as RPV lower and upper plena) accounts for the main flow structures taking place in those volumes so as to align – as far as possible – the longest side of the discretization cells with the flow

stream, and thus reduce the numerical errors associated with the spatial discretization.
In this connection, CFD can be a useful tool to investigate and understand complex 3D flows and provide guidance to the TH-SYS nodalization development.
Moreover, CFD can help checking some assumptions on which some lumped parameter models may be based, such as – for instance – the hypothesis of a uniform pressure distribution over a plenum in the presence of “internals” which could possibly introduce appreciable pressure losses.

5. ACCURACY EVALUATION

5.1. General remarks

A crucial step in the code assessment process is the evaluation of the accuracy of the code predictions with respect to the experimental or real plant behaviour. The "evaluation" involves both the "quantification" of the accuracy and a "judgment" on the resulting accuracy level.
In other words, the following two questions have to be answered:

1. How much accurate is the code prediction (for a specific code, simulation approach and problem) with respect to the experiment?
2. Is the degree of accuracy resulting from the above quantification high enough for the intended purposes?

Answering the first question requires the characterization of the target results (e.g. the time and space distribution of the coolant properties at core inlet) and of their deviation with respect to the experimental information by means of suitable local, global, integral and statistic quantities. The problem is therefore to select a set of such quantities that provide a synthetic and exhaustive picture of the accuracy level.

On the other hand, the second question involves some arbitrary elaboration of the above information to provide "acceptance thresholds" and "judgement criteria". With this purpose, the potential effects of the coolant properties perturbation on the core dynamics (e.g. reactivity insertion leading to power excursion) will have to be taken into account and a check whether the inaccuracies in code predictions are on the conservative side or not will be needed. This kind of assessment requires a thorough analysis of the complex interaction between the thermal fluid dynamics phenomena which are object of the above code predictions and the core physics, and is therefore outside the scope of the present work.
Instead, the results characterization and accuracy quantification issue will be addressed here. The current approaches, known from the literature and from technical documentation of international research projects, are examined and evaluated with their limitations. Then, some new ideas are proposed to improve the state-of-the-art.

5.2. Current approaches in accuracy evaluation

Some attempts can be found in literature to quantify the accuracy of code predictions for problems involving the perturbation of coolant properties at core inlet, but no judgment on the level of accuracy. Examples of the current best practice on this aspect can be found in Refs. [23], [82], [90] and [91].
In many cases, most of the result analysis and comparison focuses on the qualitative behaviour, while very few information is obtained from the quantitative point of view.

Let us consider, for instance, a typical simulation of in-vessel flow during a transient involving the presence of a slug of deborated of overcooled water which is transported to the RPV and then through the core. The target variable is the space and time distribution of the perturbation at core inlet, more precisely is the time history of the perturbation (in terms of temperature, or boron concentration, or mixing scalar, see Section 1.4) at each coolant channel inlet. Such information is easily obtained with the post-processing and on-line results storage interfaces available in common CFD codes, as well as in system codes with 3D capabilities. The same information may be available from experimental investigation; for example, in each of ROCOM tests (see Section A.1, and Ref. [22]) conductivity measurements are provided at the inlet of each of the 193 channels, while Gidropress experiments (see Section A.3, and Ref. [13]) provided such conductivity measurements for 90 out of the 151 channels. Thus, a common way to compare numerical results and measured data consists in a channel-by-channel comparison.
Figure 44, for example, shows such kind of comparison at three of ROCOM channels, for a test involving four pumps in steady operation and tracer injection into one loop (see Section A.1). As can be seen in the three plots, the agreement with the measured data appear very satisfactory at some locations, while relatively large discrepancies appear at other locations; moreover, the perturbation is either over-predicted or under-predicted depending on the location. A further step in the analysis may be to specify how much the relative maximum local discrepancy is. However, it is rather evident that the local comparison does not provide an overall picture of the code prediction accuracy, unless some further processing of the discrepancies is done.
This becomes even clearer if the problem of the “downcomer flow rotation” is considered. As explained in Section A.2, even with symmetric pump operation, an angular shift is usually observed in the downcomer flow in VVER-1000 reactors (and reactor scaled models); such effect is normally not predicted by CFD codes. However, a CFD code can be realistically expected to be able in the next future to accurately predict the shape of the perturbed sector, the gradients, the timing, and anything else which characterizes the perturbation apart from the angular shift. In such a case, the channel-by-channel comparison would keep showing large discrepancies and hiding the key information that the code is missing “only” the rotation.

Another example of an approach usually adopted to compare code results and experimental data is shown in Figure 45, which refers to numerical simulations (with both CFD and system codes) of a steady state problem with a temperature perturbation coming from one of the four loops of a VVER-1000 reactor. The target variable (the temperature at the inlet of each coolant channel) is compared at all FA locations on the same plot, which has the advantage of summarizing the whole information. However, since all FA are represented on a single axis, all information on the core layout and on the “shape” of the perturbation is lost. Therefore, this kind of data presentation does not bring any significant and usable quantitative and qualitative information on the accuracy.

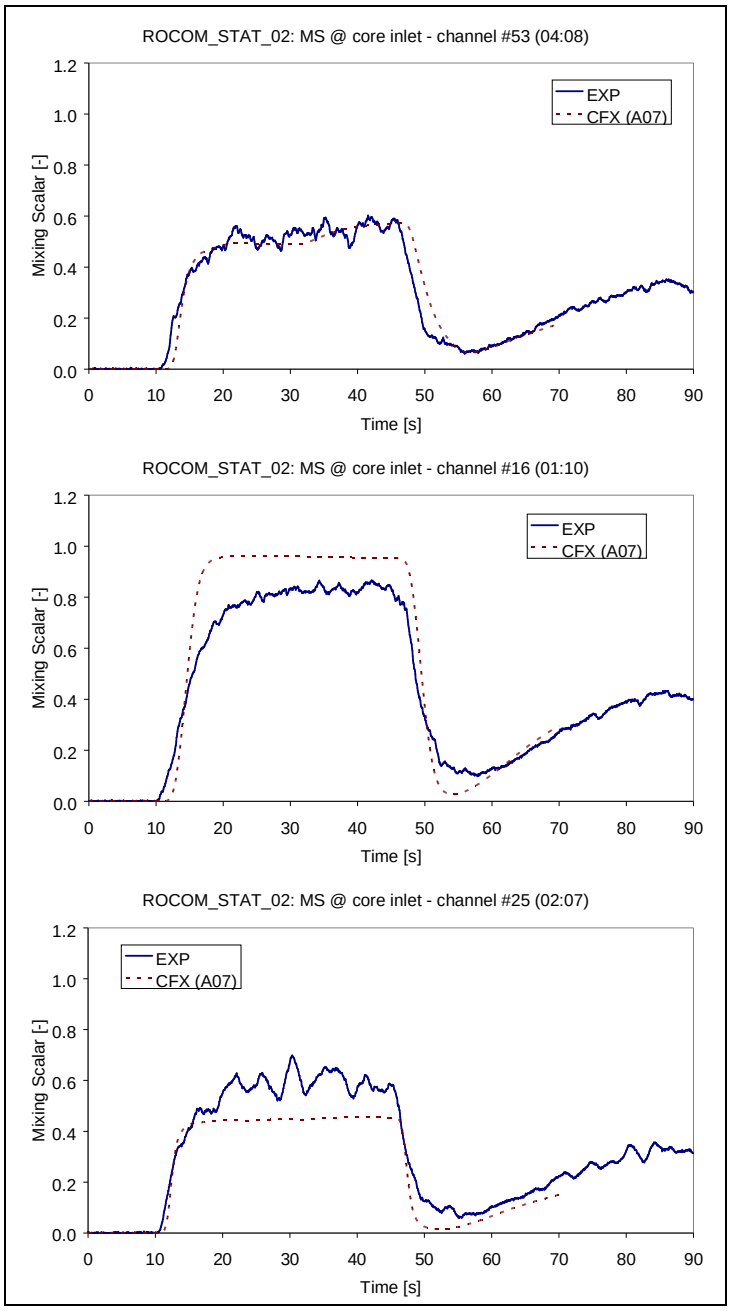

Figure 44 – Typical channel-by-channel comparison (from Ref. [31])

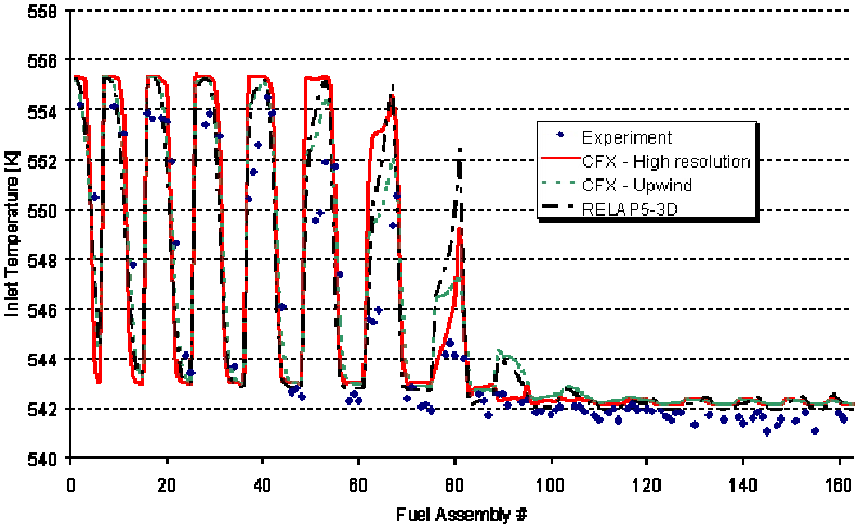

Figure 45 – Another typical comparison approach (from Ref. [7])

5.3. Proposal of a more exhaustive quantification of accuracy

A methodology for addressing the issue of quantifying the accuracy of code predictions of coolant properties perturbations at core inlet is proposed. The approach includes the following two steps:

1. qualitative analysis of the code results and comparison against the experiment;
2. quantitative analysis and comparison.

The objective is to provide an exhaustive set of quantitative information to characterize the discrepancy between code predictions and experimental data, that is – in other words – to quantify the accuracy.

As explained above, once acceptance criteria are established to judge on the accuracy, the complete evaluation of accuracy is achieved. However the definition of acceptance criteria is beyond the scope of the present work and is not addressed here.

5.3.1. Qualitative analysis

The qualitative analysis is a first mandatory step towards the quantification of accuracy. It provides the following information:

- Morphology of the flow field observed in the experiments (if measured data are available[32]) and predicted by the code:

    - flow in the downcomer mainly oriented vertically OR presence of strong horizontal components (e.g. in case of asymmetric pump operation);
    - presence of symmetries;
    - presence of swirls;
    - presence of inverse flows in idle loops;
    - presence of stagnation regions;
    - flow distribution through different parts of the lower plenum region (defined by internals).

- Morphology of the perturbation observed in the experiments and predicted by the code:

    - perturbation distribution at RPV inlet nozzle; either uniform or non uniform over the nozzle cross section (e.g. in relation to possible thermal stratification phenomena in cold leg); either sharp or smooth fronts (depending on the role played by mixing phenomena in cold leg);
    - perturbation distribution in the downcomer[33] (it is driven by the flow distribution, and this should be easily recognizable); it could either be concentrated below the inlet nozzle of the perturbed loop, or spread azimuthally and reach the opposite side (as in case of pump start-up scenarios); it could even point out buoyancy effects associated with density differences (e.g. stagnation of the perturbation on the upper part of the downcomer if hotter water is injected);
    - perturbation distribution at the core inlet; it is mostly driven by the perturbation configuration in the downcomer, and affected to some extent by the lower plenum internals; it may appear as a large well defined sector, or a spot; otherwise more than one perturbation spot may appear having different shapes and locations; the absence of any coherence in the spatial distribution of the perturbation may be related to the presence of buoyancy effects, with the perturbation stagnating either in the lower plenum or in the upper part of the downcomer;
    - spatial gradients of the perturbation both in the downcomer and in the lower plenum; the code-to-exp comparison may qualitatively reveal either under-prediction or over-prediction of turbulent diffusion (mixing effectiveness);
    - presence of “swirls” effects (due to flow angular shift in the downcomer, as usually occurs in VVER reactors).

---

[32] To the best Author’s knowledge, among the existing experimental facilities for investigation of in-vessel flow, only ROCOM provides information on the velocity distribution, by means of LDA measurements.

[33] Again, ROCOM is the only test facility providing perturbation measurements in the downcomer by means of the so-called wire mesh sensors.

The qualitative analysis basically answers the question whether the code is able or not to predict the same macroscopic flow and perturbation patterns taking place in the experiment. Before any quantitative assessment, it is necessary to understand whether the code actually describes what happens in the experiment. If not, then the adopted modelling approach is missing some phenomena, and this may be crucial from the reactor safety point of view.
An example of in-vessel flow phenomena that are usually not captured by CFD models (and *a fortiori* by system codes) is the "angular shift" or "flow rotation" or "swirl effect" observed in VVER reactors. For example, when four pumps of a VVER-1000 are running at nominal speed, the flow distribution in the DC is affected by an azimuthal shift which increases along the axial direction. This angular shift also affects the position of the perturbation at the core inlet. The physical reason for this phenomenon has not yet been fully understood (although it is common opinion that it is related to hydraulic instabilities and affected by secondary flows in the cold legs). The common CFD modelling approaches (based on RANS) have not the capability of capturing this kind of phenomenon[34], neither can the system codes.

If a code is failing to predict the phenomena that are object of the investigation, the qualitative analysis is supposed to reveal it, and then it will probably not be necessary to proceed with the quantitative analysis. On the other hand, addressing the quantitative analysis without carefully analyzing the results from the qualitative point of view is a wrong procedure because the judgment on the code behaviour will be incomplete; moreover it could be risky since possible error compensation effects affecting the results might not be revealed.

5.3.2. Quantitative analysis

Once the qualitative analysis has been performed and has shown that the code results satisfactorily reproduced the key features of the addressed phenomena (i.e. the predicted perturbation at core inlet – and elsewhere measured data are available – has the same morphology as observed in the experiment) the quantitative analysis is addressed.
The characterization of space and time distribution of coolant properties at core inlet (e.g. boron concentration, temperature) can be based on the following set of key quantities and code-to-experiment deviations and errors:

1. perturbation appearance (sub-section 5.3.2.2);
   a) location(s) of appearance (and related deviation);
   b) time of appearance (and related error);
   c) time of disappearance (and related error);
   d) perturbation transit time (and related error);
2. maximum perturbation (sub-section 5.3.2.3);
   a) location of maximum (and related deviation);
   b) time of maximum (and related error);

[34] Some chances to successfully address this issue come from the LES turbulence modelling. See for instance Bieder [41].

   c) maximum value (and related error);
3. core-averaged perturbation (sub-section 5.3.2.4);
   a) time of maximum (and related error);
   b) maximum value (and related error);
   c) mean time (and related error);
   d) standard deviation (and related error);
   e) time gradient of perturbation front (and related error);
4. accumulated perturbation (sub-section 5.3.2.5);
   a) value at plateau (and related error);
   b) average amplitude from FFTBM application;
5. perturbation barycentre (sub-section 5.3.2.6);
   a) time-averaged location;
   b) maximum standard deviation of perturbation spatial distribution (and related error);
   c) average standard deviation of perturbation spatial distribution (and related error);
6. FLOMIX deviations (sub-section 5.3.2.7);
   a) deviation #3, with sign;
   b) deviation #3, without sign;
   c) deviation #3, root mean square;
7. spatial gradients (sub-section 5.3.2.8);
   a) maximum slope (and related error);
8. 3D FFTBM (sub-section 5.3.2.9);
   a) average amplitude.

All above quantities are discussed in the following sub-sections. The perturbation is indicated by $c_{i,k}$, where *i* is the coolant channel number (ranging from 1 to N_{CH}), and *k* is the index running on a discretized time scale (from 0 to N_T).

The assumption is made that the perturbation is showing one peak, both in time and in space. In other words, only one “perturbation spot” appears at the core inlet, reaches its maximum intensity, and then disappears. This is typical for scenarios featured by steady and symmetric pump operation. However, pump start-up scenarios or the presence of buoyancy effects usually lead to more complex perturbation morphology, such as the presence of more than one perturbation spot, or more than one peak in the perturbation time histories. The above definitions can be easily extended to allow for local maxima, more perturbation appearances etc.

Some of the mentioned quantities play as “mixing indicators”, as they provide overall information on the effect of the mixing phenomena on the space and time distribution of the perturbation.

5.3.2.1. Preliminary data processing (time and space dependent quantities)

Preliminary data processing issues have already been covered in Section 4.3.7. Some specific considerations are reported here regarding the processing needed for the accuracy evaluation.
The assumption is made here that both calculated and measured data have been normalized to comparable units. A common and practical approach consists in

adopting the Mixing Scalar (MS), a non-dimensional normalized perturbation, with MS = 0 corresponding to absence of perturbation (i.e. nominal temperature or boron concentration values) and MS = 1 to a reference perturbation (i.e. the minimum boron concentration in a deborated slug entering the RPV, or the minimum temperature).

Data are usually available in table format, where the n-th vector includes the time history of the perturbation at the *n*-th channel, the number of rows being equal to the number of time discrete values.

Extremes calculation

The above data have to be processed to calculate the following "extremes":

- time-history of the maximum perturbation registered over the core inlet ($c_k^{MAX,t}$), see example in Figure 46;
- the spatial distribution of the maximum perturbation registered during the slug passage ($c_i^{MAX,sp}$).

The calculation of the former is common practice in the works encountered in the literature (see for example Refs. [23], [90] and [91]).

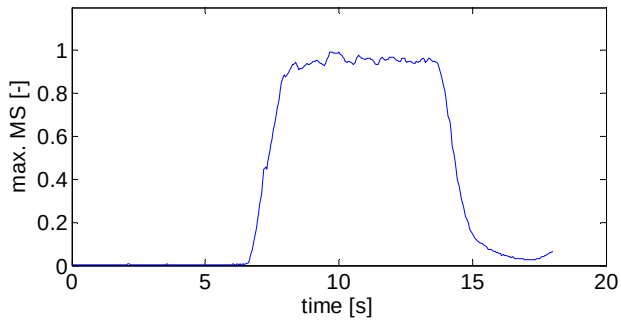

Figure 46 Example of maximum perturbation time history

Core-averaging

Preliminary processing also involves computing averages, such as:

- core-average → Time-history of the core-averaged perturbation ($\langle c \rangle_k$, see Equation 2);
- time-average → Core distribution of time-averaged perturbation ($\overline{c}_i$, see Equation 3).

$$\langle c \rangle_k = \frac{1}{N_{CH}} \cdot \sum_{i=1}^{N_{CH}} c_{i,k} \qquad \textit{Equation 2}$$

$$\bar{c}_i = \frac{1}{N_T} \cdot \sum_{k=1}^{N_T} c_{i,k} \qquad \textit{Equation 3}$$

The time-history of the core-averaged perturbation is an integral parameter that quantifies the overall amount of the deviation of coolant properties from the nominal values, and includes information related to the timing of such deviation.
Obviously, the space averaging cancels all information related to the "local" perturbation (i.e. channel by channel). An example is shown in Figure 47.

Also the calculation of core-averaged perturbation time history is rather common in the literature.

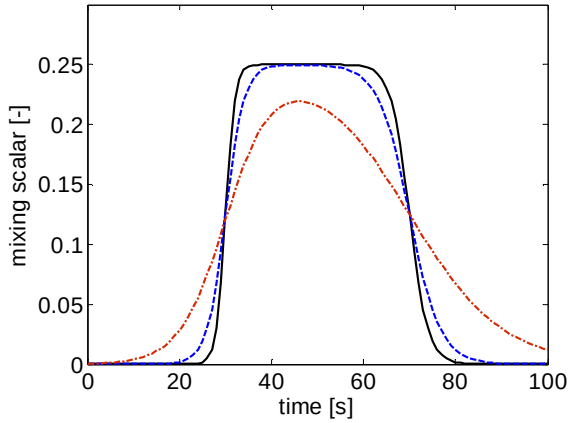

Figure 47 Examples of core-averaged perturbation time history

Accumulated perturbation

The accumulated perturbation (as a function of time) can be defined as the time integral of the core-averaged perturbation over the time interval elapsed since the beginning of the perturbation transient up to the generic time *t*. It can be calculated in the discrete form according to Equation 4.

$$AP_k = \sum_{j=2}^{k} c_{i,j} \cdot (t_j - t_{j-1}) \qquad \textit{Equation 4}$$

The accumulated perturbation always shows a monotonically increasing trend during the passage of a perturbation (see examples in Figure 48). For a simple slug problem, the accumulated perturbation finally reaches a "plateau"; if the perturbed coolant keeps circulating in the loops a new perturbation (much more diluted) will appear after a certain transit period, then the accumulated perturbation will start increasing again. The plateau value is expected to be the same both in the experiment and in the numerical simulation, even if the mixing is not appropriately modelled and the predicted perturbation distribution is totally wrong. "Acceptable" differences may be due to spatial variations of density. More "severe" discrepancies, on the other hand, are those related to ill-defined boundary conditions (e.g. in the presence of inverse flows on idle loops) or problems with

buoyancy modelling (e.g. part of the perturbation is stagnating somewhere upstream of the core inlet, and this effect is being over- or under-predicted by the code). Therefore the accumulated perturbation, although rarely referred to in the literature, is one of the most useful quantities to characterize the code results, as well as to check the modelling consistency.

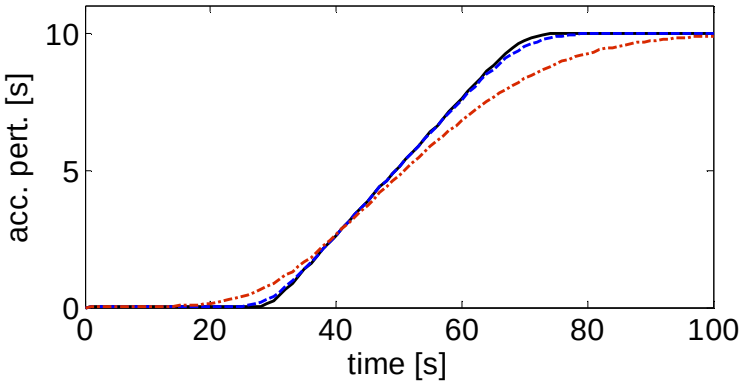

Figure 48 Examples of accumulated perturbation time history

Reactivity weight factors

Localized perturbations occurring at different locations (i.e. affecting different coolant channels) are generally expected to bring reactivity insertions of different values, owing to the different fuel operating conditions (temperature, fluence, enrichment, composition, presence of neutron poisons, etc.) This can be taken into account by weighting the perturbation distribution with suitable factors – one for each channel – provided by the NK analyst.

The calculation of the core-averaged time history would then be performed according to Equation 5:

$$\left\langle c \right\rangle_k^{(W)} = \frac{\sum_{i=1}^{N_{CH}} c_{i,k} \cdot w_i}{\sum_{i=1}^{N_{CH}} w_i} \qquad \textit{Equation 5}$$

The adoption of such a set of weighting factors can be useful to evaluate the importance of inaccuracies in predicting the location of the perturbation (e.g. because of the inability to simulate the “flow rotation effect” typical of VVER reactors), since the code prediction could indicate – for example – a perturbation of the same intensity but occurring at a less “reactive” region of the core, and in such a case the code inaccuracy could be marked as “conservative”.

This idea has been mentioned within the FLOMIX-R Project (see Ref. [90]), but no example of its application has been encountered so far.

Flowrate weight factors

A more appropriate core-averaging procedure than the simple one represented by Equation 4, consists in weighting the perturbation with the mass flowrate through each channel (see Equation 6). In this way, the non-uniform flow distribution through the core is accounted for.
However, information on the coolant channel flowrates is usually missing from experimental data; therefore this weighting approach is not easily applicable.

$$\left\langle c \right\rangle_k^{(\dot{m})} = \frac{\sum_{i=1}^{N_{CH}} c_{i,k} \cdot \dot{m}_i}{\sum_{i=1}^{N_{CH}} \dot{m}_i} \qquad \textit{Equation 6}$$

Interpolation issues
Interpolation may be needed to align the calculated data time and space distribution with the measured data, so as to allow for comparison. This operation is normally performed with the help of simple user routines. For instance, for the purposes of code validation activities performed in the frame of this research, programming languages such as Visual Basic, FORTRAN, Perl and Matlab have been extensively used. It has to be remarked that, from the Quality Assurance point of view, that user programming introduces *per se* verification issues that must addressed and solved, so as to avoid the introduction of additional error sources.

Alignment of time vectors is necessary for the calculation of exp-to-code deviations, and for the application of the FFTBM (Ref. [84]).
If the time discretization in calculated data coincides with that of measured data, then no interpolation is needed.

Space interpolation may be needed:

- when the available measured data are “incomplete” (i.e. data are not available for all coolant channels, such as in the case of the Gidropress mixing facility, see Ref. [13]);
- when the channel-by-channel set of data must be mapped on a finer grid, e.g. to allow applying multidimensional discrete Fourier transform (see Section 5.3.2.9).

It is worthwhile noticing that interpolation operations performed on experimental data may introduce some arbitrariness. For this reason, it can be recommended to perform the time interpolation by processing the calculated data to align them with the measured data, and not vice versa.
The effect may be more important when performing the spatial interpolation.

Calculation of spatial gradients
Let us consider the perturbation distribution over the core inlet at a given instant during the slug transit (an example is shown in Figure 49), and let us treat it as a continuous function of two spatial coordinates lying on the core inlet plane.

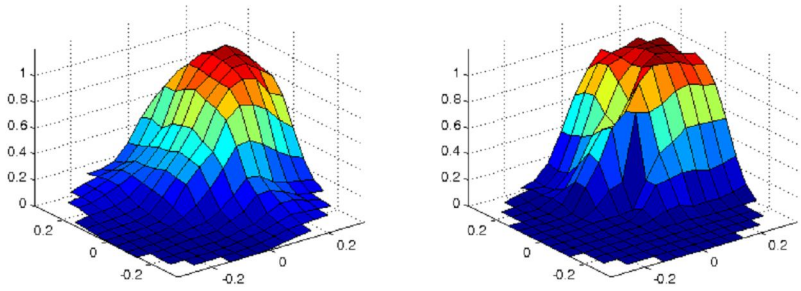

Figure 49 Example of perturbation distribution at core inlet at a given instant

As observed in the figure, different distributions may show more or less steep gradients, which are indicators of a smaller or greater diffusive behaviour, (right and left side in the figure, respectively).
Maps of the spatial gradients can be obtained, at each instant, by processing the space and time distributions with proper algorithms for slope estimation.
For example, the algorithm implemented in Matlab, calculates the slope as "the change in elevation per unit distance along the path of steepest ascent or descent from a grid cell to one of its eight immediate neighbours, expressed as the arctangent", in degrees (see Ref. [91]).
For the example shown in the figure, the maximum slope resulting from Matlab calculation is 72° and 77° respectively.

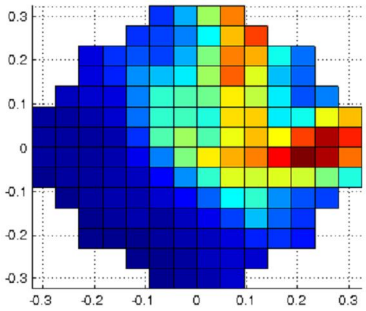

Figure 50 Example of slope map

No example of applications of this kind of processing has been found in the literature.

Calculation of perturbation barycentre location
The Cartesian coordinates of the barycentre can be calculated at each time instant as from Equation 7 and Equation 8. The instantaneous distance between calculated and experimental barycentre is obtained from Equation 9.

$$x_{B,k} = \frac{\sum_{i=1}^{N_{CH}} c_{i,k} \cdot x_i}{\sum_{i=1}^{N_{CH}} c_{i,k}} \qquad \textit{Equation 7}$$

$$y_{B,k} = \frac{\sum_{i=1}^{N_{CH}} c_{i,k} \cdot y_i}{\sum_{i=1}^{N_{CH}} c_{i,k}} \qquad \textit{Equation 8}$$

$$d_{B,k} = \left[\left(x_{B,k}^{(c)} - x_{B,k}^{(e)} \right)^2 + \left(y_{B,k}^{(c)} - y_{B,k}^{(e)} \right)^2 \right]^{\frac{1}{2}} \qquad \textit{Equation 9}$$

Calculation of standard deviation in spatial distribution with respect to the barycentre

Let us consider the spatial distribution of the perturbation over the core inlet at a given time instant. The standard deviation with respect to the barycentre of the distribution is a dispersion index and can play as a mixing indicator. It is calculated according to Equation 10 and Equation 11 ($d_{i,k}^{B}$ being the distance from the *i*-th channel centre and the perturbation barycentre at the time t_k).

$$\sigma_k^{(sp)} = \sqrt{\left[\sum_{i=1}^{N_{CH}} c_{i,k} \cdot \left(d_{i,k}^{B} \right)^2 \right] / \sum_{i=1}^{N_{CH}} c_{i,k}} \qquad \textit{Equation 10}$$

$$d_{i,k}^{B} = \sqrt{\left(x_i - x_k^{B} \right)^2 + \left(y_i - y_k^{B} \right)^2} \qquad \textit{Equation 11}$$

FLOMIX deviations (space-dependent)

As mentioned above, the only relevant attempt to define a systematic approach to the quantification of accuracy for problems involving perturbation of coolant properties at core inlet, was made in the framework of the FLOMIX-R project Ref. [90], and consisted in the definition of a set of parameters quantifying the "deviation" of the numerical results from the measured data. The same approach was then adopted in Ref. [23].

The starting point is the definition in Equation 12, which is simply the difference between calculated and experimental values, at each location and for each time value. Both the calculated and the measured values must be "aligned" on the same time vector, therefore a time interpolation procedure usually has to be applied to the code results.

$$dev1_{i,k} = c_{i,k}^{(calc)} - c_{i,k}^{(\exp)} \qquad \textit{Equation 12}$$

The next step is the definition of time-averaged deviations for each channel (Equation 13 to Equation 15):

$$dev2\_sign_i = \frac{1}{t_{N_T} - t_1} \cdot \sum_{k=2}^{N_T} dev1_{i,k} \cdot \left(t_k - t_{k-1}\right) \qquad \textit{Equation 13}$$

$$dev2\_abs_i = \frac{1}{t_{N_T} - t_1} \cdot \sum_{k=2}^{N_T} \left|dev1_{i,k}\right| \cdot \left(t_k - t_{k-1}\right) \qquad \textit{Equation 14}$$

$$dev2\_rms_i = \frac{1}{t_{N_T} - t_1} \cdot \sqrt{\sum_{k=2}^{N_T} \left(dev1_{i,k}\right)^2 \cdot \left(t_k - t_{k-1}\right)^2} \qquad \textit{Equation 15}$$

where:

- $dev2\_sign_i$ is the time integral of the deviation $dev1_{i,k}$ for each channel. In other words, it is a "cumulative" deviation, which accounts for the sign of instantaneous deviations, thus allowing for possible error cancelation effects;
- $dev2\_abs_i$ is analogous to the previous deviation, except for being based on absolute values; either errors due to over-prediction or under-prediction of the perturbation are thus cumulated without any compensation;
- the definition of $dev2\_rms_i$ involves a kind of root mean square, so that the importance of large variations is enhanced.

From the three deviations defined above, three maps can be obtained showing the deviations distribution over the core inlet. An example is shown in Figure 44; the deviations shown refer to a post-test CFD calculation of a slug-mixing experiment conducted at the Gidropress mixing facility Ref. [82]. The comparison evidences that the second and the third parameter practically give the same qualitative information (the deviation distribution over the core inlet looks exactly the same), while the first parameter reaches its largest values at different locations with respect to the other parameters.

By averaging the *dev2* deviations over the core inlet scalar quantities are obtained, defined as *dev3* deviation; they will be addressed in Section 5.3.2.7.

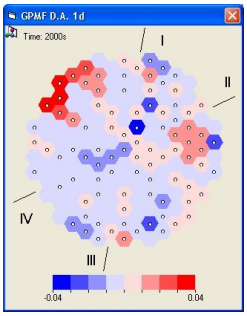

dev2_sign

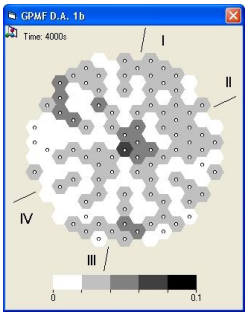

dev2_abs

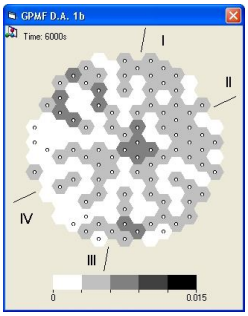

dev2_rms

Figure 51 Sample maps of "dev2"-type deviations

FLOMIX deviations (time-dependent)

Similarly, also time-dependent deviations have been defined in Ref. [90], according to Equation 16, Equation 17 and Equation 18:

$$dev4\_sign_k = \frac{1}{N_{CH}} \cdot \sum_{i=1}^{N_{CH}} dev1_{i,k} \qquad \textit{Equation 16}$$

$$dev4\_abs_k = \frac{1}{N_{CH}} \cdot \sum_{i=1}^{N_{CH}} \left| dev1_{i,k} \right| \qquad \textit{Equation 17}$$

$$dev4\_rms_k = \sqrt{\frac{1}{N_{CH}} \cdot \sum_{i=1}^{N_{CH}} \left(dev1_{i,k} \right)^2} \qquad \textit{Equation 18}$$

where:

- $dev4\_sign_k$ is the core-averaged deviation at time t_k; since the deviations are taken with their sign, opposite contributions tend to cancel reciprocally, and information on the overall over-estimation or under-estimation of the perturbation is obtained;
- $dev4\_abs_k$, instead, takes absolute values of all contributions, therefore information is obtained on the "amount of discrepancy" regardless of its sign;
- $dev4\_rms_k$ is the root mean square deviation over the core inlet at time t_k, and provides the same kind of information as $dev4\_abs_k$, except for amplifying the largest contributions.

The three above deviations can be represented on time-dependent plots, in order to show their trends during the transient evolution (see examples in Figure 52).

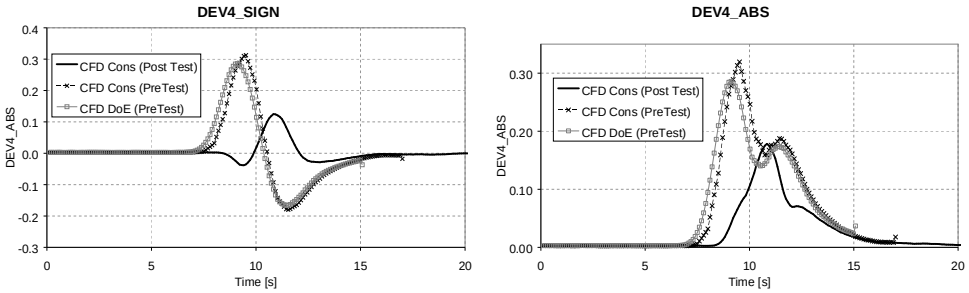

Figure 52 Sample plots of "dev4" deviations

5.3.2.2. Scalar quantities related to perturbation appearance

The definition of "perturbation appearance" is arbitrary. A threshold value has to be defined (e.g. 0.1, or 0.01), based on a suitable "sensitivity level" which should stem from neutron kinetics considerations. For instance, the NK analyst may state that perturbations below a specified limit can be neglected because the related reactivity insertion is not bringing any potential for power excursion.
The perturbation disappearance will then be defined based on the same threshold value.
The following quantities will be analysed:

1. location of perturbation appearance (Cartesian coordinates x_{PA} and y_{PA});
2. time of perturbation appearance (t_{PA});
3. time of perturbation disappearance (t_{PD});
4. perturbation transit time ($\Delta t_{PT} = t_{PD} - t_{PA}$).

Likewise, the related "code-to-experiment" deviations and errors can be introduced:

5. deviation of perturbation appearance location (d_{PA}, Equation 24, where the superscripts c and e indicate calculated and experimental values, and L is a characteristic length of the core inlet);
6. relative deviation of time of perturbation appearance (δt_{PA}), with respect to perturbation transit time (Equation 20).

$$d_{PA} = \sqrt{\left(x_{PA}^{(c)} - x_{PA}^{(e)}\right)^2 + \left(y_{PA}^{(c)} - y_{PA}^{(e)}\right)^2} / L \qquad \textit{Equation 19}$$

$$\delta t_{PA} = (t_{PA}^{(c)} - t_{PA}^{(e)}) / \Delta t_{PT} \qquad \textit{Equation 20}$$

The location of the perturbation appearance is relevant to reactor safety because of the different neutronic response of different coolant channels (see above

consideration on “weight factors”); therefore it is desirable that a code is able to predict such location accurately.
The related inaccuracy can be defined as the distance between the predicted and measured location, normalized with respect to a relevant scale such as the distance between two adjacent channels or the core diameter. Then an “acceptance threshold” might be defined on the same scale, e.g. 3 channel distances, if the predicted location is not to be more than three channels away from the measured location.

Also the time at which the perturbation appears is important. In fact, if the code predicts the perturbation arrival with a time shift (either in advance or delayed) with respect to the experiment, this may indicate that the code is failing to describe the flow distribution in the downcomer, because the vertical components of the velocity are too strong or too weak, or because the buoyancy effects are not correctly modelled, or because the turbulent mixing is under- or over-predicted.

The perturbation transit time (i.e. the time elapsing between the appearance and the disappearance of the perturbation) indicates the duration of the perturbation and is obviously a relevant parameter which determines the consequences on the core dynamics.
It is also a “mixing indicator”: the larger is its value, the greater is the mixing effectiveness along the main coolant stream direction and the smoother are the perturbation gradients in time (see below).

The literature survey showed that the analysis of parameters related to the perturbation appearance and transit is never addressed; to the Author’s opinion, this is a limitation and the mentioned parameters should be used in systematic accuracy evaluation.

5.3.2.3. Scalar quantities related to overall maximum perturbation

The quantities related to overall maximum perturbation are:

1. location (x_{MAX} and y_{MAX});
2. time (t_{MAX});
3. maximum value (c_{MAX});

with the following related deviations and errors:

4. deviation of location of maximum (d_{MAX}), Equation 21, with obvious notation;
5. deviation of time of maximum (δt_{MAX}), Equation 22;
6. relative error on maximum perturbation (ε_{MAX}), Equation 23.

$$d_{MAX} = \sqrt{\left(x_{MAX}^{(c)} - x_{MAX}^{(e)}\right)^2 + \left(y_{MAX}^{(c)} - y_{MAX}^{(e)}\right)^2} / L \qquad \textit{Equation 21}$$

$$\delta t_{MAX} = (t_{MAX}^{(c)} - t_{MAX}^{(e)}) / \Delta t_{PT} \qquad \text{Equation 22}$$

$$\varepsilon_{MAX} = \left(c_{MAX}^{(c)} / c_{MAX}^{(e)}\right) - 1 \qquad \text{Equation 23}$$

The maximum value (over time and space) is certainly one of the most useful parameters to characterize a perturbation.
It is a "mixing indicator" too: the smaller is its value, the more intense is the mixing. If the maximum perturbation at core inlet has the same value as the perturbation at the RPV inlet, this means that at least some part of the coolant has not been affected by the mixing at all. If the predicted maximum perturbation is lower than the measured one, this may indicate that the code tends to over-estimate the mixing. However this indicator is not sufficient to characterize the mixing, because of its local nature. Other indicators, of integral or global type, are necessary to draw conclusions whether the mixing is being over- or under-estimated.
In general, an overestimation of the maximum perturbation may indicate a "tendency to conservatism" in code predictions. However general conclusions in this sense cannot be drawn without analyzing the interaction with the core neutron kinetics.
An acceptance threshold for the predicted maximum perturbation could be defined as the maximum allowed deviation with respect to the measured value (e.g. ±1%).

The location and the time at which the maximum perturbation occurs are important for the same reasons discussed above about the perturbation appearance. On the other hand, if a conservative approach is followed, the NK analysis will probably assume that the maximum perturbation takes place at the most "sensitive" channel (i.e. where the same perturbation would introduce the largest amount of positive reactivity).
The inaccuracy on location prediction can be defined as above, i.e. in relation to a characteristic distance.

The maximum perturbation is often addressed in the literature when discussing the simulation results and comparing them against measured data.

5.3.2.4. Scalar quantities related to core-averaged perturbation

The quantities related to core-averaged perturbation are:

1. time of maximum ($t_{CA,MAX}$);
2. maximum value ($\langle c \rangle^{MAX}$);
3. mean time ($\bar{t}_{CA}$), Equation 24 (i.e. centre of time distribution of core-averaged perturbation);
4. standard deviation ($\sigma_{CA}^{(t)}$), Equation 25;
5. time gradient of perturbation front (c'), Equation 26;

The following deviations and errors are also defined:

6. deviation of time of maximum ($\delta t_{CA,MAX}$), Equation 27;
7. relative error on maximum value ($\varepsilon_{CA,MAX}$), Equation 28;
8. deviation of mean time ($\delta \bar{t}_{CA}$), Equation 29;
9. relative error on time gradient of perturbation front ($\varepsilon(c')$), Equation 30;
10. relative error on standard deviation of core-averaged perturbation ($\varepsilon\left[\sigma_{CA}^{(t)}\right]$), Equation 31;
11. average amplitude from application of FFTBM to core-averaged perturbation ($AA_{CA}^{(FFT)}$).

$$\bar{t}_{CA} = \left(\sum_{k=1}^{N_T} \langle c \rangle_k \cdot t_k \right) / \left(\sum_{k=1}^{N_T} \langle c \rangle_k \right) \qquad \textit{Equation 24}$$

$$\sigma_{CA}^{(t)} = \sqrt{\left(\sum_{k=1}^{N_T} \langle c \rangle_k \cdot \left(t_k - \bar{t}_{CA} \right)^2 \right) / \left(\sum_{k=1}^{N_T} \langle c \rangle_k \right)} \qquad \textit{Equation 25}$$

$$c' = \frac{\langle c \rangle^{(b)} - \langle c \rangle^{(a)}}{t^{(b)} - t^{(a)}} \qquad \textit{Equation 26}$$

$$\delta t_{CA,MAX} = (t_{CA,MAX}^{(c)} - t_{CA,MAX}^{(e)}) / \Delta t_{PT} \qquad \textit{Equation 27}$$

$$\varepsilon_{CA,MAX} = \left(c_{CA,MAX}^{(c)} / c_{CA,MAX}^{(e)} \right) - 1 \qquad \textit{Equation 28}$$

$$\delta \bar{t}_{CA} = (\bar{t}_{CA}^{(c)} - \bar{t}_{CA}^{(e)}) / \Delta t_{PT} \qquad \textit{Equation 29}$$

$$\varepsilon(c') = \left(c^{(c)\prime} / c^{(e)\prime} \right) - 1 \qquad \textit{Equation 30}$$

$$\varepsilon\left[\sigma_{CA}^{(t)}\right] = \left[\sigma_{CA}^{(t)(c)} / \sigma_{CA}^{(t)(e)}\right] - 1 \qquad \textit{Equation 31}$$

As explained above, the core-averaged perturbation is obtained as the arithmetic average – over all coolant channels – of the perturbation time histories. It is therefore an integral quantity that characterizes the whole perturbation affecting the core inlet.
Its maximum value in time is a mixing indicator; a lower value indicates a greater diffusion. On the other hand, if two trends show the same maximum value, this does not necessarily indicate the same amount of mixing. This is evident from the examples shown in Figure 53, where three different core averaged perturbation time-histories are compared (corresponding to the same volume of “perturbed slug”). Curves #1 and #2 show the same maximum value, but the latter is featured by a more diffusive behaviour (i.e. more intense mixing). In curve #3, the mixing is much stronger and is affecting the maximum value too.

The mixing intensity is better characterized by the gradients, for instance by the time gradient defined above, as indicated also in Figure 53, where $\Delta\langle c\rangle / \Delta t = \tan(\alpha)$ is the average time derivative between two points *a* and *b* arbitrarily defined (e.g. at 10% and 90% of the maximum value).
The mean time of the time distribution of the core-averaged perturbation will coincide with the time of maximum only if the distribution is symmetric. The comparison between experimental and calculated data should address at least one of the two parameters (the mean time being preferable, since its definition is unambiguous).
The standard deviation of the time distribution (i.e. the square root of the central moment of second order with respect to the mean time) is also a parameter that characterizes the diffusive behaviour: for example, curves #1 to #3 in Figure 53 will show the three values *11.9*, *12.6* and *17.1*, respectively (around the mean times *50.1*, *50.3*, *52.4*).

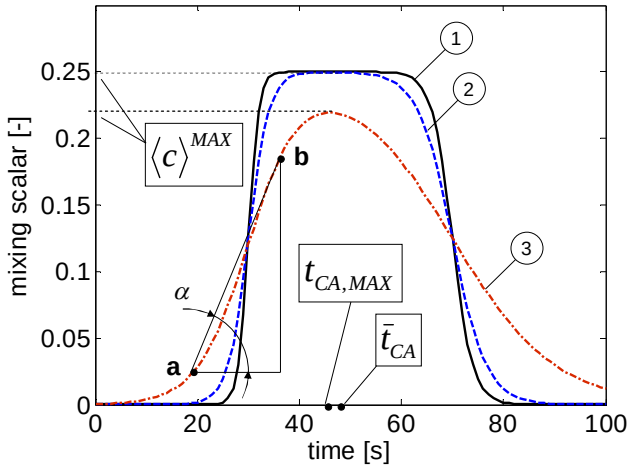

Figure 53 Possible core-averaged perturbation trends

The accuracy in predicting the core averaged perturbation can also be quantified by applying the FFTBM (see Ref. [93]), i.e. with the average amplitude of the power spectrum of the difference of both the experimental and the calculated time histories Discrete Fourier Transforms. An acceptance threshold should then be defined for such parameter too.
Referring to the sample curves shown in Figure 53, if #1 is assumed as the "experiment" and both #2 and #3 as the results from two different simulations, the resulting average amplitudes from FFTBM application would be *0.166* and *0.452* for the two calculations respectively.

The above parameters and indicators related to the core-averaged perturbation are commonly ignored in literature (apart from the maximum value and its occurrence time, see for example Refs. [23], [34] and [91]).

5.3.2.5. Scalar quantities related to accumulated perturbation

The following quantities, related to the accumulated perturbation, should be addressed in the quantitative analysis:

1. plateau value (AP_{slug}), or analogous quantity;
2. average amplitude from application of FFTBM to accumulated perturbation ($AA_{AP}^{(FFT)}$);
3. relative error of accumulated perturbation at plateau (ε_{AP}), Equation 32.

$$\varepsilon_{AP} = \left(AP_{slug}^{(c)} / AP_{slug}^{(e)} \right) - 1 \qquad \textit{Equation 32}$$

If a plateau is reached (which indicates that a perturbation slug has completely passed through the core inlet), the corresponding accumulated perturbation value quantifies the total amount of perturbation, and should be always addressed in quantitative analysis. An acceptance threshold should be defined for such important parameter.

In some cases a plateau may not be reached because a second perturbation is arriving before the "tail" of the previous one has completely disappeared. In such a case the relevant accumulated perturbation value could be that corresponding to the time of minimum core-averaged perturbation. An example of such a situation is shown in Section 5.4.

The FFTBM can be applied also to the accumulated perturbation time-history, and the resulting average amplitude is a further parameter that quantifies the accuracy. An acceptance threshold should be defined for such parameter too.

For the sample curves shown in Figure 48, if #1 is assumed as the "experiment" and both #2 and #3 as the results from two different simulations, the resulting average amplitudes from FFTBM application would be *0.013* and *0.072* for the two calculations respectively.

The accumulated perturbation was adopted for quantitative analysis within the FLOMIX-R project Ref. [90]; however it is rarely referred to in the literature. The FFTBM, on the other hand, has never been applied to this kind of problem.

5.3.2.6. Scalar quantities related to the perturbation barycentre

Relevant quantities related to the barycentre location are:

1. time-averaged location ($\overline{x}_B$, $\overline{y}_B$);
2. maximum standard deviation of perturbation spatial distribution ($\sigma_{MAX}^{(sp)}$), i.e. maximum value of $\sigma_k^{(sp)}$ (as defined in Equation 10);
3. time-averaged standard deviation of perturbation spatial distribution ($\overline{\sigma}^{(sp)}$), Equation 33.

along with the following deviations:

4. maximum distance of perturbation barycentres ($d_{B,MAX}$), i.e. maximum value of $d_{B,k}$ (as defined in Equation 9);
5. average distance of perturbation barycentres ($\overline{d}_B$), Equation 34;
6. deviation of maximum standard deviation of perturbation spatial distribution ($\varepsilon\left[\sigma_{MAX}^{(sp)}\right]$), Equation 35;
7. deviation of time-averaged standard deviation of perturbation spatial distribution ($\varepsilon\left[\overline{\sigma}^{(sp)}\right]$), Equation 36.

$$\overline{\sigma}^{(sp)} = \frac{1}{t_{N_T} - t_1} \cdot \sum_{k=2}^{N_T} \sigma_k^{(sp)} \cdot \Delta t_k \qquad \textit{Equation 33}$$

$$\overline{d}_B = \frac{1}{t_{N_T} - t_1} \cdot \sum_{k=2}^{N_T} d_{B,k} \cdot \Delta t_k \qquad \textit{Equation 34}$$

$$\varepsilon\left[\sigma_{MAX}^{(sp)}\right] = \left[\sigma_{MAX}^{(sp)(c)} / \sigma_{MAX}^{(sp)(e)}\right] - 1 \qquad \textit{Equation 35}$$

$$\varepsilon\left[\overline{\sigma}^{(sp)}\right] = \left[\overline{\sigma}^{(sp)(c)} / \overline{\sigma}^{(sp)(e)}\right] - 1 \qquad \textit{Equation 36}$$

The location of the barycentre is necessary to estimate the other quantities.
The maximum and average distances between the experimental and calculated barycentre of the perturbation help quantifying the accuracy; related acceptance values should be defined.
The standard deviation of the spatial distribution (i.e. the central moment of second order around the barycentre), with its maximum and time-averaged values, is a mixing indicator: larger values indicate a more diffused spatial distribution, that is a more effective mixing, and vice versa.

No example of application of such key parameters has been found within the surveyed literature.

5.3.2.7. FLOMIX deviations

The following scalar deviations, already mentioned in Section 5.3.2.1 can be considered:

1. overall deviation, with sign ($dev3_{sign}$), Equation 37;
2. overall deviation, without sign ($dev3_{abs}$), Equation 38;
3. overall deviation, root-mean-squared ($dev3_{rms}$), Equation 39.

$$dev3_{sign} = \frac{1}{N_{CH}} \cdot \sum_{i=1}^{N_{CH}} dev2\_sign_i \qquad \textit{Equation 37}$$

$$dev3_{abs} = \frac{1}{N_{CH}} \cdot \sum_{i=1}^{N_{CH}} dev2\_abs_i$$ *Equation 38*

$$dev3_{rms} = \frac{1}{N_{CH}} \cdot \sum_{i=1}^{N_{CH}} dev2\_rms_i$$ *Equation 39*

They derive from space-averaging of *dev2* deviations, and provide a kind of overall information on the discrepancy between numerical results and experimental data.

5.3.2.8. Spatial gradients

Another mixing indicator is the maximum slope (intended as the maximum spatial gradient over the core inlet), along with its relative error. A higher value indicates steeper spatial gradients and thus a less diffused distribution.

1. Maximum slope ($\left[\Delta c / \Delta s\right]_{MAX}$).
2. Relative error on maximum slope ($\varepsilon\left\{\left[\Delta c / \Delta s\right]_{MAX}\right\}$)

5.3.2.9. Application of 3D FFTBM

The FFTBM is a well established tool to evaluate the accuracy of system code applications. It is applied to a set of time-dependent scalar quantities featuring the NPP thermal-fluid-dynamic behaviour (such as primary and secondary pressure, pressure drops, coolant and cladding temperatures, flowrates, etc.) and for each of them provides quantification (by the "average amplitude") of the discrepancy between code prediction and experimental data. Moreover, each of such scalar quantities is assigned a weighting factor to account for their different relevance, and then all average amplitudes are averaged – with proper weighting – to obtain a single quantity that characterizes the overall discrepancy.

The information to be analyzed and compared in the present context has however a completely different nature, as it consists of a perturbation distribution over three variables: the time, and two independent spatial coordinates (which define coolant channels locations). A first simple idea is to apply the FFT to the perturbation time-history at each channel, so that N_{CH} average amplitudes are obtained: maps of the discrepancies over the core inlet can thus be plotted, and finally the average amplitudes can be core-averaged to get an overall quantification of the accuracy. However this approach does not add any useful information to the accuracy quantification already provided by the FLOMIX deviations discussed above, and does not account for the spatial correlation between the perturbations occurring at adjacent channels, since each channel is considered regardless of its location and neighbouring channels.
Nevertheless, this kind of accuracy quantification was applied, for demonstration purposes, by the Author and his colleagues, in the framework of the code validation activities against Gidropress mixing experiments Refs. [13] and [47].

Another possibility to consider is the application of multidimensional discrete Fourier transform, with the purpose of directly providing a single scalar quantity which characterizes the discrepancy between code predictions and measurements. A huge amount of literature exists regarding the application of multi-D FFT approaches to the image processing. However, very few examples were found of multi-D FFT applications to data of different nature, and in no case dealing with problems of code accuracy assessment.
What is done here, in a somewhat pioneering way, is to extend the definition of average amplitude to three dimensions. This results in the following Equation 40:

$$AA = \frac{\sum_{i,j,k} \left| \widetilde{\Delta c}_{i,j,k} \right|}{\sum_{i,j,k} \left| \widetilde{c}^{(e)}_{i,j,k} \right|} \qquad \textit{Equation 40}$$

where $\Delta c_{i,j,k} = c^{(c)}_{i,j,k} - c^{(e)}_{i,j,k}$ is the error function, the symbol ~ indicates the 3D FFT operator, and the three indices *i*, *j* and *k* span over the transformed domains.
The 3D FFT is simply defined as the successive application of the 1D FFT operator over the three dimensions (see Ref. [91]).

5.4. Sample application of the proposed approach

5.4.1. Preliminary remarks

This Annex deals with a sample application of the accuracy quantification approach already presented in Section 5.3. Such approach consists in a data processing leading to a set of scalar quantities that characterize the time and space distribution of a perturbation of coolant properties at the core inlet, as well as the deviation between code prediction and experimental information about such perturbation.
The objective of this sample application is to test the approach and to evaluate the effectiveness of the above mentioned scalar quantities in quantifying the accuracy of a code simulation.
For this purpose, thirteen experiments were selected from the experimental database available at the University of Pisa for in-vessel mixing investigation (namely, tests conducted on ROCOM and GPMF test facilities). Moreover, 24 code simulations of those experiments were also selected from the available validation database. The selected simulations had been performed either with CFD or system codes; it is thus shown that the proposed approach can be of general use and not limited to CFD codes only.

The data processing was performed with the help of MATLAB routines that were coded for this specific purpose. However, a systematic application of the proposed procedure would require the development of a software package that satisfies generality, efficiency and quality assurance requirements (through a suitable Verification and Validation process). Such a task is a possible topic for the continuation of the present research activity beyond the PhD framework.

5.4.2. Parameters for accuracy quantification

The scalar parameters used for the accuracy quantification are listed in the following two Tables. In particular, Table 2contains all those quantities that characterize the perturbation (related to perturbation appearance, maximum perturbation, core-averaged perturbation, barycentre, etc.), while Table 3 contains parameters that quantify the deviations between the calculated and the experimental perturbation.

The third column of both Tables indicates which parameters can be considered as “mixing indicators”. The fourth column shows the name that the parameters are given win the MATLAB routines (the character “%” being replaced by “c” and “e” for calculated and experimental data respectively). The last column indicates the reference Sections of this document that contain more detailed information on the parameters definition.

Table 2 – List of scalar parameters for accuracy quantification (Calc. / Exp.)

Scalar quantity	Description	M.I.	Matlab ID	Ref.
x_{PA} , y_{PA}	Location of perturbation appearance		x_pa_%, y_pa_%	
t_{PA}	Time of perturbation appearance		t_pa_%	5.3.2.2
t_{PD}	Time of perturbation disappearance		t_pd_%	
Δt_{PT}	Perturbation transit time	X	dt_pt_%	
x_{MAX} , y_{MAX}	Location of maximum perturbation		x_max_%,y_max_%	
t_{MAX}	Time of maximum perturbation		t_max_%	5.3.2.3
c_{MAX}	Maximum perturbation	X	max_c_%	
$t_{CA,MAX}$	Time of maximum of core averaged perturbation		t_max_ave_%	
$\langle c \rangle^{MAX}$	Maximum of core averaged perturbation	X	max_ave_%	
$\bar{t}_{CA}$	Mean time of core averaged perturbation		t_centre_%	5.3.2.4
$\sigma_{CA}^{(t)}$	Standard deviation of core averaged perturbation	X	t_sigma_%	
$\Delta\langle c \rangle / \Delta t$	Time gradient of perturbation front	X	grad_t_%	
AP_{slug}	Accumulated perturbation at “plateau” or end of slug passage		ap_pl	5.3.2.5
$\bar{x}_B$, $\bar{y}_B$	Time-averaged location of perturbation barycentre		xB_ave_%, yB_ave_%	
$\sigma_{MAX}^{(sp)}$	Maximum standard deviation of perturbation spatial distribution	X	std_max_%	5.3.2.6
$\bar{\sigma}^{(sp)}$	Time-averaged standard deviation of perturbation spatial distribution	X	std_ave_%	
$[\Delta c / \Delta s]_{MAX}$	Maximum spatial gradient of perturbation	X	max_slope_%	5.3.2.8

Table 3 – List of scalar parameters for accuracy quantification (Deviations)

Scalar quantity	Description	M.I.	Matlab ID	Ref.
d_{PA}	Perturbation appearance location (distance over characteristic length)		d_pa	5.3.2.2
δt_{PA}	Time of perturbation appearance (relative to transit time)		d_t_pa	
d_{MAX}	Location of maximum perturbation (distance over characteristic length)		d_max_loc	5.3.2.3
δt_{MAX}	Time of maximum perturbation (relative to transit time)		d_t_max	
ε_{MAX}	Maximum perturbation (relative error)	X	d_max	
$\delta t_{CA,MAX}$	Time of maximum of core averaged perturbation (relative to transit time)		d_t_max_ave	5.3.2.4
$\varepsilon_{CA,MAX}$	Maximum of core averaged perturbation (relative error)	X	d_max_ave	
$\delta \bar{t}_{CA}$	Mean time of core averaged perturbation (relative to transit time)		d_t_centre	
$\varepsilon\left[\Delta\langle c\rangle / \Delta t\right]$	Time gradient of perturbation front (relative error)	X	d_grad_t	
$\varepsilon\left[\sigma_{CA}^{(t)}\right]$	Standard deviation of core averaged perturbation (relative error)	X	d_t_sigma	
$AA_{CA}^{(FFT)}$	Average amplitude from FFTBM applied to core averaged perturbation		AA_ca	
ε_{AP}	Accumulated perturbation at "plateau" or end of slug passage (relative error)		d_ap	5.3.2.5
$AA_{AP}^{(FFT)}$	Average amplitude from FFTBM applied to accumulated perturbation		AA_ap	
$d_{B,MAX}$	Maximum deviation of pert. barycentre (distance over characteristic length)		d_B_max	5.3.2.6
$\bar{d}_B$	Time-ave. deviation of pert. barycentre (distance over characteristic length)		d_B_ave	
$\varepsilon\left[\sigma_{MAX}^{(sp)}\right]$	Max. standard deviation of pert. spatial distribution (relative error)	X	d_std_max	
$\varepsilon\left[\bar{\sigma}^{(sp)}\right]$	Time-averaged standard deviation of pert. spatial distribution (relative error)	X	d_std_ave	
$dev3_{sign}$	FLOMIX deviation #3, with sign		dev3_sign	5.3.2.7
$dev3_{abs}$	FLOMIX deviation #3, without sign		dev3_abs	
$dev3_{rms}$	FLOMIX deviation #3, root mean squared		dev3_rms	
$\varepsilon\left\{\left[\frac{\Delta\langle c\rangle}{\Delta s}\right]_{MAX}\right\}$	Maximum spatial gradient at $t_{CA,MAX}$ (relative error)	X	d_max_slope	5.3.2.8
AA	Average amplitude from 3D FFTBM applied to the whole perturbation		AA	5.3.2.9

5.4.3. The selected experiments

A brief description of the experiments referred to in this part of the work is given hereafter; the main features of the tests are indicated in Table 4.

The first three were conducted on ROCOM test facility. They are “slug-type” experiments, since they feature a tracer slug that enters the RPV. The tracer, in this facility, is injected for a short period of time into cold leg N°1, and the injection zone is a few decimetres far from the cold leg inlet nozzle. The first two experiments were run with all of the four pumps in steady-state operation (each test with a different flowrate and different injection duration), while in the third test the start-up of pump N°1 was simulated, the other three pumps being at rest. Measurements of the tracer concentration both at core inlet and in the downcomer were obtained with the so-called wire mesh sensors; however, only the measured data for the core inlet are referred to here.

The remaining ten experiments were conducted on the Gidropress mixing facility in the framework of the Project TACIS R2.02/02. The first five of them (i.e. #4 to #8) are slug-type experiments, with one pump being started-up and the other three pumps kept at rest. Those tests differ by the condition of the isolation valves on idle loops (either open in tests #4 and #5, or closed in tests #6-#8), and by the density ratio between the tracer slug and the pure water (lighter and heavier slug in tests #3 and #5 respectively; density ratio = 1 for all other tests).

The last five experiments are “injection-type”, i.e. they were run with a continuous tracer injection into loop #1 for a relatively long period of time (around three times the circulation period through the whole loops in normal operation) while the pumps are running at nominal flowrate, so that a tracer accumulation took place during the tests. The first two of them had four pumps symmetrically operating (with nominal and reduced flowrate respectively). The last three experiments differ by the number of pumps being operated.

It is worth remarking that the experiments featuring a pump start-up instead of the steady pumps operation are characterized by noticeably more complex flow patterns developing inside the vessel, with strong horizontal velocity components, stagnation regions and recirculation zones the simulation of which is a challenging task even for CFD codes.

Table 4 – Selected experiments

#	ID	Original ID	Slug/Inject.	Pumps	Ref.
1	R_ST_01	ROCOM_STAT_01	S	4 S-S	[89], [32], [22]
2	R_ST_02	ROCOM_STAT_02	S	4 S-S	
3	R_TR_09	ROCOM_09	S	Start-up	
4	GPMF-01	GPMF E1	S	Start-up	[13], [47], [82]
5	GPMF-02	GPMF E2	S	Start-up	
6	GPMF-03	GPMF E3	S	Start-up	
7	GPMF-04	GPMF E4	S	Start-up	
8	GPMF-05	GPMF E5	S	Start-up	
9	GPMF-06	GPMF E6	I	4 S-S	
10	GPMF-07	GPMF E7	I	4 S-S	
11	GPMF-08	GPMF E8	I	3 S-S	
12	GPMF-09	GPMF E9	I	2 S-S	
13	GPMF-10	GPMF E10	I	1 S-S	

5.4.4. The selected simulations

A large code validation database on in-vessel mixing problems has been collected at the University of Pisa, comparing numerical results against measured data obtained from – among others – the tests mentioned above. Many CFD simulations have been performed by the Author of this work for the purposes of his PhD research (see ANNEX A).

The validation database includes not only CFD analyses, but also system code calculations performed with RELAP5-3D and some Russian codes with 3D capabilities (DKM, KORSAR, TRAP-KS) in the framework of the Project TACIS R2.02/02.

A small set of calculations has been selected from the above database for demonstrating the proposed accuracy quantification approach. At least a hundred more calculations are available for future application of the approach.

The main features of the selected calculations are indicated in Table 5, along with a synthetic description of the results obtained and of their “quality” as appears from the qualitative and (preliminary) quantitative analysis. More detailed information on such calculations can be found in the same references already indicated in Table 4, as well as in Section A.1 as regards ROCOM simulations.

Table 5 – Selected simulations

#	TEST	CODE TYPE	SIMULATION FEATURES	RESULTS
1	R_ST_01	CFD	Three different meshes (RPV only); same simulation set-up; RANS turbulence modelling	Good qualitative agreement (correct prediction of "perturbation sector"). Steeper gradients predicted (mixing under-estimated).
2	R_ST_01	CFD		
3	R_ST_01	CFD		
4	R_ST_02	CFD	Same mesh as above; RANS	Same as above
5	R_TR_09	CFD	Two different meshes (RPV only); same simulation set-up; RANS turbulence modelling	Qualitative agreement less satisfactory than above (much more complex flow behaviour!). Not all features of perturbation morphology are caught.
6	R_TR_09	CFD		
7	GPMF-01	CFD	CFD: post-test; same mesh for all calculations (same size and type as ROCOM meshes); RANS; BC from experiments; tracer slug SYS: post-test; same nodalization for all calculations, with entire loops; LP mixing model;	CFD (#7, #9): Better qualitative agreement than for ROCOM test R_TR_09 (i.e. better description of perturbation morphology), perhaps owing to lower order advection scheme used. Evidence of large quantitative discrepancies. CFD (#11, #14): No coherent perturbation morphology at core inlet due to buoyancy effects. SYS: Completely unable to predict the perturbation morphology
8	GPMF-01	SYS		
9	GPMF-02	CFD		
10	GPMF-02	SYS		
11	GPMF-03	CFD		
12	GPMF-03	SYS		
13	GPMF-04	SYS		
14	GPMF-05	CFD		
15	GPMF-05	SYS		
16	GPMF-06	CFD	CFD: post-test; same mesh for all calculations; RANS; BC from experiments; tracer injection SYS: post-test; same nodalization for all calculations, with entire loops; LP mixing model;	CFD: As for #1 to #4, the morphology is relatively simple (one perturbation sector) and is well reproduced; however the flow rotation observed in the tests cannot be predicted. Calculated perturbation gradients are steeper than in the experiment. SYS: Even better results than CFD, because the flow rotation is accounted for (although artificially)
17	GPMF-06	SYS		
18	GPMF-07	CFD		
19	GPMF-07	SYS		
20	GPMF-08	CFD		
21	GPMF-08	SYS		
22	GPMF-09	CFD		
23	GPMF-09	SYS		
24	GPMF-10	SYS		

5.4.5. Results of the application of the accuracy quantification approach

The error-type parameters listed in Table 3 have been calculated for each of the 24 code simulations, with the help of the MATLAB routines mentioned above. The results are reported in Table 6 and Table 7. Some "instructions" for a proper reading of the tables are given hereafter, while a discussion on the tables' contents will be provided later.

i. The systematic calculation of the parameters for accuracy quantification is relatively easy, once proper tools have been developed to run it automatically. However, what cannot be done automatically is obviously the interpretation of the values obtained. This quantitative analysis must be strictly linked to the qualitative analysis previously performed, and the meaningfulness of each quantity must be checked, based on what has been learnt from the information on perturbation morphology, flow distribution etc. Clear examples are represented by the experiments GPMF-03 and GPMF-05 and the related code simulations #11, #12, #14 and #15 (see Table 5): in such cases the morphology of the perturbation at the core inlet is not well defined, rather it has a kind of "erratic" behaviour, due to the presence of strong buoyancy effects leading to the stagnation of the tracer either in the lower plenum or in the upper part of the downcomer, respectively; therefore, in such cases, almost all of the quantitative parameters here defined lose their meaning, except those related to the maximum, core-averaged and accumulated perturbation values.

ii. All the values suspected to be non-sense (either for the reasons above or for numerical problems encountered with the MATLAB processing) are marked with a cross in the tables.

iii. The perturbation appearance and disappearance threshold has been arbitrarily set as MS = 0.01 for the maximum perturbation (i.e. 1% of the overall maximum perturbation). In some cases, the maximum perturbation does not drop below such threshold after the slug passage, because the presence of some tracer persists quite longer, therefore the perturbation disappearance time is automatically set at the end of the available data set.

iv. The perturbation appearance location may be a "weak" parameter, in those cases when the perturbation morphology is more complex that a simple tracer spot and can appear at more than one position at (approximately) the same time.

v. All deviations on relevant times (appearance, maximum perturbation, etc.) are expressed in % of the perturbation transit time. Such deviations are indicated as δt .

vi. All deviations on distances (e.g. between perturbation appearance locations, locations of maxima, locations of barycentres, etc.) are expressed in metres, instead of being normalized. However, both experimental facilities ROCOM and GPMF have the same size (RPV diameter around 1 m), therefore the results are comparable. Spatial deviations are indicated as d .

vii. Deviations indicated as ε are relative errors (calculated minus experimental values) with respect to experimental value.

viii. Shaded columns contain the so-called “mixing indicators”. They reveal the tendency of the code either to over-predict or under-predict the effectiveness of mixing.

ix. The FFTBM was applied to the core-averaged and accumulated perturbation without defining a “cut-off” frequency common to all cases; rather, the cut-off frequency was automatically defined by the period of the each experimental data set without any further interpolation. The only interpolation performed was that necessary to align the calculated data with the measured ones. This approach can obviously be improved, with some additional computational expense, to allow for a “unified” definition of the cut-off frequency.

x. Analogous considerations apply to the definition of the “time window” to which the FFT is applied.

xi. The 3D FFTBM has been applied on data arrays mapped on a 64-by-64 node grid in space. The mapping has obviously required data interpolation in space, for both experimental and calculated data. The resulting average amplitude is – *a priori* – affected by such nodding; however no sensitivity analysis was performed on such parameter and this may be a topic for future development.

xii. The application of the 3D FFTBM to the accuracy quantification is pioneering. The mathematical issues connected with this approach have not been addressed in the framework of this research; however they should be carefully investigated and solved in order to make this methodology well founded and rigorous.

Table 6 – Results of accuracy quantification for selected calculations (first set of parameters)

#	TEST	CODE TYPE	d_{PA}	δt_{PA}	δt_{MAX}	d_{MAX}	ε_{MAX}	$\delta t_{CA,MAX}$	$\varepsilon_{CA,MAX}$	$\delta \bar{t}_{CA}$	$\varepsilon(c')$	$\varepsilon\left[\sigma_{CA}^{(t)}\right]$	$AA_{CA}^{(FFT)}$
1	R_ST_01	CFD	0.190	0.00%	10.92%	0.280	3.36%	10.04%	-6.69%	0.75%	-2.25%	-0.90%	0.164
2	R_ST_01	CFD	0.411	0.00%	4.80%	0.000	3.35%	27.95%	-5.90%	0.74%	-9.99%	-1.85%	0.161
3	R_ST_01	CFD	0.411	-0.44%	5.24%	0.000	3.35%	14.41%	-6.18%	0.86%	-20.61%	-0.72%	0.165
4	R_ST_02	CFD	0.046	0.75%	-26.80%	0.065	7.39%	0.19%	-10.87%	-1.49%	65.03%	-8.12%	0.260
5	R_TR_09	CFD	0.092	0.21%	-4.19%	0.617	183.62%	-7.28%	10.57%	-0.17%	54.18%	6.84%	0.567
6	R_TR_09	CFD	0.396	-6.18%	-6.38%	0.206	143.83%	-11.05%	-3.53%	-3.30%	23.22%	-1.86%	0.624
7	GPMF-01	CFD	0.083	0.12%	0.46%	0.127	4.82%	0.00%	33.92%	-0.40%	57.17%	5.31%	0.357
8	GPMF-01	SYS	0.221	-1.48%	0.59%	0.547	-34.47%	0.15%	-6.96%	-0.07%	-31.19%	0.39%	0.226
9	GPMF-02	CFD	0.568	-0.25%	-0.36%	0.000	-6.82%	-0.22%	16.39%	-0.32%	16.39%	-9.98%	0.565
10	GPMF-02	SYS	0.411	5.60%	-0.18%	0.501	-15.19%	-0.15%	-0.57%	-1.89%	-17.14%	-0.36%	0.387
11	GPMF-03	CFD	0.083	-24.56%	-38.24%	0.250	-7.43%	-24.56%	-0.83%	-25.15%	-3.47%	4.63%	0.846
12	GPMF-03	SYS	0.083	-16.82%	-21.21%	0.382	17.91%	-13.79%	18.45%	-18.42%	-2.74%	-8.76%	0.724
13	GPMF-04	SYS	0.464	-5.92%	3.37%	0.441	-20.87%	3.83%	-10.07%	-0.05%	-48.41%	-3.67%	0.270
14	GPMF-05	CFD	0.000	-0.88%	-8.64%	0.482	31.08%	-10.58%	52.06%	-4.49%	163.94%	-3.24%	0.525
15	GPMF-05	SYS	0.578	-6.61%	-12.87%	0.382	175.60%	-12.87%	241.14%	-16.50%	331.76%	-27.46%	2.043
16	GPMF-06	CFD	0.547	15.46%	1.11%	0.145	6.83%	0.10%	6.21%	0.06%	5.62%	2.81%	0.100
17	GPMF-06	SYS	0.521	15.61%	-1.31%	0.096	-6.59%	-0.05%	2.03%	-0.10%	10.21%	-0.16%	0.117
18	GPMF-07	CFD	0.083	-1.21%	-4.68%	0.174	-8.97%	-3.38%	-16.98%	-2.32%	-0.56%	1.92%	0.404
19	GPMF-07	SYS	0.144	9.63%	-3.90%	0.083	-11.25%	-2.95%	-13.77%	2.04%	-15.76%	7.27%	0.271
20	GPMF-08	CFD	0.255	18.41%	2.72%	0.048	17.42%	1.90%	-4.47%	0.59%	-5.46%	-2.38%	0.198
21	GPMF-08	SYS	0.293	17.46%	0.34%	0.128	-3.01%	0.41%	-4.70%	0.52%	-2.87%	-1.39%	0.107
22	GPMF-09	CFD	0.293	15.54%	2.34%	0.144	3.22%	3.10%	-7.27%	-0.17%	-9.22%	-1.87%	0.273
23	GPMF-09	SYS	0.293	6.38%	-0.22%	0.083	-9.13%	0.27%	-3.51%	0.16%	0.61%	0.08%	0.123
24	GPMF-10	SYS	0.083	9.59%	-0.40%	0.555	-3.06%	-0.40%	4.93%	-0.49%	9.18%	-1.03%	0.131

Table 7 – Results of accuracy quantification for selected calculations (second set of parameters)

#	TEST	CODE TYPE	ε_{AP}	$AA_{AP}^{(FFT)}$	$\varepsilon\left[\sigma_{MAX}^{(sp)}\right]$	$\varepsilon\left[\overline{\sigma}^{(sp)}\right]$	$\varepsilon\left\{\left[\frac{\Delta\langle c\rangle}{\Delta s}\right]_{MAX}\right\}$	$d_{B,MAX}$	$\overline{d}_B$	$dev3_{sign}$	$dev3_{abs}$	$dev3_{rms}$	$AA^{(3DFFT)}$
1	R_ST_01	CFD	-4.49%	0.047	30.26%	33.63%	269.01%	0.321	0.123	-0.00455	0.14803	0.22893	1.638
2	R_ST_01	CFD	-3.98%	0.041	-21.91%	-18.41%	45.04%	0.238	0.031	-0.00404	0.03845	0.05954	0.806
3	R_ST_01	CFD	-4.02%	0.043	-21.70%	-18.89%	48.88%	0.279	0.033	-0.00408	0.03943	0.05992	0.753
4	R_ST_02	CFD	-11.29%	0.102	-35.33%	-26.76%	48.74%	0.414	0.047	-0.01334	0.05197	0.07610	0.906
5	R_TR_09	CFD	1.43%	0.044	-90.76%	-2.65%	223.60%	3.214	0.048	0.00028	0.01844	0.03619	2.671
6	R_TR_09	CFD	13.49%	0.157	-90.52%	7.57%	386.43%	3.242	0.121	0.00261	0.01908	0.03482	2.313
7	GPMF-01	CFD	6.15%	0.085	-65.31%	10.89%	0.00%	0.621	0.032	0.00079	0.00593	0.02688	1.046
8	GPMF-01	SYS	15.76%	0.156	-69.50%	-7.06%	0.00%	0.911	0.058	0.00520	0.01461	0.03661	1.191
9	GPMF-02	CFD	6.09%	0.149	12.28%	1.48%	18.20%	0.158	0.033	0.00038	0.00357	0.02573	1.118
10	GPMF-02	SYS	1.20%	0.026	-11.54%	-2.38%	-31.83%	0.281	0.013	0.00046	0.00745	0.02869	1.323
11	GPMF-03	CFD	-1.71%	0.165	-21.67%	19.66%	6.75%	0.441	0.013	-0.00186	0.08825	0.12042	1.129
12	GPMF-03	SYS	-10.88%	0.164	-32.53%	6.21%	-44.92%	0.441	0.070	-0.01174	0.07283	0.09677	1.228
13	GPMF-04	SYS	4.94%	0.059	-11.27%	-9.78%	-37.85%	0.292	0.138	0.00408	0.05463	0.08444	1.221
14	GPMF-05	CFD	10.06%	0.137	4.22%	0.44%	74.72%	0.200	0.021	0.00342	0.01337	0.02292	1.091
15	GPMF-05	SYS	144.36%	1.615	-10.83%	-16.12%	70.51%	0.296	0.083	0.04916	0.06515	0.11034	1.662
16	GPMF-06	CFD	5.94%	0.056	-100.00%	-49.55%	47.87%	13.908	0.155	0.00418	0.04740	0.10701	1.182
17	GPMF-06	SYS	5.17%	0.052	-98.42%	-18.65%	-42.45%	13.908	0.034	0.02592	0.04169	0.05542	0.654
18	GPMF-07	CFD	-19.77%	0.197	-100.00%	-46.18%	14.86%	1.759	0.054	-0.01607	0.03558	0.05686	0.800
19	GPMF-07	SYS	-9.19%	0.105	-100.00%	-34.59%	-31.89%	1.759	0.042	-0.00748	0.02437	0.03616	0.643
20	GPMF-08	CFD	-7.74%	0.079	-100.00%	-23.61%	112.60%	8.980	0.067	-0.04498	0.23189	0.29816	1.029
21	GPMF-08	SYS	-2.26%	0.025	-100.00%	-18.63%	-5.31%	8.980	0.025	-0.01314	0.05121	0.06715	0.658
22	GPMF-09	CFD	-9.70%	0.095	-92.50%	-19.35%	114.46%	2.885	0.051	-0.06243	0.19555	0.25813	1.128
23	GPMF-09	SYS	0.31%	0.003	-92.48%	-6.76%	-6.02%	2.885	0.009	0.00207	0.02587	0.04188	0.747
24	GPMF-10	SYS	4.94%	0.052	-94.49%	-9.41%	-95.64%	3.932	0.009	0.03982	0.04805	0.07011	0.823

Some considerations from the observation and the comparison of the values reported in the two tables above are given below. They do not constitute the conclusions of a systematic assessment of the accuracy indicator proposed, which would require their application to a wider validation database.

Quantities related to the perturbation appearance (d_{PA}, δt_{PA})

- The deviation of PA location shows relatively large variations in almost all cases. It does not help much in assessing haw accurate is the simulation, but can however provide useful information if the PA location is assumed, in a specific context, as a parameter relevant to the reactor safety.
- The deviation in perturbation appearance time shows large values (>10%) in many cases among the GPMF simulations: this is mostly due to incorrect calculation of the appearance time for the experiments, since the appearance threshold arbitrarily chosen (i.e. MS = 0.01) is comparable with the background noise in the experimental measurements before the tracer arrival. This suggests that the threshold should be set to a value sufficiently large compared to the noise.

Quantities related to the maximum perturbation appearance (δt_{MAX}, d_{MAX}, ε_{MAX})

- The time of maximum is predicted with relatively small errors in many cases, except for experiments with buoyancy effects, and in ROCOM steady-state experiments (especially the second one). For the latter, the large discrepancy is explained by the fact that the “plateau” reached in the experiment is slightly sloping, then the maximum values is reached at the end of the plateau; on the other hand, the code simulation predict the maximum value at the beginning of the plateau. This evidences once more that the importance of the qualitative analysis before any accuracy quantification is made.
- As regards the maximum perturbation location, the same considerations can be made as for the location of the perturbation appearance.
- The largest errors in the maximum perturbation values are associated with system code simulations, buoyancy cases, and ROCOM transient experiment.

Quantities related to the core-averaged perturbation
($\delta t_{CA,MAX}$, $\varepsilon_{CA,MAX}$, $\delta \bar{t}_{CA}$, $\varepsilon(c')$, $\varepsilon\left[\sigma_{CA}^{(t)}\right]$, $AA_{CA}^{(FFT)}$)

- The deviation on the time of maximum for the core-averaged perturbation shows the smallest values in all GPMF cases without density effects, and in ROCOM tests except the first (for the same reason mentioned above, i.e. the slope in the plateau).
- No particular evidence arises from the errors in maximum value. As a “mixing indicator”, it seems to indicate opposite trend. Obviously it is not sufficient, if taken alone, to characterize the mixing behaviour, there it should be used combined with the other mixing indicators.
- The “centre” of the time distribution is well predicted in practically all cases without buoyancy. This can be a good check than the inlet boundary conditions are well-posed.

- No particular evidence arises from the errors in time gradient and standard deviation.
- The average amplitude from the FFTBM application is probably the quantity that better characterizes the accuracy as regards the core-averaged perturbation. Its lowest values are associated in fact with the cases which had shown, in the qualitative analysis, the closest agreement between calculation and experiment.

Quantities related to the accumulated perturbation (ε_{AP} , $AA_{AP}^{(FFT)}$)

- The error "plateau" value of the accumulated perturbation is certainly an important parameter to characterize the accuracy, since it is related to the amount of perturbation that has passed through the core. Its variations shown in the table (small in some case, much greater in other) evidence different code behaviours.
- Since the accumulated perturbation is related to the core-average by a time-integration, one would expect that the average amplitudes from the FFTBM application show the same behaviour as for the core-averaged perturbation (apart from smaller values). This is actually not always the case; the two simulations of the experiment GPMF-01, for instance, show opposite behaviours of the two average amplitudes (i.e. the SYS calculation yields a smaller value for $AA_{CA}^{(FFT)}$ and a larger value for $AA_{AP}^{(FFT)}$. This aspect deserves further investigation.

Quantities related to the perturbation barycentre ($d_{B,MAX}$, $\overline{d}_B$, $\varepsilon\left[\sigma_{MAX}^{(sp)}\right]$, $\varepsilon\left[\overline{\sigma}^{(sp)}\right]$)

- The calculated relative maximum deviations of the perturbation barycentre position appear non plausible in several cases, probably due to a bug in the Matlab routine. The average deviation, on the other hand, generally shows lower values for those cases which are indicated to be relatively "more accurate" also by other parameters (e.g. cases #2 and #3 compared to #1, #5 compared to #6, etc.).
- This tendency is also shown by the relative error on the time averaged standard deviation of the perturbation spatial distribution. Moreover, this parameter shows negative values in most cases, which indicate a tendency to under-predict the mixing.

Maximum spatial gradient ($\varepsilon\left\{\left[\frac{\Delta\langle c\rangle}{\Delta s}\right]_{MAX}\right\}$)

- This parameter shows positive values for all CFD calculations, i.e. time gradients steeper than in the experiment, in agreement with the tendency to under-predict the mixing effectiveness already indicated by other parameters.

FLOMIX deviations ($dev3_{sign}$, $dev3_{abs}$, $dev3_{rms}$)

- The first parameter, which accounts for the sign of the local deviations, shows lower magnitudes for those case which are indicated as more accurate by the other parameters. Moreover, smaller values are normally associated with CFD results rather than with system code results (except for GPMF tests no. 7 to 9). This behaviour appears consistent with the average deviation on the perturbation barycentre. It is obviously much affected by the incapability of the CFD code to predict the downcomer flow rotation.
- The same tendency is generally shown by the other two parameters.

AA from 3D FFTBM application ($AA^{(3DFFT)}$)

Apart from few exceptions (#1, #5, #6, #15) this quantity shows values ranging between 0.6 and 1.4. Its "sensitivity to accuracy" is not particularly evident from the few cases considered and certainly needs further assessment.

5.5. Concluding remarks on accuracy evaluation

The approach described above for the quantification of the accuracy was applied systematically to a number of (CFD and system) code simulations selected within the validation database that has been collected at the University of Pisa. The purpose of such application is to test the applicability of such parameters in characterizing the accuracy of a code simulation, while a thorough assessment of the proposed approach requires the application to a wider validation database, which constitutes matter for future work.
The main achievements from this demonstrative application are summarized hereafter.

- The applicability of a number of parameters for accuracy quantification in IVF investigations has been demonstrated. This has been done with the support of a small database of mixing experiments and related code simulations. Such database is just a "sample" from the wider database available at UNIPI. Moreover, it is relatively heterogeneous as it includes both CFD and system code calculations and experiments of different types.
- A "ranking" of such parameters in relation to their effectiveness in quantifying the accuracy is needed before they can be utilized in the practice. For this purpose, they will have to be assessed on a wider validation database. In particular, it is necessary to assess more in detail the sensitivity of each parameter on the features of a given experiment as well as of the code simulations, such as the steady or transient nature of the pumps operation, the symmetry in pumps operation, the numerical models adopted for the simulations, etc.
- The application of a 3D FFT technique to characterize the perturbations and their deviations is new and the related mathematical aspects still have to be analyzed in detail. This should be also matter for future research.

One final comment must be made about the uncertainty.

The experimental data are inherently affected by some uncertainty, and information should always be provided by experimentalists on the uncertainty that is associated with each measurement. Such information usually derives from statistical treatment of the data measured in different runs on the same tests (this happened for instance both with ROCOM and GPMF experiments) and is expressed in terms of “confidence intervals” bounded by one or two standard deviations.
The comparison between calculated and experimental data should then be performed taking into account the information on experimental uncertainty (as recommended also by the BPG).
Besides, also the uncertainty of calculation results should be evaluated. This obviously leads to a large number of sensitivity calculations to be performed and then to noticeable increase in the computational resources to be allocated for that (which is cause for CFD results uncertainty analysis being so rare).

The proposed approach for the accuracy quantification should be combined with the existing well-established techniques for the treatment of experimental and numerical uncertainty, and this can be also a topic for future developments of the present work.

6. FINAL REMARKS ON THE WORK DONE AND CONCLUSIONS

This doctoral thesis is a result of four-year work on application of CFD codes in the area of nuclear reactor safety, operation and design, with particular reference to the code assessment issues and to the in-vessel flow investigation. In particular, it aims at proposing a synthesis of what has been learned in the activities carried out within an exceptionally stimulating context.

The Author has been in charge of coordinating all CFD-related activities within the San Piero a Grado Group and has been continuously in touch with top-level experts from foreign research centres, institutions and industries (e.g. CEA, EDF, FZD, PSI, USNRC, ANSYS, AREVA, etc.) and international organizations (IAEA, OECD/NEA), being involved in many relevant international events.
In this context, the experience gained basically relies on two aspects:

1. the efforts spent and the results obtained in generating meshes, running calculations, comparing results, processing data, etc.;
2. the invaluable opportunity to observe the complex interaction between the worlds of CFD and nuclear technology from the perspective of those who make decisions and drive the overall R&D process.

6.1. Work, experience and framework

A large part of the work dealt with the CFD analysis of single-phase in-vessel flow, including the comparison against experimental data – whenever available – for code validation purposes. Various test facilities and nuclear reactors have been simulated, so that different geometries, scales, transient scenarios, flow phenomena and levels of complexity had to be dealt with. Such a wide variety of situations does represent really precious working material from which general lessons can be obtained.

Many CFD analyses addressed experiments conducted by the ROCOM test facility, in the frame of a research cooperation agreement between the University of Pisa and the Research Centre Dresden-Rossendorf (FZD). Simulating ROCOM experiments is a kind of “continuous action”, since new computational grids can be developed and new calculations can be performed as more computing power, improved models and code releases, and improved user’s skills become available. Thus, it took almost three years to achieve a relatively satisfactory CFD mesh for ROCOM simulations.
Amongst the scaled test facilities for investigation of in-vessel flow, ROCOM is the one equipped with the most sophisticated instrumentation for tracer concentration measurements. In particular, it permits an accurate characterization of the RPV inlet boundary conditions and then a noticeable reduction of the related uncertainties. Moreover, it allowed investigating the effects of the non-uniformities of the tracer cross-sectional distribution on the in-vessel distribution. Addressing this and other modelling issues helped to point out many essential aspects involved in the CFD analysis of in-vessel flow.

A valuable source of experience was constituted by the TACIS Project R2.02/02, and in particular by hundreds of CFD and system code simulations of Gidropress mixing experiments, performed by the participants in the project. The University of Pisa had the responsibility of coordinating the pre-test and post-test analysis tasks, as well as of performing CFD simulations of all experiments (sharing this work with FZD) and analyzing and comparing all participants' results. The result of this collaboration is a large validation database that has been exploited only for a part of its potential, and will keep playing an important role in CFD assessment process. On the UNIPI side, most of the "hands-on" work on the analysis of Gidropress experiments was done by Daniele Melideo, and constitutes the basis of his doctoral research. However, part of the results of that shared experience is present also in this work, although in a different form, i.e. both through further elaboration of the numerical and experimental data (for accuracy quantification purposes) and through the synthesis effort towards a systematic assessment procedure.

Another validation activity focused on Kozloduy VVER-1000 reactor, and was carried out in the framework of an OECD/NEA benchmark. The most interesting aspects of this work were related to modelling a real full-scale geometry, and dealing with the problem of "downcomer flow rotation".

In-vessel flow investigations have been performed also for the Atucha-II PHWR (the most directly involved person being Fulvio Terzuoli, in the frame of his PhD research). In this case, the analyses were not aimed at code assessment, but rather at observing and understanding the fluid-dynamic phenomena occurring in such a peculiar geometry, and confirming some assumptions on which some integral code analyses of Atucha-II are based. Anyhow, dealing with a noticeably different geometry helped to get a more complete view of what issues can be encountered when addressing in-vessel flow investigation.

Along with the simulations of in-vessel flows, many other CFD analyses have been performed, including two-phase flows, for example: calculations of local pressure losses through geometrical discontinuities, simulations of free-surface flows, simulations of convective boiling flows, etc. Such additional work has not been documented in this thesis as it has no direct connection with its main topics; however, it also contributed to reinforce the experiential bases of the whole work.

A great added value came from the participation in the meetings of the CSNI "Writing Groups on CFD issues". Much of the quality-and-safety-oriented attitude that supported this work derives from such an environment.

Another point worth mentioning is the editorial activity performed for the international journal Science and Technology of Nuclear Installations, in particular looking after a special issue on "Computational fluid dynamics for gas-liquid flows".

The very last part of the doctoral activity consisted in revisiting and re-elaborating (at least in part) the main achievements and the "lessons learned" from the above experiences and work, and synthesizing them in this dissertation. Those achievements are widely discussed in the central Chapters of the thesis, while a more general description is provided in the following concluding remarks.

6.2. Achievement of the objectives

The final goal of the research was to provide a contribution to the assessment of CFD codes in their application to nuclear reactor safety problems and, in particular, to the investigation of in-vessel flows. That aim was achieved in several steps, at different levels, which can be summarized as follows:

1. The validation work performed, that has been the subjects of archival publications (see Annex A), is *per se* a first, direct contribution to the code assessment. The conclusions of this activity cannot be a simplified judgement about the adequacy of CFD tools for in-vessel flow predictive analysis, for the following reasons:
   - o the code validation, even for a single specific problem such as the in-vessel flow, is quite a huge task, which requires coordinated efforts from the whole scientific community and cannot be enveloped within a PhD research;
   - o suitable criteria still have to be defined to assess the "degree of accuracy" of the CFD predictions (see below).

   However, the validation work allowed pointing out some capabilities and limitations (which confirm and extend the achievements from the code assessment work performed by other specialists, e.g. in the frame of FLOMIX-R project). Some key considerations in this respect are reported below.
   a. CFD simulations, combined with RANS turbulence modelling approaches, are generally able to provide realistic descriptions of the phenomenology involved in in-vessel flow and mixing. In particular, the main flow distribution patterns are usually well predicted, along with the morphology of the perturbations affecting the coolant properties in case of boron dilution scenarios, main steam line breaks etc.
   b. The "degree of realism" of CFD predictions is, however, quite sensitive to the different level of complexity that can be encountered in different in-vessel flow configurations, depending upon the operational configuration of the coolant loop. The flow patterns developing in case of symmetric and steady pump operation are relatively "simple" (apart from possible "downcomer flow rotation" effects) and are easily described by CFD codes. On the other hand, in the presence of strong loop flow asymmetries (e.g., in pump start-up scenarios) the flow configuration becomes much more complex, since highly three-dimensional flow structures develop, the accurate representation of which represents a challenge. Further complications can be brought by the presence of buoyancy effects. Therefore, a classification based on the type of scenarios addressed and the related flow configuration is always necessary.
   c. There are still open issues related to the quantitative prediction of the mixing effectiveness. In most of the CFD analyses performed, a tendency to under-predict the turbulent mixing was revealed by steeper gradients compared to measured data. This observation is obviously bounded to the specific scenarios analyzed and to the turbulence models used (usually two-equation eddy-viscosity models). Anyhow, it

allows identifying a weakness in the modelling capabilities and suggests a topic for future developments.

d. A closer look at the numerical results and experimental data indicates that the most critical part of in-vessel flow modelling is the downcomer flow, despite its relatively simple geometry, and that the research of model deficiencies in turbulent mixing predictions should focus here.
e. Although the influence of inlet boundary conditions and geometrical details can be expected *a priori*, it is necessary to assess it with specific sensitivity analyses. This was done, for instance, as regards the fillet on the RPV inlet nozzle edge, the non-uniformities of tracer distribution over the cold leg cross-section, the cold leg elbows, the lower plenum internals, etc.
f. Intrinsic limits have been encountered in the physical modelling, in particular as regards the downcomer flow rotation. Some geometrical and operational features (cold leg elbows, asymmetries in geometry and pumps operation, etc.) were identified which can affect such behaviour, but the origin of the phenomenon has not been fully understood yet, and the question whether the CFD can predict it or not remains open.

2. The experience on code assessment for in-vessel flow investigation was critically re-elaborated and put in the form of a general methodology, which is presented in Chapter 4. In particular, the topics listed below were addressed.
   a. The relevant phenomena and flow configurations are identified and described analytically, along with the related experimental and modelling issues.
   b. Guidance is provided on how to address the in-vessel flow investigation, through a discussion on the known issues connected with each phase of the analysis, pointing out the main limitations in the current state-of-the-art and making reference to the phenomena and flow configurations previously indentified as well as to the BPGs.
   c. The role of CFD in support to the thermal-hydraulic system code application and assessment is demonstrated, in particular as regards the interpretation of code results, the extension of the experimental database and the development of system code nodalizations.

   A synthesis effort was necessary to outline a general methodology which encompasses the experience achieved. This part of the work represents the main outcome of the research carried out.

3. Connected to the code assessment methodology mentioned above is the proposal of a systematic approach to the quantification of accuracy, discussed in Chapter 5 (which constitutes, together with Chapter 4, the core of the thesis). The study on this aspect started with the consideration, supported by the literature survey and the direct experience gathered within the international scientific context, that a weak point in the CFD code assessment process is represented by the lack of systematic approaches to accuracy evaluation when dealing with multi-dimensional data (such as, for instance, the space and time distribution of coolant propertied at the

core inlet). In other terms, the quantitative analysis of results (both from CFD and integral codes with 3D capabilities) and the comparison against measured data is usually incomplete and not exhaustive, since it focuses only on a limited set of quantitative parameters which are not sufficient to fully characterize the addressed phenomena. Therefore, an attempt has been made to identify a larger number of quantitative indicators that, together, can characterize the perturbations at the core inlet and "measure" the discrepancy between numerical predictions and experiments. Such indicators have been "tested" on a small part of the validation database available at the University of Pisa (including both CFD and system code simulations of in-vessel mixing experiments, as well as the related measured data). The potential of this approach to provide an efficient tool for quantifying the accuracy was thus proven, although further efforts are necessary for a complete assessment against a wider validation database, in order to identify the effectiveness and significance of each parameter in quantifying the accuracy.

The whole work has been inspired and driven by the concept of quality assurance, which, as far as code application and assessment are concerned, means that all practicable efforts are spent to limit sources of errors and uncertainties, and to obtain the best quality achievable from a state-of-the-art tool consistently with the available computational resources. Some guidance on how to pursue the quality in CFD for nuclear reactor safety applications is contained in the so-called best practice guidelines (such as those issued by one of the above mentioned CSNI Writing Groups). However the existing BPGs are limited and incomplete, since they do not address thoroughly any of the specific problems encountered in nuclear technology; as declared by their Authors, the BPGs are intended as a "living document", which will grow as new contributions are provided addressing specific issues in detail. It is believed that the present work can represent a useful contribution to establish best practice guidelines on the in-vessel flow analysis.

6.3. Perspectives for future research

Many topics have been identified throughout the document as matter for future research and development. The most important ones, apart from the never-ending validation work, can be summarized as follows:

- The "guidelines" included in the proposed assessment methodology are obviously far from being complete and exhaustive: as additional experience is gathered on in-vessel flow analysis (especially if improved models and grids are made available, and more sophisticated turbulence modelling approaches – such as LES – are adopted), the methodology can be further improved and enriched in the discussions upon the specific modelling issues.
- Concerning the phenomenology involved in in-vessel flow and the related modelling, many issues deserve to be further investigated, such as, for example:
  - the downcomer flow and the problem of mixing under-prediction;

  - the geometric and operational features affecting and/or triggering the downcomer flow rotation;
  - the quantification (through sensitivity analyses) of the uncertainties associated with the boundary conditions (also in relation to the coupling with system and NK codes), the models, the mesh etc.
- As mentioned above, further work is necessary to establish a systematic accuracy quantification approach. The quantitative parameters proposed (and applied at a “demonstrative” level) are a good starting point. They will have to be applied to a larger validation database, which encompasses a large variety of scenarios and modelling choices, so as to identify which parameters are most effective in characterizing the accuracy, and possibly to formulate a method for extracting, from the whole set of parameters, a global quantification of the accuracy of a single calculation. Moreover, the accuracy quantification approach should also be extended and improved to account for the treatment of numerical and experimental uncertainties.
- Accuracy quantification is only half of the job: what is then necessary is to define criteria for judging the accuracy level obtained from a calculation. In other words, after the accuracy has been quantified, it must be evaluated, in order to answer questions such as: “Is the calculation accurate *enough*?” What “enough” means must be defined, and this obviously requires a coordinated effort involving thermal-hydraulics and core physics analysis.

REFERENCES

1. Bestion D., Anglart H., Caraghiaur D., Peturaud P., Smith B., Andreani M., Niceno B., Krepper E., Lucas D., Moretti F., Galassi M. C., Macek J., Vyskocil L., Koncar B., Hazi G., Review of Available Data for Validation of NURESIM Two-Phase CFD Software Applied to CHF Investigations, Science and Technology of Nuclear Installations, Special Issue on Computational Fluid Dynamics for Gas-Liquid Flows, Volume 2009, Article ID 214512.
2. Galassi M.C., Coste P., Morel C., Moretti F., Two-phase flow simulations for PTS investigations by means of NEPTUNE_CFD code, Science and Technology of Nuclear Installations, Special Issue on Computational Fluid Dynamics for Gas-Liquid Flows, Volume 2009, Article ID 950536.
3. Moretti F., Terzuoli F., Melideo D., Creation of 3 CFD Models of Atucha-II RPV and Execution of Steady-state Calculations, TFR-3 Rev.0, Task 3 Final Report, 1st Agreement NA-SA/UNIPI, Pisa, October 2007.
4. Moretti F., Terzuoli F., Melideo D., CFD Transient Analyses for CNA-2, TFR-6 Rev.0, Task 6 Final Report, 1st Agreement NA-SA/UNIPI, Pisa, December 2007.
5. Mahaffy J. et al., **Best Practice Guidelines for the use of CFD in Nuclear Reactor Safety Applications**, NEA/CSNI/R(2007)5, May 2007.
6. Smith B. et al., **Assessment of CFD for Nuclear Reactor Safety Problems**, NEA/CSNI/R(2007)13, January 2008.
7. Moretti F., Melideo D., Terzuoli F., D'Auria F., Application of CFX-10 to the Investigation of RPV Coolant Mixing in VVER Reactors, ICONE14-89840, Proceedings of 14th International Conference on Nuclear Engineering, July 17-20, 2006, Miami, Florida, USA.
8. Kolev N. et al., VVER-1000 Coolant Transient Benchmark (V1000CT), Volume II: Specifications of the VVER-1000 Vessel Mixing Problems, OECD/NEA/CSNI, March 2004.
9. Shkarupa A., Application of RELAP5-3D to the V1000CT2 Exercise 1, Proceedings of the OECD/DOE/CEA VVER-1000 Coolant Transient Benchmark - Fourth Workshop, 24-25 April 2006, Pisa, Italy.
10. ANSYS Inc., ANSYS CFX-10.0 User Manual, (embedded in the software package), 2005.
11. ANSYS Inc., ANSYS ICEM-CFD 10.0 User Manual, (embedded in the software package), 2005.
12. Rohde U., Fluid mixing and flow distribution in the reactor circuit – measurement data base, Nuclear Engineering and Design Vol. 235, 2005, pp. 421-443.
13. Moretti F., Melideo D., Del Nevo A., D'Auria F., Pre-test Analyses of Gidropress Mixing Facility Experiments, Project TACIS R2.02/02, University of Pisa Report, DIMNP NT 611 (07) Rev. 0, December 2007.
14. Oberkampf W. L., Trucano T. G. and Hirsch C., Verification, Validation, and Predictive Capability in Computational Engineering and Physics, SAND REPORT SAND2003-3769, February 2003.
15. Bestion et al., Extension of CFD codes to two-phase flow safety problems, NEA/SEN/SIN/AMA(2006)2, August 2006.
16. WS Atkins Consultants, Best Practices Guidelines for Marine Applications of CFD, MARNET-CFD Report, 2002.

17. Casey M., Wintergerste T., Special Interest Group on 'Quality and Trust in Industrial CFD' Best Practice Guidelines, Version 1, ERCOFTAC Report, 2000.
18. Menter F., CFD Best Practice Guidelines for CFD Code Validation for Reactor-Safety Applications, European Commission 5th EURATOM FP, ECORA Project, EVOL-ECORA-D01, February 2002.
19. Use of computational fluid dynamics codes for safety analysis of reactor systems, Joint IAEA/NEA technical meeting, Pisa, Italy, November 11-13, 2002, IAEA-TECDOC-1379, IAEA, Vienna, 2003.
20. Rohde U., Höhne T., Kliem S., Scheuerer M., Hemström B., Toppila T., Dury T., Klepac J., Remis J., Műhlbauer P., Vyskocil L., Farkas I., Aszodi A., Boros I., Bezrukov Y., The European project FLOMIX-R: Fluid mixing and flow distribution in the reactor circuit - Final summary report, Scientific-technical Report, Forschungszentrum Rossendorf; FZR-432 August 2005.
21. Rohde, U. et al., "Description of the slug mixing and buoyancy related experiments at the different test facilities", EU/FP5 FLOMIX-R Project, FLOMIX-R-D09, Germany, 2004.
22. Moretti F., D. Melideo, F. D'Auria, CFX Simulations of ROCOM Experiments, University of Pisa, DIMNP NT 588 (06) Rev. 0, Pisa, November 2006.
23. Rohde U. et al., Fluid mixing and flow distribution in a primary circuit of a nuclear pressurized water reactor—Validation of CFD codes, Nuclear Engineering and Design Vol. 237, pp. 1639–1655, 2007.
24. Kliem S., Hemström, B., Bezrukov Y., Höhne T., Rohde U., Comparative evaluation of coolant mixing experiments at the ROCOM, Vattenfall, and Gidropress test facilities, Science and Technology of Nuclear Installations, Vol. 2007, Article ID 25950.
25. Höhne T., Kliem S., Rohde U., Weiss F. P., Boron dilution transients during natural circulation flow in PWR—Experiments and CFD simulations, Nuclear Engineering and Design 238 (2008) 1987-1995.
26. Kliem S., Prasser H.-M., Sühnel T., Weiss F.-P., Hansen A., Experimental determination of the boron concentration distribution in the primary circuit of a PWR after a postulated cold leg small break loss-of-coolant-accident with cold leg safety injection, Nuclear Engineering and Design Vol. 238, 2008, pp. 1788-1801.
27. Kliem S., Sühnel T., Rohde U., Höhne T., Prasser H.-M., Weiss F.-P., Experiments at the mixing test facility ROCOM for benchmarking of CFD codes, Nuclear Engineering and Design Vol. 238, 2008, pp. 566-576.
28. Cartland Glover G.M., Höhne T., Kliem S., Rohde U., Weiss F.-P., Prasser H.-M., Hydrodynamic phenomena in the downcomer during flow rate transients in the primary circuit of a PWR, Nuclear Engineering and Design, Vol. 237, 2007, pp. 732–748.
29. Höhne T., Kliem S., Bieder U., Modeling of a buoyancy-driven flow experiment at the ROCOM test facility using the CFD codes CFX-5 and Trio U, Nuclear Engineering and Design, Vol. 236, 2006, 1309-1325.
30. Höhne T., Kliem S., Rohde U., Weiss F.-P., Buoyancy driven coolant mixing studies of natural circulation flows at the ROCOM test facility using ANSYS CFX, ICONE14-89120, Proceedings of 14th International Conference on Nuclear Engineering, July 17-20, 2006, Miami, Florida, USA.
31. Moretti F., Melideo D., D'Auria F., Höhne T., Kliem S., "CFX simulations of ROCOM slug mixing experiments", ICONE15-10461, Proceedings of 15th

International Conference on Nuclear Engineering, April 22-26, 2007, Nagoya, Japan.
32. Moretti F., Melideo D., D'Auria F., Höhne T. and Kliem S., CFX simulations of ROCOM slug mixing experiments, Journal of Power and Energy Systems, vol. 2, no. 2, pp. 720-733, 2008.
33. Lisenkov E.A., Task B5: Description of experiments, Project TACIS R2.02/02, SPA Gidropress report 320-Pr-656E, October 2006.
34. Vyskocyl L., CFD simulation of slug mixing in VVER-1000 reactor, ICONE14-89079, Proceedings of 14th International Conference on Nuclear Engineering, July 17-20, 2006, Miami, Florida, USA.
35. Muehlbauer P. et al., Review of experimental database on mixing in primary loop and future needs, European Commission 5th EURATOM FP, ECORA Project, EVOL-ECORA-D03, August 2003.
36. Toppila T., CFD simulation of Fortum PTS experiment, Nuclear Engineering and Design, Vol. 238, 2008, pp. 514–521.
37. Gavrilas, M., Kiger, K.: OECD/CSNI ISP Nr. 43 Rapid Boron-Dilution Transient Tests for Code Verification, September 2000.
38. Gavrilas, M., Kiger, K.: ISP-43: Rapid Boron Dilution Transient Experiment. Comparison Report. NEA/CSNI/R(2000)22, February 2001.
39. Umminger K., Kastner W., Liebert J., Mull T., Thermal hydraulics of PWRS with respect to boron dilution phenomena. Experimental results from the test facilities PKL and UPTF, Nuclear Engineering and Design, Vol. 204, 2001, pp. 191-203.
40. Bieder U., Graffard E., Qualification of the CFD code Trio U for full scale reactor applications, Nuclear Engineering and Design, Vol. 238, 2008, pp. 671-679.
41. Gavrilas M., Kiger K., OECD/CSNI ISP Nr. 43 Rapid Boron-Dilution Transient Tests for Code Verification, September 2000.
42. Bieder U., Fauchet G., Bétin S., Kolev N., Popov D., Simulation of mixing effect in VVER-1000 reactor, Nuclear Engineering and Design, Vol. 237, 2007, 1718-1728.
43. Scheuerer M. et al., Evaluation of computational fluid dynamic methods for reactor safety analysis (ECORA), Nuclear Engineering and Design, Vol. 235, 2005, pp. 359-368.
44. Scheuerer M. et al., ECORA Project - Condensed Final Summary Report, European Commission, March 2005.
45. Scheuerer M. et al., Selection of PTS relevant cases, European Commission 5th EURATOM FP, ECORA Project, EVOL-ECORA-D05a, December 2002.
46. Muehlbauer P. et al., Review of CFD Applications in Primary Loop and Recommendations, European Commission 5th EURATOM FP, ECORA Project, EVOL-ECORA-D02, March 2003.
47. Melideo D., Moretti F., Del Nevo A., D'Auria F., Post-test Analyses of Gidropress Mixing Facility Experiments, Project TACIS R2.02/02, University of Pisa Report, DIMNP NT 632 (08) Rev. 2, June 2008.
48. Moretti, F., Del Nevo, A., D'Auria, F., Asymmetrical Boron Concentration / Temperature Events: Review of US Position and Approaches – Review of EU Framework Programmes Related to Computational Tools, DIMNP NT 575 (06), Pisa, 2006.

49. Burnett T., Westinghouse Nuclear Energy Systems, Westinghouse assessments of reactivity transients due to rapid boron dilution, Proceedings of the CSNI Specialists Meeting on Boron Dilution Reactivity Transients, October 18-20, 1995, State College, Pennsylvania, USA, NUREG/CP-0158, NEA/CSNI/R(96)3.
50. Jones R. C., USNRC, Boron dilution reactivity transients – A regulatory perspective, Proceedings of the CSNI Specialists Meeting on Boron Dilution Reactivity Transients, October 18-20, 1995, State College, Pennsylvania, USA, NUREG/CP-0158, NEA/CSNI/R(96)3.
51. Attard A. C., USNRC, Boron dilution reactivity transients – An overview of efforts, Proceedings of the CSNI Specialists Meeting on Boron Dilution Reactivity Transients, October 18-20, 1995, State College, Pennsylvania, USA, NUREG/CP-0158, NEA/CSNI/R(96)3.
52. Diamond D. J. et al., Brookhaven National Laboratory, "Analysis of boron dilution transients in PWRs", February 2004, BNL-NUREG-71996-2004-CP.
53. U.S. Nuclear Regulatory Commission, Office of Nuclear Reactor Regulation, "A Prioritization of Generic Safety Issues", NUREG-0933.
54. U.S. Nuclear Regulatory Commission Generic Letter 85-05, "Inadvertent Boron Dilution Events", January 31, 1985.
55. U.S. Nuclear Regulatory Commission Information Notice 91-54, "Foreign Experience Regarding Boron Dilution", September 6, 1991.
56. U.S. Nuclear Regulatory Commission Information Notice 93-32, "Nonconservative inputs for boron dilution event analysis", April 21, 1993.
57. Diamond D. J., et al., "Probability and Consequences of a Rapid Boron Dilution in a PWR: A Scoping Study", Brookhaven National Laboratory, U.S. NRC, June, 1992. (NUREG/CR-5819).
58. U.S. Nuclear Regulatory Commission, "Shutdown and Low Power Operation at Commercial Nuclear Power in the United States", NUREG-1449, September 1993.
59. U.S. Nuclear Regulatory Commission, Certification of System 80+, NUREG-1462, Vol. 2, August 1994.
60. U.S. Nuclear Regulatory Commission Information Notice 94-64, "Reactivity Insertion Transient and Accident Limits for High Burnup Fuels", August 31, 1994.
61. U.S. Nuclear Regulatory Commission Information Notice 94-64, "Supplement: Reactivity Insertion Transient and Accident Limits for High Burnup Fuels", April 6, 1995.
62. U.S. Nuclear Regulatory Commission Information Notice 96-69, "Operator actions affecting reactivity", December 20, 1996.
63. U.S. Nuclear Regulatory Commission, Advisory Committee on Reactor Safeguards, "Proposed resolution of Generic Safety Issue 185, 'Control of Recriticality Following SBLOCA in PWRs'", October 22, 2004, ACRSR-2099.
64. Draft NUREG-XXXX, "Avoiding Recriticality From Transport of Diluted Water From Loop Seals to Core During Small Break Loss-of-Coolant Accidents in Pressurized Water Reactors," Generic Safety Issue 185, February 2004.
65. U.S. Nuclear Regulatory Commission, Office of Nuclear Reactor Regulation, "Standard Review Plan", NUREG-0800.
66. U.S. Code of Federal Regulations.

67. CE-System 80+, Vol. U.S. Regulatory Commission, Office of Nuclear Reactor Regulation, August 1994.
68. Longo J. et al., ABB-CE, The System 80+ response to the Small Break LOCA Boron Dilution Issue, Proceedings of the CSNI Specialists Meeting on Boron Dilution Reactivity Transients, October 18-20, 1995, State College, Pennsylvania, USA, NUREG/CP-0158, NEA/CSNI/R(96)3.
69. U.S. Nuclear Regulatory Commission, "Final Safety Evaluation Report for AP1000 Related to Certification of the AP1000 Standard Design", September 2002.
70. Di Marzo M., "Ex-vessel Transport and Mixing of a Deborated Slug in a PWR Primary Geometry", Nuclear Engineering and Design 210, pp 169-175, 2001.
71. Tafreshi A. M., Di Marzo M., "Reactor coolant pump startup under degraded conditions in a scaled OTGS lowered loop PWR", Energy Conversion Engineering Conference, 1996. IECEC 96. Proceedings of the 31st Intersociety, August 1996.
72. Tuomisto H., et al., EUBORA - Concerted Action on Boron Dilution Experiments, FISA-99 Symposium on EU Research on Severe Accidents, Luxembourg, 29 November - 1 December, 1999.
73. Bestion D. et al., EUROFASTNET - EU Project for future advances in sciences and technology for nuclear engineering thermal-hydraulics, FISA 2003 Symposium on EU Research IN Reactor Safety, Luxembourg, December 10-13, 2003.
74. Paillere H. et al., ASTAR – Advanced Three-Dimensional Two-Phase Flow Simulation Tools for Application to Reactor Safety, FISA 2003 Symposium on EU Research IN Reactor Safety, Luxembourg, December 10-13, 2003.
75. Weiss F.P. et al., VALCO - Validation of Coupled Neutronics / Thermal Hydraulics Codes for VVER Reactors, FISA 2003 Symposium on EU Research IN Reactor Safety, Luxembourg, December 10-13, 2003.
76. D'Auria F. et al., CRISSUE-S Project - Condensed Final Summary Report, European Commission, 2004.
77. EURATOM 6th FP, NURESIM Integrated Project, Annex I – Description of Work, December 2004.
78. EURATOM 6th FP, BOROND (EURATOM Training Fellowship) Annex - I – Description of Work.
79. IAEA, Accident Analysis for nuclear power plants with pressurizer water reactors, Safety report series No. 30, IAEA, Austria, November 2003.
80. Cherubini M., Moretti F., D'Auria F., UNIPI-KINS cooperative research agreement final report: independent assessment of multidimensional features of the MARS code, DIMNP NT 637(08) Rev0, Pisa, February 2009.
81. Moretti F., Melideo D., D'Auria F., Set-up of computational grids for CFD simulations of Gidropress mixing facility experiments, TACIS Project R2.02/02, Working Document TP-08-03(06), December 2006.
82. Moretti F., Melideo D., Del Nevo A., D'Auria F., Höhne T., Lisenkov E., CFD Analysis of a Slug Mixing Experiment Conducted on a VVER-1000Model, Science and Technology of Nuclear Installations, Volume 2009, Article ID 436218, 2008.
83. Galassi M. C., Mazzini D., D'Auria F., Impinging jet studies for turbulent modelling assessment and code benchmarking, XXIV Congresso Nazionale UIT sulla Trasmissione del Calore, Napoli, 21-23 June 2006.

84. Glantz T., Freitas R., Validation of CATHARE 3D Code Against UPTF TRAM C3 Transients, Journal of Power and Energy Systems, Vol. 2, No. 1 (2008), pp.397-408.
85. Aumiller D.L., Tomlinson E.T., Bauer R.C., A coupled RELAP5-3D:CFD methodology with a proof-of-principle calculation, Nuclear Engineering and Design, Vol. 205, 2001, pp. 83–90.
86. Bertolotto D., Manera A., Frey S., Prasser H.-M., Chawla R., Single-phase mixing studies by means of a directly coupled CFD/system-code tool, Annals of Nuclear Energy, 2009 (*in press*).
87. Idel'cik I. E., **Memento des pertes de charge**, Collection de la Direction des Etudes et Recherches d'Electricite de France, Paris: Eyrolles, 1969.
88. Ferziger, J. H., Perić, M., 2002, **Computational Methods for Fluid Dynamics**, 3rd edition, Springer, Berlin.
89. Wilcox, D., 2000, **Turbulence Modelling for CFD**, DCW Industries, Inc., Griffin printing, California.
90. Rohde U. et al., Validation of CFD codes based on mixing experiments (Final Report of WP4, Deliverable D11), FLOMIX-R Project, 2004.
91. Dury T. V., Hemström B., Shepel S. V., CFD simulation of the Vattenfall 1/5th-scale PWR model for boron dilution studies, Nuclear Engineering and Design Vol. 238, pp. 577-589, 2008.
92. The MathWorks Inc., Matlab® 7.1 User Guide (embedded in the software package), 2005.
93. Prošek A., D'Auria F., Mavko, B., Review of quantitative accuracy assessment with fast Fourier transform based method (FFTBM), Nuclear Engineering and Design Vol. 217, pp. 179-206, 2002.

ANNEX A. CFD VALIDATION WORK

This Annex describes part of the CFD code validation activity carried out by the Author in the frame of his doctoral research. The shown contents have been included in some papers, which are also indicated.

A.1. CFD simulations of ROCOM experiments

[Moretti F., Melideo D., D'Auria F., Höhne T. and Kliem S., CFX simulations of ROCOM slug mixing experiments, Journal of Power and Energy Systems, vol. 2, no. 2, pp. 720–733, 2008.]

A.1.1. General remarks

In the safety analysis of nuclear reactors, a number of scenarios have to be addressed in which a safety-relevant role is played by the space and time distribution of primary coolant physical and/or thermodynamic properties, such as temperature, density, concentration of additives, etc. For example, transients have to be analyzed which are featured by a perturbation of the coolant properties at the reactor core inlet, since such a perturbation can introduce a positive reactivity and determine a rapid power excursion, potentially leading to core damage. Those transients include the so-called boron dilution scenarios in Pressurized Water Reactors (PWR), leading to a reduction in the boron concentration at the core inlet, and Main Steam Line Break (MSLB) accidents in PWRs, leading to an overcooling in the interested loop, and thus to relatively cold water reaching the core inlet.

Another typical problem related to the distribution of coolant properties, is whether an Emergency Core Cooling (ECC) injection following a Small Break Loss-of-Coolant Accident (SB-LOCA) may lead or not to a Pressurized Thermal Shock (PTS) scenario, due to the relatively cold injected water being not sufficiently mixed with the water already present in the cold legs.

The above mentioned scenarios are all characterized by the relevance of the turbulent mixing. In fact, the mixing between coolant flows with different properties has a mitigating effect, both when boron concentration or temperature distribution at core inlet are concerned, as well as when temperature distribution in the coolant flowing close to the vessel wall in SB-LOCA scenario is concerned.

The predictive analysis of turbulent mixing phenomena requires a local, three-dimensional approach, that is, in other words, the Computational Fluid Dynamics (CFD) approach. What have been done so far in the licensing analyses of nuclear reactor is not to simulate or the mixing phenomena, but rather to conservatively neglect them, or to account for them through highly conservative modelling assumptions. On the other hand, the dramatic increase in the power of the computing tools experienced in recent years has made credible, within reasonably short time in the future, the application of the CFD codes to practical problems relevant for the nuclear reactor safety, such as the above mentioned ones. This would allow reducing the conservatism of assumptions and thus the related safety margins. However, an extensive validation of the CFD codes is still needed before they can be reliably applied in licensing procedures.

An extensive CFD code validation activity had been carried out in the past years by European Organizations within the FLOMIX Project (Refs. [1] and [2]). Such work

was partly based on experiments conducted on the German ROCOM tests facility at Forschungszentrum Dresden-Rossendorf (FZD).
ROCOM experiments are being used also within a CFD code validation activity at the Department of Mechanics, Nuclear and Production Engineering (DIMNP) of the University of Pisa. One of such experiments, in particular, is addressed in the present work; it reproduced the injection of a de-borated water slug (simulated by a tracer) into the RPV of a PWR with all circulation pumps at steady-state operation. The experiment was simulated with the CFD code ANSYS CFX-10.0.
The results of the simulations (in terms of space and time distribution of tracer concentration) were compared against the experimental data kindly made available by FZD to DIMNP within a Cooperation Agreement, so as to further contribute to the assessment of the code capabilities in predicting the in-vessel coolant mixing.

A.1.2. ROCOM Experiments

A.1.2.1. The ROCOM Test Facility

The ROCOM (Rossendorf Coolant Mixing Model) test facility is a 1/5 scaled model of the primary circuit of a Konvoi-type PWR reactor. It was built by FZD with the purpose of investigating the coolant mixing phenomena occurring in the reactor pressure vessel (RPV) of a PWR, and to provide experimental data for CFD code validation. Experiments can be conducted on the facility, which represent typical operation or accidental scenarios involving transport and mixing of a scalar, such as temperature and/or boron concentration. The scalar is simulated by a salt tracer (sodium chloride), whose concentration is indirectly obtained through electrical conductivity measurements. Several conductivity sensors are present inside the ROCOM vessel providing detailed information on time and space distribution of the tracer during the performed test. The salt tracer allows simulating scenarios in which the transported scalar has no feedback on the flow in terms of density (and thus buoyancy effects), i.e. when the maximum boron concentrations or the temperature differences yield relatively small density variations. In such conditions the transport equations for boron concentration and for temperature (and for any other “passive” scalar) are formally identical and have the same non-dimensional solutions. From a physical point of view, the mixing of temperature and the mixing of boron concentration are governed by the same processes and turbulent exchange mechanisms. The effect of molecular diffusion of the coolant properties can be neglected, since in the facility, as well as in the real plant, the Reynolds numbers are sufficiently high to yield fully turbulent flows, even when the facility is operated at low regimes so as to reproduce natural circulation conditions. Moreover, ROCOM can also be used to study scenarios in the presence of density effects, introduced through the injection of either alcohol or glucose, together with the use of salt tracer.

The ROCOM facility is made of the following parts:

- a model of the RPV with four inlet and four outlet nozzles;
- four circulation pumps, driven by computer-controlled frequency motors;
- four “cold legs” connecting the pumps to the vessel;

- four steam generator simulators (only primary side, just to account for the volume);
- four “hot legs” connecting the vessel to the steam generators simulators;
- auxiliary components for the tracer storage and injection.

A sketch of the facility layout is shown in Figure A. 1. Descriptions of the facility and of its equipments can be found in the literature (Refs. [2], [3]).

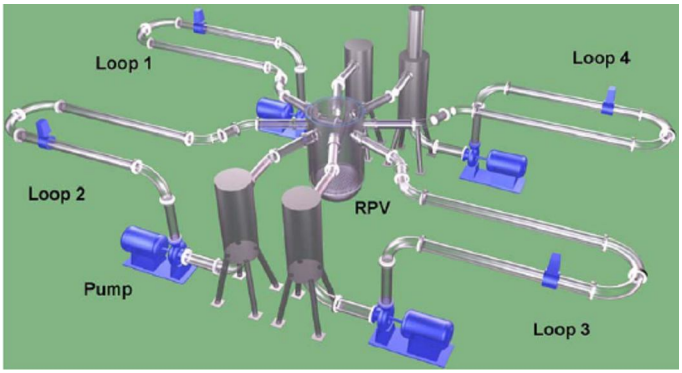

Figure A. 1 – Sketch of ROCOM facility layout

The RPV model contains the following internals:

- the barrel, which separates the downcomer region from the core region; it is simply a cylinder, going from the upper cover plate to the lower support plate; it has four holes to allow the coolant exiting from the core to enter the outlet nozzles;
- the core support plate, which is connected to the lower edge of the barrel, and distributes the coolant flow over the 193 core channels; it has a relatively complex geometry, which determines a high concentrated pressure loss at the core inlet so that pressure equalization and an almost uniform mass flow rate distribution though the core channels are achieved;
- the core simulator, made of 193 aluminum tubes (30 mm inner diameter), which has the purpose of simulating the core flow resistance; the outlet of the core simulator is connected with the upper plenum, which does not contain any internals;
- the perforated drum (or sieve drum), which is a cylinder with around 410 small holes (15 mm diameter), located in the lower plenum, just below the core support plate; it has the purpose of enhancing the coolant mixing in the lower plenum and to equalize the mass flow distribution through the core channels.

All the above listed internals, except for the core simulator, are made of Plexiglas. Each of the four circulation loops is equipped with a pump whose speed is individually controlled by a frequency transformer. Each loop can be isolated by a

gate valve located at the outlet of the corresponding pump. The aforementioned steam generator simulators are simply cylindrical tanks, having the same (scaled) volume of the original steam generators. The one connected to loop #4 is open to the atmosphere so as to allow pressure equalization. The ratio between vessel volume and loops volume is the same in the facility as in the real plant, in order to assure the same travelling times.
The facility is equipped with the following auxiliary systems:

- two tanks for pure and waste water respectively;
- pumps for water supply system and cleaning system;
- ion exchanger for water cleaning;
- injection system for introduction of salted water in loop #1 inlet nozzle, including two computer-controlled pneumatic valves;
- mixing device at tracer injection location, permitting to obtain an almost uniform distribution of injected tracer over the nozzle cross section.

The local tracer concentration is derived from measurements of the electrical conductivity of the fluid (after obtaining proper calibration curves). The conductivity is measured by the so-called “wire mesh sensors” designed by the FZD experts. The sensor is a mesh of crossing conducting wires that form an electrode at each crossing point, where a local and instantaneous conductivity measurement is achieved by sending rapid voltage signals to the wires. A special data acquisition system registers the electrical currents for each measuring point and stores them on a PC with a measuring frequency up to 300 Hz. In most performed experiments, data have been acquired with a frequency of 200 Hz, and time-averaging has been performed each 10 successive measurements before storing the data, thus obtaining a n effective measurement frequency of 20 Hz.
The facility is equipped with wire mesh sensors at the following locations (Figure A. 2):

a. loop #1 inlet nozzle;
b. upper part of the downcomer (horizontal sensor);
c. lower part of the downcomer (horizontal sensor);
d. whole downcomer;
e. lower support plate.

The sensor (a) is located in the inlet nozzle of Loop #1, across the flow direction. It is made of a 16x16 mesh of wires. 216 of the 256 measuring positions do fall inside the nozzle cross section area. This sensor permits to control the injection of a tracer slug into the reactor model, and provides maximum concentration values for normalization. The annular downcomer sensors (b) and (d) are located in the upper part of the downcomer (just below the downcomer diameter variation) and in the lower part (at the connection between downcomer and spherical bottom) respectively. Each of them has 4 radial and 64 azimuthal measuring positions, for a total of 256 measuring points. The downcomer sensor (c) has been recently installed in the facility, and was not yet available when the experiments addressed in the present paper were conducted. It is located over the whole downcomer length and has 1 radial, and several angular and axial measuring positions. The core inlet sensor (e) is integrated in the lower support plate and has 193 measuring points.

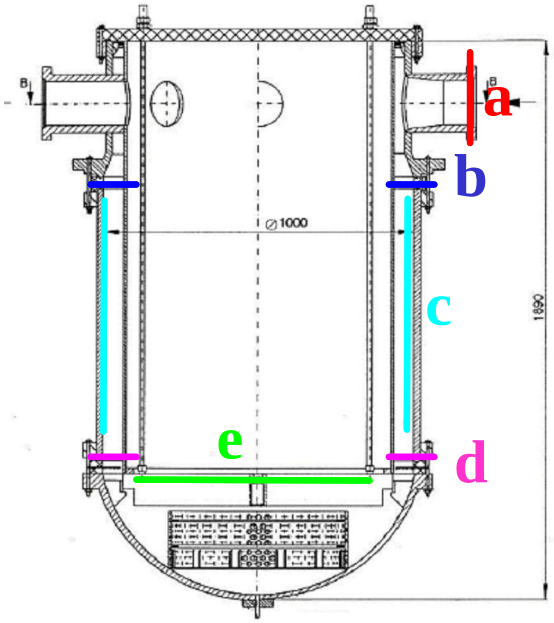

Figure A. 2 – Locations of wire-mesh sensors

When a ROCOM experiment is conducted to reproduce a boron dilution scenario, the injection of salted water is used to simulate the perturbed coolant (i.e. the coolant with low or no boron concentration), while the clear (i.e. without salt) water already present in the loops simulates the normally borated water in the real reactor. The measured values are normalized with respect to the values of conductivity that characterize the "clear water" and the "salted water", by defining a scalar quantity named the mixing scalar (MS in the following) and defined by Equation A.1.

$$\theta_{x,y,z,t} = \frac{\sigma_{x,y,z,t} - \sigma_0}{\sigma_1 - \sigma_0} = \frac{T_{x,y,z,t} - T_0}{T_1 - T_0} = \frac{C_{x,y,z,t} - C_0}{C_1 - C_0} \qquad \textit{Equation A. 1}$$

where σ, T and C indicate the conductivity, the temperature and the boron concentration respectively, while the sub-scripts *0* and *1* correspond to the unaffected water and the water subjected to the perturbation.

A.1.2.2. The simulated experiment

Both "slug mixing experiments" and "buoyancy driven mixing experiments" have been conducted at the ROCOM test facility. The one addressed in the present paper belongs to the former type. Such kind of experiments were aimed at investigating the flow mixing in the presence of a deborated water slug and various combinations of flow rates in the loops, according to postulated boron dilution scenarios, and assuming that no density effect is present (that is the mixing is

momentum-driven). Those experiments are performed using sodium chloride as a tracer, without any other additive. They are either steady-state or transient as regards the pumps operation. Steady-state tests consist in running symmetrically the four pumps at constant speed (the nominal speed, or a fraction of it), and injecting the tracer solution into on loop (usually #1) for a certain time period. Transient tests consist in starting up one or more pumps and varying its (or their) speed until the target mass flow rate is reached; furthermore, during a certain time period within this transient the tracer solution is injected so as to simulate the entrance of a deborated slug into the reactor.
The simulated experiment is a steady-state test, and is identified as ROCOM_STAT_02. It was conducted with the four pumps running at 25 % of nominal speed (i.e. 46.25 m^3/h mass flow rate per loop), and injecting the tracer for 35 s.
Figure A. 3 shows the time history of the cross-section averaged MS as measured at the inlet nozzle sensor, along with the maximum and the minimum values. The tracer concentration is thus not perfectly uniform over the nozzle cross section (despite the use of the mixing device), and maximum deviations are in the range ±15%. The Figure also shows a new increase in the measured MS after 45 s from the beginning of the test: this is because the tracer has gone through the whole circuit and enters the vessel for the second time.

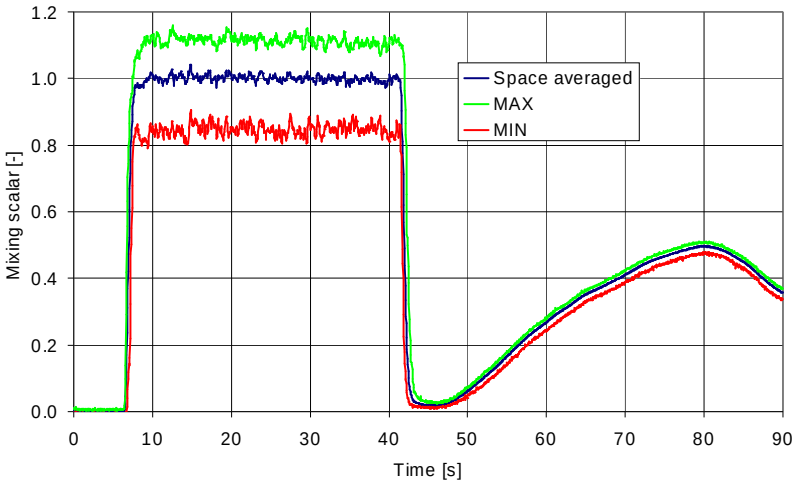

Figure A. 3 – ROCOM_STAT_02 experiment: time history of inlet MS

Five realizations of this experiment were performed, and the time histories of the measured MS at each measuring position were averaged, so as to filter the effect of the turbulent fluctuations. The maximum reference conductivity value needed for the non-dimensionalisation (i.e. to calculate the MS) is derived from the space-averaged plateau-averaged value at inlet nozzle sensor (for the steady-state experiments), or from the maximum in time space-averaged value at inlet nozzle sensor (for the transient experiments). The available experimental data include the time-dependent MS at each measuring point of each sensor, with a time step of 0.05 s (i.e. 20 Hz frequency).

A.1.3. CFD Simulations

A.1.3.1. Computational Grids

Several computational grids were prepared for the CFD simulations of ROCOM experiments. The meshing tool used is ANSYS ICEM 10.0 (Ref. [4]).
Since the considered experiments and the related CFD calculations focus on the mixing phenomena occurring inside the reactor vessel, whereas no attention is paid to the flow phenomena in the other parts of the Reactor Coolant System (RCS) such as cold and hot legs, circulation pumps, and so on), the selected computational domain includes only the following parts of the ROCOM facility:

- downcomer (DC) (including 4 inlet nozzles);
- lower plenum (LP);
- core simulator (CS);
- upper plenum (UP).

In order to solve some issue related to managing large files, and to allow easy creation of “hybrid” meshes (i.e. grids having parts meshes with different types of elements, such as hexahedra and tetrahedra), these four parts were modelled and meshed separately and then assembled in a single domain (shown in Figure A. 4), connected in CFX-10.0 by means of General Grid Interfaces (GGI, see Ref. [5]).

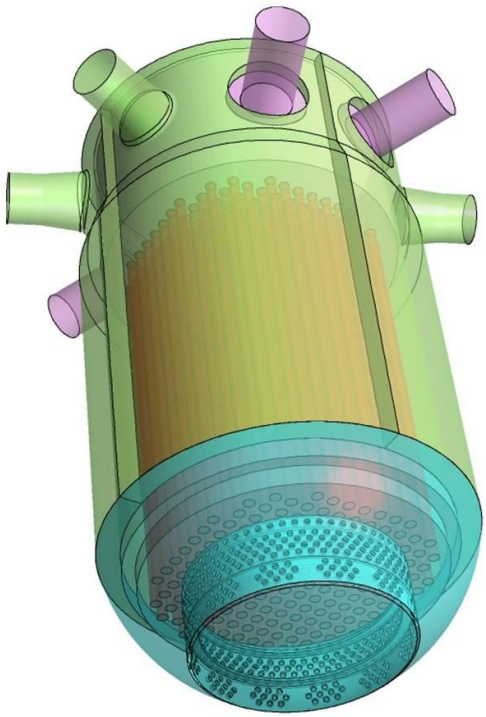

Figure A. 4 – Whole computational domain

A quarter(*) of the DC was modelled according to the real geometry of ROCOM without any simplification. In particular, the diameter variations both in the inlet nozzle and in the DC were taken into account, as well as the fillet radius in the connection between nozzle and DC, which was shown by preliminary CFD studies to sensibly affect the mass flow distribution in the DC. The LP sub-domain is defined by: the interface with DC part, the inner surface of the vessel bottom, the side and lower surfaces of the support plate, and the boundaries of the perforated drum. The drum was modelled along with its 410 holes (15 mm diameter), as shown in Figure A. 5.

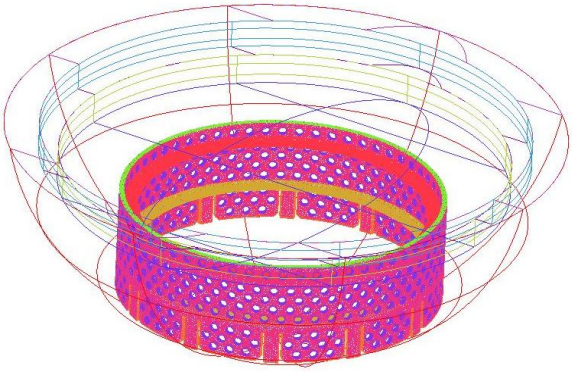

Figure A. 5 – LP solid model (drum in evidence)

The CS consists in 193 tubes connecting the LP to the UP. Its length has been extended downward so as to "replace" the complex geometry of the lower support plate with a simplified, tube-based geometry. This geometry simplification obviously affects the pressure losses that the flow encounters when crossing the plate. This was taken into account in the CFD simulations by defining additional pressure losses.

The UP has a straightforward geometry, since it is simply made of five cylinders (the plenum itself and the four outlet nozzles) and does not have any internals.

Some CFD investigations have shown that the flow velocity and pressure field that forms in ROCOM DC and LP is not sensibly affected by the CS and UP region, owing to the relatively high pressure losses encountered through the lower support plate. For this reason the complete model of ROCOM geometry can be simplifying by replacing CS and UP with a "reduced core" and a cylindrical outlet volume (see below).

Several grids of ROCOM were created, with the purpose of testing different mesh strategies, investigating the influence of some modelling assumptions and meshing choices on the CFD results, and finally assessing a general meshing strategy that can be conveniently applied when dealing with in-vessel mixing CFD analysis.

It has to be remarked that, as recommended by the ECORA Best Practice Guidelines (Ref. [6]), a mesh should be proven to yield grid-independent results,

(*) The whole part can be easily obtained from two symmetry operations on a quarter.

and systematic mesh sensitivity analyses should be performed in order to achieve the grid-independence and to select the proper grid. However, when dealing with complex geometries (such as a nuclear RPV), it is quite usual that the limitations in available computing power (in terms of number of CPUs, computing-time that can be allocated, and amount of memory) do not allow performing such expensive analyses and to utilize a sufficiently refined mesh. Due to the above reasons, the meshes used for the present study are “production meshes”, i.e. they are relatively coarse, and represent a compromise between accuracy and computing time in relation to the available computing power. A mesh strategy is usually based on the use of either hexahedral of tetrahedral elements. The use of hexahedra instead of tetrahedra usually allows reducing the total number of cells (with the same characteristic cell-size) or to improve the numerical accuracy. Hexa-based grids can be created with ICEM following a block-structured meshing technique, whose application can be however quite a tough task when dealing with complex geometries. In this case following a tetra-based meshing approach may be much easier and less time-consuming. More details concerning these (and other) possible meshing strategies can be found in Ref. [7]. Three of the several grids created were used for the simulations described in this paper. Their main features are summarized in Table 1.

Table A. 1 – Used grids

Grid		**A01**	**A04**	**A07**
Types of elements	DC	hexa	tetra	tetra
	LP	tetra	tetra	tetra, prisms
	CS	prisms, hexa	prisms, hexa	prisms
	UP	hexa	hexa	tetra
Total no. of cells		4.5 million	6.0 million	6.3 million
Notes				reduced core

In all cases, around one half of the whole number of cells is present in the LP region, due to the presence of smaller scale geometric details. The DC grid was obtained using either hexa-meshing (A01, see Figure A. 6) or tetra-meshing (A04, A07). In all cases the LP was meshed with tetrahedra (Figure A. 7), because a hexa-meshing would be too difficult to achieve due to the geometric complexity.

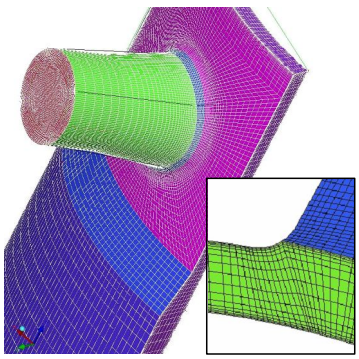

Figure A. 6 – DC mesh (A01)

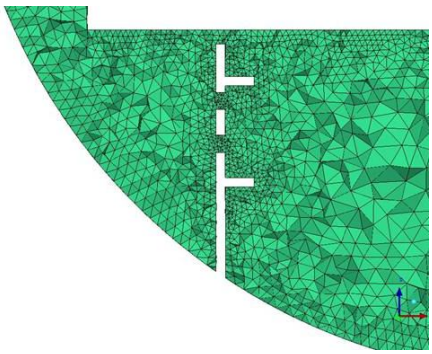

Figure A. 7 –LP mesh (A01, A04)

The LP of grid A07 has layers of prism elements to better comply with the turbulent treatment at the walls. The CS region of grids A01 and A04 was obtained through axial extrusion of 2D meshes (triangles and quadrangles) of the tubes cross sections, thus generating prisms and hexahedra, and the UP was meshed with hexahedra. In grid A07 the CS is replaced by a "reduced core" meshed with prisms (extrusion of triangles), while a cylindrical outlet volume, meshed with tetrahedral, is present instead of the UP (Figure A. 8).

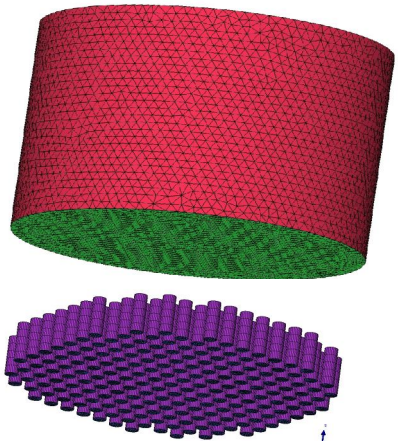

Figure A. 8 – Reduced core (A07 grid)

A.1.3.2. Simulations Set-up

The simulations were performed with the ANSYS CFX-10.0 package (CFX in the following), a general-purpose, commercial CFD code owned and developed by ANSYS Inc. The solver is based on a finite volumes – finite elements hybrid approach. More details on the code features and capabilities can be found on Ref. [5].

The simulations were set-up taking into account the best practice for this kind of applications, and the achievements of the FLOMIX Project (Refs. [1] and [2]). The following field equations have been solved:

- mass balance (continuity);
- momentum balance (Navier-Stokes);
- transport of turbulent kinetic energy (κ);
- transport of turbulent eddy dissipation (ε) or frequency (ω) depending on the turbulence model used (2-eq. turbulence model, either κ–ε or SST, respectively);
- transport of an additional, user-defined, scalar variable (i.e. the "MS").

All the calculations performed share the following features:

- working fluid: incompressible water at 1 atm, 25°C;
- density: 997 kg/m^3;
- dynamic viscosity: 8.899 x 10-4 kg m^{-1} s^{-1};

- constant inlet velocity;
- uniform inlet velocity profile (0.73 m/s, i.e. 25% of nominal mass flow rate);
- pressure-controlled outlet boundary condition;
- uniform inlet turbulent intensity profile (either 5% or 10%);
- MS injected into loop #1 inlet nozzle;
- Upwind discretization scheme for advection terms.

The most significant simulations performed of the ROCOM_STAT_02 experiment are summarized in Table A. 2. Their features are discussed hereafter.
In simulations #1 to #4 the computational domain represents the whole RPV up to the outlet nozzles (grids A01 and A04), while calculation #5 accounts for a partial RPV with a "reduced core" not including the whole CS and the UP (grid A07).
Each calculation (except for the first one) was initialized with the solution of a previous calculation, in order to accelerate the convergence. In order to do this, the old solution has to be loaded and, if the new grid is different from the old one, it has also to be adapted through an interpolation procedure. All this can be done automatically in the pre-processing.

Table A. 2 –Summary of CFX calculations for ROCOM_STAT_02 test

Run #	1	2	3	4	5
Run name	A01_case1	A01_case2	A01_case3	A04_case3	A07_case1
Comp. domain	whole RPV				with red. core
Turbulence model	$\kappa-\varepsilon$				SST
Restart from	-	A01_case1	A01_case2	A01_case2 (with interp.)	-
MS injection	Continuous				Slug
Inlet MS profile	Uniform	Non-uniform (with user function)			
Inlet turb. intensity	5 %		10 %	5 %	
Equations solved	All	MS only	All		

Since in the addressed experiment the tracer injection lasts for a relatively long time period (i.e. 35 s), sufficient to establish a quasi-stationary concentration distribution in the vessel (during the so-called "plateau"), for calculations #1 to #4 the assumption was made that the injection is continuous, therefore the problem is considered as steady-state both in relation to velocity field and concentration as well. Thus all the field equations have been solved using a fully-implicit, very robust time-advancement scheme which is available in CFX for steady-state problems, where the time-step (that can be very large) is to be intended as an "accelerating parameter" rather than time advancement. The advantage in using this scheme is that the convergence can usually be reached in a relatively small number of iterations. Moreover, calculation #2, after being initialized with results of #1, was run solving only for the MS transport equation (and thus excluding the continuity,

momentum balance and turbulent parameters transport equations). In other words, the flow field was kept “frozen”. This helps sensibly reducing the computing time. On the other hand, calculation #5 was run using the transient CFX solver and MS boundary conditions were defined so as to simulate a slug injection rather than a continuous injection.
Despite the use of a mixing device (Section A.1.2.1) the MS at injection is not perfectly uniform over the inlet nozzle cross section. This is evident from the measurements at inlet nozzle wire mesh sensor, showing spatial deviations in the range +/- 15 % with respect to the mean value (Figure A. 9). In order to take this into account and to assess the related results sensitivity, most calculations were set-up with a non-uniform MS boundary condition at loop #1 inlet nozzle. This was done by means of a user-defined function that interpolates the experimental data (supplied by a text file). The resulting boundary profile is shown in Figure A. 9.

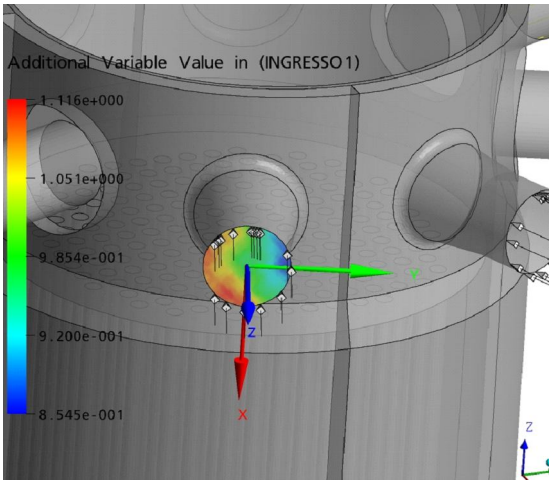

Figure A. 9 – Non uniform inlet MS profile

Another difference between simulations #1 to #4 and #5 is that for the latter the SST turbulence model was used instead of the $\kappa-\varepsilon$ one. The inlet turbulent intensity was set either to 5 % or 10 %.
Moreover, additional pressure losses have been applied in order to compensate for the simplifying assumptions made in modelling the lower support plate. This has been done defining a momentum source term in the cells corresponding to the plate holes. Namely, the directional loss model available in CFX was chosen, with a loss coefficient of 85 m^{-1} in the stream wise direction, and a loss coefficient greater by a factor 10 in the transverse direction. Such model is based on the Darcy law, written in the following form:

$$S_i = -C_{R2}\left|\vec{U}\right|U_i \qquad \textit{Equation A. 2}$$

$$C_{R2} = K_{loss}\frac{\rho}{2} \qquad \textit{Equation A. 3}$$

where S_i is a momentum source term and C_{R2} is the above loss coefficient. The value to such coefficient has been derived on the basis of available experimental information and CFD analyses on a detailed local model of the plate.

The purpose of the simulations was to calculate the local and instantaneous value of the MS, and then to compare it against the available experimental data. The following monitor points (also shown in Figure A. 10) were defined for the MS, according to the geometric location and configuration of the wire mesh sensors:

- 256 Upper DC monitor points located in the upper part of the DC (4 radial and 64 azimuthal measuring positions);
- 256 Lower DC monitor points located in the lower part of the DC (4 radial and 64 azimuthal measuring positions);
- 193 Core Inlet monitor points, located in the centre of each tube of the core simulator.

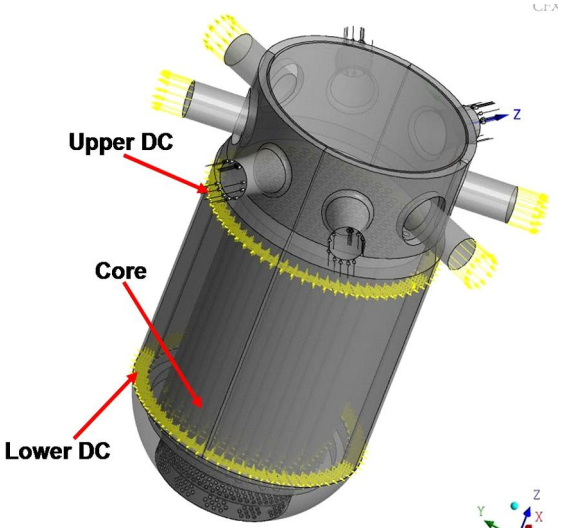

Figure A. 10 – Locations of monitor points

All the calculations were run in parallel mode on an 8-CPU Linux-cluster, using *pvm* protocol for message passing, and double precision round-off. CFX has an automatic partitioning algorithm (called MeTiS) that, in most cases, optimizes the job distribution and maximizes the parallel efficiency. This is used by default. However, in the present work a circumferential partitioning in eight parts was used instead of MeTiS, since it turned out to be more efficient for this specific case.

A.1.4. Results

The numerical results of the above discussed CFD simulations have been compared against the available experimental data. In particular, the results analysis focused on the MS distribution both in the downcomer and at the “core” inlet as well.

The results of calculations #1 to #4 are discussed first (i.e. steady-state simulations of continuous injection, and complete computational domain), while results of calculation #5 (transient simulation of slug injection, with reduced core) are presented later.

A.1.4.1. Results of Calculations #1 to #4

Since the addressed experiment involves symmetric and constant pump operation, the resulting flow field in the RPV consists of four symmetric "flow sectors", each one corresponding to one loop. The flow entering the RPV from the four inlet nozzles first impinges against the barrel outer wall, so that complex local flow patterns develop in the inlet region. However the flow in the downcomer below the diffusion zone (diameter variation) is mainly directed downwards, as shown by the streamlines in Figure A. 11-a.

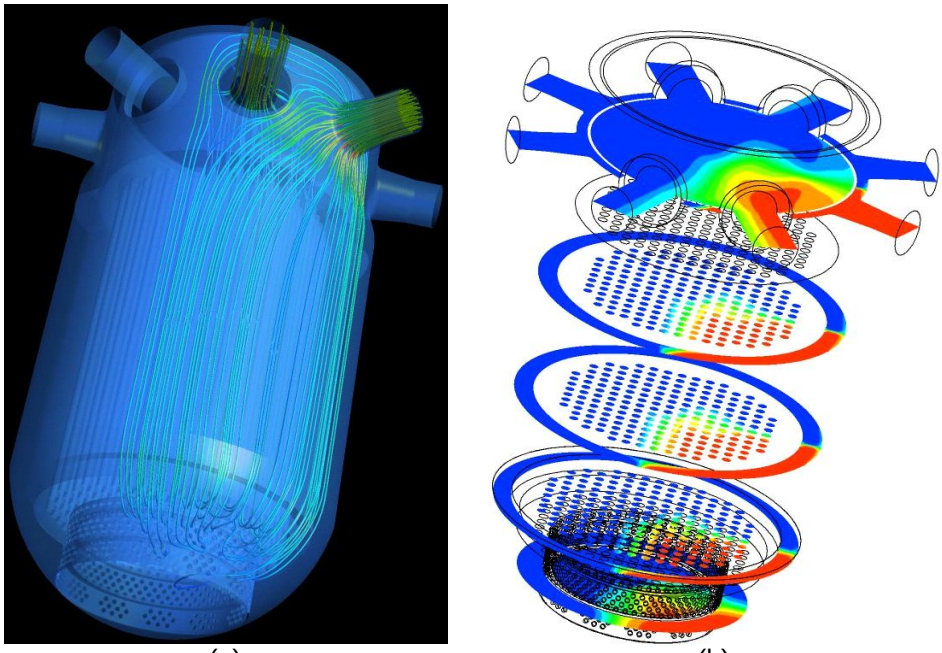

(a) (b)

Figure A. 11 – CFD results: streamlines from loop 1 (a) and MS field (b)

The downcomer flow is affected by turbulent mixing, which causes the MS field to diffuse in the transverse direction (i.e. azimuthally). This is shown by the plateau-averaged experimental data represented in Figure A. 12 and Figure A. 13. In particular, the first figure shows the comparison of MS azimuthal profile in the upper part of the downcomer: the agreement looks quite good. Slightly worse results appear for case #1, and this is probably due to the use of a uniform inlet MS profile instead of a more realistic boundary condition such as that shown in Figure A. 9.

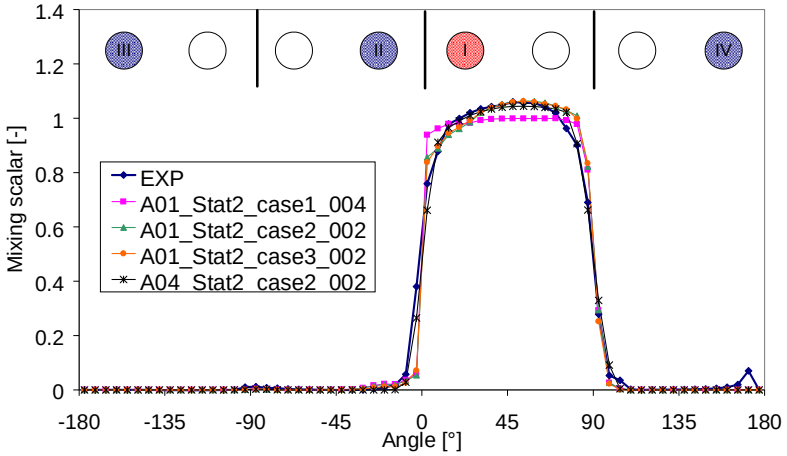

Figure A. 12 – Azimuthal profile of MS at the upper DC sensor

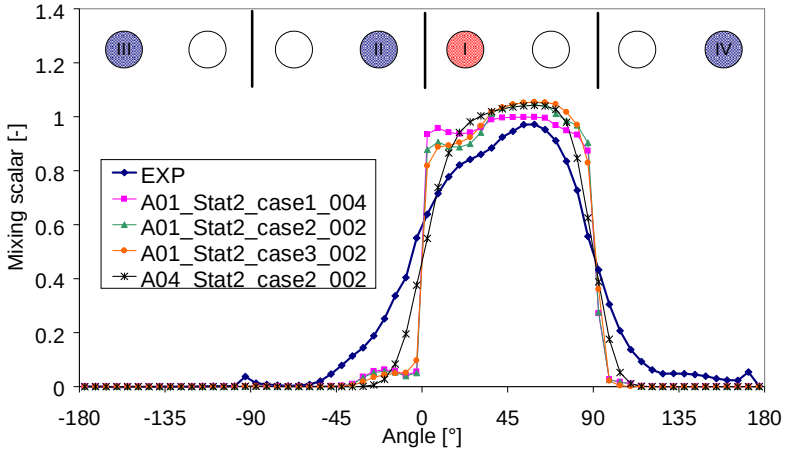

Figure A. 13 – Azimuthal profile of MS at the lower DC sensor

The agreement between numerical predictions and experiment becomes poorer in the lower part of the downcomer, as evident from Figure A. 13. The MS field experiences a relatively strong diffusion in the azimuthal direction, which “smears” the profile, while the spatial gradients predicted by the simulations keep steeper. As a consequence, the predicted maximum values are higher than experimental ones, and the MS perturbation does not sensibly interest the two adjacent sectors.
What stated above suggests that the code, despite the use of a first-order discretization scheme (i.e. “upwind”) for the advection terms, yet underestimates the turbulent diffusivity (in other words, the effectiveness of turbulent mixing). The best results are those yielded by calculation #4: this can be explained with the use of tetrahedral elements in the DC grid (instead of hexahedra), which introduce higher numerical diffusion and thus partly compensate for the above mentioned underestimation.

From these results about the mixing in the DC, one can expect that the predicted MS perturbation will affect a smaller number of channels than in the experiment, and that MS values in the most affected channels will be higher. This is confirmed by the qualitative comparison of plateau-averaged MS at core inlet shown in Figure A. 14. All the CFD simulations (including #5) give similar results in terms of shape and extension of the MS perturbation, which looks less diffused than in the experiment.

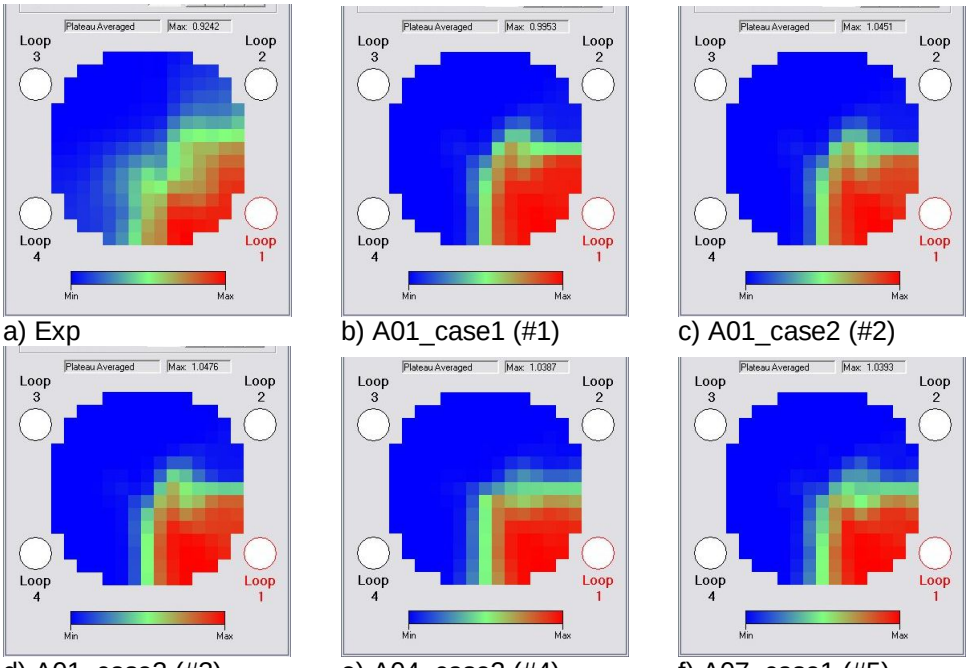

a) Exp b) A01_case1 (#1) c) A01_case2 (#2)

d) A01_case3 (#3) e) A04_case2 (#4) f) A07_case1 (#5)

Figure A. 14 – Plateau-averaged MS at core inlet

A.1.4.2. Results of Calculation #5

This calculation differs from the previous ones since it simulated the actual tracer slug injection instead of a continuous injection. Moreover, it was run using the grid A07, i.e. with a computational domain that does not include the whole CS region and the UP, but rather accounts for the plate and a fictitious outlet volume ("reduced core").

Figure A. 15 and Figure A. 16 show the numerical results related to the MS distribution in the downcomer at a given instant during the transient (within the "plateau" range), compared against the corresponding experimental profiles. As for the previous simulations, a satisfactory agreement is obtained in the upper part of the downcomer, while some underestimation of the turbulent mixing (i.e. of the MS spatial gradients) is revealed in the lower part (however, the predicted profile looks closer to the experimental one than in simulations #1 to #4).

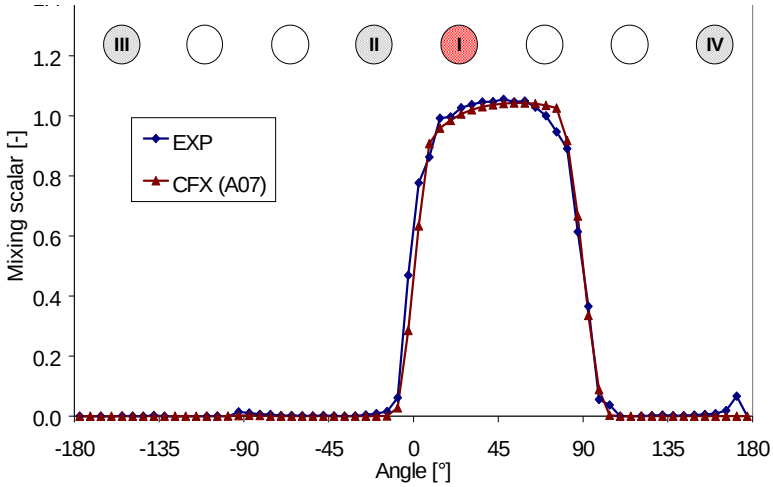

Figure A. 15 – Azimuthal profile of MS at the upper DC sensor (t=30s)

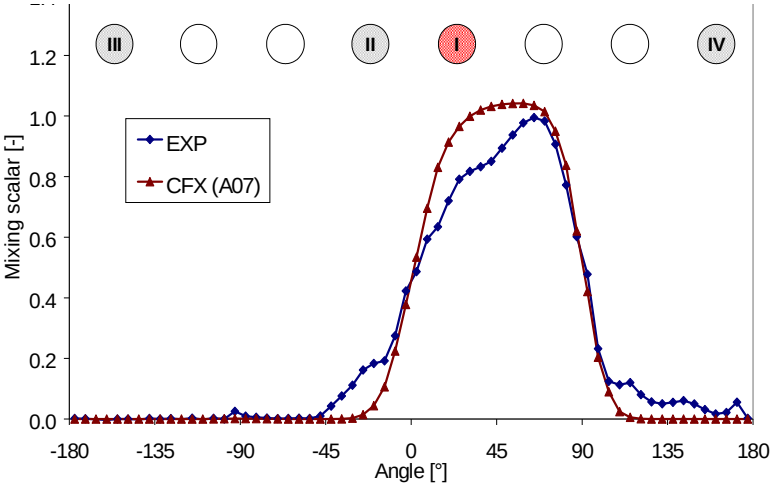

Figure A. 16 – Azimuthal profile of MS at the lower DC sensor (t=30s)

As regards the MS profile at core inlet, a code-to-experiment comparison was made for several channels selected within the perturbed region. A few examples are shown in Figure A. 17, Figure A. 18 and Figure A. 19, according to the identification map in Figure A. 20.

As expected, a good agreement is observed for those channels interested by a "medium" perturbation (e.g. channel #53, Figure A. 17), while the MS is overestimated in the middle of the perturbation (e.g. channel #16, Figure A. 18) and underestimated at the periphery of the perturbation (e.g. channel #25, Figure A. 19).

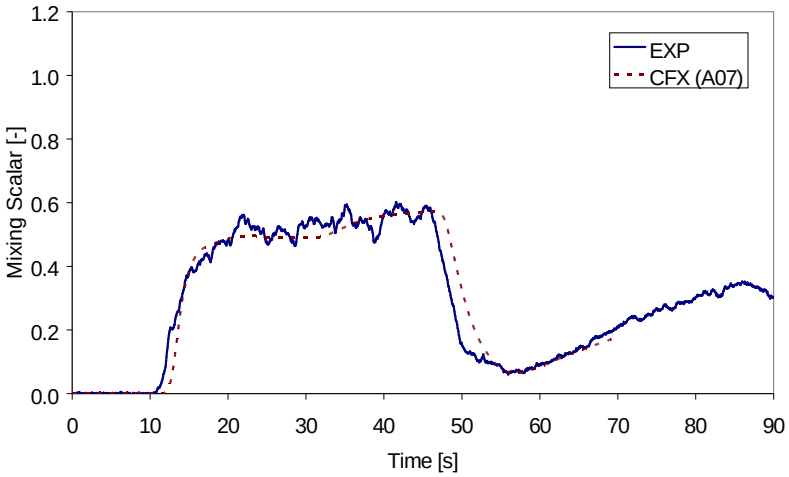

Figure A. 17 – Comparison of MS at core inlet (ch. #53)

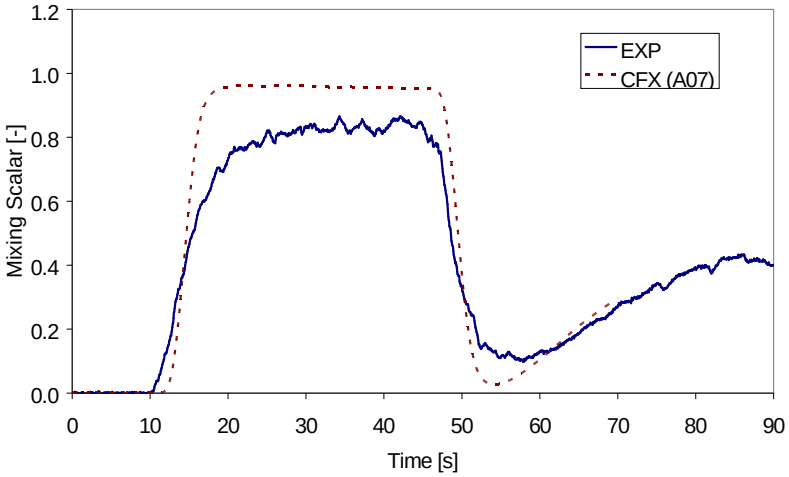

Figure A. 18 – Comparison of MS at core inlet (ch. #16)

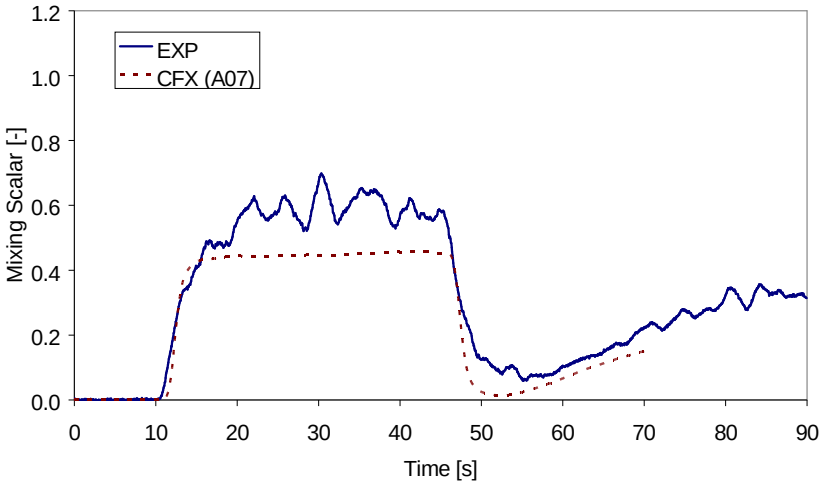

Figure A. 19 – Comparison of MS at core inlet (ch. #25)

III				135	120	105	90	75	60	45				II
		163	150	136	121	106	91	76	61	46	32	19		
	176	164	151	137	122	107	92	77	62	47	33	20	8	
	177	165	152	138	123	108	93	78	63	48	34	21	9	
187	178	166	153	139	124	109	94	79	64	49	35	22	10	1
188	179	167	154	140	125	110	95	80	65	50	36	23	11	2
189	180	168	155	141	126	111	96	81	66	51	37	24	12	3
190	181	169	156	142	127	112	97	82	67	52	38	25	13	4
191	182	170	157	143	128	113	98	83	68	53	39	26	14	5
192	183	171	158	144	129	114	99	84	69	54	40	27	15	6
193	184	172	159	145	130	115	100	85	70	55	41	28	16	7
	185	173	160	146	131	116	101	86	71	56	42	29	17	
	186	174	161	147	132	117	102	87	72	57	43	30	18	
IV		175	162	148	133	118	103	88	73	58	44	31		I
				149	134	119	104	89	74	59				

Figure A. 20 – Map for identification of measurement points at core inlet wire mesh sensor

Figure A. 21 shows the comparison between experimental and calculated MS, at a given instant within the plateau, for the channels located in the periphery of the support plate. Again, the predicted perturbation results less diffused than in the experiment.

Along with local parameters like the MS at each measuring position, also “global” parameters need to be taken in to account to characterize the perturbation and the code-to-experiment agreement. Figure A. 22 shows, for instance, the time histories of the maximum and the space-averaged MS. As regards the average value, no discrepancy resulted, because it is an “integral” parameter relatively easy to estimate for the code. On the other hand, the maximum value is obviously affected by the same overestimation discussed above.

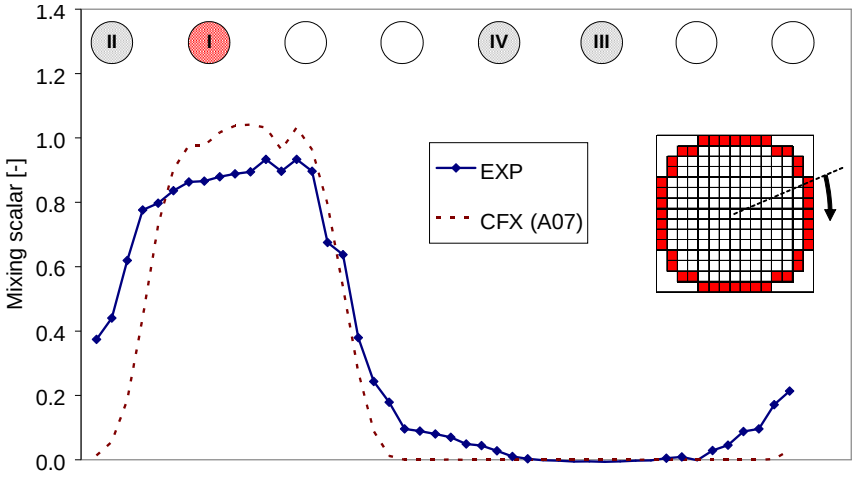

Figure A. 21 – Comparison of MS at inlet of peripheral channels (t=30s)

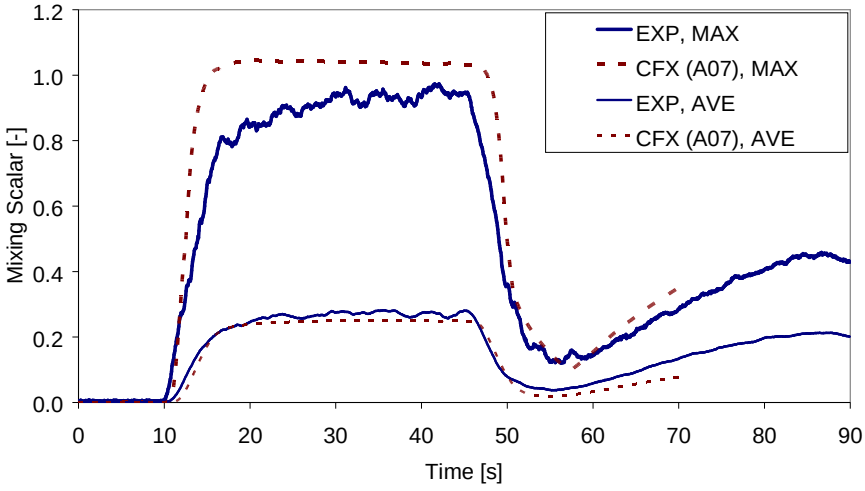

Figure A. 22 – Comparison of maximum and space-averaged MS at core inlet

Figure A. 23 shows a comparison of the MS at core inlet, for some selected instants (15 s, 30 s, and 40 s respectively), and confirms the above considerations concerning the good qualitative agreement as well as the lower mixing predicted by the CFD simulation.

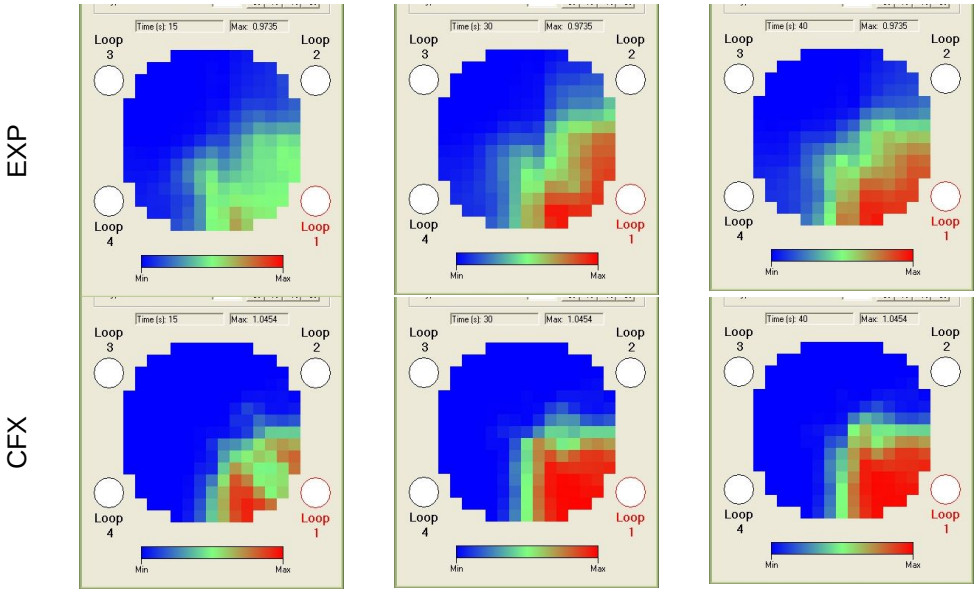

Figure A. 23 – Comparison of MS at core inlet for some selected instants (15 s, 30 s and 40 s respectively)

A.1.5. Conclusions

The CFD code CFX was used for the simulation of a slug-mixing experiment conducted on the ROCOM test facility at FZD. International Projects had already addressed ROCOM experiments for code validation purposes. This work further contributes to the assessment of CFD code capabilities for the simulation of in-vessel mixing.

Several “production” meshes were developed, which could cope both with the relatively high geometric complexity of ROCOM vessel internals, and with computing power limitations as well.

Several parallel simulations were set-up and run, based on different meshing solutions, numerical options and modelling assumptions. Then the numerical results were compared against the experimental data, in terms of tracer concentration space and time distribution both in the downcomer and at the core inlet. Qualitatively, the formation of the perturbed region in the downcomer and in the lower plenum was correctly predicted. Quantitatively, the code tends to predict steeper gradients of the concentration space profiles than in the experiment, thus the effectiveness of the turbulent mixing is generally under-predicted. The mixing underestimation appears in the DC (although it shows its effects mainly at the core inlet), and may be related to the limitations of the used 2-equation turbulence models in dealing with the high anisotropy of the turbulent structures. Slightly better

results were achieved using a grid with tetrahedra in the DC, since the higher numerical diffusion tends to compensate the mixing under-prediction.
Such mixing under-prediction had been observed also in several FLOMIX results.
Further investigation on the sensitivity of mixing prediction on different turbulence modeling approaches is needed. In particular, special care should be taken in addressing the DC mixing, which should be separately assessed with respect to the LP mixing. Additional efforts should also be spent in achieving the grid convergence, as increased computing resources become available.
Although higher accuracy in prediction of turbulent mixing would certainly be desirable for “best-estimate” purposes, it is worth considering the “conservatism” of the results obtained, since they predicted a less mitigating effect (with respect to the experiment) played by the turbulence mixing in the assumed accidental scenarios.

References to Section A.1

1. Rohde, U. et al., 2007, Fluid mixing and flow distribution in a primary circuit of a nuclear pressurized water reactor – Validation of CFD codes, Nuclear Engineering and Design, Vol. 237(2007)15-17, pp. 1639-1655.
2. Rohde, U. et al., 2004, Description of the slug mixing and buoyancy related experiments at the different test facilities, EU/FP5 FLOMIX-R Project, FLOMIX-R-D09, Germany.
3. Höhne, T., Kliem, S., Prasser, H.-M., Rohde, U., 2003, Experimental and numerical studies inside a reactor pressure vessel, *Proceedings of the 4th ASME/JSME Joint Fluids Engineering Conference*, Hawaii, USA. CD-ROM.
4. ANSYS Inc., 2005a, ANSYS ICEM-CFD 10.0 User Manual, (embedded in the software package).
5. ANSYS Inc., 2005b, ANSYS CFX-10.0 User Manual, (embedded in the software package).
6. Menter, F., 2002, CFD Best Practice Guidelines for CFD Code Validation for Reactor-Safety Applications, EU/FP5 ECORA Project “Evaluation of computational fluid dynamic methods for reactor safety analysis”, EVOL-ECORA-D01, Germany.
7. Ferziger, J. H., Perić, M., 2002, Computational Methods for Fluid Dynamics, 3rd edition, Springer, Berlin.

A.2. CFD simulations of VVER-1000

[Moretti F., Melideo D., Terzuoli F., D'Auria F., Application of CFX-10 to the Investigation of RPV Coolant Mixing in VVER Reactors, ICONE14-89840, Proceedings of 14th International Conference on Nuclear Engineering, July 17-20, 2006, Miami, Florida, USA.]

A.2.1. Introduction

The International Standard Problem No. 43 organized by the OECD, and based on the experimental data collected at the University of Maryland – College Park (UMCP) mixing facility (Ref. [4]) has constituted an important benchmarking for CFD code users and developers. Furthermore, the second V1000CT Benchmark, "Coolant Mixing Tests and Main Steam-Line Break (MSLB)", supported by OECD and USNRC (Ref. [5]), based on VVER-1000 reactor, has also constituted a chance for assessing CFD code capabilities in predicting in-vessel mixing. In such framework, measured data (in terms of temperatures at coolant channels outlet) had been made available from Kozloduy NPP Unit-6.

The present paper documents part of the CFD code assessment activity currently ongoing at University of Pisa, in particular focuses on the application of the ANSYS CFX-10 code to the simulation of mixing phenomena occurring inside a VVER-1000 RPV.

The CFD simulations were run on computational grids representing a VVER-1000/320 reactor, and characterized by rather high level of geometrical detail, although not fine enough to yield mesh-independent solutions. The simulations addressed both thermal mixing and slug-mixing problems. In the first case reference was made to the final steady-state conditions of the MSLB scenario of the V1000CT-2 Benchmark – 1st exercise (Ref. [5]). The loop-to-assembly mixing coefficient were calculated and compared to experimental values. In particular the attention was focused on the "swirl" effect that has been observed in many reactors of this kind. As regards the slug-mixing problem, a transient was simulated where a slug of deborated water is transported into the RPV by a natural circulation flow, and reaches the core inlet after experiences a certain degree of mixing in the Downcomer (DC) and in the Lower Plenum (LP). Those calculations had demonstration purposes rather validation, since no experimental data were used for comparison. All calculations were run in parallel mode on a small Linux-cluster. Some comparisons have been made also against results form RELAP5-3D calculations, presented at the Fourth V1000CT Benchmark Workshop (Ref. [6]), and kindly made available by Dr. Shkarupa of Kiev University.

Moreover, transient calculations are presented which were aimed at simulating a deborated slug mixing problem, assuming that a deborated slug has accumulated in the loop seal, and then it is transported towards the RPV by a natural circulation flow.

Like in many other works already published in the literature, the limitations related to the high computational costs of CFD analyses, especially when transient problems are addressed, as well as their great potential, are once more put in evidence.

A.2.2. Grids preparation

The VVER-1000 is a four loop PWR with hexagonal core geometry. The core contains 163 hexagonal fuel assemblies. Most of the reactor internals are contained in the core barrel, which is inserted and fixed in the reactor vessel. The primary circuit coolant flows to the core through the perforated barrel bottom and perforated fuel support columns serving as flow distributors. The fuel support columns are inserted into corresponding holes of the core support plate and welded together at the top so that no flow passes around the columns. Thus, the primary coolant flows through the slots into the columns, and then further upward through the support columns into the fuel assemblies.

Some geometrical differences exist between VVER-1000/320 reactors belonging to different Nuclear Power Plants (NPP). In this work reference was made to the Kozloduy NPP Unit 6 (Ref. [5]).

The computational domain chosen for the CFD simulations includes the inlet nozzles region, the DC, the LP up to the core inlet plate. A three-dimensional CAD model of such domain was created; many geometrical details were explicitly represented, such as the solid support columns between the core inlet plate and the elliptical shell (Figure A. 24), and the eight consoles in the DC between the internal RPV wall and the barrel (Figure A. 25). Smaller details, like the 1344 holes through the elliptical shell, and the holes through the perforated columns below the core inlet plate (violet region in Figure A. 24), were not represented, and were accounted for in the calculation model by additional pressure losses. A sketch of the overall 3D model is shown in Figure A. 26, together with a cross-section of the lower part of the computational domain. The latter includes an outlet volume above the core inlet plate, which simulates the core region and allows for pressure equalization. The “porous regions” shown in Figure A. 27 were assigned additional pressure losses when setting up the calculations.

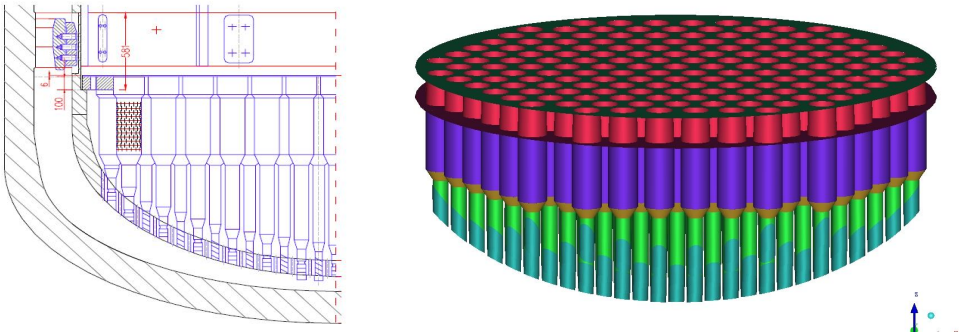

Figure A. 24 –Sketch of the LP internals (left, from Ref. [5]) and related CAD model (right)

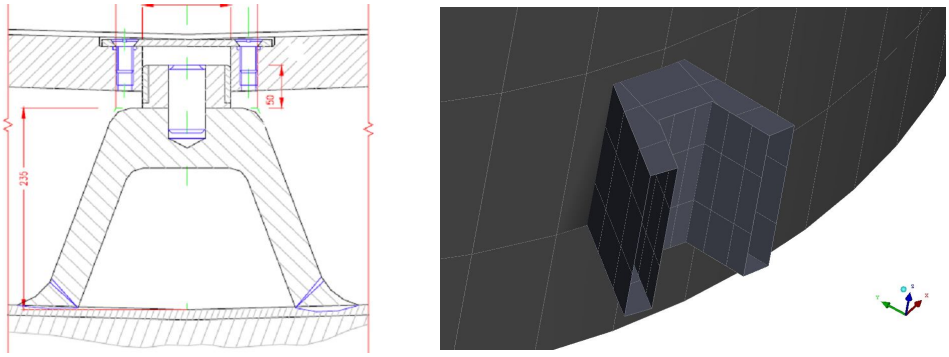

Figure A. 25 – Sketch of the consoles (left, from Ref. [5]) and related CAD model

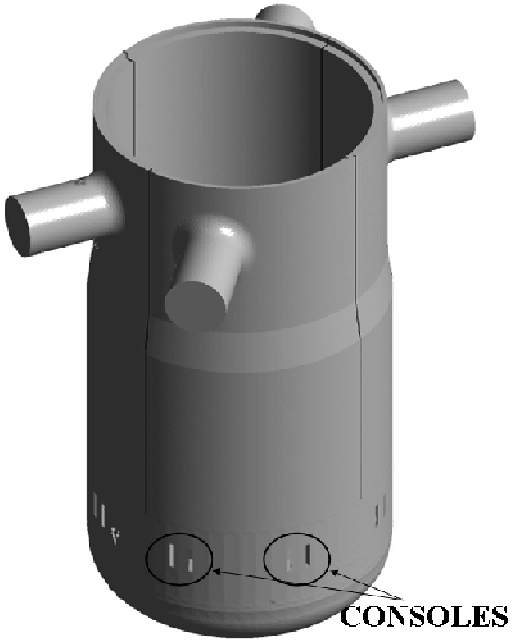

Figure A. 26 –CAD model of the computational domain

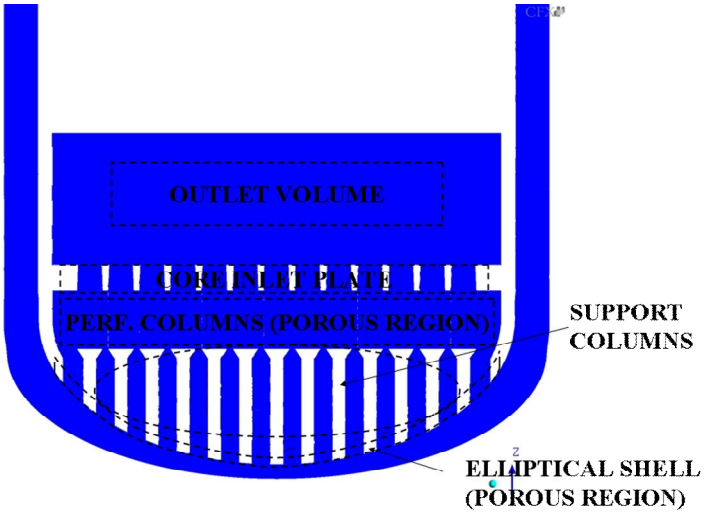

Figure A. 27 – Cross-section of the lower part of the computational domain

The computational grids were created with the ANSYS ICEM CFD package. As usual, the grid preparation was a very much time-consuming part of the work.
As a first meshing strategy, hybrid meshes were obtained, made of hexahedral elements in the inlet nozzles and DC regions (included the consoles region), and tetrahedral elements in the lower plenum region, where the complexity of the geometry would have made very difficult to mesh with hexahedral cells. In general, the use of hexahedral cells tends to minimize the mesh size, with respect to the use of tetrahedral cells, which on the other hand are more versatile for meshing complex domains. Test calculations (mentioned below) revealed some numerical problems associated with the hybrid meshes, which were thus abandoned.
As a second strategy, a mesh was created made only by tetrahedral cells. This mesh did not show the same numerical problems as the previous one, and was thus used for the main simulations. It counts around 4 200 000 cells (three millions only in the LP). Despite this large number, the mesh is relatively coarse, and then more prone to numerical diffusion. It represents a compromise between accuracy and computing time. Finer meshes would provide more accurate results, but with unacceptable calculation time in relation to the available computing power. It has to be remarked that, as suggested by Best Practice Guidelines (BPGs, see Ref. 7), a mesh should be proved to yield grid-independent results, and systematic mesh sensitivity analyses should be performed. On the other hand, such task is almost always impracticable when dealing with such complex geometries.
Some particulars of the tetrahedral mesh are shown in Figure A. 28 and Figure A. 29. The smallest cell size is lower than 30 mm. Some zones characterized by very small thickness required “manual” modifications of the mesh so as to avoid one-cell thickness (which would be seen as a “wall elements” by CFX).
A few words need to be spent concerning the symmetries. In the Kozloduy-6 reactor, the vertical symmetry planes of the nozzles do not coincide with the core symmetry planes, instead they are rotated with respect to them, around the vertical direction, by a 7° angle counter-clock wise. The consoles are equally spaced in the DC along the azimuthal direction, and their layout is symmetric with respect to the

core symmetry planes. This is shown in Figure A. 30. A higher degree of symmetry would have simplified the 3D modeling and the mesh generation process, and probably allowed the use of hybrid grids.

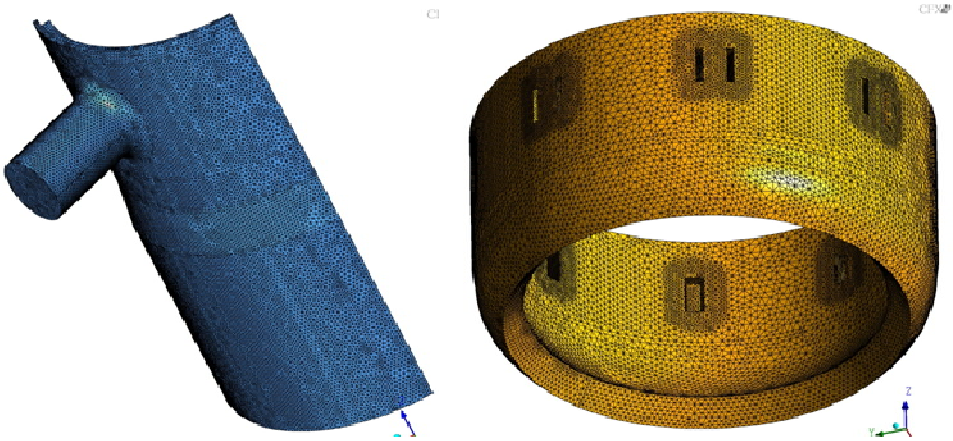

(a) (b)

Figure A. 28 – Particulars of the mesh: a) quarter of the DC; b) consoles region

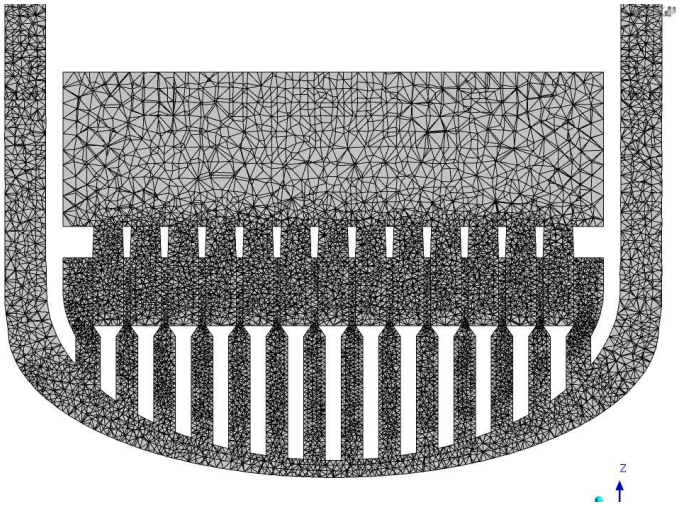

Figure A. 29 – Mesh in the LP region

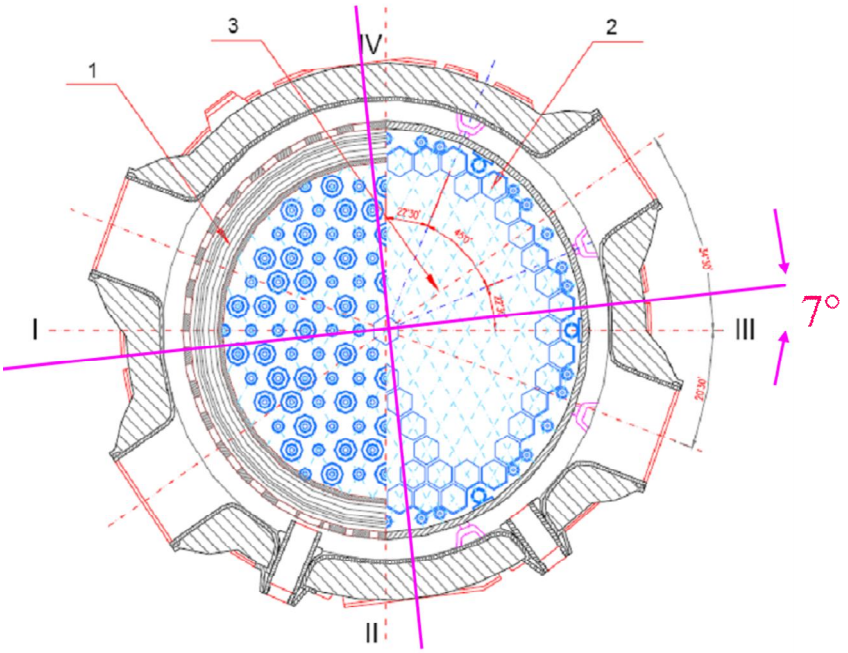

Figure A. 30 – Cross section of the Kozloduy-6 reactor at inlet nozzle level, with indication of symmetries

A.2.3. Test calculations

Some CFX calculations, with arbitrary model settings and boundary conditions, were performed to test the computational grids, before running the "production" calculations.

Some test calculations were run using the hybrid meshes described above. Some unexpected and unphysical flow field features were observed in some of them, like very large momentum diffusion in some regions where small mixing was expected.

One of the test calculations was run on a "non realistic" mesh which did not include the consoles and in which the core region and the downcomer shared the same symmetry planes. The solved problem was perfectly symmetric (both in terms of geometry and boundary conditions), but some asymmetries were revealed in the solution. It was found that those asymmetries were due to the azimuthal mesh spacing in the DC being not perfectly symmetrical.

Several tests were performed differing by the following features:

- inlet angular position (either corresponding to the design layout, or rotated by 7° clockwise so that the nozzles and the core share common symmetry planes);
- presence of the consoles (i.e. meshes were considered also without consoles);
- different meshing strategies (DC meshed either with tetrahedral or hexahedral elements);

- different discretization schemes for the convective term of the momentum equation (Upwind, High Resolution or with a user-specified blend factor).

Further test calculations were run to asses the additional pressure losses. As mentioned above those artificial losses have been applied both to the elliptical shell, and to the perforated column region, by means of source terms in the momentum conservation equation. The same approach had been previously followed by Bieder et al. (Ref. [8]).
Concerning the head losses through the elliptical, shell a directional pressure loss correlation has been used, which requires a loss coefficient for the vertical direction (chosen as a reference direction) and one for the transverse direction. The latter was imposed a value two order of magnitude greater than the former, so as to force the flow along the reference direction (i.e. to the shell holes). For the perforated columns region, an isotropic pressure loss was defined in the volume portion outside the columns (i.e. with only one coefficient, and no reference direction). For a more accurate treatment pressure losses should have been applied on each perforated column, but such solution would have required much more meshing and modeling effort.
Both the isotropic coefficient (for the columns) and the reference-direction coefficient (for the shell) were arbitrarily assigned the same value. Such value was assessed by some tuning calculations in order to obtain a pressure difference of about 200 kPa between RPV inlet and core inlet, which is the same specified for the V1000CT Benchmark – Phase 1.

A.2.4. Thermal mixing simulations

Most of the performed calculations are referred to Exercise 1 of the V1000CT Benchmark – Phase 2 (Ref. [5]), which represents a Steam Generator (SG) isolation transient reproduced at the Kozloduy-6 plant. In particular, steady-state simulations have been performed of the final state of such flow-mixing test. Transient calculations would certainly have been desirable, however the available computing power, represented by a small Linux-cluster of eight processors (2.8 MHz, and 2 MB RAM each), was not sufficient to obtain transient results in reasonable time.

The problem is characterized by asymmetrical temperature distribution at inlets. In particular, inlet temperature from loop #1 is about 12-13 K higher than from the other loops, thus one sector of the RPV (and of the core) is affected by a temperature perturbation. The simulations are aimed at predicting the thermal mixing between flows coming from the four loops, and the temperature space distribution at core inlet.
The reference fluid physical properties are those of water at 543 K and 16 MPa. Buoyancy has been neglected. The turbulence has always been taken into account by the $\kappa-\varepsilon$ model, and the “scalable” turbulence wall treatment has been used. However the used grids do not allow an accurate treatment of the wall turbulence, since no prism layer adjacent to the wall has been defined. Such improvement will be addressed in the continuation of the present assessment activity at University of Pisa.

Two reference calculations are hereafter referred to. Both use the inlet conditions reported in Table A. 3, and differ for the discretization scheme (either Upwind or High resolution) of the advection term in transport equations.
Figure A. 31 shows the fuel assemblies (FA) layout and identification numbers, along with the indication of FAs with inlet thermocouples.

Table A. 3 – Inlet boundary conditions for thermal mixing problem

Loop #	Average inlet velocity [m/s]	Inlet static temperature [K]
1	10.57	555.35
2	10.54	543.05
3	10.51	542.15
4	10.85	542.35

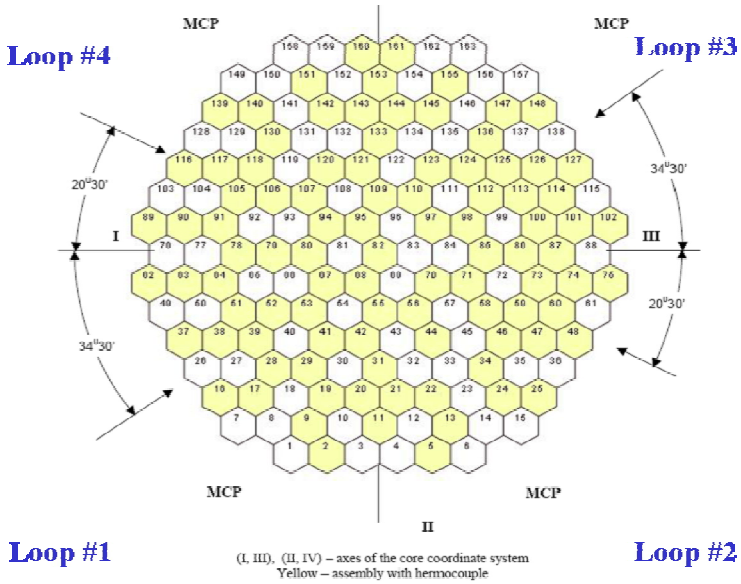

Figure A. 31 – Fuel assemblies' layout and identification. FA with inlet thermocouples are also indicated (from Ref. 5)

Some of the results obtained are shown in Figure A. 32, and compared against results from RELAP5-3D calculations (Ref. [6]) and plant data (Ref. [5]). Results from CFX simulation with Upwind scheme seems to be the most close to plant data both in terms of "shape" of the perturbation spot and of temperature spatial gradients (i.e. to mixing effectiveness), although the angular location of the spot is not correctly predicted (see below considerations about swirl effect). Results from CFX simulation with High Resolution scheme show much steeper temperature gradient, thus indicating an underestimation of the turbulent mixing. This may suggest that the overall CFD model tends to underestimate mixing (the reasons why need to be investigated), and that the use of low-order discretization schemes like the Upwind scheme, which are characterized by greater numerical diffusion,

may have a compensating effect on such deficiency, thus improving the results. Such effect would obviously be reduced by a finer spatial discretization.
As regards RELAP5-3D results, they appear quite similar to CFX – Upwind results.

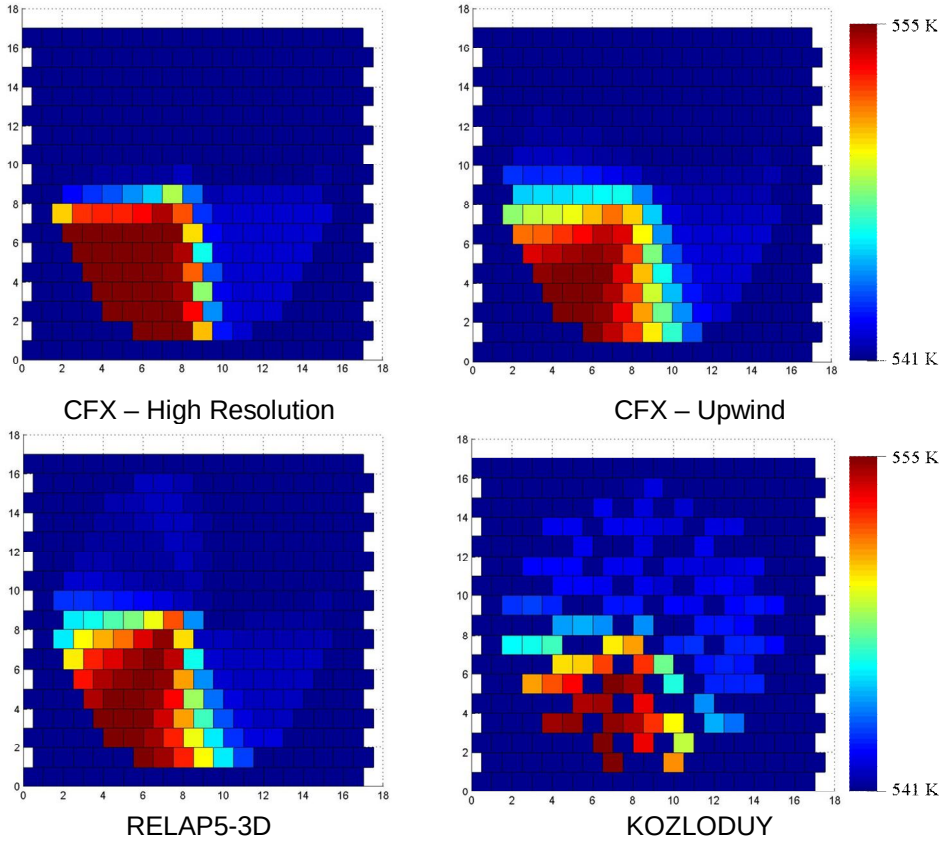

Figure A. 32 – Temperature distribution at core inlet: comparison of CFX results, RELAP5-3D results, and plant data.

A.2.4.1. The swirl effect

The swirl effect has been observed at Kozloduy-6 (Ref. [5]) and in several other VVER-1000 type plants. It consists in a rotation component of the whole downcomer flow (which is, for instance, 15-20° counter-clockwise for Kozloduy NPP), which in turn strongly affects the temperature (or any other transported scalar) distribution at core inlet.
The effect has not yet been fully explained, although some relevant insight came from recently published works, like that of Bieder et al. (Ref. [8]). The authors concluded that the swirl effect is due both to some hydraulic instabilities occurring in the DC, and to the small discrepancies existing between the design layout of the cold legs and the real plant layout (angular locations differ of a few percents). Such conclusions came from the fact that the authors' simulations (performed with Trio_U code) could predict the swirl only when a Large Eddy Simulation (LES) approach was followed and the real plant data were used.

The reference simulations presented in this work (all based on a two-equation turbulence model) could not capture the swirl effect in the case that an Upwind scheme was used, while a small swirl (about 1°) was observed with the High Resolution Scheme. The difference between simulation and real plant behavior can be seen in Figure A. 33. In order to extend the investigation on the swirl, some more hypotheses have been considered:

1. the effect of secondary motions within the inlet flows, such as – for instance – a swirling component induced by the Main Circulation Pumps (MCP);
2. the effect of asymmetrical inlet boundary conditions (i.e. different inlet flow rates);
3. the effect of the two Emergency Core Cooling (ECC) nozzles at Cold Leg (CL) level;
4. the fact that the nozzles and the core do not share the same symmetry planes.

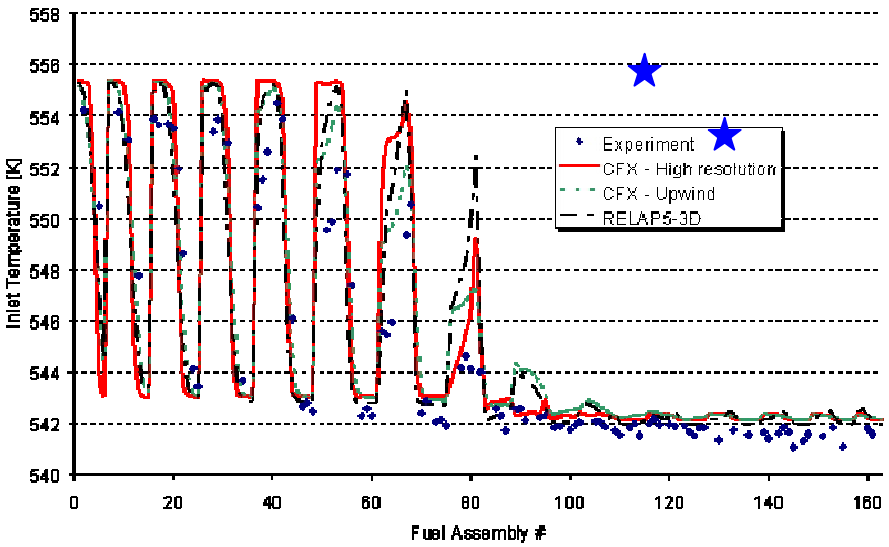

Figure A. 33 – Thermal mixing problem: comparison of fuel assembly inlet temperatures values from experiment (V1000CT-2 data), CFX simulations (both High Resolution and Upwind schemes).

Two calculations were run adding a tangential component (about 5 % of the normal component) to the inlet velocity at each nozzle, either clockwise or counter-clockwise (with respect to normal velocity component). Both showed a small swirl effect, in the order of about 2-3°, either clockwise or counter-clockwise (with respect to DC axis). This indicates that secondary motions in inlet flows may give a contribution to the rotation effect. Further parametric studies are needed to asses the relevance of such contribution.
The V1000CT mixing problem is characterized by asymmetric loop operation, in terms of both inlet velocities and temperatures (see Table A. 3), which differ by a few percents from nozzle to nozzle. Such asymmetries might also contribute to the

swirling effect. Some insight could come from experimental observation, as well as from sensitivity CFD analyses. Such analyses have not yet been performed and will be matter for further activities.
An effect due to the presence of the two ECC nozzles at CL level can be expected since they affect the local flow resistance. Investigations on this possible influence are currently ongoing at University of Pisa.
Concerning the asymmetric cold leg orientation with respect to the core (see Figure A. 30), its relevance to the addressed phenomenon can be excluded since it is known that the swirl effect has been observed also in VVER plants having symmetric configurations.

A.2.4.2. The effect of numerical diffusion

As evidence above, the choice of the discretization scheme for the convective term of the momentum equation may sensitively affect the results of mixing calculations, especially with relatively coarse meshes. An example of that is shown in Figure A. 34: the use of a first-order scheme (Upwind) yields to an overestimation of eddy diffusivity (i.e. mixing), as indicated by the smoother thermal gradients with respect to the High Resolution (2^{nd} order) scheme. On the other hand, higher order schemes (than first), lead sometimes to numerical instabilities and unphysical behavior, as show in Figure A. 34-d (upper region of the DC).

A.2.5. Slug-mixing simulations

The addressed problem is represented by the entrance of a 5 m^3 deborated slug into the RPV, being transported by a postulated natural circulation flow. Transient simulations have been performed in order to investigate the in-vessel mixing phenomena and to explore the capabilities of the code to simulate transient flow mixing problems.
The calculations assume symmetric loop operation, i.e. identical inlet velocities for each loop. Two values were considered for the mean inlet velocity: 1 m/s and 1.5 m/s (further parametric studies are ongoing).
An additional variable (referred to as the scalar) has been defined to simulate the boron concentration, which is considered as a passive scalar(+). Correspondingly, and additional transport equation is solved, without any feedback on the flow field. Time-dependent boundary conditions in terms of scalar concentration have been defined at inlet nozzle on loop #1 in order to simulate the slug entering the RPV. The timing of the injection has been defined as a function of the inlet velocity, so as to obtain a slug volume of 5 m^3. Time histories of the scalar concentration have been monitored both in the DC and at the core inlet.
Before running transient simulations, some tests were performed with inlet velocity varying from zero to the stationary value within a few instants (to simulate the natural circulation start-up) and without any scalar, in order to estimate the time interval needed for the in-vessel flow field to be fully developed. It was thus found that such interval is smaller than the time required for the boron slug to reach the

(+) The scalar concentration is defined as a non-dimensional quantity varying between 0 and 1. 0 represents the normally borated water, while 1 represents the diluted (or deborated) water.

RPV from the loop seal. This allows initializing the slug-mixing simulations with a developed steady-state flow field, and to start the scalar injection from t=0, with great advantage in terms of computing time.

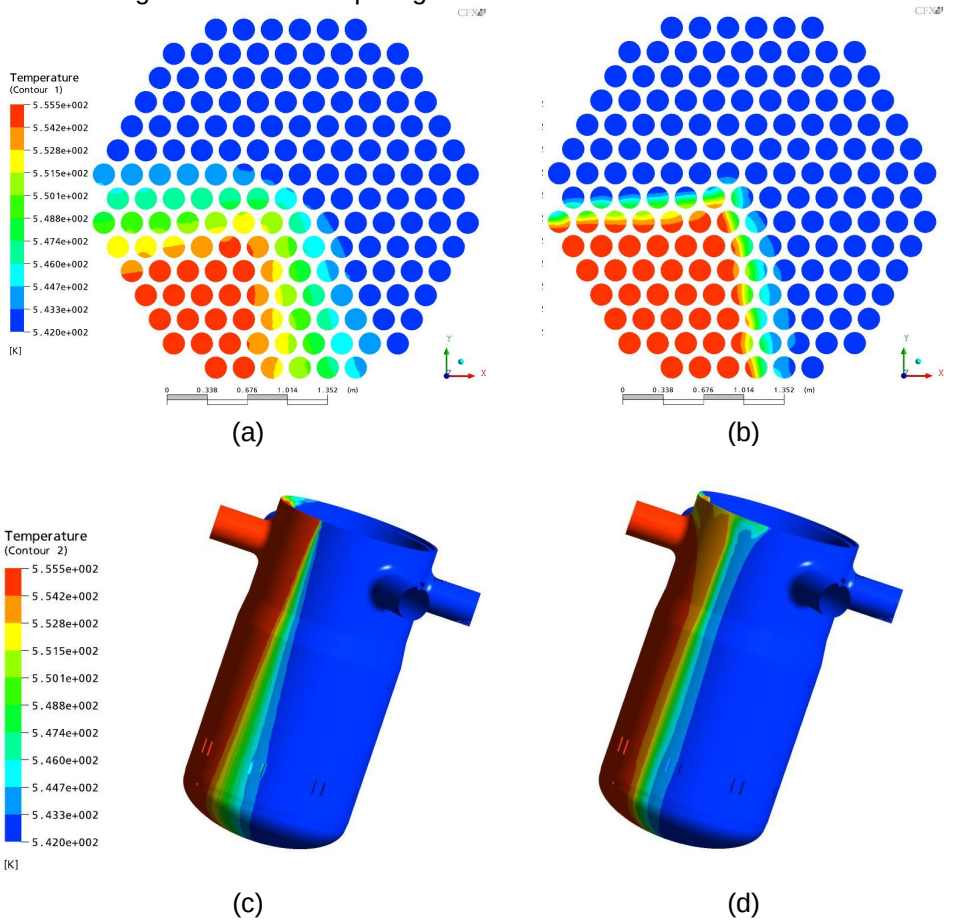

Figure A. 34 – The effect of numerical diffusion: steady-state thermal mixing calculation, with upwind scheme (a and c) and high resolution scheme (b and d)

The CFX code allows selecting which unsteady equations must be solved during a transient calculation. This allows running transient calculations only solving the scalar transport equation at each time step, and excluding the mass, momentum, energy and turbulence equations, so that only the scalar concentration is recalculated while the flow field is kept steady-state. Calculations are thus sped-up by a factor four. That kind of calculations will be referred to as “scalar transport only” (STO) calculations, while those in which the complete set of equations is solved will be referred to as the “all equations” (AE) calculations.
Three calculations are considered hereafter:

1. AE, inlet velocity = 1 m/s
2. STO, inlet velocity = 1 m/s
3. STO, inlet velocity = 1.5 m/s

AE calculations were run using the High Resolution scheme for the advection term in momentum equation.
A 0.1 s time step has been used for all calculations.
Figure A. 35 shows a comparison between results of the first and second calculation, in particular the scalar concentration time histories at some FA inlets are considered. Some discrepancies are observed for those FAs being in the high-mixing zones (# 4, 20, 42). To explain them, the hypothesis can be made that some numerical instabilities take place in the AE case, probably related to the use of High Resolution schemes. Further sensitivity analyses are needed to solve this issue.

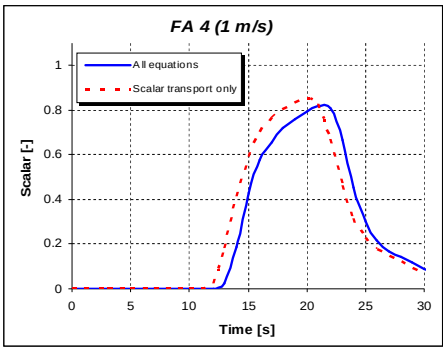

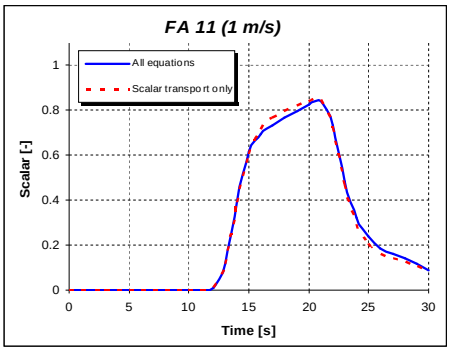

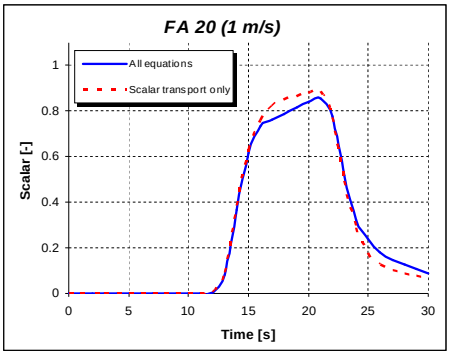

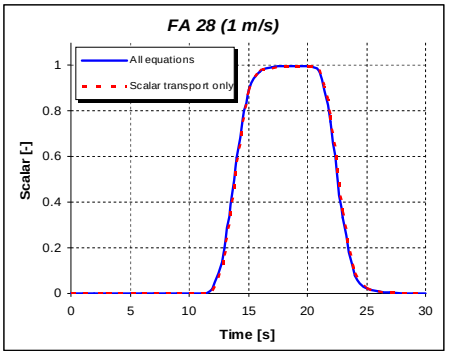

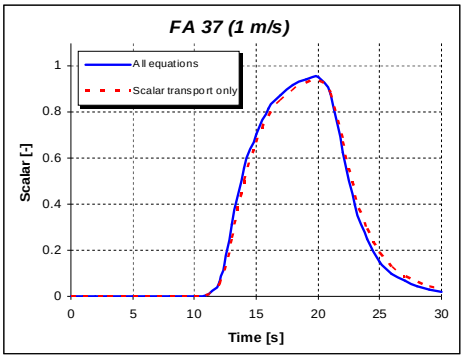

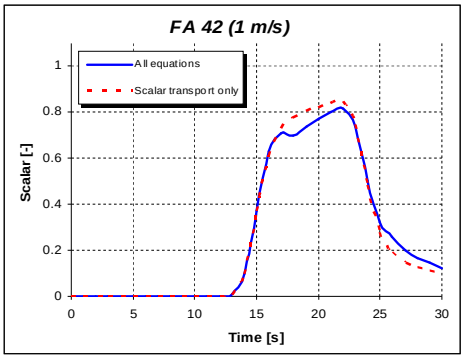

Figure A. 35 – Results of CFX calculations of the slug-mixing problem (1 m/s case), solving either the full set of equations or only the passive scalar transport equation. Time histories of scalar concentration at some selected FA inlets are compared

A.2.6. Conclusions

The CFX-10 code has been applied to the simulation of a steady-state thermal mixing problem and a transient slug-mixing problem, on a computational model representing the RPV of a VVER-1000 reactor. The results were compared against experimental results, as well as results from the RELAP5-3D system code. The calculations provided insight into the capabilities of the used code to address in-vessel mixing problems, including sensitivity on some numerical feature (like discretization schemes), and allowed identifying the main aspects needing further efforts as regards the computational model improvement and assessment.
Some improvements of the results of mixing simulations (both for temperature and scalar concentration) are expected if the following actions are undertaken:

- general mesh refinement;
- definition of prism layers at the walls;
- explicit modeling of the holes on the elliptical plate;
- more accurate modeling of pressure losses through the support columns (either by explicit modeling of holes, or directional pressure losses).

The prism creation, for a better turbulence wall treatment, is easily achievable and will be soon performed. As regards more deep mesh refinement actions, they will be practicable only if large computing power is available.

To further investigate the “swirl” effect, systematic studies should be done on the following items:

- the ECC nozzles effect on DC flow field;
- the effect of mesh refinement;
- the adoption of different turbulence models (included LES);
- the adoption of real plant data;
- the use of different inlet boundary conditions.

As regards the slug-mixing results, further CFX calculations are planned to investigate sensitivity to numerical schemes. Moreover, those results constitute a basis for a code-to-code comparison activity, since they are being compared against results from RELAP5-3D simulations. So far, the developed CFD model has yielded qualitatively good results and has been demonstrated to have the capability to address slug-mixing problems, although further model improvements, mesh refinement, and sensitivity analyses are still needed.

Nomenclature

BPG	Best Practice Guidelines
CAD	Computer Aided Design

CFD	Computational Fluid Dynamics
CL	Cold Leg
EC	European Community
ECC	Emergency Core Cooling
FA	Fuel Assembly
LES	Large Eddy Simulation
LP	Lower Plenum
MCP	Main Circulation Pump
MSLB	Main Steam Line Break
NPP	Nuclear Power Plant
OECD	Organization for the Economic Cooperation and Development
PWR	Pressurized Water Reactor
RCS	Reactor Coolant System
RPV	Reactor Pressure Vessel
SG	Steam Generator
UMCP	University of Maryland – College Park
USNRC	United States Nuclear Regulatory Commission

References to Section A.2

1. Tuomisto H., et al., EUBORA - Concerted Action on Boron Dilution Experiments, FISA-99 Symposium on EU Research on Severe Accidents, Luxembourg, 29 November - 1 December, 1999.
2. Scheuerer M. et al., ECORA Project - Condensed Final Summary Report, European Commission, March 2005.
3. Rohde U. et al., FLOMIX-R Project – Final Summary Report, European Commission.
4. Gavrilas M., Kiger K.: OECD/CSNI ISP Nr. 43 Rapid Boron-Dilution Transient Tests for Code Verification, September 2000.
5. Kolev N. et al., VVER-1000 Coolant Transient Benchmark (V1000CT), Volume II: Specifications of the VVER-1000 Vessel Mixing Problems, OECD/NEA/CSNI, March 2004.
6. Shkarupa A., Application of RELAP5-3D to the V1000CT2 Exercise 1, Proceedings of the OECD/DOE/CEA VVER-1000 Coolant Transient Benchmark - Fourth Workshop, 24-25 April 2006, Pisa, Italy.
7. Menter F., CFD Best Practice Guidelines for CFD Code Validation for Reactor-Safety Applications, EVOL-ECORA-D01, 2002.
8. Bieder U. et al., Simulation of mixing effects in a VVER-1000 reactor, The 11th International Topical Meeting on Nuclear Reactor Thermal-Hydraulics (NURETH-11), Avignon, France, October 2-6, 2005.

A.3. CFD simulations of Gidropress mixing facility

[Moretti F., Melideo D., Del Nevo A., D'Auria F., Höhne T., Lisenkov E., CFD Analysis of a Slug Mixing Experiment Conducted on a VVER-1000Model, Science and Technology of Nuclear Installations, Volume 2009, Article ID 436218, 2008.]

A.3.1. Introduction

In a pressurized water reactor (PWR) several transient scenarios can be hypothesized leading to a perturbation of the coolant time and space distribution at the core inlet (such as temperature and boron concentration), which in turn can induce positive reactivity insertion and power excursion. Transients leading to Boron dilution as well as main steam line break (MSLB) transients are examples of such scenarios.

The perturbation is influenced by the turbulent mixing phenomena occurring inside the reactor pressure vessel (RPV), that is, a perfect mixing between the perturbed coolant (e.g., a deborated slug coming from a loop) and the non-perturbed coolant is expected to lead to the smallest core response, while the absence of mixing is likely to induce a stronger and localized reactivity insertion. Obviously a quantitative assessment of the relationship between the mixing effects and their consequences in terms of reactivity is needed for demonstrating the reactor safety.

The mixing phenomena are inherently three-dimensional, therefore they can be properly analyzed and predicted by means of numerical tools having 3D capabilities, in particular the computational fluid dynamic (CFD) codes (and, to a certain extent, by system codes embedding 3D modules and mixing models).

Several international projects and experimental campaigns have been conducted in the past to investigate the in-vessel mixing phenomena and the code capabilities to predict them. Examples are the experiments carried out at Forschungszentrum Dresden-Rossendorf (FZD) ROCOM facility (Ref. [1]), University of Maryland (Ref. [2]), Vattenfall (Ref. [3]), while as far as the code assessment is concerned, the OECD/NEA International Standard Problem (ISP) no. 43 (Ref. [4]), the EC FLOMIX-R project (Ref. [5]), and the EC ECORA project (Ref. [6]) can be mentioned.

Recently, these issues have been addressed in the framework of the EC-funded TACIS project R2.02/02 "Development of safety analysis capabilities for VVER-1000 transients involving spatial variations of coolant properties (temperature or boron concentration) at core inlet" (Ref. [7]). An extensive experimental campaign was conducted at the OKB "Gidropress" mixing facility (a 1:5 scaled model of a VVER-1000 reactor) to study fluid mixing scenarios featured by different flow conditions, such as symmetric and asymmetric steady pump operation at nominal flowrates in the presence of tracer injection (5 experiments), and pump start-up scenarios in the presence of tracer slugs (5 more experiments).

All the measured data collected have been utilized for the validation of mixing models implemented in a set of Russian thermo-hydraulics system codes, with CFD being used as a valuable support to the phenomena understanding, and results interpretation, and being object of validation itself.

One of the experimental tests performed consisted in a main coolant pump (MCP) start-up, with the other three pumps switched-off and a tracer slug (simulating

deborated water) accumulated in the cold leg of the starting loop. Such experiment was then simulated both with system codes and CFD codes. In particular, pre-test and post-test simulations were run using the commercial CFD code ANSYS-CFX and the results obtained were compared against the measured data. Such CFD code validation activity is described in the present paper.
As explained above, the present work is a part of a wider and more comprehensive activity, which included the CFD grid generation, the pre-test and post-test simulations of all the experiment performed, the execution of sensitivity analyses on the main modelling parameters, in compliance with the requirements of the Best Practice Guidelines (BPGs, Refs. [8] and [9]). Additional information can be found for instance in Refs. [10] and [11].
This work is connected to the CFD code validation activity in progress at the University of Pisa, related to single phase in-vessel flows. Analogous analyses were performed, for instance, for some experiments carried out on the abovementioned ROCOM facility (Ref. [12]).
It is also worth mentioning that CFD validation activities (Ref. [13]) had been carried out in the recent past on a previous version of the same Gidropress mixing facility in the framework of the above-mentioned FLOMIX-R project.

A.3.2. Description of the experiment

The experimental facility basically consists of a RPV model, connected with four circulating loops. The RPV model (Figure A. 36-a) is made of steel and reproduces, at a 1:5 scale, practically all the geometrical features of the RPV of a VVER-1000 reactor (namely, Novovoronezh NPP reactor, Unit no. 5) which are affecting the in-vessel mixing phenomena up to the core inlet, particularly the internal components such as the barrel, the lower ellipsoidal perforated shell (with more than 1300 drillings of two different diameters), the core support columns (one for each of the 151 fuel assemblies) and the core lower plate (which separates the core region from the lower plenum region). The core region is actually not modelled; rather a structure is present made of perforated plates and guide tubes supporting 90 conductivity probes which are located just above the lower core plate.
Each loop is equipped with an independent computer-controlled circulation pump, which permits to simulate a wide range of flow conditions. An expansion tank is connected to one of the loops in lieu of the pressurizer; atmospheric conditions reign above the water level in the tank, while higher pressures (although still in the range 1 to 2 atm) occur in the RPV model due to the hydrostatic effect and to the pumps head. The experiments are conducted at ambient temperature. The circulating loops (Figure A. 36-b) do not exactly reproduce the real piping layout; however the related volumes are such that the $1:5^3$ volume scale is kept.
Some auxiliary systems are present for the tracer injection, consisting in injection pumps, fast acting valves, a tracer tank, and pipelines connecting all such components to the main loops. For instance, such systems can be operated for accumulating a tracer slug in the ascending section of one loop while the pumps are at rest, with such section being “isolated” by two fast acting valves (Figure A. 37). Furthermore, a continuous tracer injection can also be performed into the volume compensation tank located upstream of a circulation pump.

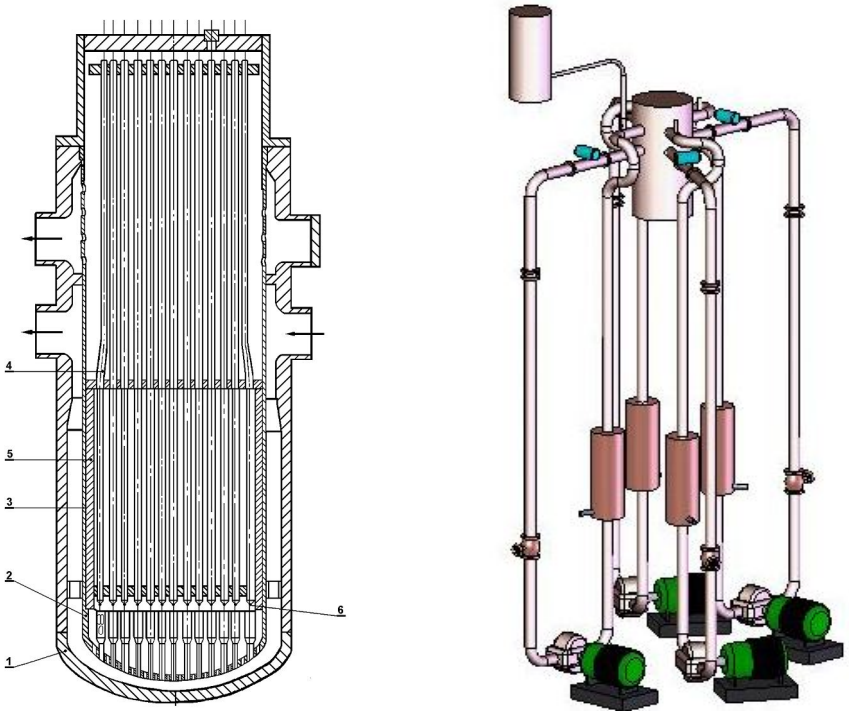

(a) (b)

Figure A. 36 – Vertical cross-section of the RPV model (a); 3D isometric sketch of the facility (b)

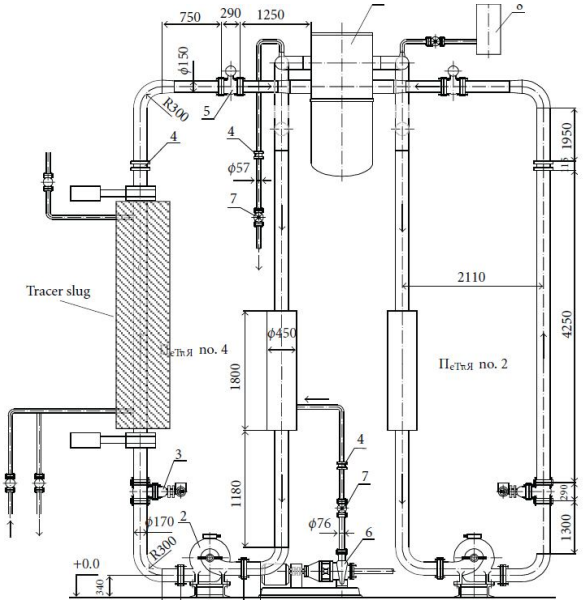

Figure A. 37 – Location of the tracer slug

The tracer utilized is sodium chloride, which alters the water electrical conductivity. Through a calibration procedure, the conductivity can be easily correlated to the salt concentration. The facility is equipped with a number of conductivity probes, providing high-frequency measurements of the local tracer concentration. As mentioned above, 90 of such probes are located above the lower core plate, each one being aligned with the centreline of one coolant channel. This means that experimental information is available for 60% of the coolant channels (90 out of 151), which is obviously not an "ideal" configuration (as it would be if all the channels were instrumented); however such measurement equipment still permits to gather valuable information of the perturbation at the core inlet. A conductivity probe is located also at each inlet and outlet nozzle; some probes are present in the tracer tank.

The loop flowrates are measured by electromagnetic flow meters located close to each inlet nozzle.
As can be understood from the description above, the facility can be operated such as to simulate a wide spectrum of operation conditions and accidental scenarios involving the perturbation of the coolant properties distribution at the core inlet. The experiment addressed in the present work was intended to reproduce the start-up of one reactor coolant pump (the other pumps remaining at rest) assuming that a "deborated slug" had previously been accumulated in the starting loop. The slug is thus transported inside the RPV, where it partially mixes with the normally borated water before reaching the core inlet and then introducing a positive reactivity in the reactor core. Namely, the deborated slug is here represented by a salted water slug (0.072 m^3 volume, which roughly corresponds to the scaled volume of the loop seal, where a deborated slug would most probably accumulate).
The starting pump is run, via the numerical control, such as to achieve an exponential growth for the flowrate, according to Equation A. 4 (the target flowrate being Q_0 = 220 m^3/h). 10 s are enough to reach ~98% of the target flowrate.

$$Q = Q_0 \cdot \left(1 - e^{-0,25 \cdot \tau}\right) \qquad \textit{Equation A. 4}$$

The isolation valves of the idle loops are left open; therefore inverse flows develop which are expected to strongly affect the flow field in the RPV model as well as the tracer distribution. The inverse flowrates are not known before the execution of the experiments, and thus constitute the main unknown parameters in the pre-test phase of the numerical analysis.

A.3.3. Description of the computational model

A.3.3.1. Computational grid

The computational domain selected for the in-vessel mixing simulations (shaded region in Figure A. 38-a) includes the following coolant regions: inlet nozzles, downcomer (DC), lower plenum (LP). The reactor core region and the upper plenum are not modelled because they are not expected to influence the coolant flow upstream of the core inlet. However, a dummy outlet volume is defined corresponding to a fraction of the core region, in order to permit the easy application of pressure-controlled outlet boundary conditions.

The identified computational domain is defined and bounded by the following solid parts:

a. inner wall of the inlet nozzles (including round surface at connection with vessel wall);
b. inner wall of the vessel (including cylindrical regions, diameter variations, elliptical bottom);
c. consoles, located in the lower part of the DC;
d. outer wall of the barrel (including elliptical bottom);
e. inner wall of the barrel (including elliptical bottom), only up to the core inlet;
f. holes through the barrel bottom (also referred to as “perforated shell” in the following);
g. support columns, located in the region between the inner wall of the barrel bottom and the lower side of the core support plate; each column includes a “solid column” part (14 mm diameter) on the bottom and a “perforated column” part on the top (a tube, 38 mm outer diameter, connected to the solid columns through a conic region, and having perforations on its wall allowing the fluid to pass from the LP to the core support plate holes and then to the core region);
h. core support plate;
i. baffle inner wall.

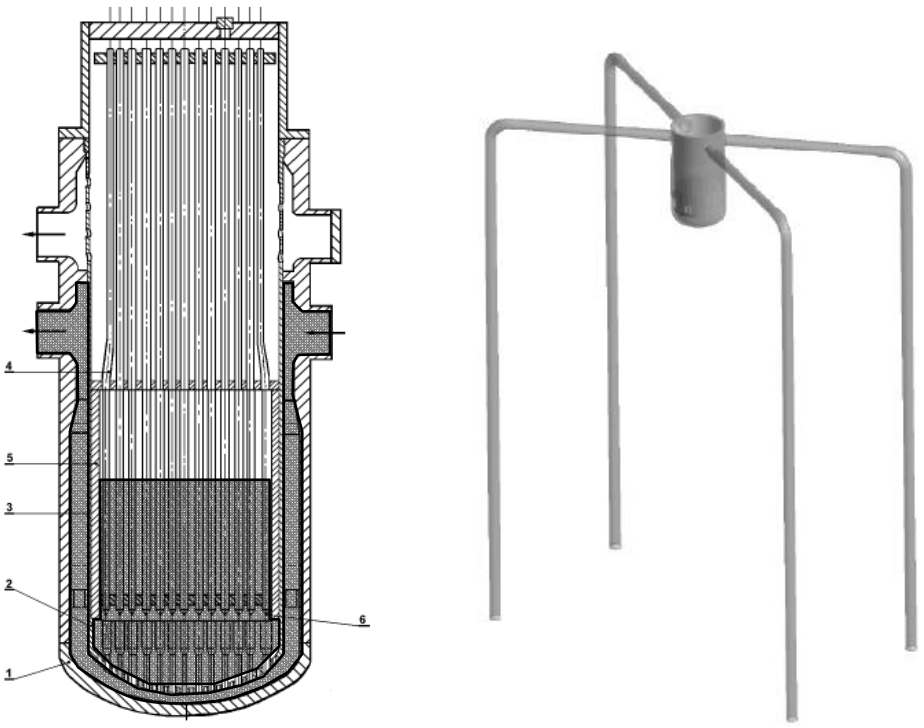

(a) (b)

Figure A. 38 – Sketch of the computational domain chosen for CFD simulations

The presence of such a large number of small geometric details (consoles, perforations through the barrel bottom, support columns, etc.) makes the achievement of a high-quality and accurate computational grid quite a tough task.

The mesh has been developed with the package ANSYS ICEM-CFD 10.0 (Ref. [14]), following a modular approach, i.e. the domain has been subdivided into several sub-domains which have been meshed separately. Then the sub-meshes obtained have been connected together by means of “interfaces”. This approach allowed adopting different mesh types in different sub-domains, namely the DC was meshed with hexahedral elements, while tetrahedra and prism layers close to the walls were used in the LP region (where the complexity of the geometry would make impracticable the hexahedral meshing). The result is a so-called hybrid grid.

Actually, several grids were generated and assembled based on different meshing approaches and sizes. Grid sensitivity analyses were performed, and a reference grid was selected, which is the one used for the present calculations. Its main features are reported in Table A. 4.

Table A. 4 – Size of reference grid ($M=10^6$)

	N°. of Nodes	N°. of Tetrahedra	N°. of Wedges	N°. of Pyramids	N°. of Hexahedra	Total No. of Elements
Reference Grid	4.3 M	3 M	630 000	32 000	2.75M	6.46 M

It is worth remarking that the reference grid is to be considered as a “production grid”, in the sense that its size results from a compromise between the need of achieving a high numerical accuracy and mesh-converged results (as recommended by the BPG) on one side, and the computational resources limitations on the other side. As usual, when addressing CFD problems having the same degree of complexity, it was not possible to demonstrate that the grid is able to provide grid-independent results. However it is believed to be a state-of-the-art grid, suitable for CFD simulation of turbulent flows, at least as far as the Reynolds-Averaged Navier-Stokes turbulence modelling is adopted.
Some pictures of the reference grid are shown in Figure A. 39 and Figure A. 40.

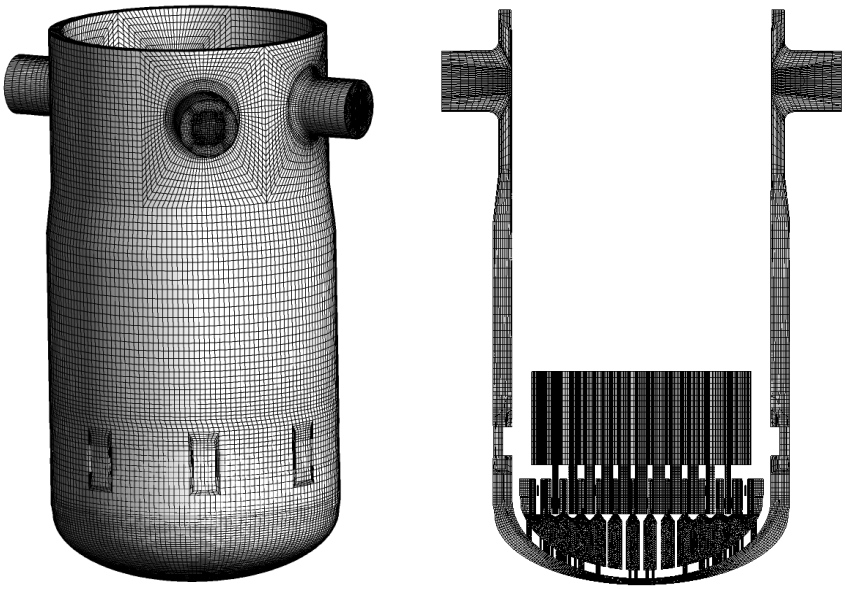

(a) (b)

Figure A. 39 – Mesh: a) overall view; b) vertical cross-section view

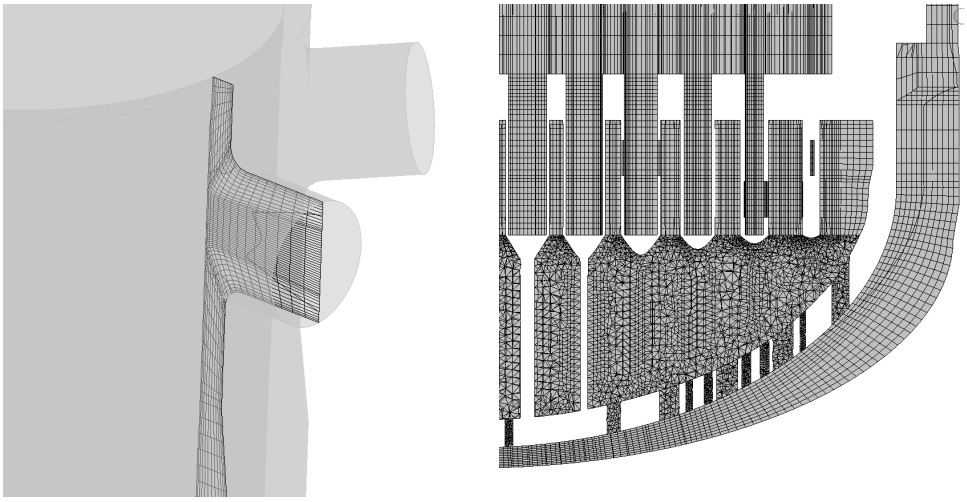

(a) (b)

Figure A. 40 – Mesh: a) inlet nozzle detail; b) LP detail

A.3.4. Simulations set-up

The simulations have been performed with the commercial, multi-purpose CFD code ANSYS CFX-10.0 (Ref. [15]), using 8 processors of a Linux-cluster available at the University of Pisa. The main features of the simulations set-up are as follows:

- working fluid: water (incompressible) at 1 atm, 25 °C;
- density: 997 kg/m^3;
- dynamic viscosity: 8.899 x 10^{-4} kg m^{-1} s^{-1};
- turbulence accounted for with SST model.

The following field equations have been solved:

- mass balance (Continuity);
- momentum balance (Navier-Stokes);
- transport of turbulent kinetic energy;
- transport of turbulent eddy frequency;
- transport of an additional, user-defined, scalar variable simulating the tracer.

The tracer concentration is handled in terms of normalized concentration (also referred to as the mixing scalar, or MS). Normalization is such that the mixing scalar ranges between the values 0 and 1, which correspond respectively to absence of tracer (i.e. full boron concentration in a hypothetical real plant transient) and initial concentration in the tracer slug (i.e. lowest boron concentration).
The transient solver available in CFX was used for both calculations, and the second-order backward Euler time advancement scheme was adopted. The Upwind scheme for the discretization of the advection terms was selected; adopting higher-order schemes is generally recommended (see for instance the BPGs, Ref. [8]), because they are less prone to numerical diffusion that first-order schemes (such as Upwind), however previous sensitivity calculations performed using the same grid had shown some non-satisfactory performance (local non-physical oscillations, bad convergence) when a higher order scheme was used, therefore it was decided to stay with Upwind scheme.
The initial conditions (for both the pre-test and the post-test calculation) consisted in zero-velocity flow over the whole domain, and zero-concentration everywhere except for the volume corresponding to the tracer slug, which was marked with mixing scalar equal to 1.
The following boundary conditions were set for the pre-test calculation:

- time-dependent flowrate at loop #4 inlet nozzle, according the theoretical law (see Equation A. 4 above);
- 5% turbulence intensity at loop #4 inlet nozzle;
- pressure-controlled “Opening” at inlet nozzles #1, 2 and 3 (to permit inverse flows), with additional concentrated pressure losses to account for the overall flow resistance of the idle loops (the pressure loss coefficients have been roughly estimated based on sensitivity calculations and experimental information on the inverse flowrates, which were known not

to exceed 10% of the nominal flowrate);
- pressure-controlled “Outlet” at the top boundary of the dummy outlet volume replacing the core region;
- no-slip condition at all walls (i.e. all boundaries not mentioned above);
- near-wall treatment of turbulence based on logarithmic law.

The post-test calculation set-up is identical to the pre-test, except for the boundary conditions at the inlet nozzles. In this case, in fact, all the flowrates (including the inverse ones) were imposed based on the measured values. The experimental flowrates are plotted in Figure A. 41, along with those resulting from the pre-test calculation.

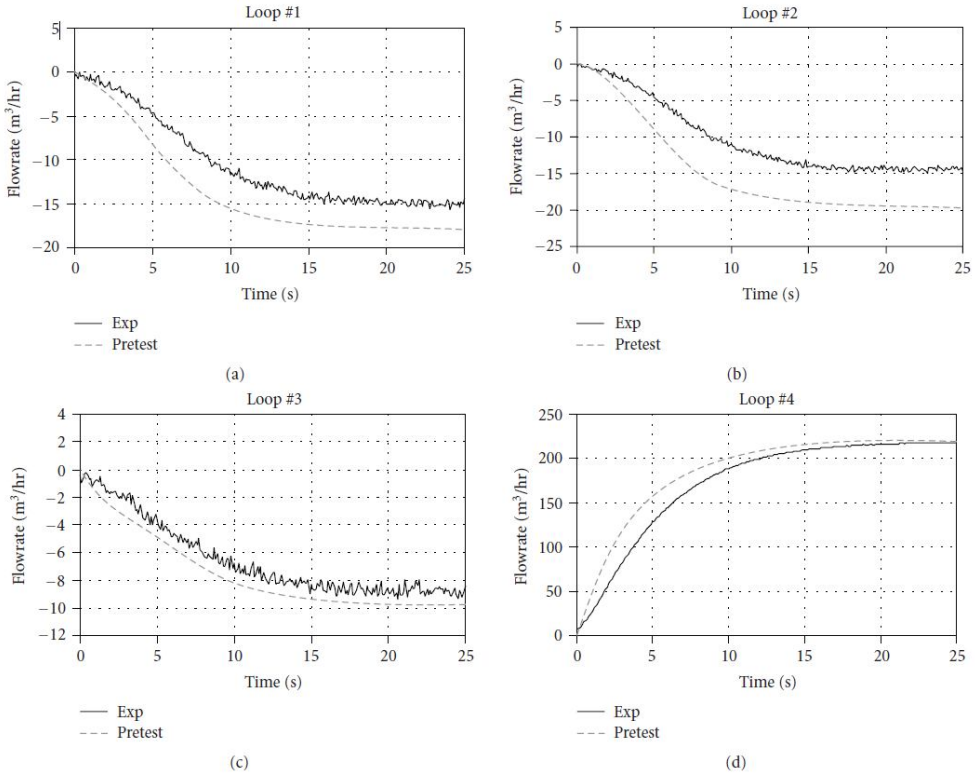

Figure A. 41 – Loop flowrates (post-test values coincide with experimental values)

A.3.5. Results

All results and experimental data are reported (and compared) in terms of normalized concentration (mixing scalar) at the core inlet, in particular at the 90 instrumented channels locations.

Figure A. 42 provides a picture of the flow pattern developing in the RPV model, by means of streamlines entering from the starting loop. The entering flow keeps a dominant horizontal component and tends to reach the opposite side before

moving downwards (towards the lower plenum). Besides, a portion of the flow leaves the RPV model through the idle loops (the related valves being kept open): such inverse flows are shown by some streamlines in the picture, and are expected to affect the amount of tracer that will reach the core inlet (since part of the tracer will exit through the idle loops). Furthermore, a stagnation region appears below the starting loop. This is also shown by the azimuthal profile of the velocity in the DC (at various instants) plotted in Figure A. 43.

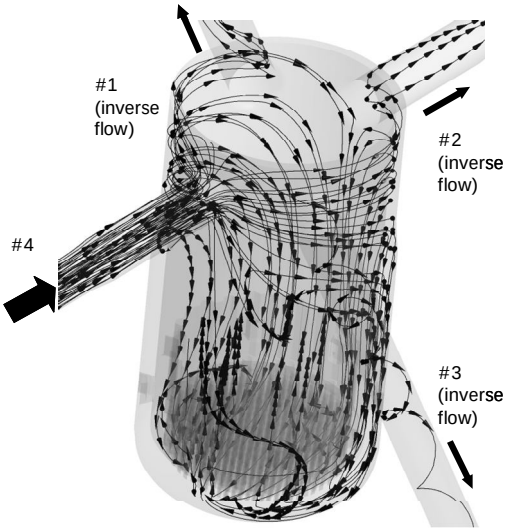

Figure A. 42 – Numerical results: velocity field (streamlines from loop 4)

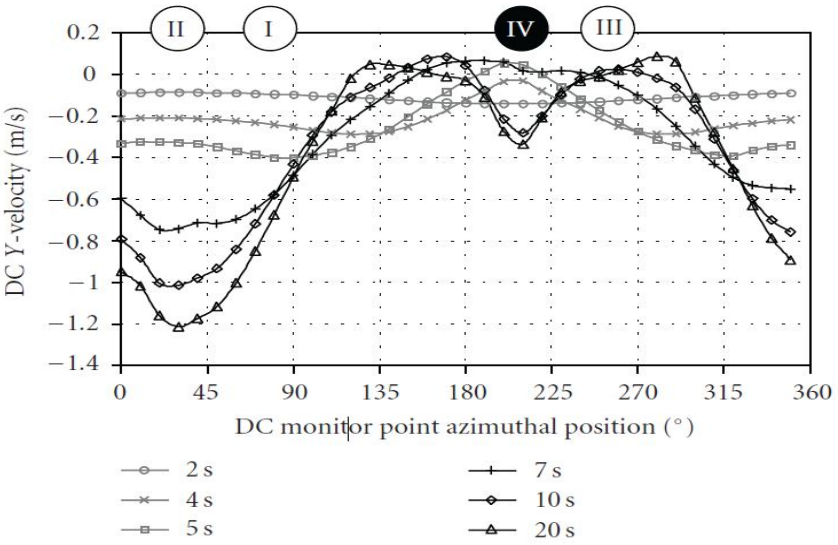

Figure A. 43 – Numerical results: azimuthal velocity profile in DC

Such a qualitative behaviour of the flow is highly dominated by three-dimensional features, so that it would be hardly described by system codes (even if with 3D capabilities). CFD codes represent the “natural” approach to deal with such behaviour, although an accurate modelling of the turbulence may still be a challenging task due to the high anisotropy of the turbulence parameters expected in a strongly bounded flow.
The correct description of the flow field developing in the downcomer is important because it determines the space distribution of the perturbation at the core inlet, particularly the location and the shape of the perturbation.

Figure A. 44 shows a qualitative code-to-experiment comparison of the mixing scalar at the core inlet at several selected instants during the slug passage. As from the experimental measurements, the first perturbation appears at the core inlet at around 9 seconds and is located below loop no. 1, that is, on the opposite side to the starting loop (i.e., no. 4). Then the perturbation extends to other peripheral channels in the clockwise direction; furthermore, a secondary perturbation spot appears just below loop no. 2. After a couple of seconds from the first perturbation appearance, almost all channels are affected, and the mixing scalar distribution has become relatively uniform. In a few more seconds, the perturbation disappears from the core inlet.

The pre-test results show the same results, from a qualitative point of view. In particular, the appearance of a primary perturbation on the opposite side with respect to the starting loop and a secondary perturbation spot below the same loop is correctly described, although with a small discrepancy in timing (1 second ahead) and somewhat larger spatial gradients. Moreover, when most of the perturbation is crossing the core inlet, the spatial distribution is quite less uniform than observed in the experiment.
As can be observed in Figure A. 41, the pre-test calculation overestimated all the inverse flowrates in idle loops. In addition, also the direct flowrate in the starting loop is larger that the measured value (as the experiment is not exactly behaving according to the theoretical law), and this explains why the perturbation reaches the core inlet in advance with respect to the test. Such time shift disappears in the post-test calculation, where the experimental loop flowrates are imposed as boundary conditions. The perturbations appearance now appears aligned with the experiment.
It is evident how the morphology of the perturbation affecting the core inlet is determined by the flow distribution in the downcomer (described above).
It is also evident that the predicted spatial distribution of the perturbation is quite less uniform than observed in the experiment. In other words, a less effective mixing is predicted, as it has previously been observed in similar works (see Ref. [12]), and this behaviour is most probably related to limitations of the RANS turbulence modelling.

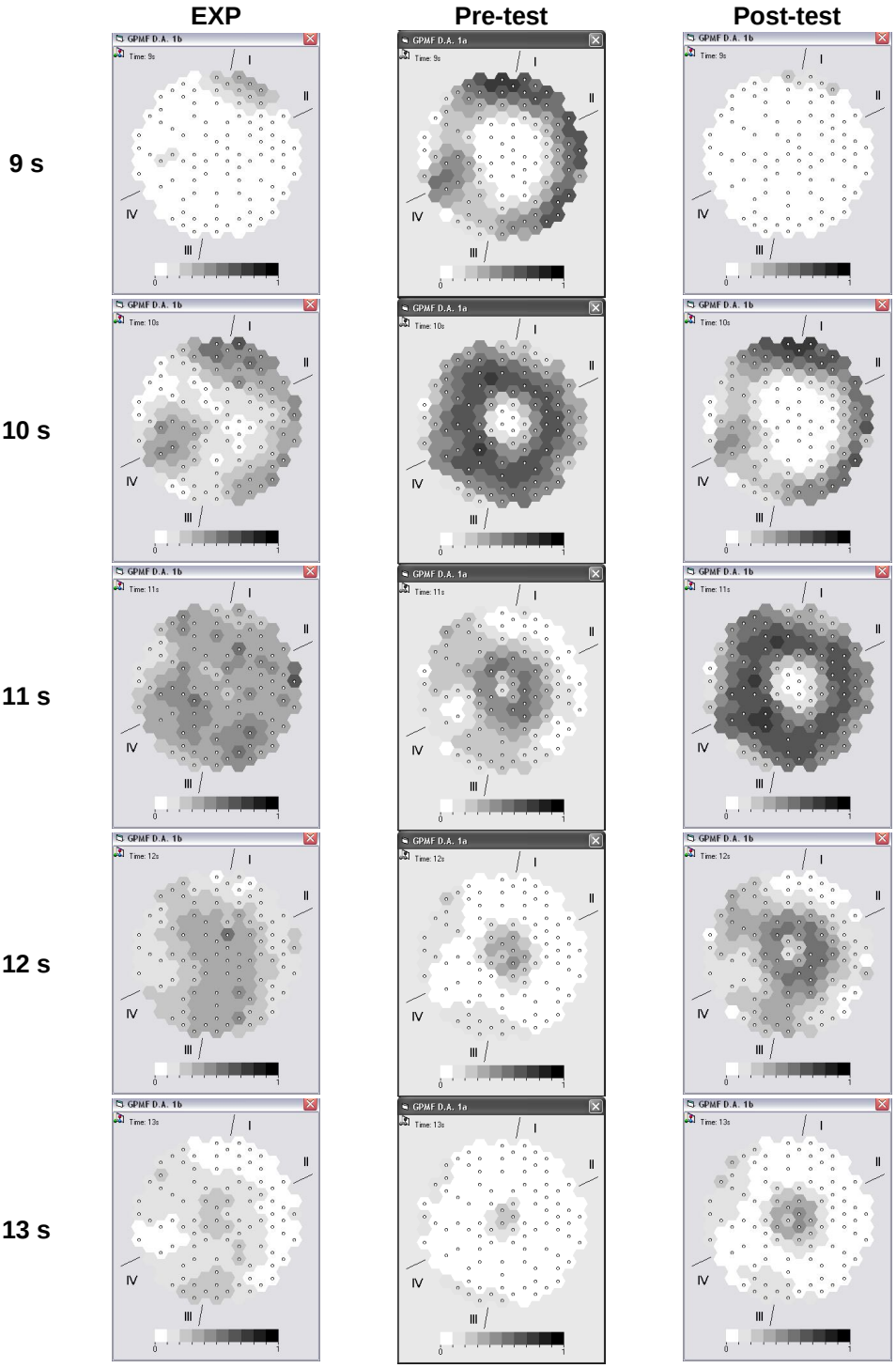

Figure A. 44 – Comparison of MS distribution at core inlet during slug passage

A key parameter affecting the core neutron kinetics response is the maximum perturbation (e.g., the lowest boron concentration, in a boron dilution scenario) reached at the core inlet. The related code predictions are plotted in Figure A. 45, where they are compared with the corresponding experimental trend. As mentioned before, five runs were conducted for this experiment, and the measured values were averaged over such data sets. The mean value of the maximum perturbation is reported in the figure, along with the two curves defining a confidence interval of one standard deviation around the mean value. It is observed that both calculations slightly over-predicted the peak of the mean value curve, although still within the confidence interval.

The pre-test results show a time shift of 1 second in advance (as already observed from Figure A. 44), which is related to the non optimized boundary conditions. The post-test results show instead an accurate timing for the peak occurrence, as well as for the first appearance of the perturbation (around 8 seconds). Later, the code prediction shows a slight delay in the maximum perturbation decrease: at 15 seconds the predicted value for the maximum perturbation is around 0.2, while the experimental value is a little above 0.1. The post-test results, although they are generally outside the confidence interval, look pretty close to the experimental behaviour.

Another key parameter is the core-averaged perturbation, and the related results comparison is shown in Figure A. 46 (the averaging is made on the 90 instrumented locations, both for measured and calculated data). The pre-test results show the same time shift observed above. The post-test results show a correct timing, and a less smooth behaviour than the experimental trend, which indicates that a less “diffused” slug is passing through the core inlet.

A time integration of the core-averaged perturbation provides a measure of the “accumulated perturbation”; this is shown in Figure A. 47. Again, the post-test results show a less diffusive trend (indicated by steeper time gradients); in other words, the perturbation —according to the code prediction— takes a somewhat smaller time to cross the core inlet than in the experiment, and reaches a higher peak.

Quite surprisingly, at the end of the slug passage both calculations predicted the same accumulated perturbation as the experiment, that is, the same amount of tracer has reached the core inlet despite the inaccurate boundary conditions in the pre-test.

The accumulated perturbation at 25 seconds for both the experiment and the post-test results is shown in Figure A. 48 for each instrumented channel. Those maps evidence that the code tends to under-predict the overall perturbation in the central region and to over-predict it in the peripheral region between loops I and IV.

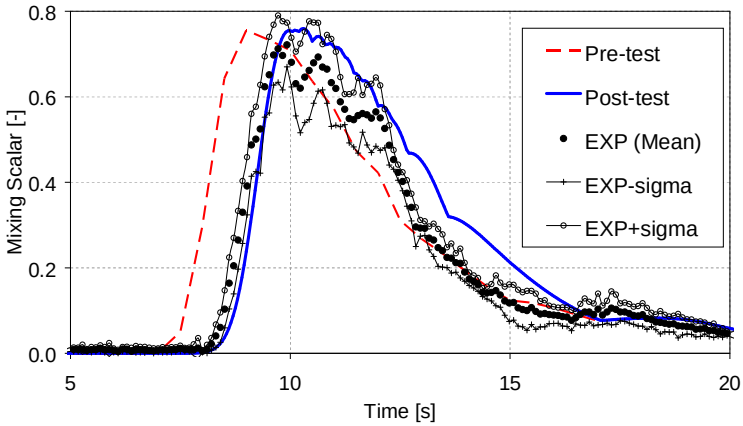

Figure A. 45 – Maximum mixing scalar at core inlet

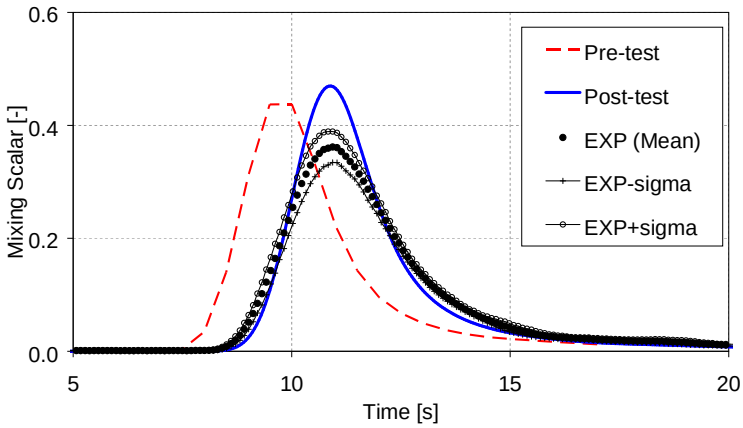

Figure A. 46 – Core-averaged mixing scalar

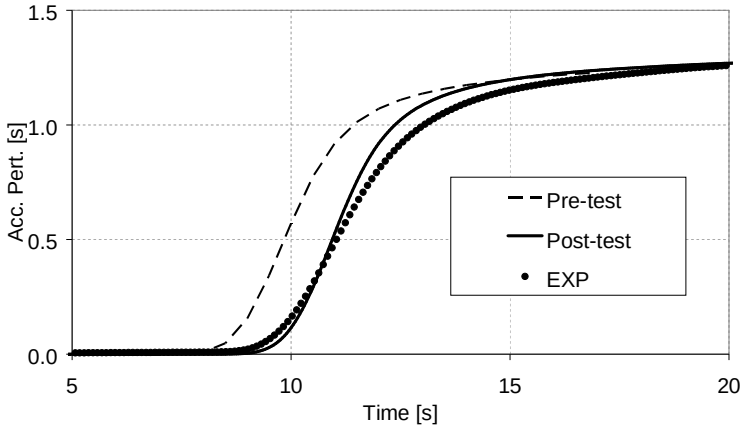

Figure A. 47 – Accumulated perturbation at core inlet

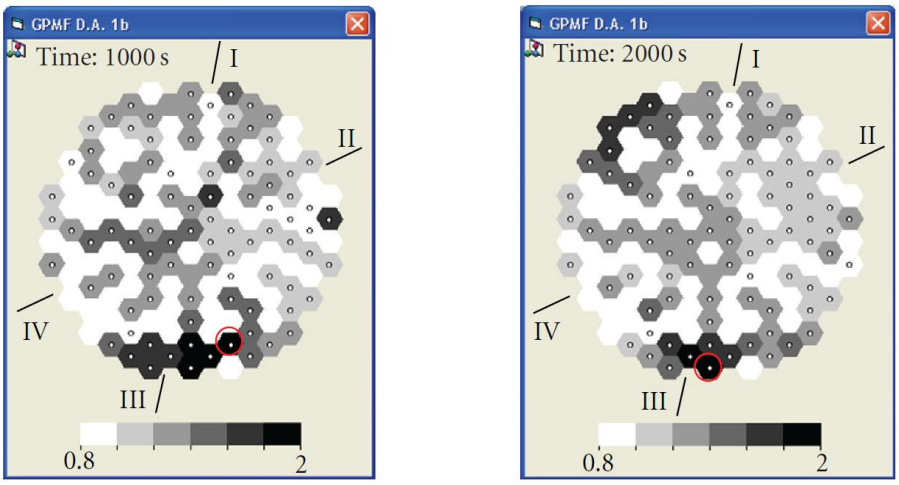

EXP POST-TEST

Figure A. 48 – Maps of channel-by-channel accumulated perturbation at 25 seconds

The measured maximum local accumulated perturbation is 2.02 (s/−), while the predicted value is 2.07 (s/−). The locations of those two maxima are indicated by red circles in Figure A. 48. Table A. 5 summarizes the results obtained for some key parameters such as the timing of perturbation appearance (defined as MS = 0.1), timing and value of the maximum perturbation, and timing and value of the core-averaged perturbation peak. As observed before, the appearance of the perturbation is predicted 1 second in advance by the pre-test calculation and with a 0.2 second delay by the post-test calculation. Similar time discrepancies (−0.9 second and +0.4 second, resp.) appear for the prediction of maximum.

The maximum value is predicted quite satisfactorily in both cases (with a 5% overestimation, which is, however, within the ±σ confidence interval).

Similar time discrepancies (−0.9 second and +0.1 second, resp.) also appear for the prediction of core-averaged peak, while the related peak value is noticeably over-predicted in both cases (27% and 35%, resp.). This seems to indicate a less effective mixing.

A quantitative analysis of the agreement between code predictions and measured data requires taking into account the results channel by channel, in addition to the core-averaged and maximum perturbations discussed above.

Table A. 5 – Comparison of results (perturbation appearance; max. perturbation; core-average)

	Exp - σ	Exp	Exp + σ	Pre-test	Post-test
Time for MS >0.1 [s]	-	8.5	-	7.5	8.7
Time of Max MS [s]	-	9.9	-	9	10.3
Max MS [-]	0.670	0.721	0.773	0.755	0.758
Time of max Ave MS [s]	-	10.9	-	10	11.0
Max Ave MS (90 ch.) [-]	0.334	0.362	0.389	0.460	0.489

However, as easily expected from the quantitative analysis shown before, an excellent agreement would be observed at some locations while at the other locations the perturbation will be either over-predicted or under-predicted by the calculations. This does not allow an easy judgement on the overall quality of the code prediction, unless some general, synthetic accuracy parameter is defined.
A local instantaneous code-to-experiment deviation can be defined as follows (based on the same approach adopted within the FLOMIX-R project, Ref. [1]):

$$DEV1_{i,t} = c_{i,t} - e_{i,t} \qquad \textit{Equation A. 5}$$

where $c_{i,t}$ and $e_{i,t}$, respectively, represent the calculated and experimental values at *i*-th location and *t*-th time-step.
The deviation DEV1 can be averaged over a time interval of interest (e.g. 0 to 17 s, corresponding to the slug passage through the core inlet). The following three deviations are thus obtained (based respectively on relative and absolute values of DEV1 deviations, and on a root mean square averaging approach):

$$DEV2\_SIGN_i = \frac{1}{t_N - t_0} \cdot \sum_{k=1}^{N} DEV1_{i,t} \cdot (t_k - t_{k-1}) \qquad \textit{Equation A. 6}$$

$$DEV2\_ABS_i = \frac{1}{t_N - t_0} \cdot \sum_{k=1}^{N} \left| DEV1_{i,t} \right| \cdot (t_k - t_{k-1}) \qquad \textit{Equation A. 7}$$

$$DEV2\_RMS_i = \frac{1}{t_N - t_0} \cdot \sqrt{\sum_{k=1}^{N} \left(DEV1_{i,t} \right)^2 \cdot (t_k - t_{k-1})^2} \qquad \textit{Equation A. 8}$$

where *N* is the number of time-steps within the selected time period, and t_k is the time value at *k*-th time-step.
Maps of the DEV2 deviations for both calculations are plotted in Figure A. 49, obviously for the 90 instrumented channels only (the others being represented by white colour). Concerning the deviations with their sign, they approximately range between −0.04 and 0.04, and no evident change is observed from pre- to post-test: this is because the two calculations actually behave similarly, except for the time shift, and thus errors with opposite sign during the transient partly compensate. Some locations are evidenced, in both cases, where the perturbation is systematically over-predicted (red) or under-predicted (blue).

Concerning the absolute deviations, it is not possible to identify specific patterns on the map of pre-test results, while on post-test map it is observed that the largest discrepancies occur in the central region and in the peripheral region around 90◦ away from loop #4 (on both directions); moreover, a noticeable improvement is noticed from pre-test to post-test. The same behaviour is observed for the root mean square deviations.

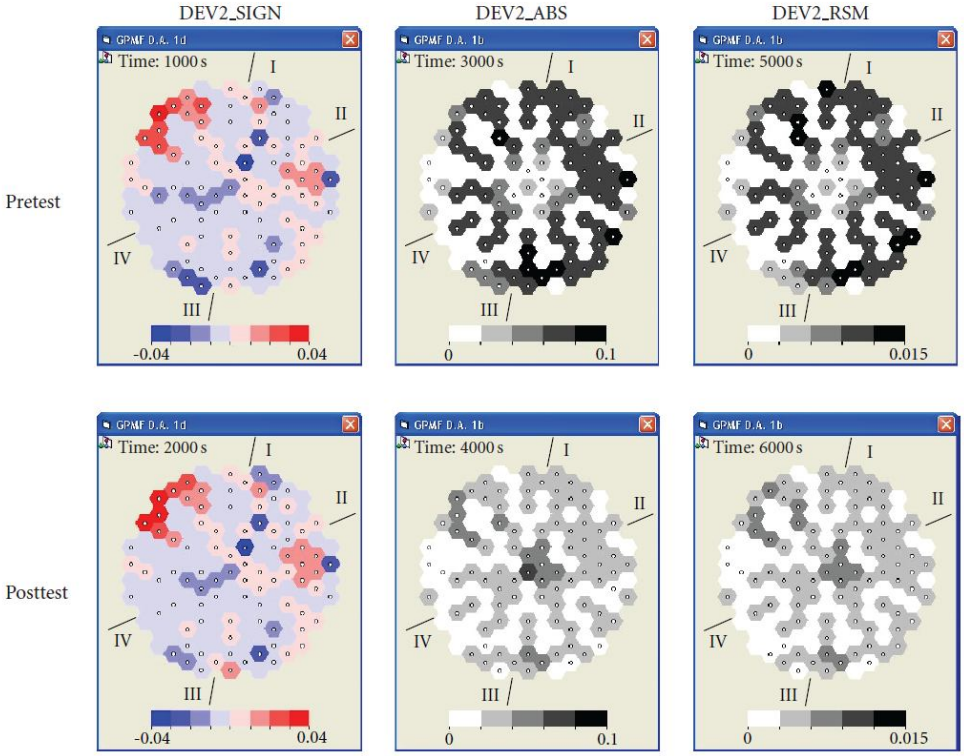

Figure A. 49 – Maps of DEV2 deviations

If the DEV2 deviations are averaged over the instrumented locations, then the results in Table A. 6 are obtained (deviations DEV3), which represent a measure of the overall accumulated deviations. Again, the higher accuracy of the post-test predictions is evidenced. Only the DEV3SIGN deviation is increased.

Table A. 6 – Core- and time-averaged deviations (DEV3)

	Pre-test	Post-test
DEV3_SIGN	0.0011	0.0020
DEV3_ABS	0.0620	0.0311
DEV3_RMS	0.0092	0.0049

The local instantaneous deviations can also be directly averaged over the instrumented locations, so as to obtain time-dependent deviations (DEV4), according to the following equations:

$$DEV4\_SIGN_t = \frac{1}{M} \cdot \sum_{k=1}^{M} DEV1_{i,t} \qquad \textit{Equation A. 9}$$

$$DEV4\_ABS_t = \frac{1}{M} \cdot \sum_{k=1}^{M} \left| DEV1_{i,t} \right| \qquad \textit{Equation A. 10}$$

$$DEV4\_RMS_t = \frac{1}{M} \cdot \sqrt{\sum_{k=1}^{M} \left(DEV1_{i,t} \right)^2} \qquad \textit{Equation A. 11}$$

The resulting plots are shown in Figure A. 50. The first plot clearly indicates that the pre-test results first over predict the perturbation (until 11 seconds), then the under prediction prevails; this is related to the time shift. The post-test results show an opposite behaviour, and generally the discrepancy is much reduced.
The second and the third plots show the same qualitative behaviour; in both cases the noticeable improvement of post-test results is evident.

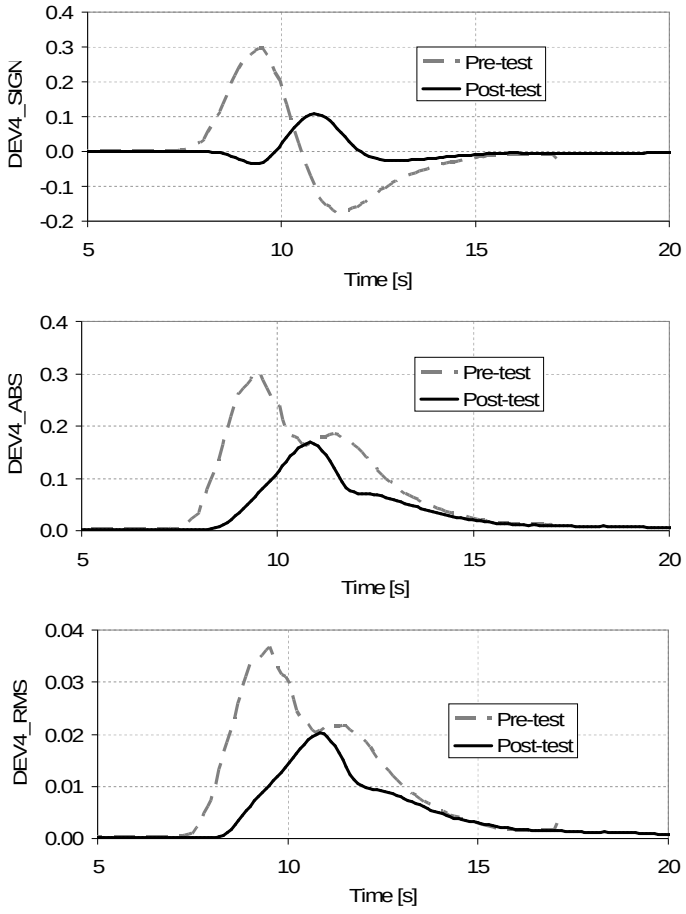

Figure A. 50 – Core-averaged deviations (DEV4): sign, abs. value, root mean square

A.3.6. Conclusions

A pump start-up experiment with the presence of a tracer slug, conducted on a Gidropress mixing facility in the framework of TACIS project R2.02/02, was simulated with the CFD code ANSYS CFX. Both a pre-test and a post-test calculation were run, differing by the boundary conditions imposed in terms of loop flowrates. The numerical results were compared against the experimental data available, which consist in tracer concentration measurements at several locations at the core inlet.

The results of both calculations showed quite a good agreement with the experiment from the qualitative point of view: in particular, the morphology of the tracer concentration distribution at the core inlet was correctly described, including the appearance of two different perturbation patterns (one on the opposite side with respect to the starting loop, and a secondary one on the same side). The only noticeable difference between the pre-test and the post-test—confirmed also by the quantitative analysis—is a time shift (in advance) of the former, due to an imposed loop flowrate which was little higher than actually obtained in the experiment. This qualitative agreement is quite an important achievement, since the addressed scenario is featured by a complex, highly three-dimensional, flow distribution in the downcomer, and its accurate numerical prediction is not a trivial task, due to the well-known limitations of the turbulence modelling based on the Reynolds-Averaged Navier-Stokes approach and particularly on the eddy viscosity concept (i.e., the difficulties in dealing with turbulence anisotropy, unsteady flows, separation phenomena, secondary motions), and typical of most industrial-scale CFD applications.

From a quantitative point of view, the results in terms of maximum perturbation (and related timing), core-averaged perturbation, and accumulated perturbation are also satisfactory. The perturbation peak is over-predicted by 5%, which is comparable with the experimental uncertainty. The predicted time history of the core-averaged perturbation shows a less smooth trend than the experiment, which seems to indicate a less effective mixing (this would be consistent with results from previous CFD validation studies against symmetric loop operation experiments, which had shown a tendency to under-predict the turbulent mixing by the CFD/2-equation turbulence modelling approach).

A further quantitative analysis of the results was done based on a set of “deviations” defined according to a similar approach to that adopted within the FLOMIX-R project. This kind of analysis of the agreement between code predictions and experiment provides a valuable tool to compare the accuracy of different code results. However, a real judgement on the results accuracy cannot be given because it would require a sort of “acceptance thresholds” (in relation to the nuclear reactor safety), which however have not been proposed yet. This is certainly an important matter for future research.

Possible future developments of the present work involve developing finer grids (as far as allowed by the available computing resources), running further sensitivity analyses (e.g., with respect to time discretization, wall roughness) and switching to large eddy simulation (LES) or LES/RANS hybrid approaches for a more accurate prediction of turbulence.

References to Section A.3

1. Rohde U. et al., Fluid mixing and flow distribution in primary circuit of a nuclear pressurized water reactor – Validation of CFD codes, Nuclear Engineering and Design 237 (2007) 1639-1655.
2. Kiger K. T., Gavelli F., Boron mixing in complex geometries: flow structure details, Nucl. Engineering and Design 208 (2001), 67 – 85.
3. Hemstroem B., Andersson N.-G., Physical modelling of a rapid boron dilution transient – II. Study of the Ringhals case, using a more complete model. Report US 97:20, Vattenfall 1997.
4. Gavrilas M., Kiger K., OECD/CSNI ISP Nr. 43 Rapid Boron-Dilution Transient Tests for Code Verification, September 2000.
5. Rohde U. et al., FLOMIX-R Project – Final Summary Report, European Commission.
6. Scheuerer M. et al., ECORA Project - Condensed Final Summary Report, European Commission, March 2005.
7. European Commission – Europeaid Cooperation Office, TACIS Project R2.02/02, "Development of safety analysis capabilities for VVER-1000 transients involving spatial variations of coolant properties (temperature or boron concentration at core inlet)", Terms of Reference.
8. Menter F., CFD Best Practice Guidelines for CFD Code Validation for Reactor-Safety Applications, EU/FP5 ECORA Project "Evaluation of computational fluid dynamic methods for reactor safety analysis", EVOL-ECORA-D01, Germany, February 2002.
9. Mahaffy J. et al., Best Practice Guidelines for the use of CFD in Nuclear Reactor Safety Applications, NEA/CSNI/R(2007)5, May 2007.
10. Hoehne T., Rohde U., Melideo D. et al., Pre-test CFD simulations of Gidropress mixing facility experiments using ANSYS CFX, Proceedings of the 17th AER Symposium on VVER Reactor Physics and Reactor Safety, Yalta, Crimea, Ukraine, September 2007.
11. Hoehne T., Rohde U., Melideo D. et al., CFD simulations of Gidropress mixing facility experiments in the framework of TACIS project R2.02/02, in Proceedings of TOPSAFE Conference, Dubrovnik, Croatia, September-October 2008.
12. Moretti F. et al., CFX Simulations of ROCOM Slug Mixing Experiments, Journal of Power and Energy Systems, Vol. 2, No. 2, 2008.
13. Vyskocil L., CFD simulation of slug mixing in VVER-1000 reactor, ICONE14-89079, Proceedings of the 14th International Conference on Nuclear Engineering (ICONE-14), July 17-20, 2006, Miami, Florida, USA.
14. ANSYS ICEM-CFD 10.0 User Manual, 2005 (embedded in the software package).
15. ANSYS CFX-10.0 User Manual, 2005 (embedded in the software package).